seit 1558

Fabrication and Characterization of Innovative Bottom-Up Plasmonic Nanostructures

Dissertation

(kumulativ)

zur Erlangung des akademischen Grades *doctor rerum naturalium*

(Dr. rer. nat.)

vorgelegt dem Rat der Chemisch-Geowissenschaftlichen Fakultät der

Friedrich-Schiller-Universität Jena

von *Master of Science* (M.Sc) Sezin Yüksel

geboren am 29. Januar 1986 in Istanbul/Türkiye

Gutachter: (1) Prof. Dr. Jürgen Popp, *Friedrich-Schiller-Universität Jena*
(2) Prof. Dr. Volker Deckert, *Friedrich-Schiller-Universität Jena*

Tag der Verteidigung: 26.04.2017, Jena

To my Family

"I am enough of the artist to draw freely upon my imagination. ***Imagination is more important than knowledge.*** *Knowledge is limited. Imagination encircles the world."*

Albert Einstein (1879-1955)

Table of Content

Abbreviation

THC	(-)-trans-Δ^9-tetrahydrocannabinol
2-AP	2-aminopruine
Al	Aluminum
Al_2O_3	Aluminum oxide
AAO	Anodic aluminum oxide
ALD	Atomic layer deposition
BSA	Bovine serum albumin
CT	Charge transfer
CE	Chemical enhancement
CVD	Chemical vapour deposition
C	Cytosine
EM	Electromagnetic enhancement
EBL	Electron beam lithography
EGNPs	Enzymatically generated nanoparticles
FCC	Face-centered-cubic
Au	Gold
AuNPs	Gold nanoparticles
Ypt1	GTP-binding protein
G	Guanine
HR-TEM	High resolution transmission electron microscopy
H_2O_2	Hydrogen peroxide
HQ	Hydroquinone
LoD	Limit of detection
LSPP	Localized surface plasmon polarition
NIL	Nanoimprint lithography
NSL	Nanosphere lithography
NIR	Near-infrared
MS-ALD	Meta stable atomic layer deposition
MW	Microwave
1D	One dimensional
p-BQ	P-benzoquinone

P. lateralis	*Phythophthora lateralis*
P. ramorum	*Phythophthora* r*amorum*
PP	Polyacrylamide polymers
PSPP	Propagating surface plasmon polarition
RSD	Relative standard deviation
SEM	Scanning electron microscopy
Ag	Silver
AgNPs	Silver nanoparticle
ssDNA	Single stranded DNA
HRP	Streptavin-horseradish peroxide
SPPs	Surface plasmon polaritons
SES	Surface enhanced spectroscopy
SERS	Surface enhanced Raman spectroscopies
SERRS	Surface enhanced resonance Raman spectroscopy
TEOS	Tetraethylorthoslicate
3D	Three dimensional
T	Thymine
TDMAS	tri-dimethyl-amino-silane
2D	Two dimensional
VIS	Visible
XRD	X-ray diffraction
EDX	X-ray spectroscopy

Figures

Abstract/*Kurzfassung*

The present thesis introduces the research of various fabrication strategies of bottom-up plasmonic nanostructures for the bio-analytical application. First, a novel label-free *Phythopthora ramorum* detection platform was realized employing SERS. This invasive plant pathogen was successfully detected and the entire analysis chain including, sample preparation, DNA isolation, amplification and hybridization on SERS-active silver substrate-immobilized adenine-free capture probes is introduced in the thesis. Later, the above introduced silver plasmonic arrays, so called EGNPs, were coated with the dielectric material Al_2O_3 using atomic layer deposition (ALD). These procedure increased their sensitivity, specificity and shelf-life. Second, hierarchically designed 3D flower-like hybrid nanostructures were developed by combining the metastable property of EGNPs substrates with plasma enhanced atomic layer deposition (PE-ALD). The resulting ultra-stable nanostructures were established as an efficient SERS-template substrate. Finally, an alternative silver nanoparticle synthesizing method using microwave radiation was proposed. This employs as a reliable, rapid, simple, reproducible and environmental friendly bottom-up fabrication strategy. The approach was implemented to the glass capillaries. An ultra-sensitive and high reproducible novel SERS-based capillary platform was developed and applied for the trace detection of THC. For this purpose, not only the physical, material and optical properties of these developed nanostructures were characterized but also their SERS efficiency was studied in detail.

The developed novel SERS-active nanostructures show improved SERS performance in terms of high SERS reproducibility, surface uniformity, easy synthesis, cost-effectiveness, easy handling and high signal to noise ratio. Finally, the great potential of those novel SERS-active substrates in the field of biochemical and trace detection of an illegal drug were highlighted.

Abstract/*Kurzfassung*

In der vorliegenden Dissertation werden verschiedene Bottom-up-Strategien zur Herstellung plasmonischer Nanostrukturen in bio-analytischen Anwendungen erforscht.

Zuerst wurde eine neuartige SERS-basierte Detektionsplattform für den kennzeichnungsfreien Nachweis von Phythopthora ramorum entwickelt. Dieses invasive Pflanzen-Pathogen konnte erfolgreich nachgewiesen werden und die komplette Detektionskette von der Probenpräparation über die DNS-Isolierung und -Amplifizierung bis zur Hybridisierung an adeninfreie Fängermoleküle, die an SERS-aktiven Silberstrukturen immobilisiert sind, vorgestellt werden. Weiterhin wurden die zuvor vorgestellten Silber-Nanostrukturen, sogenannte EGNPs, über ein ALD-Verfahren mit dem Dielektrikum Al_2O_3 beschichtet, wodurch die Sensitivität, Spezifität und die Lagerfähigkeit signifikant erhöht werden konnte. In einer zweiten Methode wurden durch die Kombination meta-stabiler EGNP-Substrat-Eigenschaften mit plasmaverstärkter Atomlagenabscheidung (PE-ALD) hierarchische blumenartige 3D-Hybrid-Nanostrukturen entwickelt, die als stabile und effiziente SERS-Template eingesetzt wurden.

Zuletzt wurde eine alternative Herstellungsmethode zur Erzeugung von Silbernanopartikeln über Mikrowellenstrahlung entworfen. Diese nutzt eine zuverlässige, schnelle, einfache, reproduzierbare und umweltfreundliche Bottom-up-Herstellungsstrategie, die in einer Glaskapillare angewendet wird. Eine hoch-sensitive und reproduzierbare, neuartige SERS-basierte Kapillar-Plattform wurde entwickelt und für den Spurennachweis von THC angewendet. Zudem wurden nicht nur die physischen, materiellen und optischen Eigenschaften der entwickelten Nanostrukturen charakterisiert, sondern auch die SERS-Effizienz im Detail betrachtet.

Die betrachteten innovativen SERS-aktiven Nanostrukturen weisen verbesserte SERS-Eigenschaften hinsichtlich Wiederverwendbarkeit, Oberflächenhomogenität, einfacher Herstellung, Kosteneffizienz, einfacher Handhabung und hohem Signal-zu-Rausch-Verhältnis auf. Das hohe Potential dieser neuartigen SERS-aktiven Strukturen im Gebiet des biochemischen Spurennachweises illegaler Drogen wurde herausgearbeitet.

1 Introduction

1.1 Motivation

Research of plasmonic materials is a fascinating branch of science having a long history of over hundreds years. [1-5]. Today these materials are of interest not only for fundamental studies in physics and chemistry but also for potential applications in trace detection of molecules, drug delivery, diagnostic imaging etc. Apart from synthesizing metallic nanoparticles by modern technology in the well-equipped laboratories, they also naturally occurred in nature as far as ancient times. The most miraculous examples of using metallic nanoparticles in ancient times were observed in the glass windows of the religious temples (see **Figure 1**). Additionally, they were used to decorate the Lycurgus cups with metallic luster of glazed ceramics. The gold nanoparticles were used to give red pigments to the glass when the Lycurgus cups were illuminated from inside. Such metallic decorations show extraordinary optical properties due to the presence of silver or gold nanoparticles within the layer of the glaze.

The remarkable scientific discovery in nanoparticle research was made by Michael Faraday, considered to be one the fathers of nanotechnology, almost 150 years ago [6-10]. He accidentally synthesized the ruby red solution and further investigated the optical properties of light and matter. His discoveries showed that the color of the solution was given by the size (and shape) of the nanoparticles. He related this to the light scattering properties of

Figure 1: Nanoparticles that are used for coloring glass windows:
The stained rose window with Flamboyant tracy at Sainte-Chapelle in central Paris, France (left).
The colored glass window showing God Rama playing flute for the gopis at Amber Fort Palace, Jaipur, Rajasthan, India (right).

suspended nanoparticles, the so called Faraday-Tyndall Effect [8]. Today, it is known that the origin of these optical properties is the localized surface plasmon polaritons (LSPP). [11]. Later, the analytical solutions of Gustav Mie for the scattering of an electromagnetic wave by a metallic sphere provided the basic building block for the understanding of the plasmonic effects of metallic nanoparticles [9, 10, 12-14]. In consequence of these important contributions, applications of metallic nanoparticles in a variety of different fields such as chemical analysis, biomolecular detection, catalysis, imaging and monitoring, detection of hazardous chemicals, single molecule tracing, food analysis have been emerged[3, 15, 16].

If one thinks about combining plasmonic materials with modern and sophisticated analytical techniques, the first that springs to mind is the development of fast and ultra-sensitive detection methods. Surface enhanced Raman spectroscopy (SERS) is highlighted one of the most powerful vibrational analytical method for understanding the fundamental properties of vibrational molecules and its applications to sensing and detection, down to single molecule detection [14, 17-25]. Since its discovery, the interest in and use of SERS has grown exponentially due to its high sensitivity and specificity. Nowadays SERS is applied in a wide variety of fields from imaging and diagnostic tool in medicine, bio and chemical sensing, investigation of catalytic reactions on plasmonic active surfaces, to detection of hazardous chemicals [23, 24, 26-28]. The SERS enhancement strongly depends on the composition, size, shape and surrounding medium of the plasmonic active nanostructures [29, 30]. The development of SERS active substrates has been concentrated into the production of novel SERS substrates with a particular emphasis on stability, uniformity, reproducibility, easy-to-synthesize, cost-effectiveness and high signal to noise ratio.

The aim of the present thesis was to develop novel and high SERS performance bottom-up plasmonic substrates for bioanalytical applications. In the first chapter of the thesis, the theory of the plasmonics and the SERS technique is briefly introduced. This is followed by a definition of an ideal SERS-active substrate and a synthesis of plasmonic nanostructures and their various fabrication methods are discussed in detail. In the second chapter of the thesis, the novel bottom-up plasmonic substrates developed during the thesis are introduced. In this chapter, the great potential of enzymatically generated nanoparticles (EGNPs) for label-free detection of plant pathogens (covering all the analytical chain) is introduced. Afterwards, an ultra-thin dielectric layer of Al_2O_3 deposited by employing the atomic layer deposition (ALD) is proposed in order to quench the SERS background signal and improve the stability of the EGNPs. Here, the SERS characterization of Al_2O_3 coated EGNPs is performed and then the substrates are compared with the uncoated EGNPs. Further on, the potential applications in SERS are mentioned. This section is followed by the introduction of the establishment of novel bottom-up fabrication strategy for preparation of the

hierarchically designed 3D flower-like silver-silica hybrid nanostructures. These were fabricated by employing SiO_2 plasma enhanced atomic layer deposition (PE-ALD). By taking the great adventage of EGNPs, as a metastable surface, innovative ALD process, so called metastable atomic layer deposition (MS-ALD) is introduced. The formation and the growth theory of these nanostructures are briefly discussed. Later, the SERS performance of these 3D hybrid nanostructures as an efficient SERS template is noted. In the last section of Chapter 2, the microwave-assisted silver nanoparticle synthesis is suggested as an easy and rapid nanoparticle fabrication. The morphological, optical and SERS characteristics of the silver nanoparticles on flat substrate are studied by employing microwave radiation. Lastly, the microwave-assisted nanoparticle synthesis method is applied for coating the glass capillaries for SERS-based applications. Similarly, the physical and SERS properties of the coated capillaries were investigated. While doing this, an ultra-sensitive SERS-based capillary platform was developed for drug detection applications. In the last chapter of the thesis, the results published in six different manuscripts are summarized highlighting the potentials and limitations of the applied analytical method.

1.2 Theoretical Background

Discovered at the beginning of the twentieth century, plasmonics has raised a new and considerable interest [31, 32]. The extraordinary capability of surface plasmons polaritons (SPPs) to concentrate and enhance the electromagnetic field on the nanometer scale has opened new fields of applications in science and technology. The surface enhanced Raman spectroscopy (SERS) is the most powerful and delicate technique to reveal the capabilities combining plasmonics with spectroscopy [26, 33, 34]. The SERS effect was first observed in 1974 while recording the Raman spectrum of pyridine on silver electrodes by Martin Fleischmann, Patric J. Hendra and A. James McQuillan [27]. Discovered more than four decays ago, SERS has raised a higher popularity in research in the last ten years [35, 36] due to it is a potential to become an analytical tool capable of detecting down to single molecular level. However, to understand the SERS enhancement mechanism, first the definition of plasmonic is introduced as follows.

SPPs were first observed with an explained features of a reflectance measurement on metallic gratings by Wood in 1902 [37]. After the proposed theory of light scattering from spherical particles by Mie in 1908 [38], Pines and Fano introduced in 1956 the term of collective oscillations of free electrons in metal, so called "plasmons" and the coupled oscillation of bound electrons, so called "polaritons", respectively in the same year [39, 40]. Thereafter Cunningham and his co-workers introduced the term of surface plasmon polaritons [41]. In recent years, SPPs based nanostructures are relevant for the many application fields in optics, data storage, solar cells, sensors and surface enhanced spectroscopies (SES) [42, 43]. Plasmons and polaritions are both the quantum quasi-particles which used to describe interaction in a solid. The free electrons in a metal such as silver (Ag), gold (Au) and aluminum (Al), can be considered as electron plasma [44, 45]. The plasmon is the quasi-particle resulting from the quantization of the plasma oscillation of the free electrons gas density. The excellent optical properties of the metals such as reflecting the light in visible region or good electrical conductivity of the metal can be described with plasmons [5, 46-48]. On the other hand, polaritons are the quasi-particles resulting from a strong coupling of electromagnetic waves with electric (*or* magnetic) excitations. SPPs are one of the types of interaction coupling of surface plasmons with light. In other words, SPPs are the electromagnetic excitations propagating at the interfaces between a conductor (i.e. metal) and a dielectric medium, resulting a field enhancement from the resonant interaction between SPPs and the electromagnetic

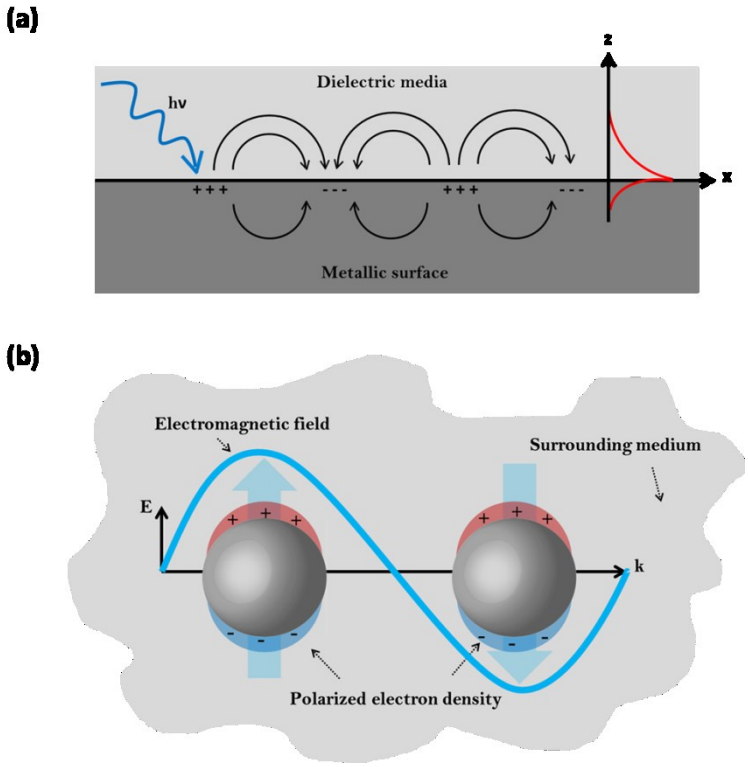

Figure 2: Schematic illustration of (a) propagating surface plasmon polarition (PSPP) and (b) localized surface plasmon polarition (LSPP).

radiation at the metallic interfaces. They are evanescently confined in the perpendicular direction. SPPs contains two other sub group of polaritons, are namely propagating surface plasmon polarition (PSPP) and localized surface plasmon polarition (LSPP) [49]. When the light interacts with the free-electrons on the metal surface, the surface electrons on the metal start to collectively oscillate, absorb and scatter light. For the electromagnetic modes, so called PSPP, propagate at the interface between metal-dielectric interfaces in the x-y direction. They decay evanescently, exponentially (e^{-1}) in z-direction both in the metal and dielectric medium (see **Figure 2(a)**). For LSPP, when the light interacts with the nanoparticle, the free electrons on the conducting band of the metal start to oscillate locally around the nanoparticle with a specific resonance frequency (see **Figure 2 (b)**). SERS relies on two main enhancement mechanisms which are widely known as electromagnetic (EM) and chemical enhancement (CE) (see Figure 2) [26, 50, 51]. From these two the EM enhancement has the main contribution to the SERS mechanism, in the order of 10^8-10^{11}, and will be further discussed in detailed [25, 50, 51]. As compared to this, the signal amplification gained from the CE enhancement is in the order of 10^2-10^3. Overall, the CE enhancement is a sum of three different of

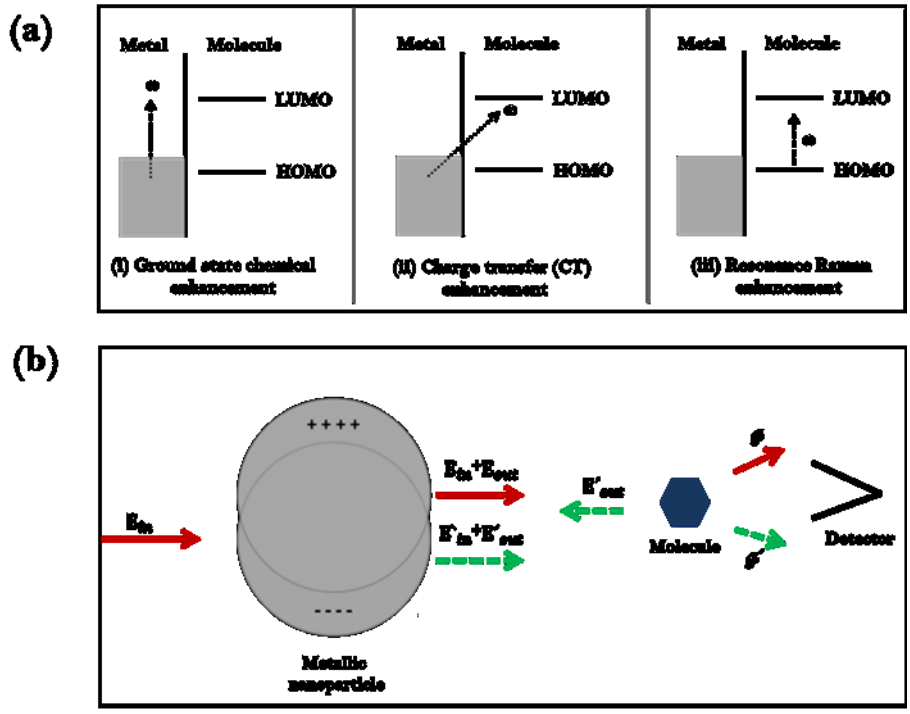

Figure 3: Illustration of the different types of enhancement mechanism in SERS (a) chemical enhancement (CE), (b) electromagnetic enhancement (EM).

contributions, see **Figure 3(a)**. Firstly, the signal amplification can be gained by the chemical interaction of the metallic surface and the molecule in the electronic ground state, known as ground-state chemical enhancement. In different situations, the charge-transfer (CT) process occurring between the molecule and the conducting band of metallic surface is responsible for the effect. That is, the charge transfer (CT) can occur between HOMO and LUMO levels of the adsorbed molecule on the metallic surface whose relative energy depends on Fermi level. The last encountered situation is represented by the resonance Raman effect of the molecule, also referred to as surface enhanced resonance Raman spectroscopy (SERRS). This is achieved by matching the laser excitation with the electronic dipole transition energy of the molecule.

A further contribution to the SERS effect is the influence of the "surface selection rules" at the hot spots, which is associated with the local field polarization effect [22, 51, 52]. The local electromagnetic field on the metallic nanoparticle shows evanescent properties and the target analyte in close vicinity to the metal surface are strongly affected by the gradient field. Due to the diagonal component over the Cartesian coordinate of the Raman tensor, the Raman modes that are perpendicular to the surface dominate in the SERS spectrum due the polarizability. Thus, forbidden Raman modes can be observable in the SERS spectra under the near-field condition. Furthermore, forbidden electronic transition which is caused by the

field gradient can be also observable in the surface resonance Raman spectrum. The SERS selection rules can be used to define the orientation of the adsorbed molecule on the metallic surface by characterizing the changes in Raman intensities of various modes.

The plasmons are the key elements for the EM mechanism which, in turn, is the main contributor to the SERS enhancement mechanism. The interaction of an electromagnetic field with metallic nanoparticles can be analyzed with a simple model employing the "*quasi-static approximation*". For this, an isolated metallic sphere whose size is much smaller than the incident wavelength ($a \ll \lambda$), having a dielectric constant ε_i is considered. Further on, the metallic sphere is embedded in medium having a dielectric constant of ε_o and it is interacting with an incident electromagnetic field, $\mathbf{E}_{in}$, which points the z-direction. Under those defined conditions, Maxwell´s equations can be solved and approximated by LaPlace´s equation and the resulted field outside the sphere $\mathbf{E}_{out}$ can be written as:

$$\mathbf{E}_{out} = E_{in}\boldsymbol{z} - \boldsymbol{\alpha} E_{in}\left[\frac{z}{r^3} - \frac{3z}{r^5}(x\boldsymbol{x} + y\boldsymbol{y} + z\boldsymbol{z})\right] \quad (1)$$

where the first term is the applied field and the second term is the polarization which is resulting from an induced dipole of the metallic sphere. Polarizability is denoted by $\boldsymbol{\alpha}$ and x, y, z are the Cartesian coordinates, r is the radial distance and the magnitude of the inside and outside of field is represented by E_{in} and E_{out} respectively. The polarizability is defined as:

$$\boldsymbol{\alpha} = \frac{\varepsilon_i + \varepsilon_o}{\varepsilon_o + 2\varepsilon_i} a^3 \quad (2)$$

When the real part of ε_i equals $-2\varepsilon_o$ and the imaginary part of ε_i is much smaller than 1, the polarizability, $\boldsymbol{\alpha}$, becomes very large and consequently, the resulting field is enhanced. The SERS enhancement factor, $\boldsymbol{\mathcal{F}}$, shows a fourth-power dependency of the electromagnetic field, $|\mathbf{E}|^4$, and can be written as [51, 53, 54]:

$$\boldsymbol{\mathcal{F}} = \boldsymbol{g}.\boldsymbol{g}' = \frac{|\mathbf{E}_{out}|^2}{|\mathbf{E}_{in}|^2}\frac{|\mathbf{E}'_{out}|^2}{|\mathbf{E}_{in}|^2} = \frac{|\mathbf{E}_{out}|^2|\mathbf{E}'_{out}|^2}{|\mathbf{E}_{in}|^4} \quad (3)$$

where $\boldsymbol{g}$ is the local field enhancement of the scatterer at the laser excitation frequency for all linear optical process and $\boldsymbol{g}'$ is the local field enhancement at the Raman frequency. The first part of the SERS enhancement, $\boldsymbol{g}$, depends on the laser frequency matching of the plasmonic profile of the SERS-active substrates. Moreover, the second part of the electromagnetic SERS enhancements, $\boldsymbol{g}'$ is the modified re-emission of the Raman modes from the nanoantenna. Even though these two terms have different definitions, the common physical origin is the coupling the surface plasmon resonances for both enhancement

mechanisms. **Figure 3 (b)** illustrates the electromagnetic enhancement mechanism in SERS. Briefly, EM arises from the optical excitation of the LSPP of the metallic nanostructure, amplifying the electromagnetic field at the particle surface, and also from the induced polarization that generates a large local field. Additional to this, the Raman signal originates from the vibrational transition of the molecule with these electromagnetic fields.

1.3 Current State of Art: Fabrication of Plasmonic Nanostructures Strategies

The SERS effect strongly depends on the optical properties of the SERS-active substrate [55, 56]. Among these, the physical morphology (such as size and shape) and the composition of the metallic nanostructure are playing an important role for the LSPP and adsorption of the target molecule [45]. Thus, design and fabrication of the SERS-active substrates has been an active research area employing nanotechnology and tailoring the features in the nanometer size scale.

The first SERS substrate was developed by employing roughened silver electrodes. Since then various plasmonic nanostructure fabrication approaches have been developed [29, 55]. Plasmonic substrates were first prepared by electrochemical oxidation and reduction cycles with random and no uniform distribution. Another preparation procedure consisted of synthesizing the nanoparticles by wet chemistry [57, 58] or laser ablation [59, 60] fabrication methods. These resulted in a large size distribution. The third substrate fabrication procedure is by employing chemical synthesis. This results in a more controlled size and shape distribution of the prepared nanoparticles. Lastly, by developing self-assembly techniques or lithographic methods over the last 20 years it was possible to better control the size and shape of the nanoparticles and to achieve a well-defined interparticle spacing by employing a template. As a consequence, SERS applications in trace-level, quantitative analysis nowadays benefit from more defined and controllable size and shape definition of the nanostructures over a large surface area coverage. Combining the concluding remarks from the literature [25, 29, 55, 61], one can define an ideal SERS array as follows:

(1) The SERS-active surface should provide large SERS enhancement down to molecular trace detection.

(2) The metallic nanoparticle should be arranged periodically or regularly or aggregated forms. The physical morphology such as the size and the shape should be well defined and well controllable.

(3) The SERS signal intensity should be homogenous and reproducible across the surface, array-to-array, point-to-point, and batch-to-batch.

(4) SERS substrates from different fabricated batches should be reproducible (batch-to-batch reproducibility).

(5) The SERS-active substrate should be insensitive to the environmental conditions such as oxygen, light and humidity.

(6) It should have long-term stability. After their storage, the SERS signal of the substrate should still be uniform and provide an efficient enhancement.
(7) The plasmonic surface should be biocompatible. The target analyte must be in close vicinity to the metallic surface and the hydrophobicity or hydrophilicity of the substrate should be easily tunable.
(8) The SERS background of the substrate should not overlap with the SERS intensity of the target molecule.
(9) The target analytes, also weak adsorbates, should be detectable without any resonance Raman Effect.
(10) The substrates should be cost-efficient and should have an easy preparation protocol.
(11) Plasmonic arrays should be easily transported at the point of sampling. The designed SERS-active substrates should be readily integrable into simple analytical system.
Based on the above criteria, different SERS substrates preparation strategies have been developed during the thesis. In the following section two main fabrication concepts are introduced: (i) top-down and (ii) bottom-up fabrication techniques [1, 16].

(i) Top-Down Techniques

The top-down fabrication strategies generally result in well-ordered and highly periodic plasmonic arrays [55, 62-69]. They can be prepared with high reproducibility and structural homogeneity. This method implies that the nanostructures are synthesized by removing building blocks from the substrate (see **Figure 4**). There are several subgroups in the top-down fabrication strategies, such as electron beam lithography (EBL), ion etching and ion beam etching EBL-based processes, nanoimprint lithography (NIL), template stripping fabrication method and etc. [55]. For example, the EBL is one of the most common and well known fabrication processes employing a focused beam of electrons to create periodic plasmonic nanostructures. Besides the advantage of the high reproducibility and periodicity, these techniques require high costs due to their laborious instruments and are time consuming. Despite their reusability as template structures, their applicability as an analytical tool has newly been introduced for the practical applications directly in field [70].

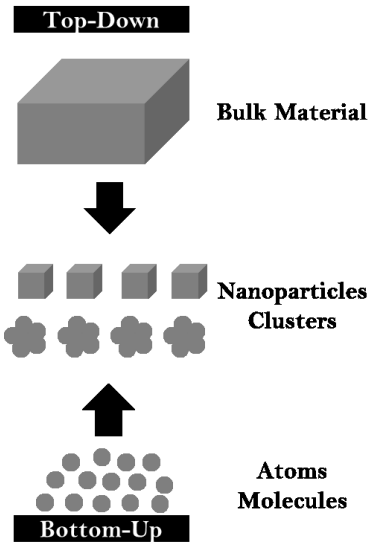

Figure 4: Schematic representation of top-down and bottom-up plasmonic nanostructure fabrication.

(ii) Bottom-Up Fabrication Techniques

The bottom-up fabrication synthesis implies that the nanostructures are prepared generally onto solid substrate by building-up the smallest elements of the molecules such as atoms by atom, or molecule by molecule, which further stack onto each other, resulting nanostructure formation [1, 16]. Thus, the bottom-up approach can be described as a synthesis approach where the building blocks are added onto each other to form nanostructures, or simply as bottom-to-top synthesis procedure (see **Figure 4**). Generally, this novel approach is conceptually imitating the nature, such as the building blocks of body: atoms to molecules, molecules to cells, cells to tissue, tissue to organs.

The bottom-up approach has many advantages compared to other existing techniques (*e.g.* top-down preparation procedures). In the case of nanoparticle synthesis employing wet chemistry, high amount of chemicals are used during the preparation, resulting in a high throughput nanostructures fabrication. The produced nanostructures then have less defects, more homogenous chemical composition and present complex physical properties. Because of employing atoms or molecules as a starting point of the fabrication process, this approach allows the achievement of smaller geometries of the nanostructures. Furthermore, it is much easier and cost-efficient to form thin films or monolayer structures. Moreover, by utilizing the chemical concept of placing molecular-scale components together, self-assembled nanostructure arrays can be formed in a well-ordered manner.

Metallic nanoparticles in an aqueous solution environment are one of the most commonly used plasmonic active materials for the SERS applications [25, 71-74]. These well-established silver and gold nanoparticle preparation methods has been used in many SERS applications. Generally, metallic nanoparticles are prepared employing wet chemical

synthesis with fast and simple procedures [55]. Among these, chemical reduction is the most common employed method for the silver nanoparticle (AgNPs) preparation [75]. The reduction of various silver ions (Ag^+) in aqueous solution leads to an elemental formation of silver (Ag^0) by employing common reductants such as borohydrides, citrate, hydroxylamine ascorbate or elemental hydrogen. The resulting colloidal silver has several nanometer size particles. Even though Lee and Meisel introduced citrate-reduced AgNPs synthesis in 1975s, this is still the most common used silver nanoparticle preparation [75, 76]. The SERS intensity dramatically depends on the number of "hot-spots" in the detection volume [77, 78]. By adding some salts *e.g.* KCl, NaCl to the silver solution silver aggregates are formed and, as a result, the SERS intensity is increased due to the formation of a higher amount of hot spots. Moreover, citrate-reduced nanoparticle preparation can be also used for gold nanoparticles (AuNPs). Besides Lee-Meisel protocol, Leopold and Lendl [79-87] in 2003 a fast and simple protocol for synthesizing AgNPs at room temperature by reducing silver nitrate with hydroxylamine hydrochloride. The resulting silver colloidal solution presents a narrow plasmonic profile and a background-free SERS intensity.

Nanoparticles in aqueous solution have several advantages by means of fast and easy preparation steps. However, their SERS performance is often hindered by the low batch-to-batch reproducibility and poor stability of metallic colloidal solution [55, 88-90]. Thus, core-shell nanoparticles synthesis offers the option of encapsulating single metallic nanoparticles with different dielectric media, such as silica [91-94]. In this manner, encapsulated nanoparticles have longer stability and longer shelf-life as compared to metallic colloidal solutions. Furthermore, the desired dimensions of the nanoparticle can be controlled and the dielectric surface modification can be easily tuned. Generally, AuNPs with silica shell are the most common used core-shell nanoparticles. For their preparation first, the gold colloidal solution is prepared by adding pH-activated sodium citrate solution to the AuNPs suspension. Desired silica thickness can be controlled [95]. These encapsulated metallic nanoparticles have been used for drug delivery, cell sensing, or chemical sensing not only due to their broad plasmon resonance covering the spectral range between 500 nm to 800 nm, but also due to their increased stability [92, 96, 97].

Further on, a straightforward way to form well-ordered plasmonic arrays is the self-assembly of bottom-up nanoparticles from the colloidal solutions [98, 99]. This fabrication method is easy-to-handle, cost-efficient and integrable to planar and non-planar surfaces. Self-assembly nanostructures can occur due to the minimum energy state caused by the electrostatic interactions between molecules and nanoparticles, biomolecular conjugation or applied external electric field. The nanoparticles can form different patterns of various complexities starting from one dimensional (1D) to three dimensional (3D) arrays [100-

106]. The main advantage of the self-assembled nanostructure method is its simple fabrication steps allowing the formation of relatively well-ordered plasmonic arrays. Even though the technique is cost-effective and allows for mass production of substrates compared to lithographic techniques, the uniformity of the arrays is not as reproducible as the one prepared by EBL.

Another method to fabricate more complex structures is using seed-mediated nanoparticle growth mechanism [58, 107]. In this approach, small metallic nanoparticles are used as a seed and are added into metal salt and reducing agent solution. To do so, the surface of the metal is used as a seed and catalyzes the reducing the metal salts. As a result, controlled physical morphology and complexity of the nanostructure in 1D to 3D can be achieved. Employing with these techniques, nanostars, nanorods, nanocages, nanowires to much more complex and hierarchical nanostructures like nanoflowers, nanoforests can be fabricated [108-115]. By using colloidal metallic nanostructures as a seed, immobilized 3D homogeneous as well as heterogeneous spiky and fractal nanostructures can be obtained on solid substrates. There are two approaches for the immobilization of the seed-mediated growth nanoparticles on the planar surface. The first approach is to link the pre-synthesized nanostructures to the substrate. The second approach is to grow the nanoparticle directly on the substrate. The most common technique is to employ a gold layer on the substrate as a seed and then use materials *e.g.* Au, ZnO, TiO_2, SiO_2 for the growth. In conclusion, these materials provide high SERS enhancement with an increased number of hot-spots and have high monodisperse properties. Fabricating plasmonic arrays with specific orientation and high stability still maintains its challenges. Template-based fabrication methods offer the opportunity of developing complex and periodically arranged nanostructures across on large scale [116]. Template synthesis refers to the use of pre-fabricated nanostructured materials with a specific orientation. Herewith, the long-term stability of the plasmonic nanostructure can be increased and these structures can be easily stored until needed and then metal coating can be applied for developing the required chemical or biochemical applications. There are several ways to create templates, among which there are colloidal templates, surface mask templates, surface templates, biological templates and sacrificial templates [116]. The most commonly used regular arrays are the polystyrene (PS) and other silica sphere ones. These were introduced by R. Van Duyne and his coworkers, and are known as nanosphere lithography (NSL) [117-127]. Here, monolayers of self-assembled nanospheres are transferred to the solid substrates and then additional silver or gold deposition is applied onto the NSL. Finally, the nanopsheres are removed and only holes with defined lattice structures remain. Similar structures can also be fabricated by assembling SiO_2 spheres or quantum dots towards building two-dimensional to three-dimensional nanostructures.

Another often enquantered templated technique is employing pre-fabricated quartz EBL structures having various geometries and only requiring a metal deposition to be performed short before the SERS measurement [128]. Further on, employing porous materials, e.g. anodic aluminum oxide (AAO) or polyacrylamide polymers (PP) particles, after the metal deposition, can result in the formation of a skeleton which allows for the diffusion of the target analyte inside the 3D hot-spots of the detection volume [116, 129]. Furthermore, 3D hierarchically designed nanostructures which are form due the specific growth mechanism can be used as templates for various metallic depositions [130]. Besides using inorganic materials as a template, biological and organic nanostructures can also be used to mask nanostructures [131-133]. A large variety of biomolecular structures, with different functionalization groups, are available to bind or to synthesis nanoparticles. DNA strands are one of the powerful options for templating the assembly of nanostructures due to their easy to use and readily existing oligonucleotides synthesis. By means of programming the chemical interactions and different chemical functionalization these allow for the building of nanostructures in 1-, 2-, 3D geometries. In addition to using biological molecules as programmable nanotemplates, biological organism also provide natural scaffold for template based nanostructures with much more complex and regular geometries [116, 134]. Butterfly wings, viruses, fungus and their spores and bacteria also can be used as template due to their excellent and inimitable geometries [135]. Lastly, one of the widespread and versatile approaches to generate complex plasmonic architectures is to use sacrificial templates. This template method undergoes destructive chemical transformation resulting in completely different and new nanomaterials maintaining its starting orientation [55, 119]. This is in contrast to core shell nanoparticle as in these synthesis approach the morphology of the nanoparticles change during the sintering process, resulting in impressive arrays of shapes. Also, destructive etching and chemical reactions can occur. By controlling the chemical reaction properties such as precursor, temperature and pressure, morphology of the nanostructure can be controlled. In conclusion, template technique has an advantage of resulting in nanostructures with simple and well-defined geometries as well as nanostructures that have much more complex morphologies. Furthermore, this approach offers control over the dimensions, morphology and an improved long-time stability. Due to the wide range of plasmonic materials that can be deposited onto templates, the desired laser excitation can be tuned for the relevant SERS application.

Besides various bottom-up plasmonic fabrication strategies, those are mentioned above, protection of those developed nanostructures against oxidation and contamination, or to create biocompatible surfaces, or to tune their plasmonic properties, is an emerging field in plasmonics [136, 137]. Thus, ultra-thin film coating on developed micro/nanostructures

employing atomic layer deposition (ALD) is one of the most promising thin-film deposition techniques and it can be counted as one of the sub-group of bottom-up fabrication strategies. It is based on sequential use of a gas phase chemical process and it is considered to be the subgroup of chemical vapour deposition (CVD). In particular, ALD is used to coat the plasmonic substrate to prolong the shelf-life or to functionalize the surface for improving its biocompatibility. Furthermore, due to its unique property of pin-hole free surface deposition, the optical properties of the plasmonic materials can be tuned easily. Moreover, a wide range of materials can be grown by ALD, including Al, Ti, Ni, Zn SiO_2, Al_2O_3, TiO_2, nitrides and sulfides [138, 139]. In a typical ALD reaction, two types of precursors (e.g. "A" and "B") sequentially react with the surface until the desired thickness is reached. **Figure 5** shows a schematic representation of ALD process. This consists of gaseous chemical precursors which react with the surface. First, the starting surface is exposed to the precursor "A" into a chamber, under vacuum, for a designed amount of time. In this process, the precursor totally reacts with the surface through a self-limiting process which forms a continuous monolayer on the surface. This is followed by purging the surface with an inert gas (typically N_2 or Ar) to remove unbounded molecules from the by-products. Then, the second precursor "B" (generally H_2O) is injected to the chamber. This is again followed by a step consisting in purging an inner gas to the chamber to remove the unbounded molecules. Each step self-saturates when all the binding sites are occupied. Furthermore, each cycle is highly reproducible. By repeating these cycles, the desired film thickness can be control with atomic precision over a large area. Thus, ALD benefits not only from pin-hole free or film density over a large surface area but also from

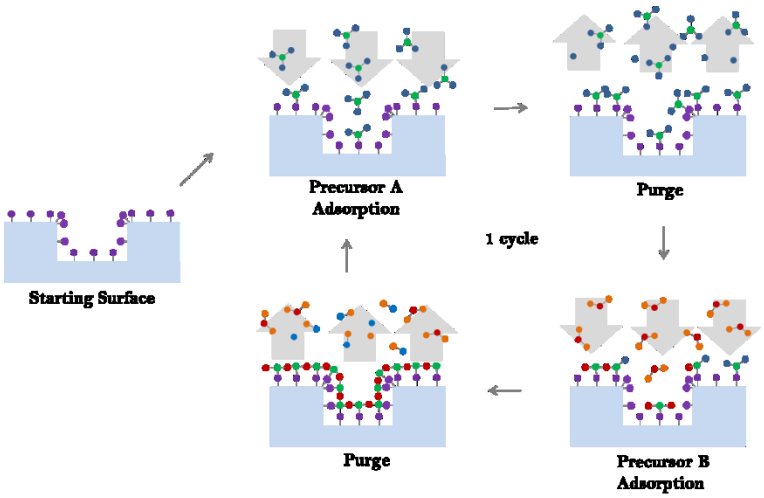

Figure 5: Schematic representation of atomic layer deposition (ALD) process.

thickness uniformity and conformity. By employing a wide range of gaseous precursors, ALD reactions can be performed at temperature 30-250°C, which is below typical CVD process. The capability of coating thin films with ALD at low temperatures, allows for the achievement of conformal films on polymers, plastics, and biological samples.

2. Own Research

2.1 Label-Free SERS-based DNA Detection Employing EGNPs as an Efficient Bottom-Up Plasmonic Arrays [SY1]

Sensitive and selective label-free DNA detection has become an emerging research in the field of gene profiling, forensic analysis, food safety, disease diagnosis, pathogen and hazardous chemical detections. There have been various DNA detection methods, including colorimetry, electrochemical, impedance, fluorescence detection, surface plasmon methods and spectroscopic techniques. One of the scopes of this thesis is to develop reliable, fast, simple, low-cost and sensitive label-free SERS-based DNA detection platform covering the entire analysis chain for the practical applications. Within this contribution, one of the most perilous plant pathogen was detected by employing novel label-free SERS-based plasmonic arrays.

To realize an ideal plasmonic substrate with high SERS performance, plasmonic arrays should fulfill some criteria. These have been already introduced and discussed in chapter 1.3. According these guidelines, enzymatically generated silver nanoparticles (EGNPs) are predominantly suitable for developing SERS based applications. These silver nanoparticles are prepared through bottom-up plasmonic technique and are relatively cost-effective and easy-to-prepare. Furthermore, these nanoparticles are readily integrable into simple analytical system and easily transportable at the point of sampling [140, 141]. EGNPs were generated by an enzyme-induced growth process on a planar substrate (see **Figure 6)**. Briefly, biotin labeled single stranded DNA (ssDNA) was immobilized onto pre-cleaned glass substrate. Streptavin-horseradish peroxide (HRP) complex was bounded to the biotin labeled ssDNA and catalyzed towards the enzymatic generation of nanoparticles from a silver solution. Closely-packed, spiky and sharp features of "desert-rose" like silver nanoparticles with a particle size approximately 500 nm were formed (see **Figure 6).** These nanoparticles are reproducible and easy-to-prepare bottom-up plasmonic arrays and have been already reported in the study of [142] and [143]. They present a broad-band plasmon absorption (450-1000 nm) covering the entire visible (VIS) and near-infrared (NIR) spectral range, which allows for the measurement of analytes by using any desired laser excitation.

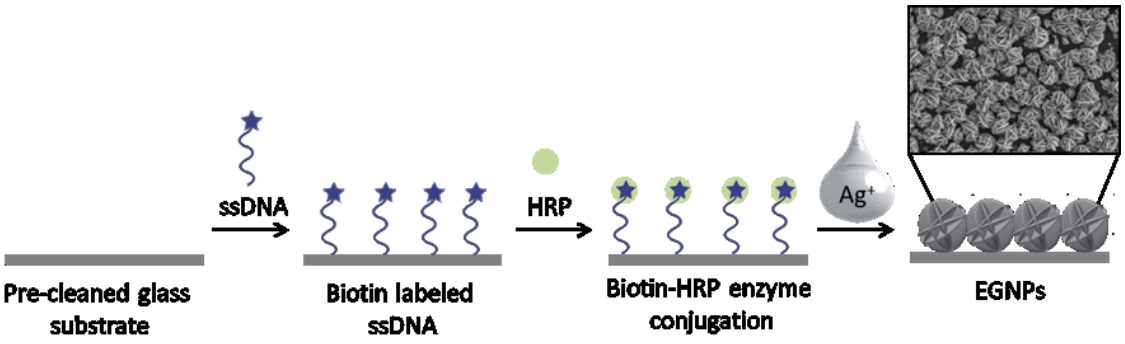

Figure 6: Schematic representation of individual steps for EGNP formation

Halas and her co-workers [144] introduce an elegant label-free detection scheme for specific DNA hybridization. As adenine presents characteristic and dominant Raman profile compared to the other nucleobases (guanine (G), thymine (T), cytosine (C)) and it can be used by the authors as a significant marker in the SERS spectra. However, due to the existence of adenine both in capture probe and target sequence, this property is hampered. This drawback was atoned by the usage of 2-aminopruine (2-AP) in the capture probe to generate adenine-free capture probes. 2-AP is an identical isomer of adenine and forms canonical Watson-Crick base pair. This was applied to record specific DNA interaction of *Phythophthora ramorum* (*P. ramorum*) plant pathogen from an infected *Rhododendron* leaves.
Within the frame work of this thesis, detection of label-free DNA hybridization, the DNA isolation and amplification play important steps for the successful pathogen detection. For this, *P. ramorum* infected plants was chosen from *Rhododendron* leaves. DNA extraction was performed by combining a mortar and pestle methods that were described at S. Julich *et al.*, 2011 [145] and T. D. Miles *et al.*, 2015 [146]. LATE-PCR was applied for the amplification of the yeast GTP-binding protein (*Ypt1*) target gene of *P. ramorum*. Thus, sufficient amount of single-stranded DNA (ssDNA) was generated. In Figure 2 [SY1] illustrates the schematic illustration of the species DNA hybridization on EGNPs is illustrated. After the production of EGNPs, species-specific capture probes which contain 2-aminopurine (2-AP) instead of adenine were immobilized on the EGNPs. Bovine serum albumin (BSA) was used for blocking the unspecific binding sites of DNA. Finally, adenine containing target DNA was used for the hybridization.DNA-based detection of *P. ramorum* was covered applying the whole analysis chain and this can be listed as follows: (i) extraction of the DNA from infected leaves; (ii) isolation gDNA that was used as a template for the amplification of Ypt1 target region by LATE-PCR; (iii) hybridization assays on EGNPs plasmonic assays; (iv) label-free SERS detection (see in Figure 3 [SY1]).

Further on, fluorescence microscopic detection was performed for the verification of the hybridization assay on the plasmonic arrays. Thus, two different capture probes, one for the target species *P. ramorum* and one for the closely related target species *P. lateralis*, were chosen and immobilized on the plasmonic arrays. Afterwards, blocking using the surface with using BSA, hybridization and washing steps were performed as previously described. Figure 4 [SY1] shows the fluorescence microscopy images for the verification of the DNA hybridization assays on EGNPs. Hybridization was performed by employing the FITC-labeled ssDNA of *P. ramorum*, which has a length of 30 nucleotides. The highest fluorescence signals were observed for the *P. ramorum*-specific capture probes that were completely matched to the target DNA. On the other hand, weak fluorescence signal were recorded for the *P. lateralis* capture probes where the hybridization did not occur. Thus, the functionality of the hybridization assay was verified successfully for the specific detection of *P. ramorum.*

After the verification of the DNA hybridization employing fluorescence microscopy, label-free SERS detection of *P. ramorum* DNA was performed. For this, short single stranded target DNA of (a length 30 nucleotides) *P. ramorum* were selected. DNA extraction was performed from the real infected plant samples, and later DNA amplification and PCR were followed by recording the SERS spectra. Two different adenine-free capture probes were selected for the target species *P. ramorum* and the non-target species *P. lateralis.* Immobilizations of the ssDNA on the EGNPs were followed by the hybridization procedure. Figure 5 [SY1] represents the mean SERS spectra of the hybridized *P. ramourm* (showed by a red line), *Phythophthora lateralis (P. lateralis)* (showed by a black line) capture probes and the background of the SERS substrates (showed by a grey line). A broad carbon signature observed in the spectral range between 1200 and 1600 cm^{-1} is visible for the SERS spectra of *P. ramorum* and *P. lateralis* capture probes. This is related to the burning effect induced by the plasmonic surface due to applying a long exposure time for the measurement, which further lead to enhanced electromagnetic effect on the surface. Characteristic Raman modes of cytosine and adenine were hampered by the high carbon background between 1200 and 1600 cm^{-1}. Furthermore, the Raman band observed in the SERS spectrum of *P. ramorum* (where the hybridization with the target DNA) at 1420 cm^{-1} was assigned to the ν(C–C) vibration of cytosine occurred. The ν(C–C) and ring breathing vibration modes of guanine were observed at 1179 cm^{-1} and 667 cm^{-1}. The most typical and dominant Raman mode of adenine at 732 cm^{-1}, which is assigned to aromatic ring breathing, was also successfully recorded. As compared to this, the SERS spectra of the non-target species *P. lateralis* did not show any characteristic adenine-related modes. This indicates that no hybridization

occurred. To sum up, the SERS spectrum of the specific binding of the *P. ramorum* target DNA to the matching capture probe was successfully recorded by employing the label-free SERS-based detection assay. Next, in order to show the applicability of the label-free SERS detection technique for the practical pathogen detection, *P. ramorum* DNA was isolated from the real infected *Rhododendron* leaves. For this the amplified PCR product, having a length of 450 nucleotides, was used. Similarly to the SERS spectra of the short target DNA fragment, Figure 6 [SY1] displays the SERS spectra of the target *P. ramorum* capture probes (showed by a red line), the non-target *P. lateralis* capture probes (showed by a black line) and the background of the SERS substrate (showed by a grey line). The characteristic Raman vibrational modes of guanine at 1081 cm^{-1} and 668 cm^{-1} were observed in the SERS spectra of *P. ramorum*. Moreover, the Raman bands of thymine at 1234 cm^{-1} and cytosine at 1292 cm^{-1} are visible in the SERS spectra of the *P. ramorum*. First, the typical vibrational modes of adenine at 1384 cm^{-1} and 732 cm^{-1} were recorded in the SERS spectra. Analogous to the previous results, the presence of the dominant peak of adenine at 732 cm^{-1} in the SERS spectra served as an endogenous marker compared to the non-target *P. lateralis*. In conclusion, by substituting adenine with 2-AP in the capture probes, the specific hybridization of the *P. ramorum* target DNA could be successfully recorded for long PCR product from real infected leaves.

Despite the fact that SERS-based DNA detection offers great potential regarding the achievement of high sensitivity and specificity, it is still challenging to record good, reproducible spectra by means of batch-to-batch and day-to-day recordings. For this reason, independent experiments were performed using developed label-free SERS-based DNA detection assay. Figure 7 [SY1] shows the normalized integrated SERS intensity at 732 cm^{-1} for the matching target (*P. ramorum*), the non-matching target (*P. lateralis*) and the background of the SERS substrate. It is clearly visible that the integrated SERS intensity at 732 cm^{-1} shows the highest values, having a relative standard deviation (RSD) between 40.6-46.4%. The high RSD of the SERS signal can be explained by three effects: (i) different orientations of the DNA on the metallic surface, (ii) inhomogeneous coverage of BSA on silver nanoparticle, (iii) oxidization of the EGNPs during the immobilization of the ssDNA and the hybridization. Thus, the results are not sufficient for quantitative analysis, but the SERS-based DNA hybridization can be monitored without employing labels for bioanalytical applications.

The well-established EGNPs provides reliable and thermally stable SERS assay for the detection of label-free *Phytophthora ramorum*. Even though the hybridization of the target DNA can be clearly and rapidly visible in the SERS spectra, the quantitative detection of

DNA is still challenging. Due to the organic solvents during the hybridization steps, the silver surface oxidizes, resulting a poor point-to-point SERS signal reproducibility and decreased sensitivity with a high RSD. Furthermore, the SERS background SERS signal of the EGNPs has characteristic Raman bands in the SERS spectrum which dominates the SERS spectra of the target analyte and decreases the sensitivity of the plasmonic arrays. Thus, precisely controlled ultra-thin dielectric coating on EGNPs was required not only for increasing the stability and sensitivity of the substrate but also for increasing the durability of the silver against the possible oxidation. In the next chapter, an ultra-thin dielectric film coating of Al_2O_s was applied on the surface of the EGNPs. The morphological as well as the SERS characterization of alumina coated EGNPs were studied.

2.2 Increased Sensitivity, Specificity and Shelf life of EGNPs by Using PE-ALD to Create Al_2O_3 [SY2]

Modelling of ideal plasmonic structures is very essential for expanding the applicability of the SERS substrates towards bioanalytical applications. This is especially important as most SERS-active substrates present high SERS background signal, poor SERS reproducibility (*e.g.* batch-to-batch, point-to-point), short shelf-life and inadequate bio compatibility. One of the objectives of this thesis was to increase the SERS performance of the EGNPs by means of achieving background-free, increased sensitivity, specificity and longtime stability for bioanalytical applications. Within this context, a thin layer of aluminum oxide (Al_2O_3) was coated on the EGNPs by employing atomic layer deposition (ALD). This well-established thin film growth technique allows pinhole-free dielectric coating with high conformity for SERS applications.

Thus, in this study [SY2] the background contribution of the EGNPs was explored in detail by employing SERS. EGNPs were produced in an arrayed order on the glass substrate as already shown in Figure 6 and Figure 1 [SY2]. Closely packed "desert-rose" like silver nanoparticles was produced via HRP catalyzed redox reaction. In this catalytical process, depicted in Figure 1 (b) [SY2], an oxygen atom is detached from the hydrogen peroxide (H_2O_2) and bound to the prostethicheme group of the enzyme. This causes a change of the iron oxidization state. In this manner, the silver ions (Ag^+) reduced to elementary silver (Ag^0) and hydroquinone (HQ) is oxidized to p-benzoquinone (p-BQ). By employing high-resolution TEM imaging, the organic residues (light grey area in the TEM image) from the redox reaction on the silver nanoparticles (dark grey area in the TEM image) can be visible, (see Figure 2 [SY2]). Here, the carbonaceous layer did not cover the whole silver surface but it varied from 2 to 25 nm. This inhomogeneous residue layer from the redox reaction causes fluctuation of the SERS signal across the surface area and decreases the reliability of the SERS substrate. Furthermore, Raman signal from the adsorbed molecules on the silver surface, further referred to as the Raman background signal of the EGNPs, was recorded is depicted in Figure 3(a) [SY2]. Here, the strong Raman mode at 1391 cm^{-1} was assigned to the combined contribution of ν(C-C) and ν(C-H) vibrations of p-BQ. Furthermore, the other vibrational modes at 945 cm^{-1}, 800 cm^{-1}, 1019 cm^{-1}, which were assigned respectively to ν(C-C) and ν(C-H) of p-BQ, in plane vibration of HQ and ν(C-C) vibration of the HQ-p-BQ complex, are also visible in the SERS spectra. Lastly, a further contribution to the background signal can be assigned to the citrate solution used during the EGNPs preparation. This band occurs at around 1400 cm^{-1} and 945

cm^{-1} due to the vibrational modes of ν(COO) and ν(C-C) respectively. This strong background signal of the plasmonic substrates not only limits the detection of the target molecule but also decrease the SERS reproducibility.

In order to remove the residues from the SERS substrates, various thickness of Al_2O_3 (0.5, 1, 5, and 10 nm) dielectric coating were applied on the EGNPs by employing ALD. Figure 3(b-f) [SY2] shows the SERS spectra of the Al_2O_3 coated EGNPs. During the first few cycles of ALD, the dielectric layer started to form island growth on the surface of the EGNPs. Upon formation of an increased layer thickness of Al_2O_3, the background signal of the SERS substrates, which is normally dominated by bands centered at 1391 cm^{-1}, 1019 cm^{-1} and 945 cm^{-1}, was relatively quenched. This could be attributed to the "cleaning effect" of the surface ALD.

To analyze the influence of the dielectric coating on the EGNPs, the SERS measurement of 10 μM of riboflavin in aqueous solution, as a model analyte, was performed. Figure 4 [SY2] shows the integrated SERS intensity at 1342 cm^{-1} of riboflavin as a function of the Al_2O_3 thickness (nm). It can be clearly visible here that the highest SERS intensity was observed in the case of the thinnest coating layer, 0.5 nm. In this case a low RSD was also achieved due to the high conformity on the surface. Furthermore, the SERS intensity decreased for the increased coating thickness. Nevertheless, in order to ensure that the dielectric layer is completely closed, 1nm of Al_2O_3 coating was chosen for the further characterization experiments.

The chemical characterization of the coated (1 nm Al_2O_3) and uncoated SERS active surface was performed by energy dispersive X-ray spectroscopy (EDX). Figure 5 [SY2] shows the EDX spectra of the coated and the uncoated EGNPs. Here, the intense peak at 2.99 keV was detected for both the coated and uncoated EGNPs and was assigned to the silver Lα emission line. The peaks at 1.49 keV and 0.52 keV observed for the coated EGNPs corresponds to the K lines of aluminum and oxygen. Their presence proves that the successful Al_2O_3 coating was achieved. In contrast to the coated EGNPs, for the case of the uncoated ones no oxygen peak was found. The peak at 0.27 keV was assigned to carbon due to the underlying material of silver nanoparticles.

After investigating the chemical characterization of the coated (1 nm Al_2O_3) and uncoated EGNPs, the point-to-point and batch-to-batch SERS reproducibility were studied. For this reason first, the characteristic Raman mode of riboflavin at

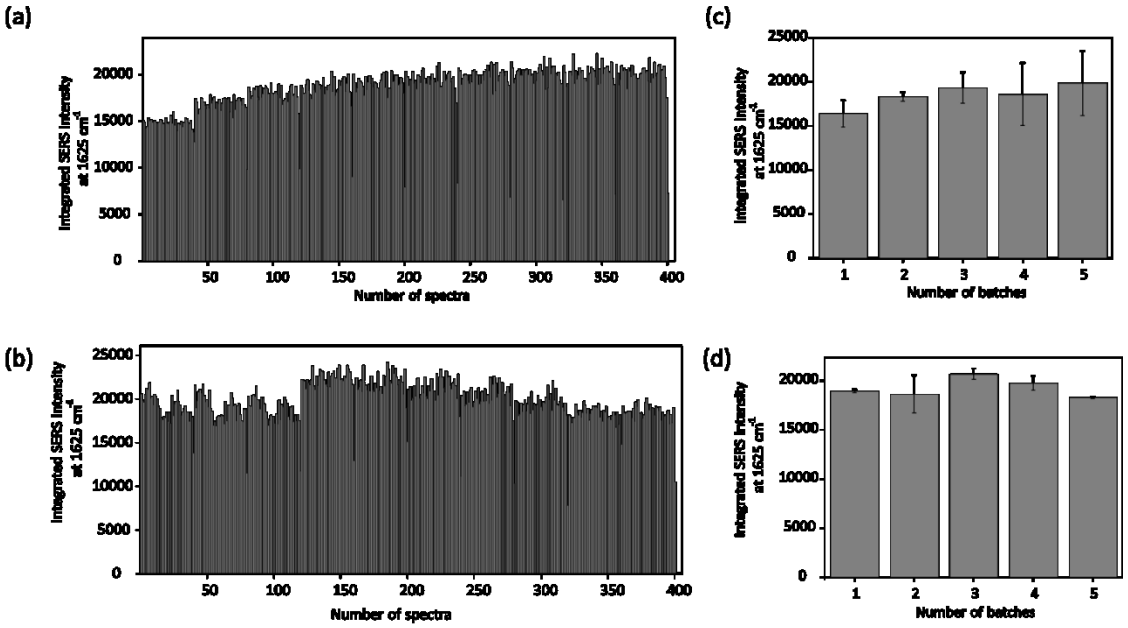

Figure 7: SERS reproducibility of uncoated and coated EGNPs: (a) Point-to-point SERS reproducibility of (a) uncoated and (b) coated (1nm Al_2O_3) EGNPs. Batch-to-batch SERS reproducibility of (c) uncoated and (d) coated (1nm Al_2O_3) EGNPs.

1625 cm^{-1} was integrated and plotted in Figure (7) (a-b) as a function of the spectrum number. As depicted in Figure (7) (a-b), the RSD of the SERS intensity for uncoated and coated EGNPs are respectively 12.95% and 10.8%. The measured RSD of SERS intensity shows that the point-to-point SERS reproducibility of the uncoated EGNPs is adequate for an ideal SERS substrate. This is due to the densely and multilayered packed silver nanoparticles. However, upon implementation of the atomic scale precision of ALD, the RSD of the point-to-point SERS reproducibility of the coated EGNPs was decreased. Similarly to the point-to-point analysis, the Raman mode at 1625 cm^{-1} was also plotted as a function for individual batches of the substrates. Figure 7(c-d) shows the batch-to-batch SERS reproducibility of the uncoated and coated EGNPs respectively. The RSD of the five different batches for uncoated EGNP substrate is between 3.8-18.5%. However, after coating the EGNPs with an ultrathin film of Al_2O_3, the RSD of the five different batches were decreased to values in between 2.6-10.3%. These investigations show that not only point-to-point but also batch-to-batch SERS reproducibility of the coated EGNPs revealed increased SERS performance compared to uncoated EGNPs.

In order to access the sensitivity of the coated and uncoated EGNPs, the quantitative detection of riboflavin at different concentrations, was studied. Figure 6 [SY2] illustrates the limit of detection (LoD) of riboflavin for coated and uncoated EGNPs. Here the characteristic Raman mode at 1625 cm^{-1}, assigned to ν(C-C) vibrational mode of the benzene ring, was integrated and plotted as function of the concentration. It has been determined

that the detection limit of riboflavin for using the uncoated EGNPs was down to 0.2 μM, with a RSD of around 20%. This high RSD was correlated to inhomogeneous residuals on the silver nanoparticle due to the redox reaction. However, the detection limit of coated EGNPs was down to 10 nM with a decreased RSD due to the existing, atomic scale precise, dielectric coating. In summary, the thin-film Al_2O_3 coating of the EGNPs not only quenched the background signal but also increased the sensitivity of the plasmonic arrays down to the detection limit of 10 nM of riboflavin.

In addition to the background-free and increased sensitivity, the ideal SERS substrate should be long-term stable. For this, the shelf-life of the coated and uncoated EGNPs was analyzed over a period of 12 weeks. In doing so, after the preparation of the coated and uncoated EGNPs, they were stored in darkness at ambient conditions for different, required previous of time and the SERS intensity of riboflavin was measured weekly. Figure 7 [SY2] shows the normalized integrated Raman intensity of riboflavin at 1625 cm^{-1} *versus* the week number. It was observed that the uncoated EGNPs were oxidized and the SERS intensity dramatically decreased after one week. In contrast to the uncoated EGNPs, 1nm Al_2O_3 coated silver nanoparticles were stable up to 4 weeks, proving the pinhole free coating on the silver surface.

Biocompatibility of the plasmonic active surface is also playing an important role for the bioanalytical applications. Within this context, retinol was chosen to show the potential of the alumina coated silver surface. Figure 8(A) [SY2] illustrates the Raman spectra of retinol and Figure 8(B-C) [SY2] shows the SERS measurements after and before retinol incubation for coated and uncoated EGNPs. When the uncoated EGNPs were incubated in the retinol solution, the most predominant Raman vibrational band detected was centered at 1583 cm^{-1}. However, when the coated EGNPs were incubated in the retinol solution, the main characteristic Raman modes of retinol are detectable due the quenching of the background substrates signal. The affinity of the retinol molecule on the alumina surface was stronger for the coated silver surface than for the uncoated EGNPs. Due to the binding of the molecule to the surface via the OH group a slight shift of the Raman band at 1585 cm^{-1} to 1555 $cm^{-1}$was observed. Thus, typical vibrational bands of retinol can be reliably detectable with coated EGNPs due the quenched background signal and high affinity to the dielectric surface.

As an alternative to an Al_2O_3 coating on EGNPs, an ultra-thin film of SiO_2 was also applied as a protection layer on EGNPs by employing plasma enhanced atomic layer deposition (PE-ALD). However, after the silica coating on EGNPs, 3D hierarchically designed silver-silica nanosponges, flower-like nanstructures were obtained. These nanostructures provide interesting morphological properties such as high 3D surface area. These 3D nanostructures

can provide excellent platform for the SERS-based application due to an increased hot-spots in 3D volume. Therefore, the morphological, and SERS respond of these new fabricated hybrid nanosponges and flower-like composite nanstructures will be investigated in the following chapter.

2.3 Hierarchically designed 3D flower-like composite nanostructures as an ultra-stable, reproducible and sensitive SERS substrate [SY3]

Conventional one dimensional (1D) and two dimensional (2D) SERS substrates are often limited by the number of hot spots in the focus volume. Furthermore, these substrates provide low detection limit for the small or non-resonant molecules due to limited number of hot spots. Thus, three dimensional (3D) SERS substrates offers large hot-spots volumes, which supplies attractive alternative for ultra-sensitive sensors for trace chemical analysis. Recent, the top-down fabrication techniques, such as EBL, provides controlled, uniform and periodic nanostructures in 3D form. However, these techniques generally require long fabrication times and are characterized by a high cost. Another way to fabricate more cost-effective 3D SERS active substrates is by creating nanotemplates. These substrates are pre-fabricated, self-standing and present well spatial oriented nanostructures. Template based SERS substrates are a convenient and versatile approach due to the various possible plasmonic material usage. After the template fabrication, nanostructures can be coated with various plasmonic materials (e.g. Ag, Au, Co, Pt etc.) which open diverse application fields. Furthermore, these prefabricated nanostructures do not only provide large scale well-aligned nanostructures but also offer long-term storability. One of the aims of this thesis is to develop novel, ultra-stable and easy-to-fabricate hierarchically designed 3D nanostructures as an efficient SERS template.

3D flower-like hybrid nanostructures were fabricated via a simple two-step process, which was already described in Chapter 2.3. Figure 1 [SY3] shows the schematic illustration of the fabrication procedure of the hierarchically designed 3D flower-like hybrid nanostructures. In the first step, EGNPs were fabricated and then various cycles of SiO_2 deposition were applied by employing PE-ALD as a second step. Figure 2 [SY3] shows the scanning electron microscopy (SEM) images of the EGNPs and various fabricated hybrid nanostructures. It can be clearly visible that the particle size of the "desert-rose" silver nanostructure was around 400 nm, presenting a structure consisting of closely packed silver plates. In order to create the 3D hybrid nanostructures, various SiO_2 cycles (5, 45, 90, 135, and 180) were applied on the EGNPs surface. After 5 cycles of SiO_2, the EGNPs morphology started to change and formed aggregated porous nanostructures instead of the previously spiky features with a size up to 4 μm (see in Figure 2(b) [SY3]).

The flower-like nanostructure pattern started to form after 45 cycles of SiO_2 deposition on the EGNPs. The increased number of SiO_2 cycle depositions on the surface of EGNPs led to

the formation of a more fractal and branch morphology (see Figure 2 (c-f) [SY3]). Furthermore, the controlled pillar size of the branches can be obtained by increasing the number of SiO_2 cycle depositions. The cracking of the surface and the nanoporosity of the silver nanostructures can be explained by purposed following mechanism. In standard ALD process, in which a stable and non-reactive substrate is used and the homogeneous dielectiric coatin is obtained on the surface. However, when the surface is meta-stable, in this case the surface is EGNPs, the standard ALD process is not valid anymore. In this study we used oxygen plasma with a high energy and pressure (300W and 160 mTorr). During the oxygen plasma step in PE-ALD process, the silver surface of the EGNPs is rapidly oxidized and this led to a highly stressed layer. Due to the high internal stress of the oxidized silver layer causes the cracking of the silver oxide plates and the silver layer above the silver oxide layer reveals through the outer surfaces. Due to the thick formation of silver oxide, inner parts of the silver oxide films lift the upper layers while the oxygen plasma exposed. By repeating these steps in a sufficient manner, the previous silver plates will continuously transform to highly stress silver oxide forming a nanoporous structure (Figure 2(b) [SY3]). Meanwhile, due to the high operating temperature (120°C) of PE-ALD, the formed silver oxides layer were not stable and eventually the silver oxide layer decomposed to elemental silver under the release of atomic oxygen. During this oxygen plasma step, a new a new metastable surface was created this new metastable substrate acts like a precursor container and releases the second precursor over a certain time due to the porosity property. By repeating the PE-ALD cycle with a sufficient time, the height of the nanostructure increases, forming a flower-like shape. Thus, various hierarchically designed 3D flowers-like hybrid nanostructures were achieved via tuning the amount of the PE-ALD cycles. Creating new meta-stable substrates during the oxygen plasma in the PE-ALD process will be refered to "metastable state assisted atomic layer deposition" (MS-ALD). This novel bottom-up nanostructure fabrication strategy was submitted for patent (Mario Ziegler, Sezin Yüksel, Dana Cialla-May, September 2016, DE 10 2016 118 440.3). In our study, EGNPs are playing a key role in the process and as already reported in [SY2], the inhomogeneous residual layer on EGNPs and the fine feature size of silver EGNPs provides excellent sacrificial template for fabricating these 3D hybrid nanostructures.

The fabricated various nanostructures do not show SERS activity. In order to measure the SERS spectra, the desired plasmonic material should be deposited on the pre-fabricated, above discussed nanotemplate. Figure 4 [SY3] shows a schematic illustration of the work flow starting from the fabrication process of the 3D hybrid nanostructures, followed by the metal deposition on the nanostructure and ending with the recording of the SERS spectra. 3D hybrid nanostructures can be used as an ultra-stable SERS template. In order to get high

SERS enhancement, differing flower-like nanostructures (45, 90, 135 and 180 cycles of SiO_2) were produced and 4 nm of silver was thermally evaporated on four different nanostructures. In order to define the optimum nanostructure, the SERS spectra of a 10 μM riboflavin solution were measured. Figure 4 [SY3] shows the SERS activity of riboflavin measured on the nanostructures (fabricated via 45, 90, 135 and 180 cycles of SiO_2). The characteristic peaks of riboflavin at 1625 cm^{-1}, 1402 cm^{-1}, 1347 cm^{-1} and1312 cm^{-1} can be reliably detected with four different 3D hybrid nanostructures. In order to define the optimized nanostructure for SERS applications, the SERS intensity at peak centered at 1625 cm^{-1} was integrated, normalized and plotted as function of SiO_2 cycle amount. The highest SERS intensity was observed for the nanostructure that was produced by 135 cycles of SiO_2 on EGNPs. This presented a RSD of 14.7%. Afterwards, the optimal silver deposition was investigated by accessing the highest SERS performance. For this, the 3D hybrid nanostructure (135 cycles of SiO_2 on EGNPs) was chosen and different silver thicknesses were applied on it. Figure 5 [SY3] shows the dependency of the SERS signal response of the 3D hybrid nanostructure to the silver thicknesses (0, 10, 20, 30, 40, 50 and 60 nm). 50 nm silver deposited hybrid nanostructure yields the highest SERS intensity with as low a RSD as 4.5%.

The surface functionalization of the SERS substrates, such as one that would provide the substrates with hydrophobic and hydrophilic properties, plays an important role for the most biomedical applications. Most of the plasmonic substrates are lipophilic and, as a consequence, the water insoluble analytes cannot be adsorbed to the metallic surface. Thus, recording the SERS spectra of hydrophobic molecules still maintains its difficulty on hydrophobic surfaces. Functionalization of the surfaces requires complex, expensive and long-time preparation procedures. Within this contribution, hierarchically designed 3D hybrid nanostructures (135 cycles of SiO_2) provide high hydrophobicity with a contact angle of approximately 111°. The influence of the EGNPs micro roughness covered with nano roughness of 50 nm silver metal deposition on the nanostructure, further increases the performance of the hydrophobicity with a contact angle as high as 125°. This super-hydrophobic property of the developed substrates serves an excellent SERS platform for the analytes solved in organic solvents.

Even though SERS offers a great potential for bioanalytical applications, plasmonic substrates have been hindered by poor batch-to-batch and array-to-array *or* point-to-point SERS reproducibility. The preparation steps of the nanostructures can cause large deviations of the SERS intensity due to the inhomogeneous distribution of metalized nanoparticles. Thus, the performance of the SERS substrates decreases because of the low SERS signal reproducibility. Due to this, several different batches of the SERS templates (135 cycles of SiO_2) with an additional 50 nm silver deposition were prepared in order to

investigate the batch-to-batch SERS reproducibility. 1 μM of riboflavin in methanol was used as a model analyte and SERS spectra were recorded. Figure 6(a) [SY3] shows the integrated SERS intensity at 1625 cm^{-1} *versus* the number of different batches. The RSD of the five different batches varies between 8.3 and 17.2%. Likewise, for the point-to-point SERS reproducibility, the characteristic Raman mode at 1625 cm^{-1} was integrated and plotted for 400 individual spectra (see Figure 6(b) [SY3]. The RSD of the SERS intensity was 16%, which was highlighted as a light grey area. These investigations reveal the potential of the developed 3D composite SERS templates to provide high point-to-point and batch-to-batch reproducibility of the SERS intensity.

The quantitative detection of the riboflavin is illustrated in Figure 7(a-b) [SY3]. Here, the SERS signal at 1625 cm^{-1} was integrated and plotted as a function of concentration. It can be visible in this plot that the range between 5 to 0.025 μM of riboflavin was detected (see Figure 7(a) [SY3]). The comparison of the data with the LOD proves that by employing the 3D ultra-stable SERS template as a sensor platform, riboflavin can reliably be detected down to a concentration of 50 nM.

Even though hierarchically designed 3D silver-silica nanostructures offers promising SERS template for the SERS applications, the fabrication time of these complex nanostructures is longer than three hours. Furthermore, complex equipment and specialized operators, that increases the overall cost of the fabrication procedure, are needed. To establish reliable SERS-active platform that can be easily and rapidly fabricated with an environmental-friendly procedure and low-costs, high number of batch-to batch fabrication as an alternative and novel silver nanoparticle synthesis is introduced by employing using microwave radiation in the following chapter.

2.4 Simple, Fast, One-Step Silver Nanoparticle Formation Employing Microwave Irradiation (MW) for SERS Application [SY4]

Several approaches have been reported for the synthesis of Ag NPs and the traditional preparation procedures are in-phase reductions solution. The mostly common ways to produce AgNPs are in ones requiring the presence of capping agents, stabilizers and organic solvents, so employing wet chemistry. These preparation strategies are often risky for the environmental ecosystem and might require a long preparation time. Due to the fast and high homogeneity of the locally produced microwave heating, the uniform and rapid synthesis of nanostructures can be obtained with high control over the shape and dimensions, allowing for a rapid synthesis of the nanostructures with high controllable shape and dimensions.

In this part of the thesis [SY4] an easy, fast and environmentally friendly method will be introduced for the production of thin films based on self-assembled and homogenously covered silver nanoparticles. Furthermore, this closely packed thin film silver is formed without using any stabilizing or strong reducing agent. The film can be obtained from the mixture of silver acetate and an ethanol/water solution. Different types of reducing agents were tested. The morphological, hydrophilic and optical properties of the silver films are characterized. The controlled shape and size of various stable films with covering objects is documented. To demonstrate their potential, the SERS activity of the obtained AgNPs covered substrate was tested with riboflavin as a model analyte.

In order to optimize the experimental conditions, three different reducing agents were chosen, namely ethanol, ethylene glycol and glycerol. These three alcohol based solvents were chosen due to their high dielectric loss for MW irradiation, which made them ideal solvents for the rapid reduction reactions. Additional to those solvents, silver acetate was used as a silver source and the glass substrates were employed as the solid support. Figure 1 [SY4] shows a photograph of the AgNPs formation, was composed by 2 mL of water, 1 mL of ethanol and 1 mg of silver acetate solution, at the glass support employing MW radiation at 170°C for 2 minutes. It is clearly visible that the glass substrate was homogenously covered with yellowish metallic layer.

In order to obtain a homogeneous and compact layer, several aspects such as the role of temperature, Ag salt concentration and reducing agent amount were investigated first (see the supplementary information [SY4]). The optimized reaction mixture (1 mL of ethanol, 2 mL of water and 1 mg of silver acetate) reacted at a temperature of 170

°C, resulting in a compact and well-defined silver film formation. By using this optimized reaction mixture, the particle formation kinetics during the irradiation time was studied. In order to investigate the particle formation kinetics, first the temperature was raised about 2.6 minutes and then the irradiation power was fixed in order to ensure that the temperature is constant inside the vial. Then, the microwave irradiation was stopped after 1, 2, 3 and 4 minutes and the substrates were collected and quickly cooled down to the room temperature. Figure 2 (a-d) [SY4] shows the top-view SEM images of the AgNPs films obtained after 1, 2, 3 and 4 minutes stopping the MW irradiation. The Figure 2(e) [SY4] shows the top-view SEM images of the film that resulted from 2 min irradiation at a constant temperature of 170°C and initial heating time of 2.6 min. Figure 2(f) [SY4] illustrates the variation of temperature and pressure during the reaction as a function of time. The silver film was transparent with few particles on the surface and a particle size of approximately 30 nm when the pressure was 1 bar and temperature was 110°C (see Figure 2(a) [SY4]). After two minutes, the surface was covered with nanoparticles with a yellowish color when the pressure was 7 bars and the temperature was 150°C (see Figure 2(b) [SY4]). When the temperature and pressure reached 170°C and 12 bars, after 3 minutes, the film appeared to be more homogeneous and more densely packed (see Figure 2(c) [SY4]). After four minutes at 170°C and 13 bars, the particle size increased and revealed more aggregated and round shaped nanoparticles (see Figure 2(d) [SY4]). Figure 2(e) [SY4] illustrates the SEM images of the nanoparticles after 2 minutes at 170°C. In this case, the best homogeneity of the film was obtained for narrow size distribution of the particles. There was no changed recorded on the surface by increasing the reaction time. Briefly, 2 minutes at 170°C was the shortest reaction time at which the nanoparticles had the best homogeneity with a narrow particle size distribution. Figure 3 [SY4] shows the UV-Vis spectrum of the AgNPs covered substrate obtained after 2 minutes at 170°C. The maximum absorption of the obtained nanoparticles is around 390 nm. The cross sections of the silver nanoparticles revealed in the SEM picture that the silver layer thickness is between 5-6 μm, with a high surface reproducibility (see Figure 4(a-c) [SY4]). It is clearly visible that silver nanoparticles formed large aggregates with densely packed arrays. The particles were reproducible for different batches. Figure 4(b) [SY4] shows colossal aggregates with a size of between 1-2 μm. It is observed from the high magnified images that much smaller round shaped particles formed well-packed aggregates. These particles had a diameter between 30-35 nm and they were homogenous over the surface (see Figure 4(c) [SY4]).

The morphological characters of these nanoparticles were analyzed by high resolution transmission electron microscopy (HR-TEM). The film was scratched onto the TEM grid in order to investigate the particles inside the layer. Figure 4(d) [SY4] shows the projected

image of the few Ag NPs which was densely packed together. Clear lattice fringes can be seen due to the high crystallinity of the particles with a lattice spacing of 0.23 nm, corresponds to the (111) planes of silver.

The TEM investigation was supported by the X-ray diffraction pattern of the silver nanoparticles film obtained after 2 minutes at 170°C using ethanol as a reducing agent (see Figure 5 [SY4]). The silver crystal structure was face-centered-cubic (fcc) with a lattice constant of 4.080 Å. The average crystallite diameter was found to be 28 nm by using the Scherrer equation [147]. The investigations of the SEM and TEM images proved that the silver nanoparticles were single crystals. The calculated crystallite size was slightly smaller than the one detected in the SEM images. However, the study reported in the reference [147] that the Scherrer equation might underestimate the real size of the nanoparticle due to the structural stress or instrumental effects.

Additionally, the stability and the aging test of the nanoparticles were investigated. The SEM analysis was performed for two hour and one week after the synthesis. There is no significant change found on the morphology of the nanoparticles due to the high electron voltage during the SEM measurements. The mechanical tests of the film were investigated employing the scotch tape tests. No changes were observed on the surface by naked eye after the tape removal. Furthermore, the substrates were sonicated in water for ten minutes and no significant detachment of the nanoparticles was seen in the solution. These tests prove that silver nanoparticles have good adhesion properties on the glass substrates.

Based on these promising results, various reducing agents were tested. Ethylene glycol and glycerol are well-known reducing agents in the literature and they were used due to their chemical similarities to ethanol. In the first case, ethylene glycol was used as a reducing agent because of its temperature-dependent reducing power, high boiling point and relative permittivity and the ability to solvate many metal precursors. However, using ethylene glycol as reducing agent did not provide satisfying results compared to ethanol. The SEM pictures show that the substrate covered developed a lightly yellowish color without any control of shape and size of the nanoparticles during the occurrence of the reaction in the suspension (see Figure S6 [SY4]). This can be explained by the good suspending ability of ethylene glycol. In this situation the particle growth and the nucleation preferentially develops in suspension rather than onto the substrate. In the second case, glycerol was tested as an alternative reducing agent. The solvent is less frequently used compared to ethanol and ethylene glycol for the nanoparticle synthesis. However, the stability of the nanoparticles in glycerol is much more even without using any stabilizer agent. The high stability in glycerol is due to the higher viscosity of ethylene glycol, which results in slower diffusion. Likewise, for the case of the synthesis of nanoparticles employing ethanol, the

films were obtained in a same manner. However, the amount of the silver acetate was lowered to 0.5 mg order to obtain a more homogeneous surface coverage. The results of this preparation protocol were different compared to using ethanol and ethylene glycol as reducing agent. The solution was yellowish-white suspension with an opaque color. A significant color change, greenish-metallic color with a strong yellowish reflection, was observed on the substrate. The SEM pictures and the cross section of the film is illustrated in Figure 6(a-b) [SY4]. It is visible here that the obtained nanoparticles have broad size distribution, between 80-150 nm, with a spherical like shape. The film was inhomogeneous and single layer instead of multiple layers. The particles were still self-assembled on the surface but forming loose surface attachment. However, this property of the nanoparticle might be used for the investigation and applications of a single nanoparticle. Figure 6(c) [SY4] shows the UV-Vis spectra of the film. The maximum absorption of the film was located at 443 nm with a much broader peak, which further proves that the nanoparticle size is larger, about 90-100 nm, due to the higher scattering.

After the morphological and optical characterization, the interaction of AgNPs with the supporting substrate and various wettability of the glass plate were investigated. First, the hydrophilicity and the hydrophobicity of the surface were studied. For this, the glass substrate was covered by self-assembled monolayer of OTS to create the surface hydrophobicity. Within this contribution, the contact angle of the surface reached about 108° without any surface morphology change. After covering the glass substrate with silver nanoparticle by using the reducing agent of ethanol, SEM and UV-Vis spectroscopic analysis were performed (see Figure S10 and Figure S11 [SY4]). These results proved that the Ag nanoparticles on OTS substrate were comparable with the hydrophilic glass substrate. Furthermore, TEFLON® was also used as a supporting material and covered with AgNPs. However, it was observed that TEFLON® was poorly covered with nanoparticles due to the high hydrophilic properties of the surface. Furthermore, silicon wafer and titanium dioxide thin layer surfaces were tested and successfully covered with silver nanoparticles. To sum up, the preferential nucleation of the silver nanoparticles during the microwave synthesis was promoted due to the high dielectric constant properties of the surface. Specifically, the local increase of the temperature, so called hot-spots, (up to 200°C) dramatically change the thermodynamics of the reactions. This instantaneous local temperature increase induces formation of round shaped small nanoparticles, promoting nucleation of new particles. Furthermore, the layer formation of the silver nanoparticles can be seen significantly while employing ethanol to ethylene glycol and glycerol see Table 1SI [SY4]). This can be explained by the different dielectric loss constant of the solvents under the microwave radiation. As showed Table 1SI [SY4], ethanol has the lowest dielectric loss

constant with lowest viscosity, thus the self-assembled nanoparticles simultaneously aggregates and nucleates directly on the surface easily. However, in the case of glycerol, the kinetics of nanoparticle nucleation was slowed down due to the high dielectric constant, or high viscosity of the medium. Moreover, the ethylene glycol has intermediate properties compared to ethanol and glycerol. In this case, the growth and the nucleation of the nanoparticles continued in the liquid phase. This led to different particle sizes and shapes due to the different nucleation hot spots and due to the local temperature.

After investigating the morphological and optical properties of the film formation by employing microwave synthesis, it was concluded that the fabricated substrates have a great potential for the SERS application. Reliable and homogenous coating of silver nanoparticles on various surfaces such as concave or hollow objects not only allows enhancing the sensitivity of the Raman measurements but also enables their applicability in different bioanalytical fields. Thus, uniformly coated nanoparticles were tested by employing SERS. Within this contribution, 0.1 mM riboflavin solution was tested as model analyte. Figure 8(a) shows the point-to-point SERS reproducibility of the Ag nanoparticle coated substrate. The Raman mode assigned to ν(C-C) stretching at 1625 cm^{-1} is integrated and plotted as a function of measured spectrum number. The RSD of the SERS intensity is 18.8%. Similar analysis of the point-to-point signal reproducibility investigations were performed for five different batches of SERS substrates. Figure 8(b) shows the batch-to-batch SERS reproducibility. The RSD of the five different batches were in between 4.7-8.5%. Based on the point-to-point and batch-to-batch reproducibility investigations, it was concluded that the microwave-assisted

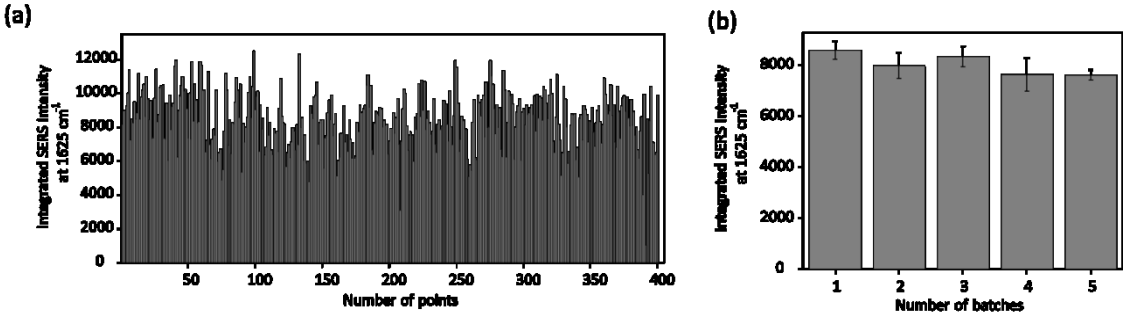

Figure 8: SERS reproducibility of AgNPs on planar substrates employing microwave radiation: (a) Point-to-point (b) batch-to-batch SERS reproducibility.

silver nanoparticle synthesis provides high SERS signal intensity. In order to determine the sensitivity of the SERS substrates, different concentrations of riboflavin were measured. Figure 7 [SY4] shows the LoD of riboflavin. For analyzing this, the characteristic Raman mode at 1625 cm^{-1} was integrated and plotted versus different concentrations. Repeatedly, it

is clearly visible that the LoD is down to 0.01 μM of riboflavin. Thus, microwave assisted silver nanoparticle synthesis results in the formation of promising SERS-active substrates due their uniform coating on various surfaces and their high SERS performance, allowing detecting concentrations down to sub-μM and nM range.

Finally, by taking the advantage of reliable, rapid and feasible Ag nanoparticle synthesis employing microwave radiation, the technique was implemented to coating glass capillaries for the practical applications. By doing so, silver nanoparticle coated glass capillaries provides easy handling in terms of sample collection, integratable and applicable to the field, pointing towards an application in routine analytics. Finally, the developed SERS based capillary platform was applied for the drug monitoring, which will be introduced in the next chapter.

2.5 SERS-Based Capillary Platform Prepared by the *In Situ* Microwave Synthesis of AgNPs for Trace Detection of Tetrahydrocannabinol (THC) [SY5]

This last section of the thesis reports an ultra-sensitive and high reproducible novel SERS-based capillary platform by employing microwave-assisted silver nanoparticle synthesis for detection of tetrahydrocannabinol (THC). Using the advantage of microwave-assisted silver nanoparticle coating on various surfaces, glass capillaries were reproducibly coated in a batch fabrication process. The glass capillaries can be coated within three minutes without any pre-surface modifications by using the capillary force. Coated glass capillaries displayed reliable and high reproducible SERS signal that enables for trace detection. The developed platform was first characterized by SERS employing adenine as a model analyte and then the Raman characterization of THC molecule was investigated.

Figure 1 [SY5] shows the schematic representation of the whole experimental procedure including, the preparation of the capillaries, collection of the sample, and SERS measurements. First, the capillaries were filled with silver salt solution and placed inside the reaction vial. Then, the capillaries were coated with silver nanoparticles within three minutes by employing microwave radiation (see Figure 1(i) [SY5]). In the second part, the target analyte was incubated for a few second by employing the capillary forces and then the SERS investigations were performed (see Figure 1(i) [SY5]). Finally, the platform was applied for drug monitoring or spectroscopic investigations.

Glass capillaries which are used for blood sample collection or thermal analysis were commercially purchased. They were coated by applying the microwave-assisted silver nanoparticle synthesis protocol that was already described in Chapter 2.5. By taking advantage of the advantages of the microwave synthesis, such as rapid heating, short reaction times and batch processing, the capillaries were reliably and uniformly coated with silver nanoparticles. The AgNPs coating was performed by using silver acetate and ethanol mixed solution without using any stabilizers and any stirring tools. Similarly to the previous study [SY4], the single-mode microwave oven was used and the reaction temperature was operated in power-controlled mode and with a constant irradiation power. The whole microwave process took less than three minutes, including cooling time, and 90 seconds of microwave irradiation (for a detailed discussion see SI 1 [SY5]). The typical reaction temperature was between 190 to 200°C with a pressure of 10-15 bars (see Figure S1 [SY5]). Always five capillaries were prepared and homogenously coated in one batch, as shown in

the Figure 1(i) [SY5]. The yellowish color of silver nanoparticles was visible along the capillary.

The physical morphology of the capillaries was investigated by employing SEM. Figure 2 [SY5] shows the SEM images of the capillaries, which were taken from different sections of the capillary. It can be visible here that the inside of the capillary was covered with dense and uniform monolayer silver nanoparticles over a large area (see Figure 2(A-C) [SY5]). Figure 2(E) [SY5] shows the photograph of a representative coated capillary and Figure 2(D) [SY5] shows the SEM images of the coated capillary from three different areas. The corresponding particle size distribution was shown in Figure 2(F) [SY5]. It can be clearly observed here that the glass capillary was coated with silver nanoparticles over more than a length of 3 cm, having particle sizes around 45±15 nm. The size of the nanoparticles can be controlled by changing the reaction time or the concentration of the silver salt in the mixed solution. Higher silver salt concentration results in more efficient microwave absorption due to accelerated heating and decreased synthesis time. Furthermore, the filling level inside the capillary has also an effect to the reaction time. This is due to the large volume of the reactants which needs longer heating time. In this study, 0.3 mL of the precursor solution was enough to fill the capillaries and the filling level in the vial was approximately 1.5 cm. However due to the capillary force, the liquid level inside the capillary was 3-5 cm. Consequently, fast, reliable and homogenous silver nanoparticle coating was achieved over a large range.

After morphological investigations of the coated capillaries, the SERS-activity of the developed platform was tested. To define the optimal SERS measurement conditions, 0.1 mM of adenine solution was used as a model analyte. By using adenine no resonance Raman effect was expected as adenine is a non-resonant molecule in the visible spectral range. The capillaries were fastly filled with adenine solution by employing capillary forces. Only 4 µl of adenine was necessary for achieving a filling level up to 3 cm and no incubation time was required. Figure 3(A) [SY5] shows the SERS background of the capillary and the SERS spectrum of adenine. The SERS measurements were recorded as single point measurements by focusing through the capillary wall. The characteristic ring vibrational mode at 733 cm^{-1} was reliably detected. Furthermore, there is no background contribution of the capillary to the target analyte. However, the carbon spectrum between 1200 cm^{-1} and 1600 cm^{-1} is visible due to the longer exposure time and can be attributed to the "burning effect" or decomposition of the target analyte on the nanoparticle surface due to the amplified local electric field. In other words, the signal-to-noise ratio of the adenine decreases during the long exposure time while the carbon background increases. In order to prevent the contribution of the burning effect in reaching a conclusion regarding the enhancement

properties of the substrate, the SERS intensity of adenine at 733 cm^{-1} was integrated and plotted as a function of time (see Figure 3(B) [SY5]). The maximum SERS intensity was observed after a time period of 10 s and then the SERS intensity has dramatically decreased. This is related to the SERS intensity fluctuation. Consequently, short integration time per spot was used to prevent the burning effect while recording the SERS spectra along the capillary. Scanning along the capillary during the SERS measurement provides a high number of recorded SERS spectra, which improves the statistics analysis of the data.

SEM investigations showed that the capillaries were uniformly coated with silver nanoparticles across a large area. To characterize the point-to-point and the batch-to-batch SERS signal reproducibility, SERS spectra were recorded along the capillary within a 40 μm line from 20 different measurement points. This measurement was repeated for 10 random area measurements, which finally resulted in recording 200 SERS spectra. Similarly to the previous section, the capillary was filled with 0.1 mM of adenine for the point-to-point SERS reproducibility. Figure 4(A) [SY5] presents the point-to-point SERS reproducibility of the coated capillary. The dominant vibrational band of adenine at 733 cm^{-1} was integrated and plotted as function of the SERS spectra number. It is observed that the relative standard deviation (RSD) of the SERS intensity was approximately 8.1%. Furthermore, the RSD was marked in the figure with light grey area and most of the recorded SERS spectra were located within this region. Additionally, five different broker batches of capillaries were prepared and similarly to the point-to-point analysis, SERS measurements were performed for different batches. Figure 4(B) [SY5] shows the integrated SERS intensity of adenine at 733 cm^{-1} as a function of batch numbers. The RSD of the five different batches were between 6.6-9.2%. The results revealed that the developed SERS-based capillary platform has high point-to-point and batch-to-batch reproducibility of the SERS intensity.

This novel, rapid and high SERS reproducible capillary platform was applied to drug monitoring to illustrate the potential applications of the SERS substrate. Thus, the (-)-trans-Δ^9-tetrahydrocannabinol (THC) molecule was studied. THC is the main psychoactive component of cannabis and its chemical structure is depicted in Figure 5(A) [SY5]. Detection of THC by employing easy to applicable, cost-effective and reliable test devices is significant for pharmacokinetic studies, drug treatment, and drug testing and traffic sobriety checks. The SERS spectra of THC in methanol, the spectrum of pure methanol and the one of the capillary background were measured (see in Figure 5(B) [SY5]). It is observed here that the vibrational modes of THC have rich fingerprints between 800-1600 cm^{-1}. However, due to the lack of detailed vibrational assignments of the THC molecule in the literature, the density functional theory (DFT) calculations were performed in order to assign the Raman

modes in the SERS spectrum. Table 1 [SY5] shows the calculated and measured vibrational modes of the THC molecule together with the tentative assignments. The most of the Raman bands are the result of several atoms and, consequently, assigning these modes is still ongoing challenge. However, the characteristic Raman modes of THC can be identified at 1390 cm^{-1}, 1236 cm^{-1}, 1006 cm^{-1} and 712 cm^{-1}, which can be assigned to the (=C-H) deformation, (C-H) deformation, (CC) stretching and (C-H) deformation respectively. It can be observed that the background signal of the capillary has no contribution to the spectra of the measured target analyte. However, the Raman modes of pure methanol at 1033 cm^{-1} and 1590 cm^{-1} might interfere with the recorded THC spectrum. Additionally, the quantitative measurement of the THC molecule was tested. Figure 5(C-D) [SY5] shows the limit of detection (LoD) of the THC molecule. The most intense SERS peak of THC at 1390 cm^{-1} was integrated and normalized as a function of concentration. The concentration range between 100 and 0.25 nM THC was monitored. To reliably conclude on the LoD, the definition of IUPAC was applied. Within this contribution, three times the standard deviation ($+3\sigma$) of the mean value of the background was used and set as a threshold. This threshold was shown with black dashed line (see Figure 5(D) [SY5]). Based on this THC can be reliable detectable by SERS-based capillary platform down to 1 nM of.

3. Summary and Outlook

Plasmonics is a rapidly growing branch of nanophotonics that opens various applications. Precisely engineered, the physical properties of these nanostructures have facilitated the development of a wide range of materials. SERS is one of the most powerful techniques which benefits from amplified Raman signal of the plasmonics nanomaterials. Engineering the physical properties of the nanostructures plays an important role to strengthen the SERS performance.

The aim of this thesis was to develop novel, easy-to-prepare, cost-effective, long-term stable, portable and biocompatible plasmonic nanostructures with high performance as SERS substrates by employing bottom-up fabrication techniques. To record reliable SERS signal for bioanalytical application, the well-established EGNPs provide good SERS performance for label-free pathogen detection. By covering the entire analysis chain including sample preparation, DNA isolation, amplification and hybridization on EGNPs adenine-free capture probes, label-free detection of an important plant pathogen, *P. ramorum*, was easily achieved by SERS. This is the first study successfully covering the whole analysis chain with employing reliable and thermal SERS substrates for label-free plant pathogen detection. Even though SERS-based label-free DNA detection offers great potential compared to other techniques by means of simple validation of yes and no question, it has been still hampered by the spectral reproducibility of batch-to-batch or day-to-day measurements recordings. Furthermore, the SERS background signal of EGNPs is presenting characteristic Raman bands due to the residuals of the redox reaction. This predominant SERS background overlaps with the SERS spectra of the target molecule that decreases the SERS performance of the EGNPs. Furthermore, the shelf-life of these "desert-rose" like nanostructures is short due to the fast oxidization under ambient conditions. Within this thesis, an ultra-thin layer of Al_2O_3 (1 nm) was applied on EGNPs as a protection layer by employing ALD. By coating the substrates with an ultra-thin dielectric layer not only the residuals were removed from the surface of silver nanoparticles and therefore the background SERS signal was also quenched significantly. Here, background-free SERS substrates were obtained. Also, the detection sensitivity of the target analyte riboflavin was improved 20 times by using ultra-thin film coating. Moreover, taking the advantage of the atomic scale precision of ALD, the point-to-point and the batch-to-batch SERS reproducibility were also improved. Furthermore, the shelf-life of the coated EGNPs was approximately four times better than the one of the uncoated EGNPs. Lastly, the improved specificity of the developed background-free EGNPs was demonstrated by the detection of retinol.

The engineering of hierarchically designed complex micro- and nanostructures in 3D form is still an ongoing challenge due to the complex equipment required for the fabrication procedure, time requirements and its consequently overall high costs. These man-kind developed complex nanostructures open various application fields in life sciences and bioanalytical applications, for example in SERS. Here, new and novel fabrication technique of complex and hierarchically designed 3D hybrid nanostructures employing PE-ALD were introduced as a result of the work developed within the thesis. A standard ALD process is based on sequential self-limiting reactions on stable surfaces, offering an exceptional conformality on high-aspect ratio. In contrast to the standard ALD, the metastable property of EGNPs such as the redox residuals on the surface and easy oxidization, was used to create 3D hierarchically designed hybrid nanostructures. New fabrication technique of hierarchically designed hybrid nanostructures is introduced by employing metastability surface of the EGNPs and the PE-ALD. By doing so, new hybrid nanostructures were created. The formation process and the morphological properties of these hybrid nanostructures were successfully discussed. Within this contribution, the fabricated 3D hybrid nanostructures were used as SERS templates. In order to record the SERS signal, the template was activated by the desired metal deposition. The metalized hierarchically designed 3D flower-like silver-silica SERS substrate provided an increased number of hot spots in the focus volume in comparison to the 2D plasmonic arrays. This 3D hybrid nanostructure yields substrates with high hydrophobic surface property, which serves an excellent plasmonic platform for the detection of analytes solved in organic solvents. Furthermore, the LoD of the 3D hybrid nanostructures for the detection of the target analyte riboflavin is four times better than the LoD of EGNPs. However, the SERS signal reproducibility investigations show that the RSD of the 3D hybrid nanostructure is comparable with the SERS reproducibility of the EGNPs. Finally, these structures can preserve their stability at least one year without any morphological deformations, which means that the shelf life of the morphology of the developed SERS templates can be stable at least one year without any degeneracy.

As an alternative to the introduced bottom-up plasmonic fabrications mentioned above, microwave-assisted silver nanoparticle synthesis is introduced. Here, fast, reliable, reproducible, facile, environmental-friendly and one-step procedure of silver nanoparticle synthesis is presented. A thin and robust film of silver nanoparticles was obtained by using a mixture of silver acetate with ethanol and by employing microwave radiation. Furthermore, other reducing agents such as ethylene glycol and glycerol were also tested and a dense layer of silver nanoparticle film was successfully obtained. The silver film formation was obtained within 2 minutes for all tested reducing agents. In this way, microwave-assisted

silver nanoparticle formation is 90 times faster than the EGNP formation. These mechanically robust silver nanoparticles are an excellent candidate for bioanalytical applications. Within this contribution, to demonstrate the potential application, the target analyte riboflavin was detected down to 10 nM, which translated in a sensitivity of 20 times improved in comparison to EGNPs. Furthermore, the capability of coating silver nanoparticles on various geometrical objects allows for new potential applications. Thus, the final aim of this thesis is to combine microwave-assisted nanoparticle synthesis, plasmonics and capillary forces for drug detection. By doing so, an ultra-sensitive and highly reproducible novel SERS-based capillary platform was developed for the trace detection of THC. The glass capillaries were reliable coated with Ag NPs in a batch synthesis method. The processing time of silver nanoparticle coating was three minutes and no pre-surface modification was needed. The coated glass capillaries exhibit excellent SERS reproducibility. Furthermore, the incubation time and the amount of analyte resulted in a simple and short procedure. To show the potential applications of SERS based capillary platform, THC was spectroscopically characterized and its concentration level was detected by SERS down to nanomolar range.

In conclusion, various and different bottom-up plasmonics nanostructures were fabricated during this thesis. The developed plasmonic arrays conform to the definetion of an ideal SERS substrate. These SERS-active platforms provide as high SERS reproducibility (point-to-point and batch-to-batch), long shelf-life, sensitive and specific for the detetction the target analyte, easy preparation procedure, cost-effective. The well-established EGNPs have great potential for the rapid analysis of biomolecules. However, these silver arrays are not convenient for the analysis which takes long analyte preparation steps. Thus, alumina coated EGNPs and hierarchically designed 3D hybrid nanostructures supply more robust and long-term stable platform for the SERS applications that takes moresample preparation. Furthermore, considering the short preperation time, easy handling and readily integrabile into the routine analytical systems, microwave-assisted AgNPs SERS platform shows great potential for the trace detection of illegal drugs. Future investigation should be devoted to integrate all these developed substrates towards practical applications such as drug monitoring in body fluids, or cell diagnostics.

4. Publications

In the present section the reprints of the publications included in the frame of the thesis are shown. Details regarding the copyright are stated on each title page.

[SY1] Label-free detection of *Phytophthora ramorum* using surface-enhanced Raman spectroscopy

Sezin Yüksel*, Lydia Schwenkbier*, Sibyll Pollok, Karina Weber, Dana Cialla-May, Jürgen Popp.

Analyst, 2015, **140**, p.7254-7262

DOI: 10.1039/c5an01156f

[SY2] Background-free Bottom-up plasmonic arrays with increased sensitivity, specificity and shelf life for SERS detection schemes

Sezin Yüksel, Mario Ziegler, Sebastian Goerke, Uwe Hübner, Kilian Pollok, Falko Langenhorst, Karina Weber, Dana Cialla-May, and Jürgen Popp.

The Journal of Physical Chemistry C, 2015, **119**, p. 13791-13798

DOI: 10.1021/acs.jpcc.5b01389

[SY3] Hierarchically designed 3D flower-like composite nanostructures as an ultra-stable, reproducible and sensitive SERS substrate

Sezin, Yüksel*, Mario Ziegler*, Sebastian Goerke, Uwe Hübner, Karina Weber, Peter Schaaf, Hans-Georg Meyer, Dana Cialla-May, Jürgen Popp.

Submitted to ACS Applied Materials and Interfaces 2017

[SY4] Microwave-assisted silver nanoparticle film formation for SERS applications

Guido Soliveri, Silvia Ardizzone, Sezin Yüksel, Dana Cialla-May, Jürgen Popp, Ulrich S. Schubert, Stephanie Hoeppener.

The Journal of Physical Chemistry C, 2016, **120**, p. 1237-1344

DOI: 10.1021/acs.jpcc.5b10833

[SY5] Trace detection of tetrahydrocannabinol (THC) with a SERS-based capillary platform prepared by the in situ microwave synthesis of AgNPs

S. Yüksel*, Almut M. Schwenke*, Silvia Ardizzone, Karina Weber, Dana Cialla-May, Stephanie Hoeppener, Jürgen Popp.

Analytica Chimica Acta, 2016, **939**, p. 93-100
http://dx.doi.org/10.1016/j.aca.2016.08.033

*both authors contributed equally

4.1 Label-free detection of *Phytophthora ramorum* using surface-enhanced Raman spectroscopy [SY1]

Sezin Yüksel*, Lydia Schwenkbier*, Sibyll Pollok, Karina Weber Dana Cialla-May, Jürgen Popp

Analyst, 2015, **140**, p.7254-7262
DOI: 10.1039/c5an01156f

*both authors contributed equally

Authorship of the publication

*Sezin Yüksel**	*Concept development* *Experimental design* *Raman measurements* *Data analysis and interpretation* *Writing the manuscript*
*Lydia Schwenkbier**	Concept development Experimental design DNA hybridization and fluorescence measurement Data analysis and interpretation Writing the manuscript
Sibyll Pollok	Concept development Experimental design Proofreading of manuscript
Karina Weber	Discussion of experimental concept and results Proofreading of manuscript
Dana Cialla-May	Discussion of experimental concepts and results Proofreading of manuscript
Jürgen Popp	Project management Discussion of concepts and results Proofreading of manuscript

*both authors contributed equally

Erklärung zu den Eigenanteilen der Promovendin sowie der weiteren Doktoranden/ Doktorandinnen als Koautoren an der Publikation und Zweitpublikationsrechten bei einer kumulativen Dissertation

Publication: **S. Yüksel, L. Schwenkbier, S. Pollok, K. Weber, D. Cialla-May and J. Popp** ***Label-free detection of Phytophthora ramorum using surface-enhanced Raman spectroscopy*** **Analyst, 2015, 140, p.7254-7262**		
Beteiligt an		
	Sezin Yüksel	**Lydia Schwenkbier**
Konzeption des Forschungsansatzes	**X**	**X**
Planung der Untersuchungen	**X**	**X**
Datenerhebung	**X**	**X**
Datenanalyse und -interpretation	**X**	**X**
Schreiben des Manuskripts	**X**	**X**
Vorschlag Anrechnung Publikationsäquevalente	**1.0**	**1.0**

*both authors contributed equally

Analyst

PAPER

Cite this: *Analyst*, 2015, **140**, 7254

Label-free detection of *Phytophthora ramorum* using surface-enhanced Raman spectroscopy†

Sezin Yüksel,‡[a,b,c] Lydia Schwenkbier,‡[a,b,c] Sibyll Pollok,[a,d] Karina Weber,*[a,b,c] Dana Cialla-May*[a,b,c] and Jürgen Popp[a,b,c]

Received 9th June 2015,
Accepted 3rd September 2015

DOI: 10.1039/c5an01156f

www.rsc.org/analyst

In this study, we report on a novel approach for the label-free and species-specific detection of the plant pathogen *Phytophthora ramorum* from real samples using surface enhanced Raman scattering (SERS). In this context, we consider the entire analysis chain including sample preparation, DNA isolation, amplification and hybridization on SERS substrate-immobilized adenine-free capture probes. Thus, the SERS-based detection of target DNA is verified by the strong spectral feature of adenine which indicates the presence of hybridized target DNA. This property was realized by replacing adenine moieties in the species-specific capture probes with 2-aminopurine. In the case of the matching capture and target sequence, the characteristic adenine peak serves as an indicator for specific DNA hybridization. Altogether, this is the first assay demonstrating the detection of a plant pathogen from an infected plant material by label-free SERS employing DNA hybridization on planar SERS substrates consisting of silver nanoparticles.

Introduction

In recent decades a vast number of invasive plant pathogens have spread across European and North American countries. Members of the genus *Phytophthora* are among these. They belong to the most important and aggressive plant pathogens worldwide and pose serious threats to plants in natural and landscaped environments as well as in plant cultivation.[1] One prominent species is *Phytophthora ramorum*[2] which is responsible for the dramatic die back of oaks in North America (sudden oak death) and the *Larix* decline in the United Kingdom.[3] In order to prevent the spread of this pathogen across borders, its reliable and specific detection is mandatory. To date *Phytophthora* diagnosis has been mainly realized by microbiological or PCR-based techniques.[4–8] However, its specific and reliable detection directly in the field from real samples and without much effort remains an on-going challenge. In this context, DNA hybridization assays have been developed which are based on the immobilization of specific capture probes and their interaction with complementary target sequences.[9,10] DNA hybridization can be detected by fluorescent dyes, radioactivity or enzyme induced color changes.[11–13] Recently, surface enhanced Raman spectroscopy (SERS) was highlighted as an attractive analytical tool for the identification of molecular interactions. In terms of high sensitivity and cost effectiveness, it represents an emerging and promising field in bioanalytical research.[14–17] While applying SERS, it is important to consider the interaction between light and molecules as well as metallic nanostructures. The latter are eminent for the amplification of the Raman signal,[18,19] which is increased by several orders of magnitude.[20,21] Thus, SERS combines high molecular specificity, attributed to the Raman effect, with a high sensitivity.[22–24] Therefore it is an excellent tool for both quantitative and qualitative analysis, offering almost unlimited possibilities for multiplexing.[25–27] Moreover, SERS-based DNA detection provides several advantages compared to classical fluorescence techniques. Fluorescence detection requires expensive dyes and complex conjugation chemistry, resulting in a limited number of specific labels. The SERS approach enables the selection of various Raman labels, without bleaching or quenching problems.[28] Furthermore, short data processing times point to the direction of implementing SERS in the development of

[a]*Leibniz Institute of Photonic Technology Jena (IPHT), Albert-Einstein-Straße 9, 07745 Jena, Germany. E-mail: karina.weber@ipht-jena.de; Tel: +49 (0)3641-948390*
[b]*Friedrich Schiller University Jena, Institute of Physical Chemistry and Abbe Center of Photonics, Helmholtzweg 4, 07743 Jena, Germany. E-mail: dana.cialla-may@uni-jena.de; Tel: +49 (0)3641-206309*
[c]*InfectoGnostics Forschungscampus Jena, Zentrum für Angewandte Forschung, Philosophenweg 7, 07743 Jena, Germany*
[d]*Ernst-Abbe-Hochschule Jena, University of Applied Sciences, Carl-Zeiss-Promenade 2, 07745 Jena, Germany*
†Electronic supplementary information (ESI) available. See DOI: 10.1039/c5an01156f
‡Both authors contributed equally to the paper.

rapid and low-cost detection platforms for pathogen diagnosis.[14]

In the last few decades a wide range of SERS-based DNA hybridization assays have been explored. Commonly, the hybridization between specific capture probes and the corresponding target molecules is indicated by a change in the signal of the dye label.[27,29–39] More recently, an elegant label-free detection scheme for specific DNA hybridization was introduced by Halas and co-workers.[40] Usually the DNA spectrum is represented by the four nucleobases: adenine (A), guanine (G), cytosine (C) and thymine (T). Adenine exhibits a more prominent Raman profile than the other nucleobases and strongly dominates the SERS spectra of DNA.[33,41,42] Thus, the adenine signal can serve as an endogenous marker for SERS-based DNA detection. However, in general both capture probes and target sequences consist of multiple adenine moieties, which hamper the SERS-based detection of DNA hybridization. This drawback was circumvented by the substitution of adenine by 2-aminopurine (2-AP) in order to generate adenine-free capture probes.[40] 2-AP serves as an adenine analogue or isomer, exhibiting identical hybridization characteristics.[43–45] It forms a canonical Watson–Crick base pair with thymine and enables the study of nucleic acid structures and their dynamics. Thus, only the SERS spectra of the hybridized target DNA, containing adenine in the sequence, provide the related adenine characteristics. Inspired by this unique feature, we expanded the principle of label-free SERS-based detection to *Phytophthora ramorum* plant pathogens in infected *Rhododendron* leaves. This illustrates, to the best of our knowledge for the first time, the application of label-free SERS towards PCR products from real samples. To this end, we considered a combination of plant sampling, DNA isolation, amplification, hybridization and SERS-based DNA detection to reflect the complete analysis chain.

Experimental section

Plant infection and DNA extraction of *Phytophthora ramorum*

The genomic DNA (gDNA) of *P. ramorum* BBA9/95 was extracted from artificially infected *Rhododendron* leaves (see detached leaf assay, described in detail elsewhere[46]) by homogenizing the samples with a mortar and pestle.[9] The lysate was placed into a micro reaction tube and DNA extraction was performed using the magnetic bead based innuPREP MP Basic Kit according to the recommendations of the manufacturer (Analytik Jena AG, Jena, Germany).

Amplification of target DNA by PCR

Linear-after-the-exponential polymerase chain reaction (LATE-PCR) was carried out to amplify a fragment within the yeast GTP-binding protein (*Ypt*1) target gene region. The conditions for LATE-PCR are described elsewhere[10] (Table 1). DNA of inoculated *Rhododendron* leaves was used in a concentration of 50 ng per reaction. The amplified *Ypt*1-fragments had a length of approximately 450 bp.

SERS substrate preparation

As the SERS substrate, we applied enzymatically generated silver nanoparticles (EGNPs). In extensive studies they were proven as low-cost, highly reproducible and stable bottom-up SERS active substrates.[47,48]

These nanoparticles were generated by an enzyme-induced growth process on glass substrates, described in detail elsewhere.[47] Briefly, a biotin-labeled single-stranded DNA was immobilized onto planar substrates. A streptavidin horseradish peroxidase (HRP) conjugate bound to the biotin and catalyzed the enzymatic generation of nanoparticles from a silver solution. For this purpose the EnzMet™ kit from Nanoprobes Inc., (Yaphank, NY, USA) was used.

Finally, an array of individual EGNP deposits was produced, where closely packed 'desert-rose-like' silver nanostructures with a particle size of approximately 400 nm could be observed (Fig. 1). The strongest electromagnetic field enhancement was located at the sharp and spiky features of the silver intertwined plates.

Scanning electron microscopy (SEM)

The scanning electron microscopy (SEM) images were recorded with a high resolution field emission scanning electron microscope JEOL JSM-6300F (Tokyo, Japan), applying 5 keV accelerating voltage with an accumulation time of 300 s.

Table 1 Primers, capture probes, and single-stranded DNA (ssDNA)

		Sequence 5′–3′	Modification
Capture probes	*P. ramorum*	CCC CCC **A***CT TTC CGT GGG TG**A*** GTT TCC TTT	5′-SH internal 2-AP
	P. lateralis	CGG G**A***G **A***TT TTT TCC CGC TTT CCT TGG GGT **A*A***G	5′-SH internal 2-AP
Primers	YPh1F_LATE	CAT CTC GAC CAT KGG TGT GGA CTT T	w/o
	YPh2R	ACG TTC TCM CAG GCG TAT CT	
ssDNA complementary to *P. ramorum*	*P. ramorum*	AAA GGA AAC TCA CCC ACG GAA AGT GGG GGG	w/o (SERS) 5′-FITC (fluorescence)

A* indicates the substitution of adenine by 2-aminopurine.

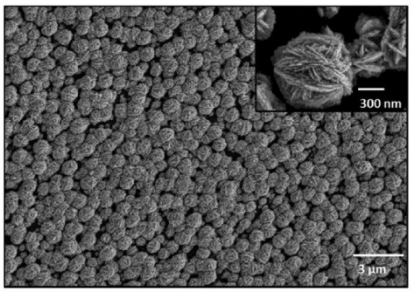

Fig. 1 SEM image of EGNPs. High-resolution scanning electron microscopy (SEM) image of closely packed EGNPs, having a particle size around 400 nm with sharp and spiky features of the EGNPs (*cf.* zoomed image).

Immobilization of adenine-free capture probes and DNA hybridization on EGNP array

The capture probes, primers and complementary ssDNA were purchased from Eurofins MWG Operon (Ebersberg, Germany; Table 1).

For either fluorescence or SERS-based detection, the capture probes were immobilized in triplicate directly on top of the EGNP array *via* their thiol groups (Fig. 2). Thereto they were dissolved in 5× PBS buffer to a final concentration of 20 µM and spotted on the EGNPs with a Nanoplotter 2.1 (GeSim, Germany). After UV-linking at 254 nm for 5 min the substrates were washed with 1× PBS for 2 min. A 0.5% (w/v) solution of bovine serum albumin (BSA) (Carl Roth, Karlsruhe, Germany) in 1× PBST was used to block unspecific binding sites. For the DNA hybridization either 20 µl of the LATE-PCR product or 1 µM of complementary ssDNA (Table 1) were dissolved in 3 × SSC/0.5% SDS and incubated on the substrates for two hours at 58 °C in a humidity chamber. The subsequent washing steps were performed at room temperature (2 × SSC/0.1% SDS, 0.2 × SSC and finally with 0.1 × SSC, 5 min each). Afterwards, fluorescence or SERS detection was performed.

Fluorescence microscopy

Fluorescence images were recorded with the light microscope Axio Imager Z1 (Carl Zeiss Jena GmbH, Jena, Germany). The samples were measured using a 20× objective with an exposure time of 435 ms.

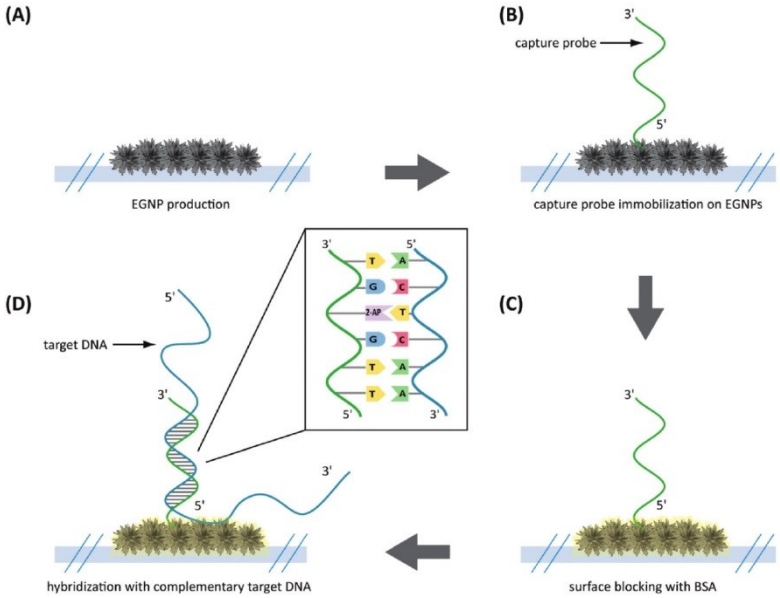

Fig. 2 Schematic illustration of specific DNA hybridization on EGNP immobilized adenine-free capture probes. (A) EGNPs were produced on planar glass substrates. (B) Species-specific capture probes containing 2-aminopurine instead of adenine were immobilized on the EGNP array. (C) DNA-free positions were blocked with BSA. (D) Hybridization of the complementary target DNA (adenine within sequence) was performed.

SERS

SERS spectra were recorded using a confocal Raman microscope (WITec GmbH, Ulm, Germany) equipped with a 488 nm excitation laser line. For the irradiation of the samples a 100× Olympus objective (NA 0.9) with a laser power of 35 μW was employed. The same objective was applied for recording the backscattered light with a spectrometer, equipped with 600 lines per mm grating and a 1024 × 127 pixel CCD camera cooled to 208 K. Average SERS spectra were calculated from ten different measurement points with an integration time of 10 s.

Results and discussion

The study focused on the reliable and label-free detection of *P. ramorum* plant pathogen from infected *Rhododendron* leaves. We applied a label-free SERS-based detection approach to record the specific DNA interaction on a planar SERS substrate (Fig. 3). The assay started with the sampling of the infected plant material and the isolation of pathogenic gDNA, which was used as a template for the amplification of the *Ypt*1 target region by LATE-PCR. This target DNA was then used for hybridization with immobilized capture probes that possessed 2-AP instead of adenine on the EGNP array. Thus, we took advantage of the strong spectral feature of adenine in the SERS spectrum of the target DNA. The presence of adenine exclusively in the target DNA sequence served as an endogenous marker for the label-free SERS-based detection of the hybridization event. Furthermore, the entire analysis chain was considered in order to prove the near-future application of SERS for implementation in an on-site detection system.

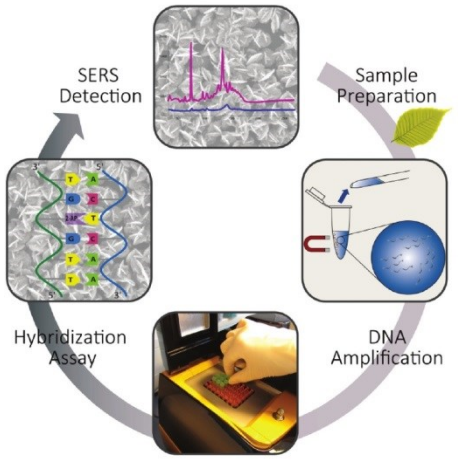

Fig. 3 Label-free SERS-based detection of *P. ramorum*. DNA-based detection of *Phytophthora ramorum* by SERS covering the whole analysis chain. Sample preparation was realized using a mortar and pestle followed by magnetic bead based gDNA isolation, DNA amplification by LATE-PCR and the subsequent hybridization was followed by label-free SERS detection of the molecular DNA–DNA interaction.

DNA isolation and amplification

The preparation of the samples is the first critical step in the successful detection of pathogens. As an example for a proof-of-concept analysis we chose *Rhododendron* leaves of *P. ramorum*-infected plants. The DNA extraction was performed by combining a mortar and pestle for effective cell disruption in conjunction with nucleic acid release.[9,49] This manually operated homogenization is applicable for softer tissues such as *Rhododendron* leaves and provided an incredibly facile way to release gDNA from the plant material. Subsequently, magnetic particle-based DNA isolation enabled easy handling as well as short processing times. Thus, the first step of DNA extraction and purification was realized in a straightforward manner for a potential field application.

LATE-PCR allowed the amplification of the yeast GTP-binding protein (*Ypt*1) target gene of *P. ramorum*. This particular region is located within a single-copy gene, which implies the presence of only one copy per genome. Therefore, a prior DNA amplification was mandatory for proper detection. Accordingly, LATE-PCR was carried out to generate sufficient amounts of single-stranded target DNA.[10] The successful generation of ssDNA was indicated by the appearance of two bands in the analytical gel. The faster migrating DNA represented single-stranded DNA (450 nt) and the higher molecular weight band of 450 bp was double-stranded (see ESI Fig. S1†). By applying asymmetric PCR post-amplification treatment could be omitted.

Fluorescence microscopic detection of target DNA hybridization

In order to verify the functionality of the hybridization assay on the SERS substrate, fluorescence microscopy was performed as a reference method. For this purpose two different capture probes, one for the target species *P. ramorum* (Fig. 4A) and one for the closely related species *P. lateralis* (Fig. 4B), were immobilized on the corresponding EGNP spots. Moreover, EGNPs without any capture probes were analyzed after identical processing steps for blocking, hybridization and washing (Fig. 4C).

Subsequently, hybridization was accomplished using FITC-labeled single-stranded target DNA of *P. ramorum* with a length of 30 nucleotides (Table 1). The selection of this particular *Phytophthora* species relied upon previous studies which focused on the specificity and sensitivity of the *Ypt*1 target gene region.[46] The highest signals were recorded for *P. ramorum*-specific capture probes that entirely matched the target DNA sequence (Fig. 4A). In contrast, only weak signals were detected for the *P. lateralis* capture probes (Fig. 4B). In comparison with the background fluorescence (Fig. 4C) those signals were negligible. Consequently, the functionality of the hybridization assay for the specific detection of *P. ramorum* is

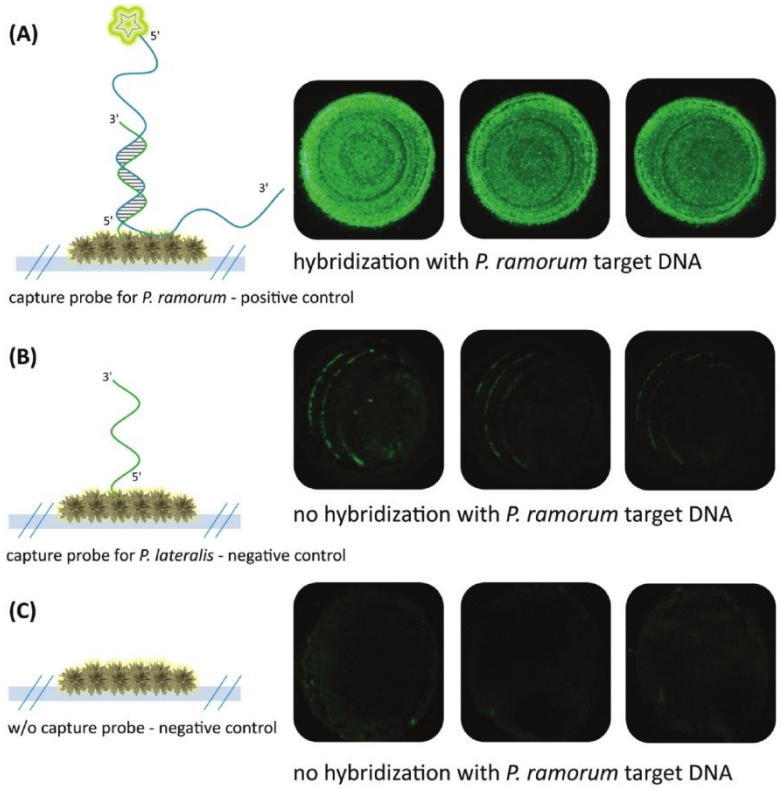

Fig. 4 Fluorescence microscopy to verify the functionality of the hybridization assay on the SERS substrate. (A) Specific hybridization signals (FITC fluorescence) for *P. ramorum* target DNA with matching *P. ramorum* capture probes. (B) Absence of hybridization signals for *P. ramorum* target DNA with non-matching *P. lateralis* capture probes. (C) Background signals of EGNPs. The respective fluorescence signals were depicted as triplicates.

proven. The adenine isomer, 2-AP, in the capture probes exhibited the same hybridization characteristics.

SERS detection of target DNA hybridization

In the next step, the label-free SERS detection of *P. ramorum* DNA was investigated. First, DNA hybridization was accomplished using a short single-stranded target DNA of *P. ramorum* with a length of 30 nucleotides. After that we applied the PCR product isolated from real plant samples and recorded the corresponding SERS spectra.

Hybridization experiments were performed with the 30 nucleotide single-stranded target DNA of *P. ramorum*. Two different adenine-free capture probes, one for the target species *P. ramorum* and one for the non-target species *P. lateralis* were immobilized on the SERS substrate and hybridization was conducted. In Fig. 5, the respective SERS spectra of the hybridized *P. ramorum* capture probes (indicated by a red line), the *P. lateralis* capture probes (indicated by a black line) and the background of the SERS substrate (indicated by a grey line) are displayed as mean values. In the recorded spectra for *P. ramorum* and *P. lateralis* capture probes, the broad carbon spectra are visible between 1200 and 1600 cm^{-1}. This burning effect of the surface is caused by an enhanced electromagnetic field due to applying a relatively long exposure time. Owing to the high carbon background, the Raman vibrational modes of cytosine and adenine were barely detectable between 1200 and 1600 cm^{-1}. In the SERS spectra of *P. ramorum*, where hybridization with the target DNA occurred (see Fig. 5A, red line), one characteristic band of ν(C–C) for cytosine at 1420 cm^{-1} could be observed.[41,50] Moreover, the vibrational modes of guanine

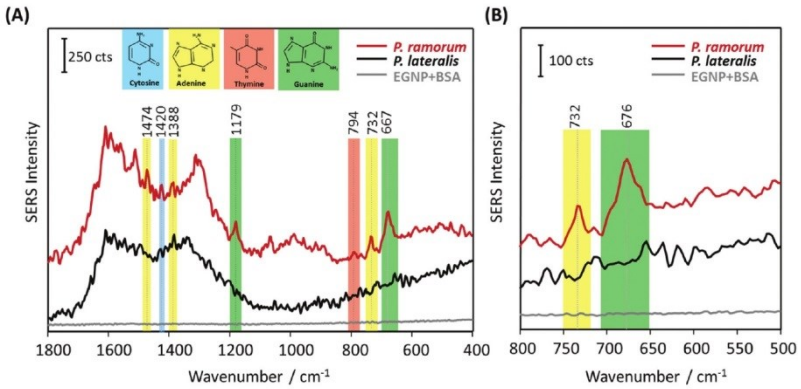

Fig. 5 SERS-based label-free detection of *P. ramorum* target DNA (30 nucleotides) based on adenine-free capture probes. (A) *P. ramorum* capture probes hybridized with complementary target DNA of 30 nucleotides (red line), *P. lateralis* capture probes with no hybridization (black line) and background of the SERS substrate blocked with BSA (grey line). (B) Zoomed view of the spectral range between 500–800 cm^{-1}.

at 1179 cm^{-1} and 667 cm^{-1} were assigned to the ν(C–C) and ring breathing vibrations. The typical Raman bands of adenine were marked with yellow colored frames. The two Raman modes of adenine at 1474 cm^{-1} and 1388 cm^{-1} are referred to as ν(C–N) and ν(C═N) stretching modes respectively. Additionally, the most prominent peak of adenine at 732 cm^{-1} is related to the aromatic ring breathing. Fig. 5B shows the spectral zoom of the region of interest between 500 and 800 cm^{-1}. Accordingly, *P. ramorum* (Fig. 5B, red line) was identified by the dominant peak of adenine at 732 cm^{-1}. In contrast, the SERS spectra of the non-target species *P. lateralis* do not show any characteristic adenine-related modes, indicating that no hybridization occurred (Fig. 5B, black line). Thus, the specific binding of the *P. ramorum* target DNA to the matching capture probe was monitored by the presence of adenine.

In order to demonstrate the applicability of the label-free technique for bioanalytical purposes in terms of pathogen detection, we adapted the SERS approach for DNA isolated from real plant samples, infected with the pathogen *P. ramorum*. The implementation of SERS as a novel tool for pathogen detection resulted in a plethora of publications in the last few years. However, the main challenge of this promising technique is the confirmation of its applicability for on-site use with real samples, *e.g.* from infected plant tissue. Therefore, the main objective of the present study was to demonstrate the application of label-free SERS detection for the plant pathogen DNA, extracted from *Phytophthora* infected *Rhododendron* leaves. Fig. 6 displays the mean SERS spectra of the DNA-hybrid between *P. ramorum*-specific capture probes and *P. ramorum* target DNA, which was amplified by PCR as 450 nucleotide fragments (indicated by a red line), the non-target *P. lateralis* (black line) and the background of the SERS substrate (grey line). In accordance with the findings for the short target DNA fragment, typical vibrational bands at 1081 cm^{-1} and 668 cm^{-1} were observed for guanine in the SERS spectra of *P. ramorum* (see Fig. 6A, red line). Also the less strong Raman bands of thymine at 1234 cm^{-1} and cytosine at 1292 cm^{-1} were depicted in the SERS spectra of the target DNA. However, focusing on adenine as the endogenous marker, very dominant Raman modes at 1384 cm^{-1} and 732 cm^{-1} were monitored for the DNA extracted and amplified from the infected *Rhododendron*. Moreover, the characteristic Raman mode of adenine at 1336 cm^{-1} could be detected due to the presence of a higher amount of the respective nucleobase in the target DNA strand. Similar to previous results the dominant peak at 732 cm^{-1} indicating the presence of adenine served as a significant marker band in comparison with the non-target *P. lateralis* (see Fig. 6B). Altogether, by substituting adenine with 2-AP in the capture probes, the specific hybridization of the *P. ramorum* target DNA could be successfully monitored even while applying this very long PCR product. A proper discrimination between *P. ramorum* (target) and *P. lateralis* (non-target) is possible. Thus, the label-free SERS detection of DNA was exemplarily demonstrated for the important plant pathogen *P. ramorum*.

Reproducibility of the SERS spectra

Despite the fact that SERS-based DNA detection offers great potential regarding a higher sensitivity and specificity, it is still in competition with more common techniques such as fluorescence spectroscopy. One drawback for SERS measurements is the lack of good spectral reproducibility as well as precise batch-to-batch and day-to-day recordings. For this reason the current study also addressed the batch-to-batch reproducibility of the SERS signals occurring in the case of DNA hybridization. Independent experiments were performed

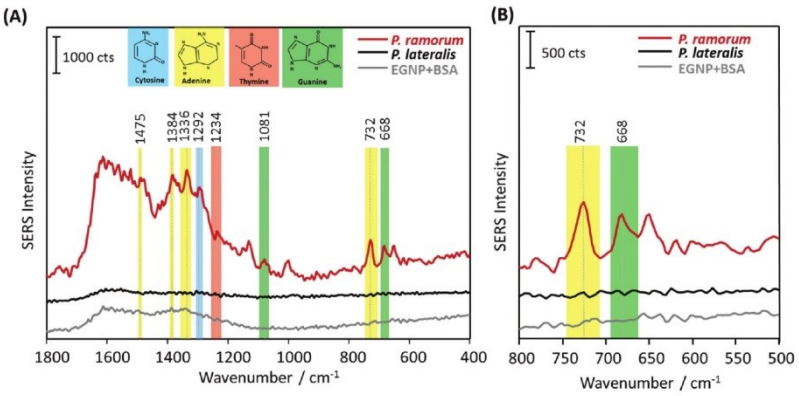

Fig. 6 SERS-based label-free detection of *P. ramorum* target DNA (450 nucleotide PCR product) based on adenine-free capture probes. (A) *P. ramorum* capture probes hybridized with the complementary target DNA of 450 nucleotide PCR product (red line), *P. lateralis* capture probes with no hybridization (black line) and background of the SERS substrate blocked with BSA (grey line). (B) Zoomed view of the spectral range between 500–800 cm^{-1}.

using various DNA extracts, conducting individual PCR runs and hybridization assays. Fig. 7 depicts the normalized integrated SERS intensity for various batches. The adenine peak at 732 cm^{-1} was integrated for the SERS spectra of the matching target (*P. ramorum*), the non-matching control (*P. lateralis*) and the background of the SERS substrate and then normalized to the peak of the highest intensity. In comparison with the capture probes and the background, the integrated SERS intensity at 732 cm^{-1} showed the highest values, having a relative standard deviation (RSD) around 40% (see Fig. 7). The high relative standard deviation can be explained by the different orientations of the DNA on the metallic surface and by an inhomogeneous coverage of BSA on silver nanoparticles. Due to the surface blocking, the SERS intensity can vary during point-to-point measurements. Hence, the results are not sufficient for quantitative detection. However, monitoring the DNA hybridization event without employing labels in SERS based detection is demonstrated. It is clearly visible that the presence of adenine in the SERS spectra of the target DNA served as an indicator for the DNA hybridization.

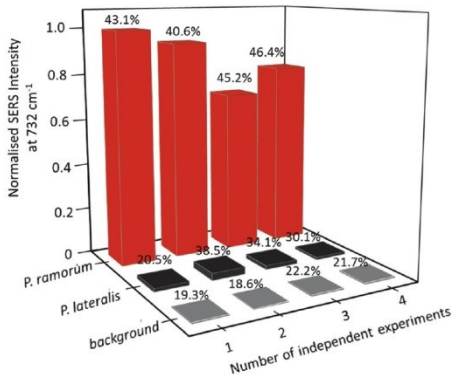

Fig. 7 Spectral reproducibility considering independent experiments. Discrimination between positive (red columns – *P. ramorum*) and negative hybridization signals (black columns – *P. lateralis*, grey columns – EGNP background) generated for AP-2 capture probes. The standard deviation is illustrated by the percentage values.

Conclusions and outlook

In recent years, SERS has been applied for a variety of analyses in the life science sector. Due to its high sensitivity and specificity, it offers great potential for the development of novel biosensors. In this study we expanded its application for the label-free detection of important plant pathogens using the example of *Phytophthora ramorum*. To the best of our knowledge, this is the first report on the label-free detection of the PCR product, isolated from infected plant tissue. Here, DNA-based detection of *P. ramorum* was achieved by covering the whole analytical chain. The sample preparation was realized by an easy tissue disruption procedure combined with magnetic bead-based nucleic acid isolation. The subsequent DNA amplification was performed by LATE-PCR, which enabled the generation of single-stranded target DNA. Thus, a post-PCR processing step for the generation of ssDNA could be omitted. In order to improve the detection and achieve a putative in-

field application, novel isothermal amplification techniques could be implemented.[51,52] Moreover, the SERS-based DNA detection, relying on DNA–DNA-hybrid formation, could be performed in a handheld Raman device, that allows the applicability at the point-of-need due to its portability.

In summary, a reliable, reproducible and thermally stable SERS assay has been developed for the detection of specific DNA hybridization between immobilized capture probes and the sequence-matching target DNA. We have highlighted the application of SERS to identify the adenine-containing target DNA isolated and amplified from infected *Rhododendron* leaves, in conjunction with adenine-free capture probes.

Acknowledgements

We thank Stephan König and Sabine Werres from the Julius Kühn–Institute Braunschweig, Germany for capture probe design, preparation of artificially inoculated *Rhododendron* leaves and extraction and reprocessing of the *Phytophthora* DNA. The project "PhytoChip-Validierung" (28-1-54.081-10) is financed by the Federal Ministry of Food and Agriculture (BMEL) based on a decision of the Parliament of the Federal Republic of Germany *via* the Federal Office for Agriculture and Food (BLE) under the innovation support program. Funding of the project "JBCI 2.0" (03IPT513Y) within the framework "InnoProfile Transfer – Unternehmen Region", the Federal Ministry of Education and Research, Germany (BMBF) is gratefully acknowledged.

References

1 O. K. Ribeiro and K. Lamour, *Phytophthora: Global Perspect.*, 2013, **2**, 1.
2 S. Werres, R. Marwitz, W. Veld, A. De Cock, P. J. M. Bonants, M. De Weerdt, K. Themann, E. Ilieva and R. P. Baayen, *Mycol. Res.*, 2001, **105**, 1155–1165.
3 C. Brasier and J. Webber, *Nature*, 2010, **466**, 824–825.
4 G. J. Bilodeau, C. A. Levesque, A. W. A. M. de Cock, C. Duchaine, S. Briere, P. Uribe, F. N. Martin and R. C. Hamelin, *Phytopathology*, 2007, **97**, 632–642.
5 F. N. Martin, *Phytophthora: Global Perspect.*, 2013, **2**, 19.
6 P. A. O'Brien, N. Williams and G. E. S. Hardy, *Crit. Rev. Microbiol.*, 2009, **35**, 169–181.
7 L. Schena and D. E. L. Cooke, *J. Microbiol. Methods*, 2006, **67**, 70–85.
8 L. Schena, J. M. Duncan and D. E. L. Cooke, *Plant Pathol.*, 2008, **57**, 64–75.
9 S. Julich, M. Riedel, M. Kielpinski, M. Urban, R. Kretschmer, S. Wagner, W. Fritzsche, T. Henkel, R. Moeller and S. Werres, *Biosens. Bioelectron.*, 2011, **26**, 4070–4075.
10 L. Schwenkbier, S. Koenig, S. Wagner, S. Pollok, J. Weber, M. Hentschel, J. Popp, S. Werres and K. Weber, *Microchim. Acta*, 2014, **181**, 1669–1679.
11 D. Cialla, K. Weber, R. Boehme, U. Huebner, H. Schneidewind, M. Zeisberger, R. Mattheis, R. Moeller and J. Popp, *Beilstein J. Nanotechnol.*, 2011, **2**, 501–508.
12 M. R. Hartman, R. C. H. Ruiz, S. Hamada, C. Xu, K. G. Yancey, Y. Yu, W. Han and D. Luo, *Nanoscale*, 2013, **5**, 10141–10154.
13 G. M. Santos, F. Zhao, J. Zeng, M. Li and W. C. Shih, *J. Biophotonics*, 2015, 9999.
14 D. Cialla, S. Pollok, C. Steinbruecker, K. Weber and J. Popp, *Nanophotonics*, 2014, **3**, 383–411.
15 X. Guo, *J. Biophotonics*, 2012, **5**, 483–501.
16 S. Mahajan, J. Richardson, T. Brown and P. N. Bartlett, *J. Am. Chem. Soc.*, 2008, **130**, 15589–15601.
17 T. Vo-Dinh, H.-N. Wang and J. Scaffidi, *J. Biophotonics*, 2010, **3**, 89–102.
18 M. Baia, L. Baia, S. Astilean and J. Popp, *Appl. Phys. Lett.*, 2006, 88.
19 S. Schluecker, *Angew. Chem., Int. Ed.*, 2014, **53**, 4756–4795.
20 E. C. Le Ru and P. G. Etchegoin, *Annu. Rev. Phys. Chem.*, 2012, **63**, 65–87.
21 M. Moskovits, *J. Raman Spectrosc.*, 2005, **36**, 485–496.
22 D. Cialla, U. Huebner, H. Schneidewind, R. Moeller and J. Popp, *ChemPhysChem*, 2008, **9**, 758–762.
23 K. K. Hering, R. Moeller, W. Fritzsche and J. Popp, *ChemPhysChem*, 2008, **9**, 867–872.
24 N. Pavillon, K. Bando, K. Fujita and N. I. Smith, *J. Biophotonics*, 2013, **6**, 587–597.
25 Y. Lai, S. Sun, T. He, S. Schlucker and Y. Wang, *RSC Adv.*, 2015, **5**, 13762–13767.
26 S. Niebling, H. Y. Kuchelmeister, C. Schmuck and S. Schluecker, *Chem. Sci.*, 2012, **3**, 3371–3377.
27 K. K. Strelau, A. Brinker, C. Schnee, K. Weber, R. Moeller and J. Popp, *J. Raman Spectrosc.*, 2011, **42**, 243–250.
28 A. J. Driscoll, M. H. Harpster and P. A. Johnson, *Phys. Chem. Chem. Phys.*, 2013, **15**, 20415–20433.
29 J. L. Abell, J. M. Garren, J. D. Driskell, R. A. Tripp and Y. Zhao, *J. Am. Chem. Soc.*, 2012, **134**, 12889–12892.
30 K. Faulds, W. E. Smith and D. Graham, *Analyst*, 2005, **130**, 1125–1131.
31 K. Gracie, E. Correa, S. Mabbott, J. A. Dougan, D. Graham, R. Goodacre and K. Faulds, *Chem. Sci.*, 2014, **5**, 1030–1040.
32 D. Graham, B. J. Mallinder, D. Whitecombe, N. D. Watson and W. E. Smith, *Anal. Chem.*, 2002, **74**, 1069–1074.
33 M. Green, F. M. Liu, L. Cohen, P. Kollensperger and T. Cass, *Faraday Discuss.*, 2006, **132**, 269–280.
34 Y. Lu, Q. Huang, G. Meng, L. Wu and J. Zhang, *Analyst*, 2014, **139**, 3083–3087.
35 N. E. Marotta, K. R. Beavers and L. A. Bottomley, *Anal. Chem.*, 2013, **85**, 1440–1446.
36 C. M. Muntean, N. Leopold, A. Halmagyi and S. Valimareanu, *J. Raman Spectrosc.*, 2011, **42**, 844–850.
37 H. T. Ngo, H.-N. Wang, A. M. Fales, B. P. Nicholson, C. W. Woods and T. Vo-Dinh, *Analyst*, 2014, **139**, 5655–5659.
38 E. Papadopoulou and S. E. J. Bell, *Chem. Commun.*, 2011, **47**, 10966–10968.

39 D. van Lierop, I. A. Larmour, K. Faulds and D. Graham, *Anal. Chem.*, 2013, **85**, 1408–1414.

40 A. Barhoumi and N. J. Halas, *J. Am. Chem. Soc.*, 2010, **132**, 12792–12793.

41 A. Barhoumi, D. Zhang, F. Tam and N. J. Halas, *J. Am. Chem. Soc.*, 2008, **130**, 5523–5529.

42 C. Otto, F. F. M. Demul, A. Huizinga and J. Greve, *J. Phys. Chem.*, 1988, **92**, 1239–1244.

43 A. Dallmann, L. Dehmel, T. Peters, C. Muegge, C. Griesinger, J. Tuma and N. P. Ernsting, *Angew. Chem., Int. Ed.*, 2010, **49**, 5989–5992.

44 J. M. Jean and K. B. Hall, *Proc. Natl. Acad. Sci. U. S. A.*, 2001, **98**, 37–41.

45 L. C. Sowers, G. V. Fazakerley, R. Eritja, B. E. Kaplan and M. F. Goodman, *Proc. Natl. Acad. Sci. U. S. A.*, 1986, **83**, 5434–5438.

46 S. König, L. Schwenkbier, S. Pollok, M. Riedel, S. Wagner, J. Popp, K. Weber and S. Werres, *Plant Pathol.*, 2015, **64**, 1176–1189.

47 H. Schneidewind, T. Schueler, K. K. Strelau, K. Weber, D. Cialla, M. Diegel, R. Mattheis, A. Berger, R. Moeller and J. Popp, *Beilstein J. Nanotechnol.*, 2012, **3**, 404–414.

48 T. Schueler, A. Steinbrueck, G. Festag, R. Moeller and W. Fritzsche, *J. Nanopart. Res.*, 2009, **11**, 939–946.

49 T. D. Miles, F. N. Martin and M. D. Coffey, *Phytopathology*, 2015, **105**, 265–278.

50 N. H. Jang, *Bull. Korean Chem. Soc.*, 2002, **23**, 1790–1800.

51 L. Schwenkbier, S. Pollok, S. Koenig, M. Urban, S. Werres, D. Cialla-May, K. Weber and J. Popp, *Anal. Methods*, 2015, **7**, 211–217.

52 J. A. Tomlinson, M. J. Dickinson and N. Boonham, *Phytopathology*, 2010, **100**, 143–149.

Electronic Supplementary Material (ESI) for Analyst.

Supplemental figure S1:

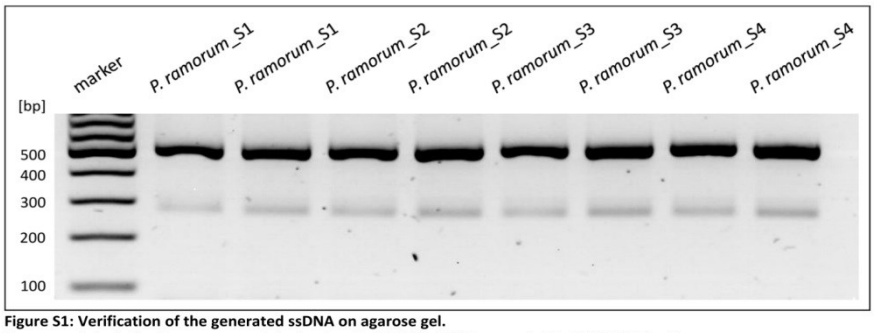

Figure S1: Verification of the generated ssDNA on agarose gel.
Agarose gel depicting the presence of single-stranded DNA (ssDNA) generated by LATE-PCR for *P. ramorum*.
dsDNA = 450 bp fat band, ssDNA = 450 nt faint band

4.2 Background-free bottom-up plasmonic arrays with increased sensitivity, specificity and shelf life for SERS detection schemes [SY2]

Sezin Yüksel, Mario Ziegler, Sebastian Goerke, Uwe Hübner, Killian Pollok, Falko Langenhorst, Karina Weber Dana Cialla-May, Jürgen Popp

The Journal of Physical Chemistry C, 2015, **119**, p. 13791-13798
DOI: 10.1021/acs.jpcc.5b01389

Authorship of the publication

Sezin Yüksel	*Concept development* *Experimental design* *Raman measurements* *Data analysis and interpretation* *Writing the manuscript*
Mario Ziegler	Experimental design ALD deposition Data analysis and interpretation Writing the manuscript
Sebastian Goerke	Experimental design Proof reading of manuscript
Uwe Hübner	Proof reading of manuscript
Kilian Pollok	TEM measurements Data analysis and interpretation Proof reading of manuscript
Falko Langenhorst	Proof reading of manuscript
Karina Weber	Discussion of experimental concept and results Proofreading of manuscript
Dana Cialla-May	Discussion of experimental concepts and results Proof reading of manuscript
Jürgen Popp	Project management Discussion of concepts and results Proof reading of manuscript

Erklärung zu den Eigenanteilen der Promovendin sowie der weiteren Doktoranden/ Doktorandinnen als Koautoren an der Publikation und Zweitpublikationsrechten bei einer kumulativen Dissertation

Publikation: **S. Yüksel, M. Ziegler, S. Goerke, U. Hübner, K. Pollok, F. Langenhorst, K. Weber,** **D. Cialla-May and J. Popp** ***Background-free bottom-up plasmonic arrays with increased sensitivity, specificity and shelf life for SERS detection schemes*** **Journal of Physical Chemistry C, 2015, 119, p.13791-13798**		
Beteiligt an		
	Sezin Yüksel	**Mario Ziegler**
Konzeption des Forschungsansatzes	**X**	
Planung der Untersuchungen	**X**	
Datenerhebung	**X**	
Datenanalyse und -interpretation	**X**	
Schreiben des Manuskripts	**X**	**X**
Vorschlag Anrechnung Publikationsäquevalente	**1.0**	**0.25**

*both authors contributed equally

THE JOURNAL OF PHYSICAL CHEMISTRY C

Article

pubs.acs.org/JPCC

Background-Free Bottom-Up Plasmonic Arrays with Increased Sensitivity, Specificity and Shelf Life for SERS Detection Schemes

Sezin Yüksel,[†,§] Mario Ziegler,[§] Sebastian Goerke,[§] Uwe Hübner,[§] Kilian Pollok,[‡] Falko Langenhorst,[‡] Karina Weber,[†,§] Dana Cialla-May,[*,†,§] and Jürgen Popp[†,§]

[†]Institute of Physical Chemistry and Abbe Center of Photonics, Friedrich Schiller University Jena, Helmholtzweg 4, 07743, Jena, Germany

[§]IPHT−Leibniz Institute of Photonic Technology, Albert-Einstein-Strasse 9, 07745, Jena, Germany

[‡]Institute of Geoscience, Friedrich Schiller University Jena, Carl-Zeiss-Promenade 10, 07745, Jena, Germany

Supporting Information

ABSTRACT: In utilizing the exceptional optical properties of metallic nanoparticles, surface enhanced Raman spectroscopy (SERS) is an excellent candidate for analytical detection schemes due to its molecular specificity and high sensitivity. To record reliable SERS signals, impurifications on the metallic surface contributing to the overall SERS signal, have to be removed. In this context, it is important to improve the nanostructures' quality to implement SERS in routine analytical applications. Here, we report about an easy to handle and fast protocol for the generation of SERS active nanoparticles by enzymatically reducing silver ions to their elementary state and oxidizing hydroquinone (HQ) to *p*-benzoquinone (*p*-BQ). However, these SERS substrates lead to a strong background signal overlapping with the actual analyte Raman bands. In order to quench this background signal and to protect the silver nanoparticles from oxidation we covered metallic nanoparticles with a dielectric layer of alumina (Al_2O_3) by applying plasma enhanced atomic layer deposition (PE-ALD). This coating guarantees the stability of these SERS substrates for at least 4 weeks after preparation under ambient storing conditions. The sensitivity of these enzymatically generated nanoparticles (EGNPs) coated with a 1 nm Al_2O_3 layer allows for a background free detection of riboflavin down to less than 10 nM. Furthermore, the improved specificity of these background-free and bottom-up produced plasmonic arrays has also been demonstrated by detecting a retinol monolayer.

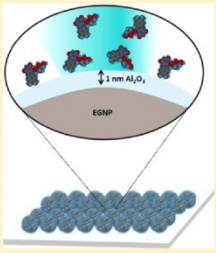

1. INTRODUCTION

Surface enhanced Raman spectroscopy (SERS) combining the high molecular specificity of Raman spectroscopy with the high sensitivity of fluorescence spectroscopy has gained remarkable interest in analytics within the last few years. Nowadays, a plethora of analytical SERS application schemes as for example the detection of proteins and DNA, drug monitoring, and cell analysis, as well as pathogen detection, are available.[1−20] The SERS mechanism is mainly based on two effects, namely the electromagnetic and the chemical enhancement effect.[3] The electromagnetic enhancement effect results from an optical phenomenon known as localized surface plasmon polariton (LSPP). When light interacts with a metallic nanoparticle surface, the electrons in the conducting band oscillate coherently and collectively with a resonant frequency. Thus, an amplification of the intrinsically weak Raman scattering for analytes in close proximity to the metal surface is obtained. The electromagnetic field enhancement is particularly concentrated at nanometer-sized gaps between nanoparticle arrangements as well as at sharp features of metal nanostructures due to the lightning rod effect.[21] The second mechanism is usually referred to a signal enhancement resulting from a chemical interaction between the analyte and the SERS active nanoparticle.[1−10,21,22]

In general, the SERS enhancement strongly depends on the composition, size, shape, and surrounding medium of the SERS active plasmonic nanostructures.[23] To expand the applicability of the SERS technique nanomaterial engineering and modeling of plasmonic structures becomes very important.[1] One important feature is the reproducibility of the plasmonic structure to ensure a homogeneous SERS intensity for each individual array. Second, it should be long-term stable without the susceptibility to any destabilizing or destructing environmental conditions, like oxidation. Third, the background signals from the SERS substrate itself should be as low as possible allowing for a clear discrimination between the vibrational bands of the analyte present in low concentrations. In this context enzymatically generated silver nanoparticles (EGNPs) are promising SERS substrates predominantly fulfilling these conditions. However, the routine application of EGNPs or silver nanoparticles in general is hampered by their chemical

Received: February 10, 2015
Revised: May 22, 2015
Published: May 22, 2015

DOI: 10.1021/acs.jpcc.5b01389
J. Phys. Chem. C 2015, 119, 13791−13798

stability, which needs to be improved.[24] Furthermore, background contribution of the EGNPs themselves to the Raman spectrum limits their widespread use as an appropriate SERS substrate. Quite some research effort has been invested in reducing or subtracting the background signal by computational methods such as frequency domain filtering, first and second derivatives and polynomial fits.[25] It is also possible to use principal component analysis (PCA) to separate the actual Raman signal from the intense background signal.[26] However, these computational approaches require preprocessing of the experimental data and therefore decrease the broad and easy applicability of the SERS technique.

To circumvent these severe limitations of metallic nanoparticles as SERS active substrates, coating the silver nanoparticles represents an interesting solution.[27,28] As an example, aluminum oxide (Al_2O_3) is commonly used as passivation layer resulting in an increased chemical stability. More importantly the oxide layer plays a significant role in tuning the LSPP resonance.[29,30] Covering the nanoparticle surface with a layer of aluminum oxide offers a great potential with respect to other important aspects such as tunable hydrophobicity, biocompatibility and resistance to high temperatures which predestines its implementation for the production of stable SERS substrates.[29−37]

Considering that the SERS enhancement is a distance-dependent phenomenon,[38] i.e., the SERS intensity of Raman modes is decreasing tremendously when the distance between analyte and metal nanoparticles increases,[39] the homogeneity and thickness of the passivation layer becomes quite crucial. Atomic layer deposition (ALD) is a well-established thin film growth technique based on the self-terminating reaction between precursor molecules and the surface of the substrate. The possibility of generating pinhole free coatings with a high conformity, due to the atomic scale precision of ALD, offers a great advantage for SERS.

Here, we characterize the background contribution of EGNPs, mainly caused by redox reaction products. Furthermore, we utilize plasma enhanced atomic layer deposition (PE-ALD) for quenching the EGNP background to clean and passivate the SERS-active surface. By doing so, the SERS enhancement is preserved for at least 4 weeks under ambient storing conditions. By using 1 nm Al_2O_3 modified EGNP substrates we were able to increase the limit of detection (LoD) for riboflavin down to 10 nM. Finally the increased specificity has been utilized for the detection of a retinol monolayer.

2. MATERIALS AND METHODS

Chemicals and Reagents. Riboflavin and retinol (≥95% pure) were purchased from Sigma-Aldrich (Steinheim, Germany). A 1 mM stock solution of riboflavin in distilled water was prepared and appropriate concentrations of these solutions were diluted for subsequent measurements. Similarly, a 5 mM solution of retinol in *n*-hexane was prepared. For the silver solution, silver acetate (99%) was provided from Sigma-Aldrich (Steinheim, Germany) and hydroquinone and hydrogen peroxide (30%) was purchased from Carl Roth GmbH (Karlsruhe, Germany).

EGNP Preparation. Plasmonic silver nanostructures were fabricated by a modified enzymatically induced redox reaction described previously.[34−36] Glass substrates (Carl Roth/Menzel) were cleaned by a series of acetone, ethanol, and water washing steps in an ultrasonic bath. As a linker molecule, single-stranded biotinylated DNA dissolved in 5 × phosphate buffered saline (PBS) was spotted in a concentration of 20 μM on the glass surface and exposed for 10 min to UV light (254 nm) for binding the molecules to the surface. The glass slides were then washed for 10 min with 0.1 × saline−sodium citrate/0.5 sodium dodecyl sulfate. The binding of a streptavidin horseradish peroxidase (HRP) complex to the biotin moieties of the immobilized DNA is realized by incubating the enzyme diluted in 1 × PBS/0.05% Tween (PBST) for 1 h at room temperature. Thereafter, the substrates were washed six times with PBST for 2 min to remove any unbound enzyme. Silver nanoparticles were formed by incubating with a silver containing solution, which consists of H_2O_2, silver acetate in distilled water solution and hydroquinone (HQ) in citrate buffer, for 5 min. Finally, the reaction was stopped by rinsing the substrates with water and drying them with compressed air. For energy-dispersive X-ray (EDX) emission spectroscopy, the EGNPs was produced on highly polished carbon substrates (12.7 mm diameter) purchased from Plano GmbH (Wetzlar, Germany) modified with (3-glycidyloxypropyl) trimethoxysilane (GOPS). Nanoparticles were cautiously scratched from the glass substrate and transferred onto copper grids, coated by Lacey carbon film (Plano GmbH, Wetzlar, Germany) and the transmission electron microscopy (TEM) images were recorded.

Plasma Enhanced Atomic Layer Deposition (PE-ALD). The EGNPs were coated with a dielectric layer by using an ALD reactor (Oxford Plasma Technology, OpAL, Bristol, U.K.) equipped with a double stage rotary vane pump. As ALD configuration, the showerhead procedure is applied. The entire process was performed under vacuum conditions with a base pressure of 2 mTorr. As passivation Al_2O_3 layers were prepared on the EGNPs in different layer thicknesses (0.5 nm, 2 cycles; 1.0 nm, 4 cycles; 2.0 nm, 9 cycles; 5.0 nm, 22 cycles; 10 nm, 45 cycles) at an operating temperature of 30 °C. Here, a low operating temperature is applied to avoid a disturbance of the fine structure of the metallic nanoparticles. The conformality of ultrathin film coatings[40] were measured by employing spectroscopic ellipsometry (J. A. Woollam Co., Nebraska, USA) equipped with a wavelength range of 246−1600 nm. The ellipsometric model was validated by a profilometer (Veeco Dektak 8, New York, USA). Subnanometer film thicknesses were calculated using the linear dependency between the film thickness and the film growth per cycle (GPC). The GPC value was constant at 2.2 Å per cycle during the measurement.

Al_2O_3 coated and uncoated EGNPs were incubated with an appropriate concentration of riboflavin and retinol for 30 min. After the incubation, the SERS-active substrates were cleaned with water and then dried with compressed air.

Instrumentation. The EDX measurements were performed using the high resolution field emission scanning electron microscope JEOL JSM−6300F (Tokyo, Japan), applying 6 keV accelerating voltage and a measuring surface area of 100 μm^2 with an accumulation time of 300 s. TEM images were taken with a FEI Tecnai G2 F20 S-TWIN (Oregon, USA) operating at an accelerating voltage of 200 kV. Raman and SERS spectra were recorded with a confocal Raman microscope (WITec GmbH, Ulm, Germany) equipped with 488 and 785 nm excitation laser lines. The backscattered light is collected by the same objective which is used for irradiation and detected by a spectrometer equipped with a 600 lines/mm grating and a 1024 × 127 pixel CCD camera cooled down to 208 K. Reference Raman spectra were recorded with a 10× Nikon objective (NA 0.25), an excitation wavelength of 785 nm with a laser power of

DOI: 10.1021/acs.jpcc.5b01389
J. Phys. Chem. C 2015, 119, 13791−13798

4 mW incident on the sample and with an integration time of 1 s. For the SERS measurements of riboflavin and retinol, 488 nm was employed as the excitation source (see the Supporting Information, Figures SI-1 and SI-2, for the UV−vis spectra of the target molecules and the extinction spectrum of the EGNPs), a 100× Olympus objective (NA 0.9) was used to irradiate the sample and to collect the Raman scattered light and the laser power onto the surface was set to 35 μW. For each measurement, a 60 × 60 μm^2 area was scanned, recording 400 spectra with 0.2 s of integration time for riboflavin and recording 1500 spectra with an integration time of 0.5 s for retinol.

3. RESULTS AND DISCUSIONS

Characterization of Silver Nanoparticles as Arrayed SERS Substrate. In order to provide reliable SERS substrates for routine analytics, the work presented in the following reports on exploring the background contribution of the metallic nanoparticles to the Raman spectra and upgrading the SERS performance of this substrate by coating the substrates with ultrathin Al_2O_3 films. Enzymatically generated silver nanoparticles were produced in an arrayed order on glass substrates as shown in Figure 1A. For that purpose single-stranded DNA was spotted onto the planar glass surface in an ordered array layout. Afterward a streptavidin-horseradish peroxidase complex (HRP) was bound to the immobilized DNA. Finally, the deposition of "desert-rose like" silver nanoparticles, was catalyzed by HRP via a redox reaction. In this catalytic process an oxygen atom is detached from hydrogen peroxide and bound to the prostethicheme group of the enzyme, causing a change of the iron oxidization state. The silver ions are electron acceptors and hydroquinone (HQ) is the corresponding electron donor, which is oxidized to p-benzoquinone (p-BQ) (Figure 1B).[34] In Figure 1, SEM images of these nanoparticles are depicted. The "desert-rose like" structure is clearly visible, which is characterized by flat plates orientated on top of each other under different angles.

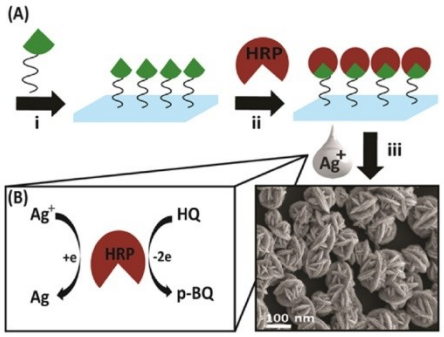

Figure 1. (A) Scheme representing the individual steps for EGNP deposition. (B) Redox reaction mechanism for the silver nanoparticle formation.

TEM images from the surface region of the silver nanoparticles reveal a thin coating which apparently represents organic residues from the redox reaction (Figure 2A). This carbonaceous and sometimes porous layer does not cover the EGNP surface homogeneously, but varies in thickness from 2−25 nm. It is stable under vacuum conditions and electron bombardment in the TEM. Figure 2B clearly shows the amorphous state of the coating in contrast to the well visible (111) lattice fringes of silver (d_{111} = 0.235 nm). This layer is critical for the SERS enhancement, which is highly dependent on the distance from the surface of the metallic nanoparticle to the adsorbate molecule.[21,41] The theoretical distance dependency of SERS intensity has been approximated as

$$I = \left(1 + \frac{d}{r}\right)^{-10}$$

where I is the intensity of the Raman mode, d is the distance between the adsorbate molecule and the surface of the metallic nanoparticle, and r is the diameter of the silver nanoparticle. For a 20 nm sized particle, 5 nm of separation between the target molecule and the surface will lead to a decreased SERS intensity by 1 order of magnitude.

Thus, the molecule−surface distance dependency is playing an important role for the SERS enhancement. Since, the redox products originating from the formation of EGNPs remain on the surface, the overall SERS enhancement will fluctuate across the surface area, which decreases the reliability of the SERS

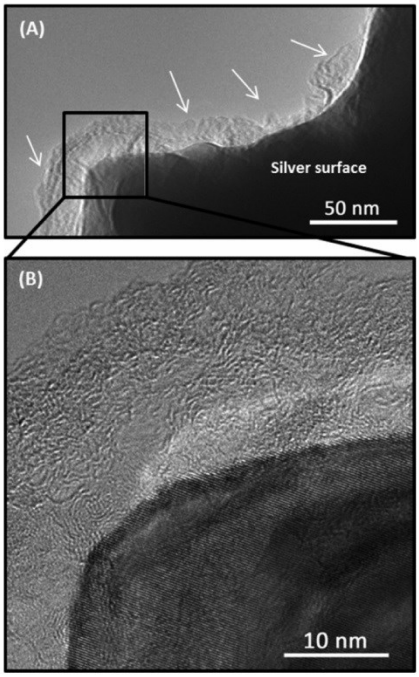

Figure 2. (A) TEM image of EGNPs (dark gray area) illustrating a thin layer of reaction products (light gray area) onto the surface. (B) High resolved image, showing the amorphous state of the layer and the lattice fringes of the silver.

DOI: 10.1021/acs.jpcc.5b01389
J. Phys. Chem. C 2015, 119, 13791−13798

substrates. Moreover, when the target molecule is incubated on this nonhomogeneously covered silver surface, the redox products will contaminate the Raman spectrum of the analyte molecule.

To investigate the adsorbed molecules on the surface of the EGNP deposits, the Raman background signals of the plasmonic nanoparticles are recorded. In Figure 3a, the

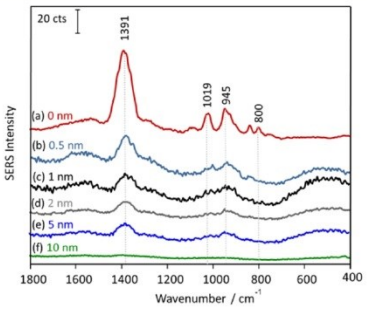

Figure 3. SERS background of EGNPs characterizing the contribution of the redox agents (a) and EGNP-related SERS background signals after the deposition of Al_2O_3 in various thicknesses (b−f). The SERS spectra were recorded applying 488 nm as excitation wavelength.

corresponding Raman signal is depicted in red. The strong Raman mode at 1391 cm^{-1} is assigned to the combined ν(C−C) and β(C−H) vibrational band of p-BQ.[36,37] The band at 945 cm^{-1} is due to the combined bending mode of β(C−C) and β(C−H) of p-BQ. The band at 800 cm^{-1} is attributed to the out of plane vibration of HQ and the mode at 1019 cm^{-1} is assigned to the ν(C−C) vibration of the HQ-p-BQ complex. A further contribution to the background signal might be caused by the citrate buffer used for the silver deposition.[42,43] The typical Raman modes of citrate are the ν(COO) around 1400 cm^{-1} and the ν(C−C) at 945 cm^{-1}. To summarize, the strong background signal of the SERS substrate limits the detection of molecules in low concentrations and with a high reproducibility.

PE-ALD Coating of EGNPs with Al_2O_3 to Significantly Reduce the SERS Background. In order to remove residues from the SERS substrate and therewith to quench the background signal as well as to passivate the metal surface, a subsequent coating of the silver nanoparticles deposit with the dielectric material Al_2O_3 in various controllable layer thicknesses (0.5, 1, 2, 5, and 10 nm) was realized by PE-ALD. Here, by utilizing the oxygen plasma during the production, the residue layer on the metal surface will be removed. In a next step, an Al_2O_3 layer is prepared based on the ALD process. In Figure 3b−f, the SERS background signal of the coated silver nanoparticles is shown in comparison to the unmodified silver substrates (0 nm Al_2O_3 thickness). Because of the various substrate surfaces, the ALD process can lead to different growth mechanisms.[44] During the first cycles of ALD, the Al_2O_3 layer might form islands on the surface of the EGNPs. With an increased layer thickness of Al_2O_3, the layer is predominantly closed. Therefore, The Raman modes at 1391 cm^{-1}, 1019 and 945 cm^{-1} (which are attributed to the redox residues at the metal surface) are quenched due to an increasing passivation layer thickness (Figure 3, 0.5−10 nm Al_2O_3 thickness). These results also illustrate the cleaning capability of the PE-ALD process which is an important feature for wet chemically fabricated bottom-up structures.

The influence of this passivation layer to the SERS activity is analyzed using the analyte riboflavin. Here, a 10 μM aqueous riboflavin solution was incubated on the substrates for 30 min. Since the electromagnetic mechanism exhibits the strongest contribution to the SERS effect, the molecule of interest does not require a binding to the metal surface via chemisorption to record high quality SERS spectra. However, a distance between analyte and metal surface in the range of a few nanometer should be present.[38] In Figure 4A, the SERS intensity of the

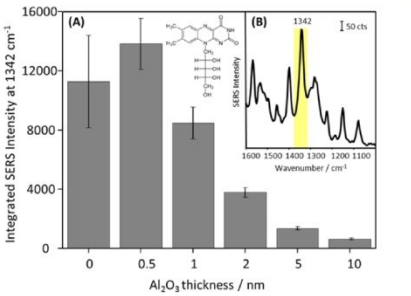

Figure 4. (A) Integrated SERS intensity of riboflavin at 1342 cm^{-1} is plotted as a function of different Al_2O_3 layer thicknesses. (B) Marked Raman mode of riboflavin used for the analysis.

model analyte riboflavin employing EGNP structures with various Al_2O_3 layer thicknesses are presented (see Supporting Information, Figure SI-3, for the SERS spectra in the spectral range of 1800−400 cm^{-1}). Characteristic bands of riboflavin are reliably detected even up to an Al_2O_3 layer thickness of 10 nm. The peak at 1342 cm^{-1} (see Figure 4B) which is assigned to the in plane aromatic ring vibrational mode is integrated and plotted as a function of the thickness of Al_2O_3.

On the basis of the distance dependency of the electromagnetic enhancement, the highest SERS intensity is expected for metallic nanostructures allowing for the closest possible distance between them and the analyte molecule. Here, the SERS intensity shows the highest value in the case of the thinnest coating layer of 0.5 nm. This could be explained by the removal of the inhomogeneous residue layer which is present on the uncoated silver nanostructures. Furthermore, by employing the PE-ALD process, the standard deviation of the SERS intensity is reduced by half which reflects the increased controllability and reproducibility of the coated surface. In comparability with the distance dependency of SERS, it is distinctly visible that the SERS intensity is decreasing with increasing thicknesses of the Al_2O_3 layer. In order to ensure the Al_2O_3 layer's homogeneously closed packing as well as a balanced ratio of signal intensity and RSD, we employed an Al_2O_3 layer thickness of 1 nm for further characterization experiments.

Characterization of the Al_2O_3 Coating Layers. The composition of the SERS active surfaces was checked by SEM-EDX measurements. In Figure 5, the EDX spectra of uncoated EGNPs and EGNPs with a 1 nm Al_2O_3 layer are depicted. The

DOI: 10.1021/acs.jpcc.5b01389
J. Phys. Chem. C 2015, 119, 13791−13798

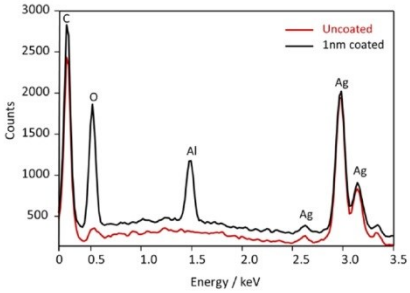

Figure 5. EDX spectra of uncoated EGNPs (red line) and EGNPs coated with 1 nm Al_2O_3 (black line).

strong peak at 2.99 keV, detected for both the coated and uncoated substrates, is due to the silver Lα emission line. The peaks at 1.49 and 0.52 keV in the recorded spectrum of the coated EGNPs are assigned to the K lines of aluminum and oxygen, respectively. This demonstrates the successful coating process with Al_2O_3. In the case of uncoated EGNPs, no oxygen peak is found, the small peak at 0.56 keV is due to a M line of silver. The peak at 0.27 keV is attributed to carbon, the material of the underlying planar substrate. Additionally, by employing the advantage of the low operating temperature of 30 °C during the PE-ALD process, no change in the fine structure of EGNPs is observed (see, the Figure SI-4).

Determining the Increased Sensitivity by Using Al_2O_3-Modified EGNPs. To characterize the sensitivity of the coated and uncoated EGNP substrates, the limit of detection (LoD) of the system was determined following the definition below.[45] Generally, all measurements possess a normal distribution with a mean value at the center of the curve. The normal distribution curve is symmetric and the standard deviation (σ) of the measurements circumscribes the tail of the curve. The limit of detection is defined as the smallest concentration, at which 3σ of the recorded SERS signal and 3σ of the background signal is not overlapping, allowing for a confidence level of 99.8%.

The quantitative relation between the SERS activity and the riboflavin concentration is illustrated in Figure 6A. The SERS signal at 1625 cm^{-1}, assigned to the ν(C−C) vibrational mode of the benzene ring,[46] is integrated and plotted as a function of the concentration. To prove the 99.8% confidence level of the data points, Figure 6B presents the low-concentration range. Here, the SERS intensity is plotted with 3σ as a function of the concentration. By employing the uncoated EGNPs as SERS substrate (Figure 6B, red squares) the integrated SERS intensity for the riboflavin concentrations of 0.01, 0.02, 0.05, and 0.1 μM are estimated with a standard deviation of 25.8%, 20.4%, 20.8%, and 23.3%, respectively. These relatively high values are attributed to the inhomogeneous layer of redox products on the silver nanoparticle surface of uncoated EGNPs. Because of the overlap of the standard deviation for low concentrations (see Figure 6B) a reliable quantitative detection is not possible for concentrations lower than 0.2 μM.

As discussed before, due to the preparation conditions during the PE-ALD process, the inhomogeneous residual layer of the EGNPs is successfully removed from the nanoparticle surface. As a consequence, no background contribution from the coated EGNPs to the overall SERS spectra is detected at low riboflavin concentrations. Similarly to the previous analysis, the SERS intensity at 1625 cm^{-1} of riboflavin is integrated and plotted as a function of the concentration. In Figure 6B, the separation of all data points (black circles) with a 3σ confidence level is shown, allowing for a quantitative detection of riboflavin down to 10 nM. Furthermore, the improved homogeneity of the SERS signals is illustrated by the standard deviations, which are reduced by half in comparison to the uncoated EGNPs as SERS-active substrates. Within the Supporting Information (Figure SI-5), the average SERS spectra of riboflavin for the lowest concentration as well as the background contribution is depicted. Additionally, the quantitative analysis based on the integration of the Raman modes at 1402 and 1083 cm^{-1} result in a similar LoD of riboflavin (see Figure SI-6).

In summary, the Al_2O_3 coating of the EGNP surface removes not only the background signal (cleaning effect), but additionally provides a high SERS sensitivity. The LoD of riboflavin is estimated to 10 nM.

Characterizing the Shelf Life of Uncoated and Coated EGNPs. In addition to a negligible background contribution, an ideal SERS substrate should be a long-term resistant against oxidation processes. Even though having excellent optical properties for SERS applications, the morphological reliability

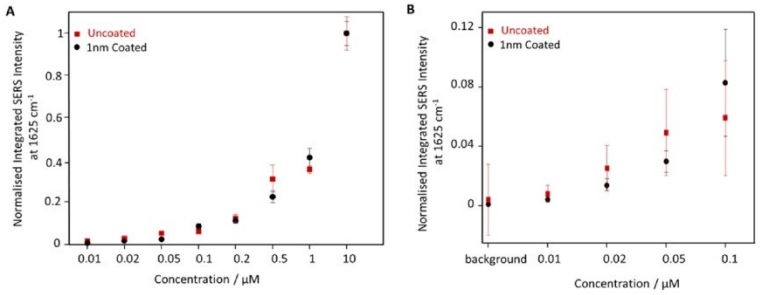

Figure 6. (A) Quantitative analysis of uncoated and 1 nm coated EGNPs: Normalized integrated SERS intensity of the peak at 1625 cm^{-1} versus different concentrations of riboflavin. (B) Detailed view of the quantitative analysis for the low concentrations in comparison with the background contribution. The error bars are illustrating a 3σ confidence level of the data points.

DOI: 10.1021/acs.jpcc.5b01389
J. Phys. Chem. C 2015, 119, 13791−13798

of silver nanoparticles can be easily changed due to oxidization processes under ambient storing conditions. In the Supporting Information, Figure SI-7, SEM images of the EGNPs before and after 7 days of storage under ambient conditions shows the oxidation of the EGNP's surface. In order to characterize the shelf life of the SERS-active substrates, the SERS intensity of riboflavin were investigated for 12 weeks by using EGNPs coated with 1 nm Al_2O_3 and uncoated EGNPs as SERS substrates (Figure 7). Both uncoated and coated substrates

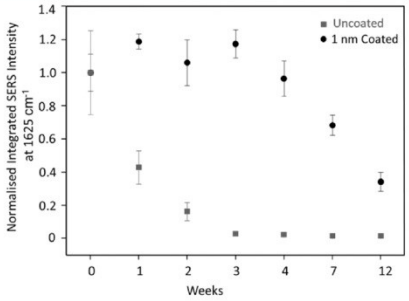

Figure 7. Normalized Raman intensity over time for uncoated and coated EGNPs by employing ethanol as an external calibration method.

were stored in darkness under ambient conditions. The substrates were applied for weekly SERS measurements of riboflavin (10 μM). To normalize the SERS spectra by weekly manner, the Raman band of ethanol at 882 cm^{-1} was used as an external standard.[47] Even though different substrate surfaces can lead to different growth rates and growth mechanisms,[44] the coated silver nanoparticles are stable at least for 4 weeks. This also ensures that the coating is predominantly closed across the surface by means of the deposition of 1 nm Al_2O_3 on EGNPs. In contrast, the SERS activity of uncoated silver deposits significantly decreased after 1 week of storage.

Specificity Improvement Using Background-Free EGNPs. Finally, to show the potential of the alumina coated EGNPs as biosensors, the detection of retinol, which is not observable by applying the unmodified EGNPs, was investigated. Figure 8A shows the characteristic Raman modes of solid retinol. The Raman modes between 1500 and 1600 cm^{-1} can be assigned to the C=C stretching vibrations in the polyene structure of retinol.[48] The recorded bands between 1250 and 1400 cm^{-1} are attributed to CCH in-plane rocking vibrations and the bands between 1100 and 1250 cm^{-1} are related with C−C stretches. Approximately at 1000 cm^{-1}, hydrogen out-of-plane wagging modes are detectable.

When retinol is incubated onto uncoated EGNPs, the most dominant vibrational band at 1583 cm^{-1} of retinol is not detectable (Figure 8B). However, when retinol is incubated onto EGNPs coated with a 1 nm thick Al_2O_3 layer, vibrational Raman bands specific for retinol are recorded, due to the decreased background signal (see Figure 8C). Furthermore, the affinity of the retinol molecule toward the sensor surface might be affected by the modified metallic surface. The Raman peak at 1585 cm^{-1} is shifted under SERS conditions to 1555 cm^{-1} due to the binding of the molecule toward the surface via the OH group and a resulting reduced electron density in the C=C

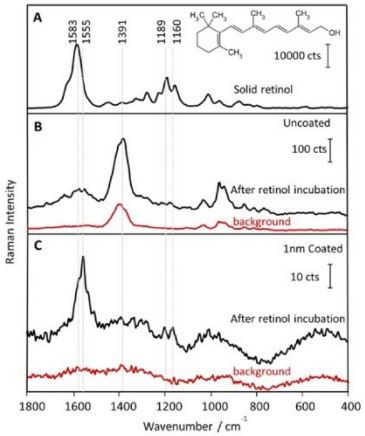

Figure 8. (A) Raman spectra of retinol were recorded utilizing the excitation wavelength at 785 nm. The SERS measurement of retinol incubated on uncoated EGNPs (B) and 1 nm Al_2O_3 coated EGNPs substrates (C) were measured applying 488 nm excitation wavelength.

double bonds. Furthermore, bands at 1189 and 1160 cm^{-1} (C−C stretching vibrations) are recorded. Thus, significant molecular vibrational fingerprints of retinol are only detectable by applying EGNPs coated with a 1 nm thick Al_2O_3 layer in SERS-based detection schemes, illustrating the increased specificity of the coated EGNPs.

4. CONCLUSION

Within this contribution, a modification strategy of bottom-up produced SERS-active EGNP substrates is presented to enable sensitive and specific SERS-based detection schemes. By employing PE-ALD, the silver surface is cleaned from reaction residues and a passivation layer consisting of Al_2O_3 is prepared. By doing so, the LoD is increased by approximately two magnitudes down to 10 nM for riboflavin. Furthermore, the shelf life of the EGNPs is significantly increased after coating with Al_2O_3 allowing for storing under ambient conditions for 4 weeks. Finally, the possibility of detecting a monolayer of retinol (which is not detectable with uncoated EGNPs) shows the improved specificity of coated substrates. In summary, EGNPs coated with ultrathin films of Al_2O_3 are promising background-free SERS substrates with an increased SERS signal reproducibility, a high sensitivity and specificity as well as with a long storage shelf life. This approach is transferable for all SERS nanostructures arranged on a substrate. In particularly, bottom-up produced nanostructures will benefit from the cleaning effect, since in most cases reaction products are found on the metal surface and limiting with this the applicability in SERS-based detection protocols.

■ ASSOCIATED CONTENT

Supporting Information

UV−vis spectra and chemical structures of riboflavin and retinol; extinction spectra of uncoated EGNPs and 1 nm Al_2O_3-coated EGNPs; SERS spectra of 10 μM of riboflavin versus different Al_2O_3 thickness; SEM image of Al_2O_3 coated EGNPs;

DOI: 10.1021/acs.jpcc.5b01389
J. Phys. Chem. C 2015, 119, 13791−13798

SERS spectra of 0.1, 0.05, 0.02, and 0.01 μM concentrated riboflavin incubated on uncoated and coated EGNPs in contrast to the background contribution; normalized integrated SERS intensity at 1402 and 1083 cm^{-1} versus different concentration of riboflavin; and backscatter electron image of the FIB cuts investigating oxizidized silver nanoparticles after 7 days of storage at ambient conditions. The Supporting Information is available free of charge on the ACS Publications website at DOI: 10.1021/acs.jpcc.5b01389.

■ AUTHOR INFORMATION

Corresponding Author

* E-mail: dana.cialla-may@uni-jena.de. Telephone: +49 (0) 3641-206309. Fax: +49 (0)3641-206399.

Notes

The authors declare no competing financial interest.

■ ACKNOWLEDGMENTS

Funding the projects "QuantiSERS" (03IPT513A) and "JBCI 2.0" (03IPT513Y) within the framework "InnoProfile Transfer−Unternehmen Region" the Federal Ministry of Education and Research, Germany (BMBF) is gratefully acknowledged. Furthermore, this study is supported by the Deutsche Forschungsgemeinschaft (LA830/14, Gottfried Wilhelm Leibniz program). The authors also thank Andrea Dellith (IPHT Jena, Germany) for SEM and EDX measurements.

■ REFERENCES

(1) Cialla, D.; März, A.; Böhme, R.; Theil, F.; Weber, K.; Schmit, M.; Popp, J. Surface-Enhanced Raman Spectroscopy (SERS): Progress and Trends. *Anal. Bioanal. Chem.* **2012**, *403*, 27−54.

(2) Larmour, I. A.; Graham, D. Surface Enhanced Optical Spectroscopies for Bioanalysis. *Analyst* **2011**, *136*, 3831−3853.

(3) Willets, K. A.; Van Duyne, R. P. Localized Surface Plasmon Resonance Spectroscopy and Sensing. *Annu. Rev. Phys. Chem.* **2007**, *58*, 267−297.

(4) Cialla, D.; Pollok, S.; Steinbrücker, C.; Weber, K.; Popp, J. SERS-Based Detection of Biomolecules. *Nanophotonics* **2014**, *3*, 383−411.

(5) Tian, Z. Q. Surface-Enhanced Raman Spectroscopy: Advancements and Applications. *J. Raman Spectrosc.* **2005**, *36*, 466−470.

(6) Avarez-Puebla, R. A.; Liz-Marzan, L. M. Traps and Cages for Universal SERS Detection. *Chem. Soc. Rev.* **2012**, *41*, 43−51.

(7) Le Ru, E. C.; Etchegoin, P. G. Single-Molecule Surface-Enhanced Raman Spectroscopy. *Annu. Rev. Phys. Chem.* **2012**, *63*, 65−87.

(8) Halas, N. J.; Moskovits, M. Surface-Enhanced Raman Spectroscopy: Substrates and Materials for Research and Applications. *MRS Bull.* **2013**, *38*, 607−611.

(9) Schlücker, S. Surface-Enhanced Raman Spectroscopy: Concepts and Chemical Applications. *Angew. Rev.* **2014**, *53*, 4756−4795.

(10) Pahlow, S.; März, A.; Seise, B.; Hartmann, K.; Freitag, I.; Kämmer, E.; Böhme, R.; Deckert, V.; Weber, K.; Cialla, D.; et al. Bioanalytical Application of Surface- and Tip-Enhanced Raman Spectroscopy. *Eng. Life Sci.* **2012**, *12*, 131−143.

(11) Jiang, C.; Liu, R.; Han, G.; Zhang, Z. A Chemically Reactive Raman Probe for Ultrasensitively Monitoring and Imaging the *In Vivo* Generation of Femtomolar Oxidative Species as Induced by Anti-Tumor Drugs in Living Cells. *Chem. Commun.* **2013**, *49*, 6647−6649.

(12) Zhang, L.; Jiang, C.; Zhang, Z. Graphene Oxide Embedded Sandwich Nanostructures for Enhanced Raman Readout and Their Applications in Pesticide Monitoring. *Nanoscale* **2013**, *5*, 3773−3779.

(13) Vendrell, M.; Maiti, K. K.; Dhaliwal, K.; Chang, Y.-T. Surface-Enhanced Raman Scattering in Cancer Detection and Imaging. *Trends Biotechnol.* **2013**, *31*, 249−257.

(14) Liu, B.; Han, G.; Zhang, Z.; Liu, R.; Jiang, C.; Wang, S.; Han, M.-Y. Shell Thickness-Dependent Raman Enhancement for Rapid Identification and Detection of Pesticide Residues at Fruit Peels. *Anal. Chem.* **2011**, *84*, 255−261.

(15) Lim, D.-K.; Jeon, K.-S.; Hwang, J.-H.; Kim, H.; Kwon, S.; Suh, Y. D. Highly Uniform and Reproducible Surface-Enhanced Raman Scattering from DNA-Tailorable Nanoparticles with 1-nm Interior Gap. *Nat. Nanotechnol.* **2011**, *6*, 452−460.

(16) Schlücker, S. Surface-Enhanced Raman Spectroscopy: Concepts and Chemical Applications. *Angew. Chem., Int. Ed.* **2014**, *53*, 4756−4797.

(17) Mahajaan, S.; Richardson, J.; Brown, T.; Bartlett, P. N. SERS-Melting: A New Method for Discriminating Mutations in DNA Sequences. *J. Am. Chem. Soc.* **2008**, *130*, 15589−15601.

(18) Vo-Dinh, T.; Wang, H.-N.; Scaffidi, J. Plasmonic Nanoprobes for SERS Biosensing and Bioimaging. *J. Biophoton.* **2010**, *3*, 89−102.

(19) Gracie, K.; Correa, E.; Mabbott, S.; Dougan, J. A.; Graham, D.; Goodacre, R.; Faulds, K. Simultaneous Detection and Quantification of Three Bacterial Meningitis Pathogens by SERS. *Chem. Sci.* **2014**, *5*, 1030−1040.

(20) Betz, J. F.; Yu, W. W.; Cheng, Y.; White, I. M.; Rubloff, G. W. Simple SERS Substrates: Powerful, Portable and Full of Potential. *Phys. Chem. Chem. Phys.* **2014**, *16*, 2224−2239.

(21) Moskovits, M. Surface-Enhanced Raman Spectroscopy: A Brief Retospective. *J. Raman Spectrosc.* **2005**, *36*, 485−496.

(22) McNay, G.; Eustace, D.; Smith, W. E.; Faulds, K.; Graham, D. Surface-Enhanced Raman Scattering (SERS) and Surface-Enhanced Resonance Raman Scattering (SERRS):A Review of Applications. *Appl. Spectrosc.* **2011**, *65*, 825−837.

(23) Murray, W. A.; Suckling, J. R.; Barnes, W. L. Overlayers on Silver Nanotriangles: Field Confinement and Spectral Position of Localized Surface Plasmon Resonances. *Nano Lett.* **2006**, *6*, 1772−1777.

(24) Kelly, K. L.; Coronado, E.; Zhao, L. L.; Schatz, G. C. The Optical Properties of Metal Nanoparticles: The influence of Size Shape, and Dielectric Environment. *J. Phys. Chem. B* **2003**, *107*, 668−677.

(25) Beier, B. D.; Berger, A. J. Method for Automated Background Substratcion from Raman Spectra Containing Known Contaminants. *Analyst* **2009**, *134*, 1198−1202.

(26) Hasegawa, T.; Nishijoa, J. Umemure, Separation of Raman Spectra from Fluorescence Emission Background by Principle Component Analysis. *Chem. Phys. Lett.* **2000**, *317*, 642−646.

(27) Hayazawa, N.; Motohashi, M.; Saito, Y.; Kawata, S. Highly Sensitive Strain Detection in Strained Silicon by Surface-Enhanced Raman Spectroscopy. *Appl. Phys. Lett.* **2005**, *86*, 263114−3.

(28) Kasim, J.; Tee, X. Y.; You, Y. M.; Ni, Z. H.; Setiawan, Y.; Lee, P. S.; Chan, L.; Shen, Z. X. Plasmon-Enhanced Polarized Raman Spectroscopy for Sensitive Surface Characterization. *J. Raman Spectrosc.* **2008**, *39*, 1338−1342.

(29) Lin, M. C.; Nien, L. W.; Chen, C. H.; Lee, C. W.; Chen, M. J. Surface Enhanced Raman Scattering and Localized Surface Plasmon Resonance of Nanoscale Ultrathin Films Prepared by Atomic Layer Deposition. *Appl. Phys. Lett.* **2012**, *101*, 023112.

(30) D'Agostino, S.; Della Sala, F. Active Role of Oxide Layers on the Polarization of Plasmonic Nanostructures. *ACS Nano* **2010**, *4*, 117−4225.

(31) Ingham, C. J.; ter Maat, J.; de Vos, W. M. Where Bio Meets Nano: The Many Uses for Nanoporous Aluminum Oxide in Biotechnology. *Biotechnology Advances* **2012**, *30*, 1089−1099.

(32) Szczepanski, V.; Vlassiouk, I.; Smirnov, S. Stability of Silane Modifier on Alumina Nanoprous Membranes. *J. Membr. Sci.* **2006**, *281*, 587−591.

(33) Kim, H.; Kosuda, K. M.; Van Duyne, R. P.; Stair, P. C. In-Situ Characterization of Heterogeneous Catalysts Themed Issue. *Chem. Soc. Rev.* **2010**, *39*, 4820−4844.

(34) Schneidewind, H.; Schüler, T.; Strelau, K. K.; Weber, K.; Cialla, D.; Diegel, M.; Mattheis, R.; Berger, A.; Möller, R.; Popp, J. The Morphology of Silver Nanoparticles Prepared by Enzyme-Induzed Reduction. *Beilstein J. Nanotechnol.* **2012**, *3*, 404−414.

DOI: 10.1021/acs.jpcc.5b01389
J. Phys. Chem. C 2015, 119, 13791−13798

(35) Schüler, T.; Steinbrück, A.; Festag, G.; Möller, R.; Fritzsche, W. Enzyme-Induced Growth of Silver Nanoparticles Studied on Single Particle Level. *J. Nanopart. Res.* **2008**, *11*, 939−946.
(36) Zhang, H.; Liu, F.; Wang, Y.; Wang, X.; Zuo, J.; Xu, C.; He, T.; Xin, H. Surface-Enhanced Raman Scattering Observation of Quinhydrones Formation from the Reaction of Hydroquinone Reducing Silver Bromide Sol. *Spectrochim. Acta, Part A* **1995**, *51*, 2501−2510.
(37) Kubinyi, M.; Kersztury, G. Infrared and Raman Spectroscopic Study of Molecular Interations in Quinhydrone Crystals. *Spectrochim Acta, Part A* **1989**, *45A*, 421−429.
(38) Cialla, D.; Weber, K.; Böhme, R.; Hübner, U.; Schneidewind, H.; Zeisberger, M.; Mattheis, R.; Möller, R.; Popp, J. Towards Multiple Readout Application of Plasmonic Arrays. *Beilstein J. Nanotechnol.* **2011**, *2*, 501−508.
(39) Stiles, P. L.; Dieringer, J. A.; Shah, N. C.; Van Duyne, R. P. Surface-Enhanced Raman Spectroscopy. *Annu. Rev. Anal. Chem.* **2008**, *1*, 601−626.
(40) Valdesueiro, D.; Meesters, G. M. H.; Kreutzer, M. T.; van Ommen, J. R. Gas-Phase Deposition of Ultrathin Aluminium Oxide Films on Nanoparticles at Ambient Conditions. *Materials* **2015**, *8*, 1249−1263.
(41) Dieringer, J. A.; McFarland, A. D.; Shah, N. C.; Stuart, D. A.; Whitney, A. V.; Yonzon, C. R.; Young, M.-A.; Zhang, X.; Van Duyne, R. P. Surfaced-Enhanced Raman Spectroscopy: New Materials, Concepts, Characterization Tools, and Applications. *Faraday Discuss.* **2006**, *55*, 712−724.
(42) Munro, C. H.; Smith, W. E.; Garner, M.; Clarkson, J.; White, P. C. Characterization of the Surface of a Citrate-Reduced Colloid Optimized for Use as a Substrate for Surface-Enhanced Resonance Raman Scattering. *Langmuir* **1995**, *11*, 3712−3720.
(43) Blatchford, C. G.; Sllman, O.; Kerker, M. Potential Dependence of Surface-Enhanced Raman Scattering from Citrate on Colloidal Silver. *J. Phys. Chem.* **1983**, *87*, 2503−2508.
(44) Satta, A.; Vantimme, A.; Schuhmacher, J.; Whelan, C. M.; Sutcliffe, V.; Maex, K. Initial Growth Mechanism of Atomic Layer Deposited TiN. *Appl. Phys. Lett.* **2004**, *84*, 4571−4573.
(45) Long, G. L.; Winefordner, J. D. Limit of Detection A −Closer Look at the IUPAC Definifition. *Anal. Chem.* **1983**, *55*, 712−724.
(46) Liu, F.; Gu, H.; Lin, Y.; Qi, Y.; Dong, X.; Gao, J.; Cai, T. Surface-Enhanced Raman Scattering Study of Riboflavin on Borohydride-Reduced Silver Colloids: Dependence of Concentration, Halide Anions and pH Values. *Spectrochim. Acta, Part A* **2012**, *85*, 111−119.
(47) Nah, S.; Kim, D.; Chung, H.; Han, S.-H.; Yoon, M.-Y. A New Quantitative Raman Measurment Scheme Using Teflon as a Novel Intensity Correction Standard As Well As the Sample Container. *J. Raman Spectrosc.* **2007**, *38*, 475−482.
(48) Morjani, H.; Beljebbar, A.; Sockalingum, G. D.; Mattioli, T. A.; Bonnier, D.; Gronemeyer, H.; Manfait, M. Surface-enhanced Raman Scattering and Fluorescence Spectroscopy Reveal Molecular Interactions of All-Trans Retinoic Acid and RARγ Ligand-Binding Domain. *Biospectroscopy* **1998**, *4*, 297−302.

DOI: 10.1021/acs.jpcc.5b01389
J. Phys. Chem. C 2015, 119, 13791−13798

Background-Free Bottom-Up Plasmonic Arrays with Increased Sensitivity, Specificity and Shelf Life for SERS Detection Schemes

Supporting Information

Sezin Yüksel [§,¥], *Mario Ziegler* [¥], *Sebastian Goerke* [¥], *Uwe Hübner* [¥], *Kilian Pollok* [‡], *Falko Langenhorst* [‡], *Karina Weber* [§,¥], *Dana Cialla-May* [*,§,¥], *and Jürgen Popp* [§,¥],

[§] Institute of Physical Chemistry and Abbe Center of Photonics, Friedrich Schiller University Jena, Helmholtzweg 4, 07743, Jena, Germany

[¥] IPHT – Leibniz Institute of Photonic Technology, Albert-Einstein-Strasse 9, 07745, Jena, Germany

[‡] Institute of Geoscience, Friedrich Schiller University Jena, Carl-Zeiss-Promenade 10, 07745, Jena, Germany

KEYWORDS: SERS, ALD, Al_2O_3, SERS substrates, stability, retinol

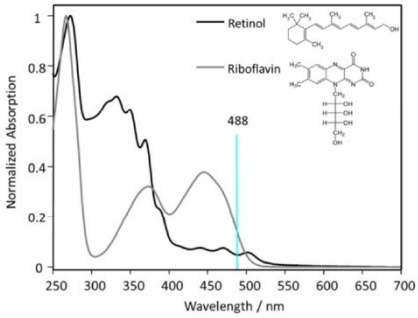

Figure SI-1: UV-Vis spectra and chemical structures of riboflavin and retinol. UV-Vis spectra of riboflavin and retinol were recorded by a Jasco V650 diode-array spectrophotometer in the wavelength range of 250–700 nm, as shown in **Figure 1**. Since the applied excitation wavelength in SERS experiments was 488 nm, an additional resonance Raman contribution to the SERS spectra is expected.

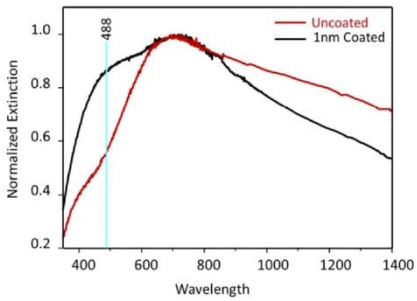

Figure SI-2: Extinction spectra of uncoated EGNPs and 1 nm Al_2O_3-coated EGNPs. Extinction measurements were performed employing a fiber-based UV-Vis extinction spectrometer. Areas of 200 μm^2 were illuminated via a halogen lamp; the reflected light is coupled into a fiber and detected by a fiber spectrometer. The Al_2O_3 coating of EGNPs results in an additional shoulder of the plasmonic profile around 480 nm due to the changed dielectric environment on the metallic surface.

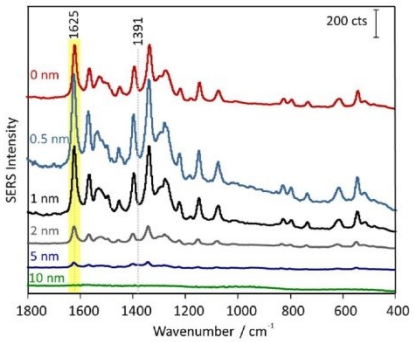

Figure SI-3: SERS spectra of 10µM of riboflavin versus different Al_2O_3 thickness. The silver nanostructures with different Al_2O_3 layers were incubated in a riboflavin solution (10 µM) for 30 minutes. **Figure SI-3** shows that the SERS intensity is decreasing when the thickness of the passivation layer of EGNPs is increasing.

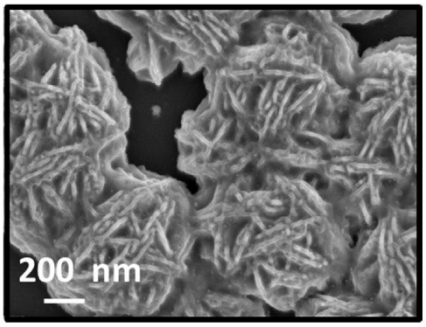

Figure SI-4: SEM image of Al_2O_3 coated EGNPs (layer thickness is 1 nm). **Figure SI-4** shows the SEM image of Al_2O_3 coated EGNPs with a layer thickness of 1 nm. The fine structures of EGNPs are visible after ultra-thin film coating with alumina due to the low operating temperature of PE-ALD.

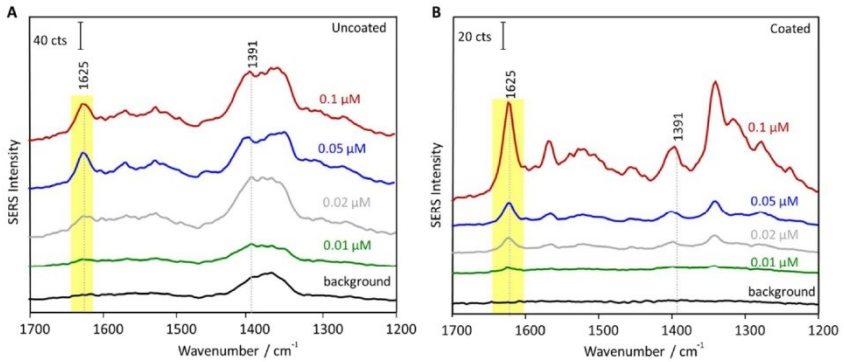

Figure SI-5: SERS spectra of 0.1 µM, 0.05 µM, 0.02 µM, 0.01 µM concentrated riboflavin incubated on **(A)** uncoated and **(B)** coated EGNPs in contrast to the background contribution. **Figure SI-5** shows the SERS spectra for different concentrations (0.1 µM, 0.05 µM, 0.02 µM, 0.01 µM) of riboflavin. The background contribution from the uncoated surface of the nanostructure interferes with the spectra of the low concentrated riboflavin (see, the **Figure SI-5 (A)**). In contrast to the uncoated EGNPs, fingerprint spectra of 0.02 µM and 0.01 µM concentrated riboflavin are detectable by using coated EGNPs as SERS substrate (see, the **Figure SI-5 (B)**).

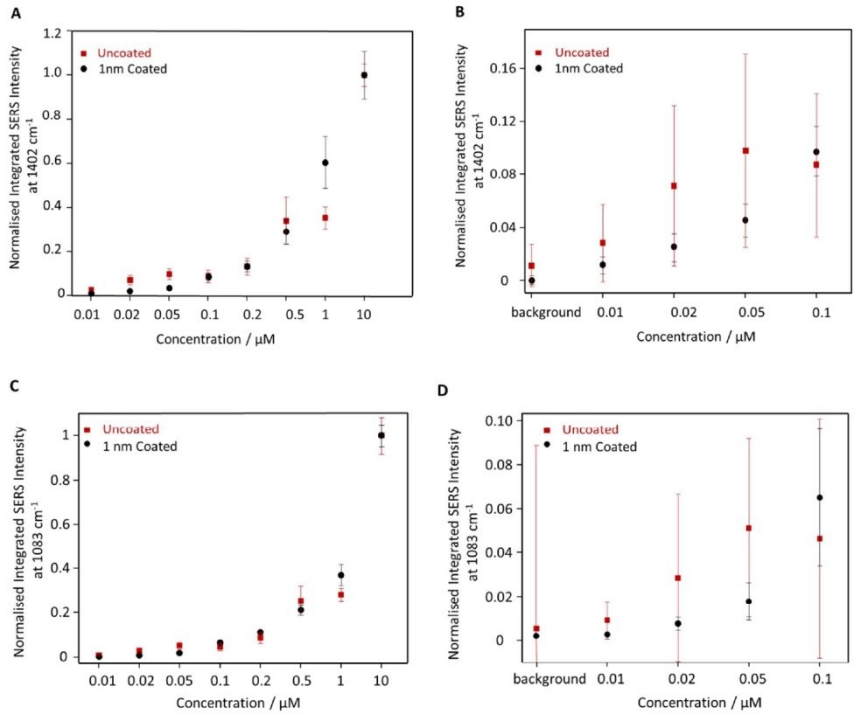

Figure SI-6: Normalized integrated SERS intensity at 1402 cm^{-1} **(A, B)** and 1083 cm^{-1} **(C, D)** versus different concentration of riboflavin. **Figure SI-6** demonstrates the normalized integrated SERS intensity of the Raman modes at 1402 cm^{-1} and 1083 cm^{-1} as function of the riboflavin concentration. Similar to the **Figure 6,** the integrated SERS intensity of 0.01 µM of riboflavin is overlapping with the integrated SERS intensity of the background at 1402 cm^{-1} as well as at 1083 cm^{-1} for uncoated EGNPs. Also, the relative standard deviations (RSDs) of the individual concentration rows of the riboflavin are between 25-44%. However, the 1 nm Al_2O_3 coated EGNPs shows improved quantitative results compared to the uncoated EGNPs. In the case of

coated EGNPs, 0.01 µM of riboflavin is easily detectable. Also, the RSDs of the individual concentration are in the range of 8-12% for coated EGNPs. The data points in **Figure SI-6 (B)** and **Figure SI-6 (D)** are plotted in order to show the 99.8% confidence level (3σ). It is clear that with integrating different Raman modes of riboflavin, 10 nM of riboflavin can be easily detected with coated EGNPs, which is far from possible with uncoated EGNPs. By employing PE-ALD, the reliability of the quantitative detection is highly increased.

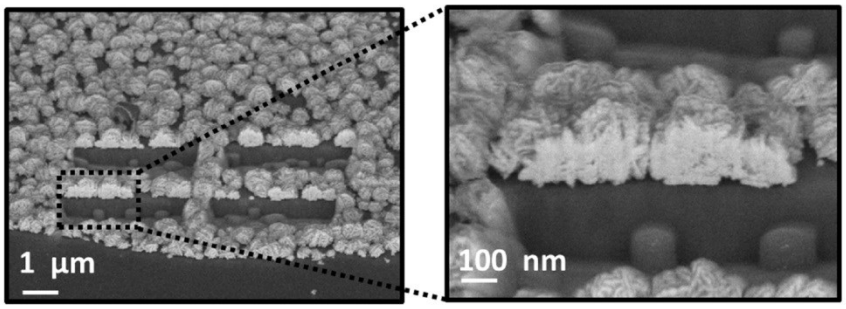

Figure SI-7: Back scatter electron image of the FIB cuts investigating oxizidized silver nanoparticles after 7 days of storage at ambient conditions. Silver nanoparticles are stored in ambient room conditions for 7 days after the production. Focused ion beam (FIB) cuts are done at a tilting angle of 55°. By analyzing the recorded the back scatter electron images, a clear contrast difference between the outer and the inner part of the nanoparticles is visible due to the oxidization of the outer part (darker) compared to the inner part (brighter) of the nanostructures.

4.3 Hierarchically designed 3D flower-like composite nanostructures as an ultra-stable, reproducible and sensitive SERS substrate [SY3]

Sezin Yüksel*, Mario Ziegler*, Sebastian Goerke, Uwe Hübner, Karina Weber, Dana Cialla-May, Peter Schaaf, Hans Georg Meyer, Jürgen Popp

ACS Applied Material& Interfaces, 2017, **9**, p. 38854-388662
DOI: 10.1021/acsami.7b14833

*both authors contributed equally

Autorenschaft der Publikation

Sezin Yüksel	*Concept development* *Experimental design* *Raman measurements* *Data analysis and interpretation* *Writing the manuscript*
Mario Ziegler	*Concept development* Experimental design ALD deposition Data analysis and interpretation Writing the manuscript
Sebastian Goerke	Experimental design Proof reading of manuscript
Uwe Hübner	Proof reading of manuscript
Karina Weber	Discussion of experimental concept and results Proofreading of manuscript
Dana Cialla-May	Discussion of experimental concepts and results Proof reading of manuscript
Peter Schaaf	Project management Discussion of concepts and results Proof reading of manuscript
Hans-Georg Meyer	Project management Discussion of concepts and results Proof reading of manuscript
Jürgen Popp	Project management Discussion of concepts and results Proof reading of manuscript

*both authors contributed equally

Erklärung zu den Eigenanteilen der Promovendin sowie der weiteren Doktoranden/ Doktorandinnen als Koautoren an der Publikation und Zweitpublikationsrechten bei einer kumulativen Dissertation

Publication:

S. Yüksel*, M. Ziegler*, S. Goerke, U. Hübner, K. Weber, D. Cialla-May, P. Schaaf, H. G. Meyer and J. Popp

Hierarchically designed 3D flower-like composite nanostructures as an ultra-stable, reproducible and sensitive SERS substrate

***ACS Applied Material& Interfaces*, 2017, 9, p. 38854-388662**

Beteiligt an		
	Sezin Yüksel	Mario Ziegler
Konzeption des Forschungsansatzes	**X**	**X**
Planung der Untersuchungen	**X**	**X**
Datenerhebung	**X**	**X**
Datenanalyse und -interpretation	**X**	**X**
Schreiben des Manuskripts	**X**	**X**
Vorschlag Anrechnung Publikationsäquevalente	**1.0**	**1.0**

*both authors contributed equally

ACS APPLIED MATERIALS & INTERFACES

Research Article

Cite This: ACS Appl. Mater. Interfaces 2017, 9, 38854-38862

www.acsami.org

Hierarchically-Designed 3D Flower-Like Composite Nanostructures as an Ultrastable, Reproducible, and Sensitive SERS Substrate

Sezin Yüksel,[†,‡,§,⊥] Mario Ziegler,[†,∥,⊥] Sebastian Goerke,[†] Uwe Huebner,[†] Karina Weber,[†,‡,§] Peter Schaaf,[∥] Hans-Georg Meyer,[†] Dana Cialla-May,[*,†,‡,§] and Jürgen Popp[†,‡,§]

[†]Leibniz Institute of Photonic Technology Jena (IPHT), Albert-Einstein-Straße 9, 07745 Jena, Germany

[‡]Institute of Physical Chemistry and Abbe Center of Photonics, Friedrich Schiller University Jena, Helmholtzweg 4, 07743 Jena, Germany

[§]InfectoGnostics Forschungscampus Jena, Zentrum für Angewandte Forschung, Philosophenweg 7, 07743 Jena, Germany

[∥]Department of Electrical Engineering and Information Technology, Institute of Materials Science and Engineering and Institute of Micro and Nanotechnologies MacroNano, TU Ilmenau, Gustav-Kirchhoff-Str. 5, 98693 Ilmenau, Germany

Supporting Information

ABSTRACT: Surface-enhanced Raman spectroscopy (SERS) is an attractive tool in the analytical sciences due to its high specificity and sensitivity. Because SERS-active substrates are only available as two-dimensional arrays, the fabrication of three-dimensional (3D) nanostructures allows for an increased number of hot spots in the focus volume, thus further amplifying the SERS signal. Although a great number of fabrication strategies for powerful SERS substrates exist, the generation of 3D nanostructures with high complexity and periodicity is still challenging. For this purpose, we report an easy fabrication technique for 3D nanostructures following a bottom-up preparation protocol. Enzymatically generated silver nanoparticles (EGNPs) are prepared, and the growth of hierarchically-designed 3D flower-like silica−silver composite nanostructures is induced by applying plasma-enhanced atomic layer deposition (PE-ALD) on the EGNPs. The morphology of these nanocomposites can be varied by changes in the PE-ALD cycle number, and a flower height of up to 10 μm is found. Moreover, the metallized (e.g., silver or gold) 3D nanostructures resulting from 135 PE-ALD cycles of silica creation provide highly reproducible SERS signals across the hydrophobic surface. Within this contribution, the morphological studies, optical properties, as well as the SERS response of these metallized silica−silver composite nanostructures applying vitamin B2 as a model analyte are introduced.

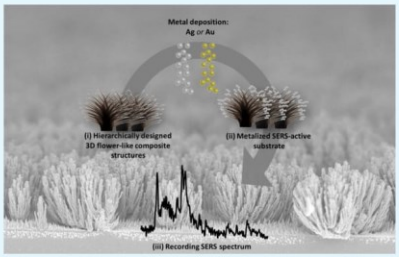

KEYWORDS: *3D flower-like silica−silver nanostructures, hybrid materials, PE-ALD, SERS templates, SERS substrates, riboflavin (vitamin B2)*

INTRODUCTION

One of the best technological benefits arising from metallic nanoparticles is their extraordinary optical properties that allow for plasmon-induced high field intensities in the near field, which can be combined with spectroscopic techniques for the detection of trace amounts of molecular substances. Surface-enhanced Raman spectroscopy (SERS), as one of these technologies, benefits not only from its high molecular specificity and sensitivity, but also from its rapid response and applicability in diverse research areas, including medicine, environmental monitoring, and trace-level chemical analysis.[1−16]

The SERS effect greatly depends on the optical properties of the plasmonic material, i.e., meeting the plasmon resonance condition.[3] Thus, morphological parameters, such as the size, shape, and composition of the metallic nanostructures, as well as the dielectric constant of the surrounding medium, play a key role in influencing the optical properties, e.g., electromagnetic field enhancement, and thus, the overall SERS intensity. Conventional one-dimensional and two-dimensional SERS substrates can be limited in detecting small and nonresonant organic molecules due to the poor controllability of the surface structures and limited number of hot spots in the detection volume.[3,10,17−35] Therefore, hierarchically-designed three-dimensional (3D) SERS substrates have attracted considerable interest due to their strong plasmonic enhancement as well as their well-ordered morphological properties. Furthermore, these 3D metallized nanostructures can offer great advantages by allowing the target molecule to diffuse efficiently and by increasing the number of hot spots in the focus volume to gain

Received: September 29, 2017
Accepted: October 20, 2017
Published: October 20, 2017

DOI: 10.1021/acsami.7b14833
ACS Appl. Mater. Interfaces 2017, 9, 38854−38862

ACS Applied Materials & Interfaces Research Article

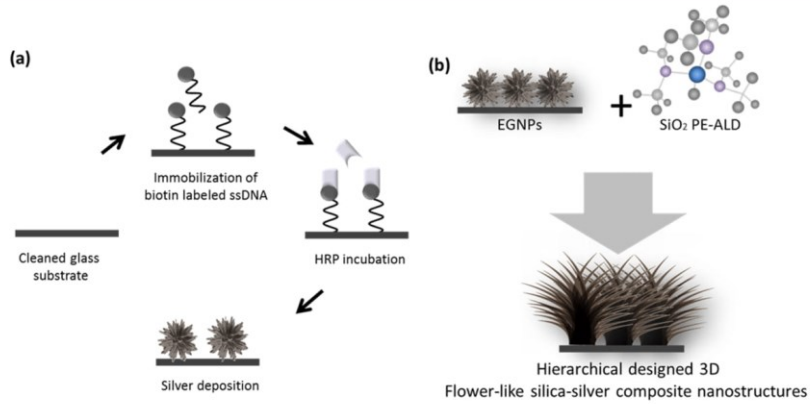

Figure 1. Schematic illustration of the fabrication process of the hierarchically-designed 3D silica composite nanostructures. (a) EGNPs were produced by a bottom-up technique. (b) Various amounts of PE-ALD cycles of SiO_2 creation were applied on the EGNPs.

detection limits down to the sub-nanomolar level. These 3D nanostructured substrates require highly reproducible fabrication methods that keep deviations in the surface morphology and arrangement of nanostructures to a minimum.[3,17] Complex-shaped nanostructures can be fabricated via different bottom-up fabrication techniques. One of the most common fabrication approaches is the seed-mediated growth mechanism where the metallic seeds are added to a growth solution containing metal salts and reducing agents.[36−39] Another fabrication method for nanostructures with various degrees of complexity is the self-assembly of nanoparticles to form regular arrays and clusters via bottom-up fabrication processes, providing cost efficient and simple-to-perform preparation procedures.[3,40] Furthermore, electrodeposition is one of the simplest 3D nanostructure fabrication methods, providing cost-effective, mass-produced nanostructures with freestanding complex geometries.[41−43] Bottom-up fabrication techniques are favorable due to their rapidity and cost-effectiveness; however, they suffer from low reproducibility over different fabricated batches. In contrast, top-down techniques offer precise surface control and high reproducibility across large surface areas in micro- and nanoscale dimensions, but these conventional lithographic techniques are expensive and time consuming.

In this study, we report an alternative, easy, cost-effective, and large-scale fabrication technique to obtain hierarchically-designed 3D flower-like silica−silver composite nanostructures by applying bottom-up fabrication methods. In the first step, enzymatically generated silver nanoparticles (EGNPs) were produced via an enzyme-induced redox reaction. Then, different numbers of plasma-enhanced atomic layer deposition (PE-ALD) cycles (5, 45, 90, 135, and 180 cycles to create SiO_2) were applied on the EGNPs. After applying five PE-ALD cycles on the EGNPs, the physical structure of the silver changed to a porous-like nanostructure. A flower-like nanostructured surface is observable after 45 PE-ALD cycles. Physical characteristics, e.g., size, shape, and pillar size, can be controlled by changing the number of PE-ALD cycles, which create Ag−SiO_2 needles. Because the EGNPs are completely covered with Ag−SiO_2 pillars, these composite nanostructures are not SERS active but provide an ultrastable and reproducible template. To become SERS-active, the composite nanostructured templates were coated with a plasmonic-active metal prior to their application as a SERS substrate. Utilizing the unique nanostructured features, SERS measurements were performed by using vitamin B2 as a model analyte. It was found that the deposition of 50 nm of silver on the composite nanostructured templates (135 PE-ALD cycles of SiO_2 creation) provides a highly reproducible SERS signal along the highly hydrophobic surface (the contact angle of water droplets was found to be up to 120°). Furthermore, point-to-point and batch-to-batch SERS reproducibility was obtained with a relative standard deviation (RSD) between 8.3 and 17.1%. Finally, the limit of detection (LOD) was estimated to be 50 nM by employing B2 as a model analyte. To the best of our knowledge, this is the first report of hierarchically-designed 3D flower-like silica−silver composite nanostructures with high-throughput, large surface area, and an effortless nanofabrication process for use as an efficient and ultrastable SERS template for bioanalytical applications.

MATERIALS AND METHODS

Chemicals and Reagents. Glass substrates were obtained from Carl Roth GmbH (Karlsruhe, Germany). Biotin-labeled single-stranded DNA (ssDNA) was purchased from Eurofins MWG Operon (Ebersberg, Germany), and riboflavin was obtained from Sigma-Aldrich (Steinheim, Germany). To perform the SERS measurements, a 10 μM methanolic stock solution of riboflavin was prepared and diluted to the desired concentrations.

Fabrication of Hierarchically-Designed 3D Flower-Like Silver−Silica Composite Nanostructures. Hierarchically-designed 3D flower-like silica−silver composite nanostructures were fabricated by an easy two-step process by utilizing a bottom-up preparation protocol for enzymatically generated silver nanoparticles, followed by various cycles of SiO_2 deposition by plasma-enhanced atomic layer deposition (see Figure 1).

In the first step, EGNPs were fabricated via an enzymatically induced redox reaction described previously (see Figure 1a).[44−46] First, biotin-labeled single-stranded DNA (ssDNA) was immobilized onto a precleaned glass substrate as a linker molecule. Afterwards, a streptavidin−horseradish peroxidase (HRP) complex was bound to

DOI: 10.1021/acsami.7b14833
ACS Appl. Mater. Interfaces 2017, 9, 38854−38862

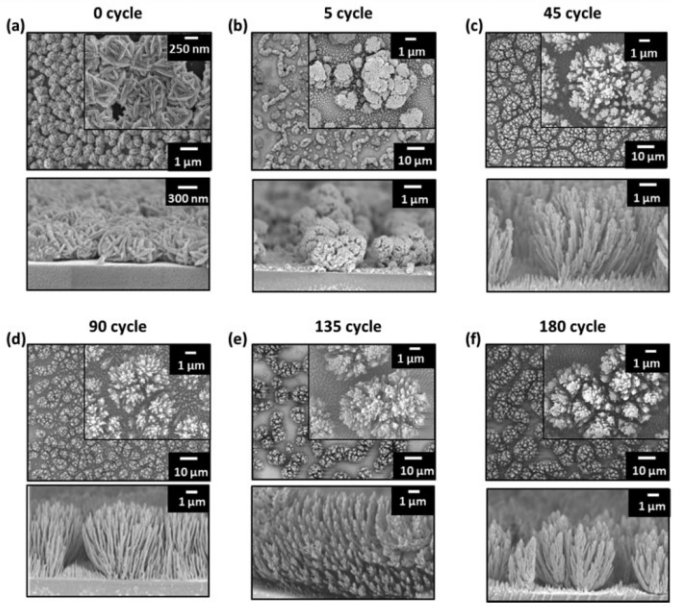

Figure 2. SEM images of the EGNPs and 3D flower-like nanostructures. High-resolution scanning electron microscopy of (a) the EGNPs and after (b) 5 cycles, (c) 45 cycles, (d) 90 cycles, (e) 135 cycles, and (f) 180 cycles of SiO_2 deposition by PE-ALD on the EGNPs.

the immobilized ssDNA. Then, the preparation of EGNPs was catalyzed by HRP via a redox reaction by using an EnzMet kit from Nanoprobes Inc. (Yaphank, NY). Finally, "desert-rose-like" silver nanoparticles were formed. The redox reaction was stopped by rinsing the substrates with distilled water, and the substrates were dried in a stream of compressed air.

Plasma-Enhanced Atomic Layer Deposition. In the second step, SiO_2 layers were applied on the EGNPs by employing different numbers of PE-ALD cycles (5, 45, 90, 135, and 180 cycles) at an operating temperature of 120° (see Figure 1b). A PE-ALD reactor OpAL (Oxford Plasma Technology, Bristol, U.K.) built in shower head configuration and equipped with a double-stage rotary vane pump as well as an inductively coupled plasma source was used. In ALD, the shower head configuration was used. The entire process was performed under vacuum conditions with a base pressure of 2 mTorr.

Under the selected conditions, the growth per cycle (GPC) was saturated at 1.11 Å per cycle. The GPC was calculated by the deposited film thickness divided by the corresponding cycle number. To measure the film thickness, silica was deposited on a standard flat boron-doped silicon chip as reference. Afterwards, spectroscopic ellipsometry (J.A. Woollam Co., Nebraska), equipped with a light source ranging from 246 to 1600 nm, was applied. The ellipsometric model was validated by a profilometer (Veeco Dektak 8, New York). Film thicknesses smaller than 5 nm were estimated using the linear dependency of the film thickness on the film growth per cycle.[47,48]

Morphological Investigation. Scanning electron microscopy (SEM) measurements were performed using a JEOL 6700FM SEM high-resolution field emission scanning electron microscope (JEOL Ltd., Tokyo, Japan), applying a 1−20 keV accelerating voltage.

Silver Deposition. Silver thin films were deposited using a Roth & Rau Microsys 200 system (Meyer Burger AG, Germany) designed for thermal evaporation. A high-purity silver target was vaporized, and the thickness was measured using a quartz crystal microbalance (QCM). The QCM was calibrated by determining the tooling factor right before the silver deposition. For this purpose, 100 nm of silver was deposited onto a 4 in. wafer and the thickness was verified at well-defined steps using a profilometer (Veeco Instruments Inc., Munich, Germany).

Raman Measurements. The SERS substrates were incubated in the riboflavin stock solution for 30 min and dried under a stream of air. SERS measurements were carried out using a confocal Raman microscope (WITec GmbH, Ulm, Germany), equipped with a 488 nm excitation laser line. A 100× objective (NA 0.8) was applied to illuminate the sample as well as to collect the backscattered light. The spectra were recorded with a spectrometer, equipped with a 600 lines/mm grating and a 1024 × 127 pixel charge-coupled device camera, cooled to 208 K. The SERS spectra were measured by scanning a 25 × 25 μm^2 area with an integration time of 0.2 s, recording 400 spectra in a total time of 80 s.

■ RESULTS AND DISCUSSION

To illustrate the morphology of the prepared nanostructures, SEM images were recorded. The results are illustrated in Figure 2. As the initial structure, EGNPs were examined, and their spiky and sharp surface morphology is illustrated in Figure 2a. The particle size is approximately 400 nm. It can also be seen that the EGNPs are closely packed. Because of the fast oxidation of silver, we initially planned to create a silica-based protection layer on top of the EGNPs. Thus, an improved shelf-life of the SERS-active nanostructures was expected, as is reported in the literature.[44,49−51] However, as shown in Figure 2b, after five PE-ALD cycles of SiO_2 creation, the morphological properties of the EGNPs changed to round-shaped aggregated porous composite nanostructures with sizes

DOI: 10.1021/acsami.7b14833
ACS Appl. Mater. Interfaces 2017, 9, 38854−38862

between 1 and 4 μm. These structures were created due to the metastable behavior of silver under the ALD deposition conditions, and the related study is already published by our work group.[52] In this study, we used EGNPs due to the fine and rough surface of the silver, where the silver surface quickly oxidizes within the oxygen plasma, which causes a metastable silver oxide substrate for a short period of time. During the oxygen-plasma step, which is associated with a higher energy as well as a higher pressure (300 W and 160 mTorr) during the PE-ALD process, the silver surface of the EGNPs is oxidized, resulting in exposed cracks on the EGNP surface and the creation of sponge-like nanostructures. This phenomenon was already observed by Ross and co-workers.[53] Here, silver(I) oxidizes to silver(II) oxide when a low energy plasma at 130 W and 75 mTorr is employed. After applying tris(dimethylamino)-silane (TDMAS) during the PE-ALD step, the previously formed silver oxide (during exposure with oxygen plasma) decomposed to elemental silver due to the operating temperature (120 °C) within the PE-ALD process. The released oxygen enhances the silica deposition and leads to the generation of hierarchically-designed 3D hybrid nanostructures. By repeating the PE-ALD step, which is the interaction between the newly created metastable surface and the highly reactive precursor TDMAS, uncontrollable side-reactions near the surface occur. Thus, more fractal-like and more branched flower-like nanostructures were generated by increasing the number of PE-ALD cycles. Figure 2c–f shows the SEM images of the various fabricated nanostructures. As shown in the images, after applying 45 PE-ALD cycles, flower-like structures were grown. The size of the nanostructures increased from 600 nm initially to 12 μm for the structures formed after 90 PE-ALD cycles of SiO_2 creation. An increase in the amount of PE-ALD cycles results in a decrease in the pillar diameter and an increase in the size of the features. On the basis of these experiments, it was concluded that a large variety of 3D silica–silver composite nanostructures can be produced on a large scale by combining two bottom-up processes, i.e., the enzymatically driven fabrication of silver nanostructures to create EGNPs and the deposition of SiO_2 by PE-ALD.

Three-Dimensional Flower-Like Silver–Silica Composite Nanostructures as Templates for SERS Substrates. The controlled size and shape of the flower-like composite nanostructures are considered to be advantageous for SERS applications. Here, these structures are applied as templates for SERS substrates, which is beneficial due to their long shelf-life based on the stability of SiO_2. Furthermore, the possibility of depositing various metals, such as silver, gold, copper, and platinum, allows one to obtain the desired excitation wavelength, and thus, this unique characteristic extends the applicability of SERS in various research fields. Even though the starting point to fabricate 3D flower-like composite nanostructures is the EGNPs, the pure composite nanostructures are not SERS active. Hence, to record SERS spectra, the deposition of an additional plasmonic material on top of these SERS templates is required.

Figure 3 shows a schematic illustration of the 3D flower-like silica–silver nanostructures as an ultrastable SERS template. Various nanostructures, resulting from 5, 45, 90, 135, and 180 PE-ALD cycles of SiO_2 creation (Figure 3a), were fabricated, and 4 nm of silver was thermally evaporated onto the structures for SERS measurement (Figure 3b). To define the optimized nanostructure to obtain the highest SERS activity, 10 μM riboflavin (vitamin 2) in methanol was used as model analyte

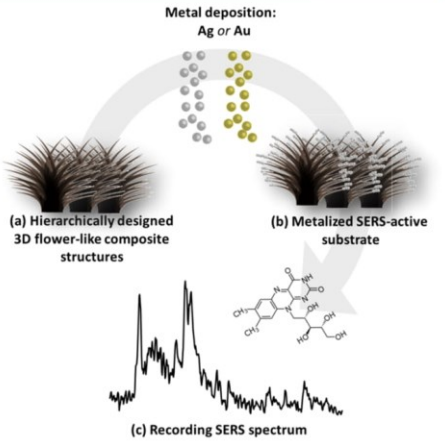

Figure 3. Schematic illustration of the hierarchically-designed 3D flower-like silica–silver composite nanostructure as a SERS template. (a) Hierarchically-designed 3D flower-like silica–silver composite nanostructures were fabricated using a varied number of PE-ALD cycles. (b) Plasmonic materials like silver and gold can be coated on the nanostructures to create a powerful SERS substrate. (c) The SERS spectra of 10 μM riboflavin in methanol can be recorded by employing the metallized template structures.

for SERS characterization (Figure 3c). Furthermore, riboflavin is biologically essential for living organisms where a deficiency of vitamin B2 may result in eye fatigue, extreme unusual sensitivity to light, digestive problems, and a form of anemia.[54] Figure 4a shows the recorded SERS spectra of 10 μM riboflavin using various composite nanostructures as SERS templates with an additional 4 nm of deposited silver.

The Raman modes characteristic of riboflavin at 1625, 1402, 1347, and 1312 cm^{-1}, which are related to ν(C–C), $\delta(CH_3)$, aromatic ring vibration, and δ(C–H) vibrational modes, respectively,[55,56] were reliably detected with all SERS templates. A complete band assignment can be found in the literature, accordingly.[55,56] However, it can be seen that the SERS template fabricated by employing 45 PE-ALD cycles of SiO_2 deposition possessed a lower SERS activity. To analyze which SERS template allows the highest SERS performance, the ν(C–C) vibrational mode of the benzene ring of riboflavin at 1625 cm^{-1} was integrated, normalized, and plotted as a function of the number of PE-ALD cycles.[44] The normalized integrated SERS intensity at 1625 cm^{-1} for various nanostructures based on 45, 90, 135, and 180 PE-ALD cycles has relative standard deviations (RSDs) of 32.3, 15.2, 14.7, and 17.4%, respectively. It is clearly visible that the SERS intensity of the silica–silver composite nanostructure employing 135 PE-ALD cycles to create SiO_2 pillars exhibited the highest SERS intensity with an RSD of 14.7%. Moreover, the morphological stability of this hybrid nanostructure was analyzed by SEM. Figure S1a–d shows the SEM and the focused ion beam images of the hybrid nanostructures. It is clearly visible that the EGNPs, which were used as a template, comprise the core of the hybrid nanostructure whereas the needles are formed of silver–silica composite material. Due to the composite material of silver and

DOI: 10.1021/acsami.7b14833
ACS Appl. Mater. Interfaces 2017, 9, 38854–38862

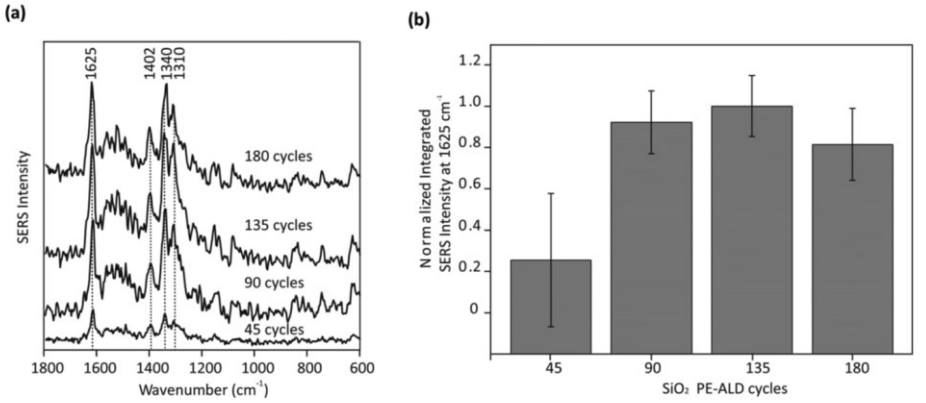

Figure 4. (a) SERS spectra of 10 μM riboflavin detected by 3D hierarchically-designed flower-like silica−silver nanostructures. (b) Normalized integrated SERS intensity at 1625 cm^{-1} vs various nanostructures based on a different number of PE-ALD cycles to create SiO_2.

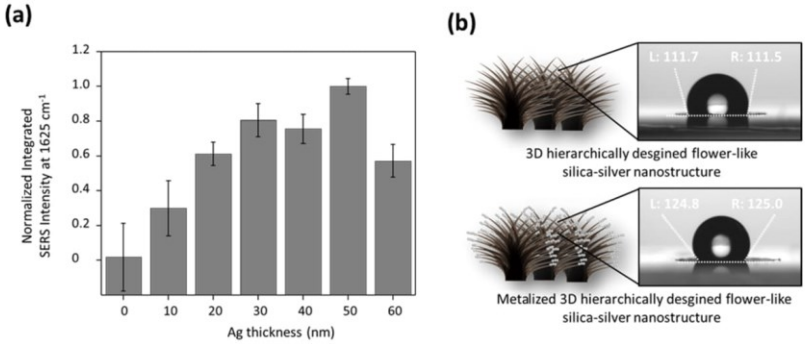

Figure 5. (a) Integrated SERS intensity of the template fabricated after 135 PE-ALD cycles as a function of silver deposition. (b) Contact angle measurement of the nonmetalized and silver-deposited composite nanostructures (based on 135 PE-ALD cycles of SiO_2 creation).

silica, the hybrid nanostructures are stable under ambient conditions (see Figure S1d). It was observed that there was no physical deformation of the fabricated SERS template, which was stable for at least 1 year of storage under ambient conditions. A desired silver deposition can be applied on these 3D hybrid nanostructures to activate the SERS properties (see Figure S1c). Furthermore, the detailed growth theory of these nanostructures and the formation of these branches has already been published by our group.[52]

To reflect these results, further experiments were carried out by applying the nanostructure resulting from 135 PE-ALD cycles as an ultrastable SERS template.

The controlled size and shape of the flower-like nanostructures resulting from 135 PE-ALD cycles were considered to provide the highest SERS performance for bioanalytical detection. To estimate the optimal silver deposition to obtain the highest possible SERS signal, several silver thicknesses (0, 10, 20, 30, 40, 50, and 60 nm) were deposited on the structure. Figure 5a shows the SERS intensity of riboflavin plotted as a function of the applied nanostructure, i.e., templates based on 135 PE-ALD cycles coated with different silver thicknesses. Again, the Raman band characteristic of riboflavin at 1625 cm^{-1} was integrated and normalized. The intensity was plotted as a function of silver deposition thickness. The SERS intensity without silver deposition and with silver deposition of 10, 20, 30, 40, 50, and 60 nm has RSDs of 19.5, 15.7, 6.6, 9.6, 8.3, 4.5, and 9.4%, respectively. It can be clearly observed that the pure structures without additional silver deposition show no Raman response (see Figure S2). Thus, the SERS signal of the pure hybrid nanostructure does not interfere with the SERS signal of the target analyte due to the background-free SERS spectra. Moreover, Figure S3 shows the SEM images representing different thicknesses of silver (0, 10, 20, 30, 40, 50, and 60 nm Ag) deposited on the hierarchically-designed 3D flower-like composite nanostructures. It is observable that up to 50 nm silver deposition, the tips and the branches of the nanostructure are clearly separated and freestanding. However, applying 60 nm silver deposition results in a leaning of the tips and

DOI: 10.1021/acsami.7b14833
ACS Appl. Mater. Interfaces 2017, 9, 38854−38862

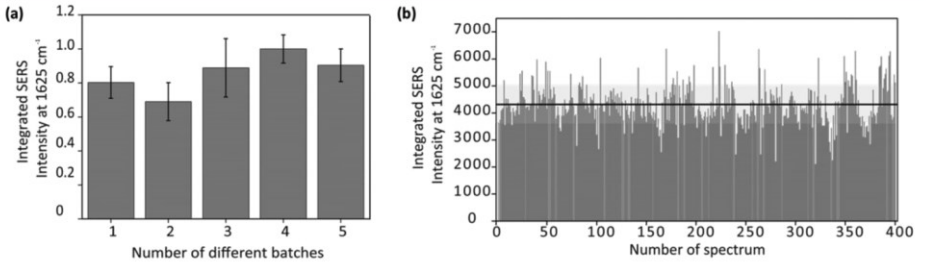

Figure 6. (a) Batch-to-batch SERS reproducibility and (b) point-to-point SERS reproducibility of our applied SERS substrate (fabricated by employing 135 PE-ALD cycles and 50 nm silver deposition).

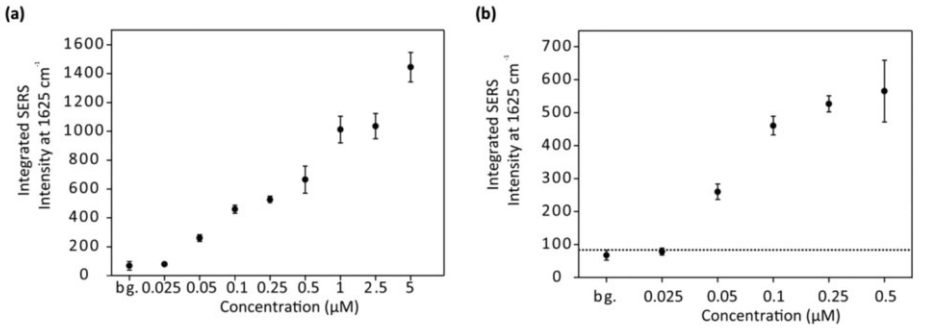

Figure 7. (a) Integrated SERS intensity of the peak at 1625 cm^{-1} vs different concentrations of riboflavin employing the SERS-active nanocomposite substrate (135 PE-ALD cycles, 50 nm silver deposition). (b) Magnified image of the low concentration range. The LOD is illustrated by the dashed line. The error bars are illustrated at a 3σ confidence level of the data points.

branches. Therefore the analyte molecules cannot occupy the hot spots efficiently, which is associated with a lower SERS intensity. It was found that the 50 nm silver-deposited nanostructure exhibited the highest SERS intensity and the lowest RSD compared to that of the 60 nm silver-deposited nanostructures. This can be explained by a homogenous distribution of silver nanoparticles across the branches as well as optimized conditions for sufficient enhancement of the Raman signals. For further investigations, 50 nm silver-deposited nanostructures (135 PE-ALD cycles) were used.

Moreover, due to the exceptional morphology of the flower-like template, hydrophobic surface characteristics were expected. These are advantageous over common hydrophilic SERS substrates when investigating water-insoluble analytes solvated in organic solvents. Thus, the interaction of the water-insoluble analytes with the metallic surface could be improved, and the SERS signal could be further amplified because more molecules are in the near field of the plasmonic surface. Consequently, a number of research studies have been published to generate hydrophobic surfaces.[49,57−61] One common surface functionalization to achieve hydrophobic surfaces is by combining micro/nanostructures using top-down techniques, such as lithography and plasma treatment.[50,62−64] However, these techniques require complex preparation steps and are often expensive and time consuming. The hierarchically-designed 3D flower-like silica−silver composite nanostructures presented in this study not only function as SERS templates but also provide highly hydrophobic surfaces, which were investigated through contact angle measurements of the nonmetalized composite nanostructure (135 PE-ALD cycles) and the 50 nm silver metallized composite nanostructure depicted in Figure 5b. A remarkable difference between the measured contact angles for the SERS template without metal deposition and the silver-deposited SERS template is visible. For the nonmetallized template, the contact angle is approximately 111°, whereas after silver deposition, it increases to 120°. This hydrophobic behavior of the substrate provides an excellent SERS platform for analytes solvated in organic solvents.

Batch-to-Batch and Point-to-Point SERS Reproducibility. Even though SERS-based techniques offer huge potential in bioapplications due to their high molecular fingerprint specificity and potential single molecule sensitivity, SERS intensity suffers from poor batch-to-batch and array-to-array or point-to-point reproducibility. During the preparation of the nanostructures, large deviations in SERS intensity can be observed due to the inhomogeneous distribution of metal nanoparticles. Thus, quantitative analysis or on-line monitoring employing the plasmonic substrates would be hampered due to the low reproducibility of the SERS signal. To illustrate the batch-to-batch reproducibility, several different batches of SERS templates (fabricated with 135 PE-ALD cycles of SiO_2

DOI: 10.1021/acsami.7b14833
ACS Appl. Mater. Interfaces 2017, 9, 38854−38862

creation) with an additional 50 nm of silver deposition were prepared. Figure S4 shows the SEM images with lower magnification of the SERS template. It is clearly visible from Figure S4 that the nanostructures are homogenously covered on the surface. The SERS reproducibility measurements were performed by randomly taking 10 different measurement areas with dimensions of 25 × 25 μm^2 and recording 400 SERS spectra (see Figure S4a). Moreover, the standard deviation was calculated based on using the average signal from scans resulting in a better standard deviation due to averaging across the surface. The SERS substrate was incubated in a 10 μM methanolic solution of riboflavin for 30 min and dried with a stream of air. The Raman mode characteristic of riboflavin at 1625 cm^{-1} was integrated and plotted versus the number of applied batches (see Figure 6a). The RSDs of the five different batches were between 8.3 and 17.2%. Likewise, as for the batch-to-batch analysis, the Raman mode at 1625 cm^{-1} of 400 individual spectra recorded for one substrate was integrated and plotted as a function of the spectral number to illustrate the point-to-point reproducibility (see Figure 6b). The RSD of the SERS intensity was 16%, which is highlighted by the light gray area. These investigations reveal the high point-to-point and batch-to-batch SERS reproducibility of our fabricated composite nanostructures.

Determining the Sensitivity of the Hierarchically-Designed 3D Flower-Like Silica−Silver Composite Nanostructures. To estimate the applicability to trace analytics, the SERS-active substrates were incubated with methanolic solutions of riboflavin down to sub-micrometer concentrations, and the LOD was calculated. In Figure S5 (Supporting Information), the average SERS spectra of riboflavin for the lowest concentration, as well as the background contribution, are depicted. The quantitative relation between the integrated SERS intensity at 1625 cm^{-1} and the riboflavin concentration is illustrated in Figure 7a,b. Riboflavin was detected in the range of 5−0.025 μM (see Figure 7a). For better visibility, Figure 7b presents the integrated SERS intensity at 1625 cm^{-1} over the low concentration range between 0.025 and 0.5 μM. The SERS background signal of the substrate, abbreviated as bg., illustrates that no signal from the substrate itself interferes with the analyte signal. To determine the LOD and to maintain a 99.8% confidence level of the data points, 3 times the standard deviation (3σ) was added to the blank value, according to the IUPAC definition, to set a threshold, which is shown as a black dashed line (see Figure 7b). Comparison of the data with the LOD proves that by employing the 3D ultrastable SERS template as a sensor platform, riboflavin can reliably be detected down to a concentration of 50 nM. In comparison to the pure EGNPs applied as SERS substrate for the detection of riboflavin,[44] the LOD value is improved from 200 to 50 nM. This is attributed to the fact that in the case of pure EGNPs, an inhomogeneous layer of redox products from the fabrication is present. The 3D flower-like silica−silver composite nanostructures exhibit a background-free SERS signal. Thus, a 4 times better reliable quantitative detection was achieved by employing hierarchically-designed 3D flower-like silica−silver composite nanostructures.

■ CONCLUSIONS

The fabrication process of ultrastable hierarchically-designed 3D flower-like silica−silver composite nanostructures was illustrated. The process combines the bottom-up synthesis of enzymatically generated silver nanoparticles with plasma-enhanced atomic layer deposition to create SiO_2 pillars. This simple two-step fabrication method significantly reduces the processing time and allows for the cost-effective batch production of consumable template substrates with a high structural variability without using any complex conventional lithography processes. The fabrication method is an efficient, simple, and fast way to assemble geometrically complex nanoparticles into a 3D architecture with high physical stability under ambient conditions. The drawback of this technique is that cleanroom facilities are needed for the fabrication of these nanostructures. However, once the template is formed, the hierarchically-designed nanostructures can be stored under ambient conditions and additional silver deposition can be applied without any cleanroom facilities. The morphology of the nanostructures can be controlled by simply tuning the number of PE-ALD cycles for SiO_2 creation. Flower-like branched nanostructures started to form after 45 PE-ALD cycles. The investigated nanostructures do not show any background Raman contribution, making them ideal templates, where the plasmonic material can be modified by employing different evaporation techniques. In our study, silver was applied as the enhancing metal, and excellent point-to-point as well as batch-to-batch reproducibility was presented. By applying these 3D SERS template platforms to a SERS-based detection scheme, riboflavin was quantitatively detected in trace concentrations down to 50 nM.

■ ASSOCIATED CONTENT

Supporting Information

The Supporting Information is available free of charge on the ACS Publications website at DOI: 10.1021/acsami.7b14833.

Additional information about the morphological and spectroscopic characteristics of the hierarchically-designed 3D flower-like composite nanostructures (PDF).

■ AUTHOR INFORMATION

Corresponding Author

*E-mail: dana.cialla-may@leibniz-ipht.de. Tel: +49 (0)3641-206309. Fax: +49 (0)3641-206399.

ORCID

Dana Cialla-May: 0000-0002-8577-1490

Author Contributions

⊥S.Y. and M.Z. contributed equally to this article.

Notes

The authors declare no competing financial interest.

■ ACKNOWLEDGMENTS

Funding of the research projects "JBCI 2.0" (03IPT513Y) within the framework "Unternehmen Region - InnoProfile Transfer" by the Federal Ministry of Education and Research, Germany (BMBF), is gratefully acknowledged. The work is also partly supported by the Deutsche Forschungsgemeinschaft (DFG grant Scha 632/24).

■ REFERENCES

(1) Cialla, D.; März, A.; Bohme, R.; Theil, F.; Weber, K.; Schmitt, M.; Popp, J. Surface-Enhanced Raman Spectroscopy (SERS): Progress and Trends. *Anal. Bioanal. Chem.* **2012**, *403*, 27−54.

(2) Cialla, D.; Pollok, S.; Steinbrücker, C.; Weber, K.; Popp, J. SERS-based Detection of Biomolecules. *Nanophotonics* **2014**, *3*, 383−411.

DOI: 10.1021/acsami.7b14833
ACS Appl. Mater. Interfaces 2017, 9, 38854−38862

(3) Jahn, M.; Patze, S.; Hidi, I. J.; Knipper, R.; Radu, A. I.; Muhlig, A.; Yuksel, S.; Peksa, V.; Weber, K.; Mayerhofer, T.; Cialla-May, D.; Popp, J. Plasmonic Nanostructures for Surface Enhanced Spectroscopic Methods. *Analyst* **2016**, *141*, 756−793.
(4) Pahlow, S.; März, A.; Seise, B.; Hartmann, K.; Freitag, I.; Kämmer, E.; Böhme, R.; Deckert, V.; Weber, K.; Cialla, D.; Popp, J. Bioanalytical Application of Surface- and Tip-enhanced Raman Spectroscopy. *Eng. Life Sci.* **2012**, *12*, 131−143.
(5) Schlücker, S. Surface-enhanced Raman Spectroscopy: Concepts and Chemical Applications. *Angew. Chem., Int. Ed.* **2014**, *53*, 4756−4795.
(6) Larmour, I. A.; Graham, D. Surface enhanced optical Spectroscopies for Bioanalysis. *Analyst* **2011**, *136*, 3831−3853.
(7) Moskovits, M. Surface-enhanced Raman Spectroscopy: a brief Retrospective. *J. Raman Spectrosc.* **2005**, *36*, 485−496.
(8) Sharma, B.; Frontiera, R. R.; Henry, A.-I.; Ringe, E.; Van Duyne, R. P. SERS: Materials, Applications, and the Future. *Mater. Today* **2012**, *15*, 16−25.
(9) Zhou, Q.; Kim, T. Review of Microfluidic Approaches for Surface-enhanced Raman Scattering. *Sens. Actuators, B* **2016**, *227*, 504−514.
(10) Betz, J. F.; Yu, W. W.; Cheng, Y.; White, I. M.; Rubloff, G. W. Simple SERS Substrates: Powerful, Portable, and full of Potential. *Phys. Chem. Chem. Phys.* **2014**, *16*, 2224−2239.
(11) Lane, L. A.; Qian, X.; Nie, S. SERS Nanoparticles in Medicine: From Label-Free Detection to Spectroscopic Tagging. *Chem. Rev.* **2015**, *115*, 10489−10529.
(12) Luo, S. C.; Sivashanmugan, K.; Liao, J. D.; Yao, C. K.; Peng, H. C. Nanofabricated SERS-active Substrates for Single-Molecule to Virus Detection in vitro: a Review. *Biosens. Bioelectron.* **2014**, *61*, 232−240.
(13) Kumar, G. V. P. Plasmonic Nano-Architectures for surface enhanced Raman Scattering: a Review. *J. Nanophotonics* **2012**, *6*, No. 064503.
(14) Wang, Y.; Yan, B.; Chen, L. SERS tags: Novel Optical Nanoprobes for Bioanalysis. *Chem. Rev.* **2013**, *113*, 1391−1428.
(15) Yamamoto, Y. S.; Ishikawa, M.; Ozaki, Y.; Itoh, T. Fundamental Studies on Enhancement and Blinking mechanism of surface-enhanced Raman Scattering (SERS) and basic Applications of SERS biological Sensing. *Front. Phys.* **2014**, *9*, 31−46.
(16) Cialla, D.; Hubner, U.; Schneidewind, H.; Moller, R.; Popp, J. Probing innovative Microfabricated Substrates for their reproducible SERS Activity. *ChemPhysChem* **2008**, *9*, 758−762.
(17) Wang, A. X.; Kong, X. Review of Recent Progress of Plasmonic Materials and Nano-Structures for Surface-Enhanced Raman Scattering. *Materials* **2015**, *8*, 3024−3052.
(18) Lin, X. M.; Cui, Y.; Xu, Y. H.; Ren, B.; Tian, Z. Q. Surface-enhanced Raman Spectroscopy: Substrate-related Issues. *Anal. Bioanal. Chem.* **2009**, *394*, 1729−1745.
(19) Stoerzinger, K. A.; Lin, J. Y.; Odom, T. W. Nanoparticle SERS substrates with 3D Raman-active Volumes. *Chem. Sci.* **2011**, *2*, 1435−1439.
(20) Bantz, K. C.; Meyer, A. F.; Wittenberg, N. J.; Im, H.; Kurtulus, O.; Lee, S. H.; Lindquist, N. C.; Oh, S. H.; Haynes, C. L. Recent Progress in SERS Biosensing. *Phys. Chem. Chem. Phys.* **2011**, *13*, 11551−11567.
(21) Sharma, B.; Fernanda Cardinal, M.; Kleinman, S. L.; Greeneltch, N. G.; Frontiera, R. R.; Blaber, M. G.; Schatz, G. C.; Van Duyne, R. P. High-performance SERS Substrates: Advances and Challenges. *MRS Bull.* **2013**, *38*, 615−624.
(22) Yang, L.; Liab, P.; Liuab, J. Progress in Multifunctional Surface-enhanced Raman Scattering Substrate for Detection. *RSC Adv.* **2014**, *4*, 49635−49646.
(23) Giner-Casares, J. J.; Liz-Marzán, L. M. Plasmonic Nanoparticles in 2D for biological Applications: Toward active multipurpose Platforms. *Nano Today* **2014**, *9*, 365−377.
(24) Fateixa, S.; Nogueira, H. I. S.; Trindade, T. Hybrid Nanostructures for SERS: Materials Development and Chemical Detection. *Phys. Chem. Chem. Phys.* **2015**, *17*, 21046−21071.
(25) Shiohara, A.; Wang, Y.; Liz-Marzán, L. M. Recent Approaches toward Creation of Hot Spots for SERS Detection. *J. Photochem. Photobiol., C* **2014**, *21*, 2−25.
(26) Golightly, R. S.; Doering, W. E.; Natan, M. J. Surface-Enhanced Raman Spectroscopy and Homeland Security: A Perfect Match? *ACS Nano* **2009**, 2859−2869.
(27) Fan, M.; Andrade, G. F.; Brolo, A. G. A Review on the Fabrication of Substrates for Surface Enhanced Raman Spectroscopy and their Applications in Analytical Chemistry. *Anal. Chim. Acta* **2011**, *693*, 7−25.
(28) Tripp, R. A.; Dluhy, R. A.; Zhao, Y. P. Novel Nanostructures for SERS Biosensing. *Nano Today* **2008**, *3*, 31−37.
(29) Lal, S.; Grady, N. K.; Kundu, J.; Levin, C. S.; Lassiter, J. B.; Halas, N. J. Tailoring Plasmonic Substrates for Surface Enhanced Spectroscopies. *Chem. Soc. Rev.* **2008**, *37*, 898−911.
(30) Brown, R. J. C.; Milton, M. J. T. Nanostructures and Nanostructured Substrates for Surface-enhanced Raman Scattering (SERS). *J. Raman Spectrosc.* **2008**, *39*, 1313−1326.
(31) Kleinman, S. L.; Frontiera, R. R.; Henry, A. I.; Dieringer, J. A.; Van Duyne, R. P. Creating, Characterizing, and Controlling Chemistry with SERS Hot Spots. *Phys. Chem. Chem. Phys.* **2013**, *15*, 21−36.
(32) Huebner, U.; Boucher, R.; Schneidewind, H.; Cialla, D.; Popp, J. Microfabricated SERS-Arrays with sharp-edged Metallic Nanostructures. *Microelectron. Eng.* **2008**, *85*, 1792−1794.
(33) Hering, K. K.; Moller, R.; Fritzsche, W.; Popp, J. Microarray-based Detection of dye-labeled DNA by SERRS using Particles formed by Enzymatic Silver Deposition. *ChemPhysChem* **2008**, *9*, 867−872.
(34) Petschulat, J.; Cialla, D.; Janunts, N.; Rockstuhl, C.; Hübner, U.; Möller, R.; Schneidewind, H.; Mattheis, R.; Tünnermann, A.; Lederer, F.; Pertsch, T.; Popp, J. Doubly resonant optical Nanoantenna Arrays for polarization resolved Measurements of surface-enhanced Raman Scattering. *Opt. Express* **2010**, *18*, 4184−4197.
(35) Yan, Y.; Radu, A. I.; Rao, W.; Wang, H.; Chen, G.; Weber, K.; Wang, D.; Cialla-May, D.; Popp, J.; Schaaf, P. Mesoscopically Bicontinuous Ag−Au Hybrid Nanosponges with Tunable Plasmon Resonances as Bottom-Up Substrates for Surface-Enhanced Raman Spectroscopy. *Chem. Mater.* **2016**, *28*, 7673−7682.
(36) Niu, W.; Zhang, L.; Xu, G. Seed-mediated Growth Method for high-quality noble metal Nanocrystals. *Sci. China: Chem.* **2012**, *55*, 2311−2317.
(37) Hinman, J. G.; Stork, A. J.; Varnell, J. A.; Gewirth, A. A.; Murphy, C. J. Seed mediated Growth of Gold Nanorods: towards Nanorod Matryoshkas. *Faraday Discuss.* **2016**, *191*, 9−33.
(38) Liu, A.; Wang, G.; Wang, F.; Zhang, Y. Gold Nanostructures with near-infrared plasmonic Resonance: Synthesis and Surface Functionalization. *Coord. Chem. Rev.* **2017**, *336*, 28−42.
(39) Xia, Y.; Gilroy, K. D.; Peng, H.-C.; Xia, X. Seed-Mediated Growth of Colloidal Metal Nanocrystals. *Angew. Chem., Int. Ed.* **2017**, *56*, 60−95.
(40) Liu, H.; Yang, Z.; Meng, L.; Sun, Y.; Wang, J.; Yang, L.; Liu, J.; Tian, Z. Three-dimensional and time-ordered surface-enhanced Raman Scattering Hotspot Matrix. *J. Am. Chem. Soc.* **2014**, *136*, 5332−5341.
(41) Bian, J.; Li, Z.; Chen, Z.; Zhang, X.; Li, Q.; Jiang, S.; He, J.; Han, G. Double-potentiostatic electrodeposition of Ag Nanoflowers on ITO glass for reproducible surface-enhanced (resonance) Raman Scattering Application. *Electrochim. Acta* **2012**, *67*, 12−17.
(42) Bian, J.; Shu, S.; Li, J.; Huang, C.; Li, Y. Y.; Zhang, R.-Q. Reproducible and Recyclable SERS Substrates: Flower-like Ag Structures with concave Surfaces formed by Electrodeposition. *Appl. Surf. Sci.* **2015**, *333*, 126−133.
(43) Bian, J.-C.; Chen, Z.-D.; Li, Z.; Yang, F.; He, H.-Y.; Wang, J.; Tan, J. Z. Y.; Zeng, J.-L.; Peng, R.-Q.; Zhang, X.-W.; Han, G.-R. Electrodeposition of hierarchical Ag Nanostructures on ITO glass for reproducible and sensitive SERS Application. *Appl. Surf. Sci.* **2012**, *258*, 6632−6636.
(44) Yüksel, S.; Ziegler, M.; Goerke, S.; Hübner, U.; Pollok, K.; Langenhorst, F.; Weber, K.; Cialla-May, D.; Popp, J. Background-Free Bottom-Up Plasmonic Arrays with Increased Sensitivity, Specificity

DOI: 10.1021/acsami.7b14833
ACS Appl. Mater. Interfaces 2017, 9, 38854−38862

and Shelf Life for SERS Detection Schemes. *J. Phys. Chem. C* **2015**, *119*, 13791−13798.
(45) Schneidewind, H.; Schuler, T.; Strelau, K. K.; Weber, K.; Cialla, D.; Diegel, M.; Mattheis, R.; Berger, A.; Moller, R.; Popp, J. The Morphology of Silver Nanoparticles prepared by Enzyme-induced Reduction. *Beilstein J. Nanotechnol.* **2012**, *3*, 404−414.
(46) Schüler, T.; Steinbrück, A.; Festag, G.; Möller, R.; Fritsche, W. Enzyme-induced Growth of Silver Nanoparticles studied on Single Particle Level. *J. Nanopart. Res.* **2009**, *11*, 939−946.
(47) Puurunen, R. L. Surface Chemistry of Atomic Layer Deposition: A Case Study for the Trimethylaluminum/Water Process. *J. Appl. Phys.* **2005**, *97*, No. 121301.
(48) Valdesueiro, D.; Meesters, G.; Kreutzer, M.; van Ommen, J. Gas-Phase Deposition of Ultrathin Aluminium Oxide Films on Nanoparticles at Ambient Conditions. *Materials* **2015**, *8*, 1249−1263.
(49) Zhang, X.; Zhao, J.; Whitney, A. V.; Elam, J. W.; Van Duyne, R. P. Ultrastable Substrates for Surface-Enhanced Raman Spectroscopy: Al_2O_3 Overlayers Fabricated by Atomic Layer Deposition Yield Improved Anthrax Biomarker Detection. *J. Am. Chem. Soc.* **2006**, *128*, 10304−10309.
(50) Ma, L.; Huang, Y.; Hou, M.; Xie, Z.; Zhang, Z. Ag Nanorods Coated with Ultrathin TiO_2 Shells as Stable and Recyclable SERS Substrates. *Sci. Rep.* **2015**, *5*, 15442.
(51) Yang, L.; Ma, L.; Chen, G.; Liu, J.; Tian, Z. Q. Ultrasensitive SERS Detection of TNT by Imprinting Molecular Recognition using a new Type of stable Substrate. *Chem. − Eur. J.* **2010**, *16*, 12683−12693.
(52) Ziegler, M.; Yüksel, S.; Goerke, S.; Weber, K.; Cialla-May, D.; Popp, J.; Pollok, K.; Wang, D.; Langenhorst, F.; Hübner, U.; Schaaf, P.; Meyer, H.-G. Growth of Hierarchically 3D Silver-Silica Hybrid Nanostructures by Metastable State Assisted Atomic Layer Deposition (MS-ALD). *Adv. Mater. Technol.* **2017**, *2*, No. 1700015.
(53) Ross, R. C.; Sherman, R.; Bunger, R. A.; Nadel, S. J. Plasma Oxidation of Silver and Zinc in Low-emissivity Stacks, Optical Materials Technology for Energy Efficiency and Solar Energy Conversion VI 1987, Proc. SPIE 0823, pp 47−53.
(54) Radu, A. I.; Kuellmer, M.; Giese, B.; Huebner, U.; Weber, K.; Cialla-May, D.; Popp, J. Surface-Enhanced Raman Spectroscopy (SERS) in Food Analytics: Detection of Vitamins B2 and B12 in Cereals. *Talanta* **2016**, *160*, 289−297.
(55) Liu, F.; Gu, H.; Lin, Y.; Qi, Y.; Dong, X.; Gao, J.; Cai, T. Surface-enhanced Raman Scattering Study of Riboflavin on Borohydride-reduced Silver Colloids: Dependence of Concentration, Halide Anions and pH Values. *Spectrochim. Acta, Part A* **2012**, *85*, 111−119.
(56) Dendisová-Vyškovská, M.; Kokaislová, A.; Ončák, M.; Matějka, P. SERS and in situ SERS Spectroscopy of Riboflavin adsorbed on Silver, Gold and Copper substrates. Elucidation of Variability of Surface Orientation based on both Experimental and Theoretical Approach. *J. Mol. Struct.* **2013**, *1038*, 19−28.
(57) Jahn, M.; Patze, S.; Bocklitz, T.; Weber, K.; Cialla-May, D.; Popp, J. Towards SERS based Applications in Food Analytics: Lipophilic Sensor Layers for the Detection of Sudan III in Food Matrices. *Anal. Chim. Acta* **2015**, *860*, 43−50.
(58) Tebbe, M.; Cherepanov, P.; Skorb, E. V.; Poznyak, S. K.; de Abajo, J. G.; Fery, A.; Andreeva, D. V.; Puebla, R. A. A.; Pazos-Perez, N. SERS Platforms of Plasmonic Hydrophobic Surfaces for Analyte Concentration: Hierarchically Assembled Gold Nanorods on Anodized Aluminum. *Part. Part. Syst. Charact.* **2014**, *31*, 1134−1140.
(59) Leiterer, C.; Zopf, D.; Seise, B.; Jahn, F.; Weber, K.; Popp, J.; Cialla-May, D.; Fritzsche, W. Fast Self-assembly of Silver Nanoparticle Monolayer in Hydrophobic Environment and its Application as SERS Substrate. *J. Nanopart. Res.* **2014**, *16*, 2467.
(60) Lovera, P.; Creedon, N.; Alatawi, H.; Mitchell, M.; Burke, M.; Quinn, A. J.; O'Riordan, A. Low-cost Silver Capped Polystyrene Nanotube Arrays as Super-hydrophobic Substrates for SERS Applications. *Nanotechnology* **2014**, *25*, No. 175502.
(61) Li, Z.; Zhu, K.; Zhao, Q.; Meng, A. The enhanced SERS Effect of Ag/ZnO Nanoparticles through Surface Hydrophobic Modification. *Appl. Surf. Sci.* **2016**, *377*, 23−29.
(62) Yu, E.; Kim, S. C.; Lee, H. J.; Oh, K. H.; Moon, M. W. Extreme Wettability of Nanostructured Glass Fabricated by Non-lithographic, Anisotropic Etching. *Sci. Rep.* **2015**, *5*, 9362.
(63) Chen, F.; Xu, W.; Huang, S.; Liu, J.; Song, J.; Liu, X. Plasma Hydrophilization of Superhydrophobic Surface and Its Aging Behavior: The Effect of Micro/nanostructured Surface. *Surf. Interface Anal.* **2016**, *48*, 368−372.
(64) Fernández-Blázquez, J. P.; Fell, D.; Bonaccurso, E.; del Campo, A. Superhydrophilic and Superhydrophobic Nanostructured Surfaces via Plasma Treatment. *J. Colloid Interface Sci.* **2011**, *357*, 234−238.

DOI: 10.1021/acsami.7b14833
ACS Appl. Mater. Interfaces 2017, 9, 38854−38862

Supporting Information

Hierarchically designed 3D flower-like composite nanostructures as an ultra-stable, reproducible and sensitive SERS substrate

Sezin Yüksel[abc§], Mario Ziegler[ad§], Sebastian Goerke[a], Uwe Huebner[a], Karina Weber[abc], Peter Schaaf[d], Hans-Georg Meyer[a], Dana Cialla-May[abc]* and Jürgen Popp[abc]

[§]Both authors contributed equally to this paper.

[a]Leibniz Institute of Photonic Technology Jena (IPHT), Albert-Einstein-Straße 9, 07745 Jena, Germany

[b]Friedrich Schiller University Jena, Institute of Physical Chemistry and Abbe Center of Photonics, Helmholtzweg 4, 07743 Jena, Germany

[c]InfectoGnostics Forschungscampus Jena, Zentrum für Angewandte Forschung, Philosophenweg 7, 07743 Jena, Germany

[d]TU Ilmenau, Department of Electrical Engineering and Information Technology, Institute of Materials Science and Engineering, Institute of Micro and Nanotechnologies MacroNano®, Gustav-Kirchhoff-Str. 5, 98693 Ilmenau, Germany

*corresponding author:

*Dr. Dana Cialla-May

Leibniz Institute of Photonic Technology Jena (IPHT), Albert-Einstein-Straße 9, 07745 Jena, Germany

07743 Jena

Phone: +49 (0)3641-206309

Fax: +49 (0)3641-206399

E-mail: dana.cialla-may@leibniz-ipht.de

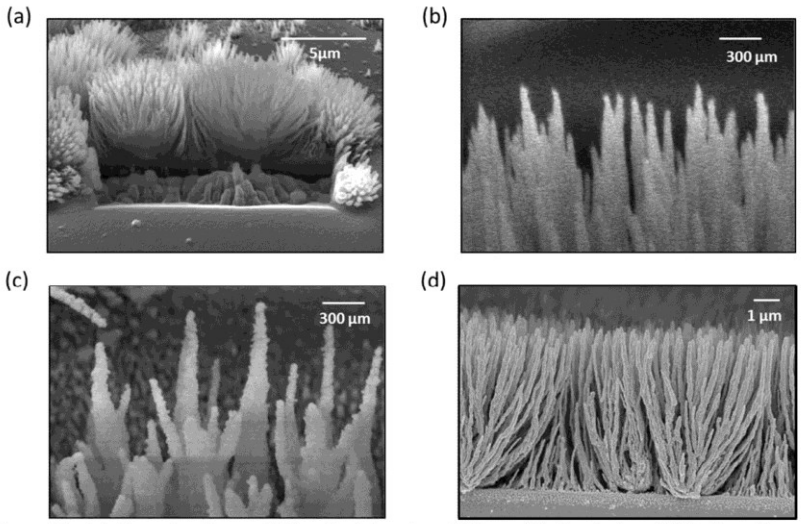

Figure S1: (a) Focus ion beam (FIB) cut of developed hierarchically designed 3D silica-silver composite nanostructure (135 cycles of PE-ALD). Scanning electron microscope (SEM) images of **(b)** the silver-silica composite needles and **(c)** the silver silica composite needles after 50 nm silver deposition, **(d)** hierarchically designed 3D silica-silver composite nanostructure (without additional silver deposition) after one year of storage under ambient conditions.

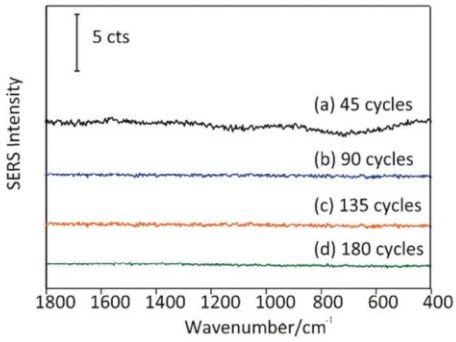

Figure S2: Raman response of the pure nanostructures fabricated with (a) 45, (b) 90, (c) 135 and (d) 180 cycles of PE-ALD after incubation with 10 µM riboflavin illustrates no signal enhancement.

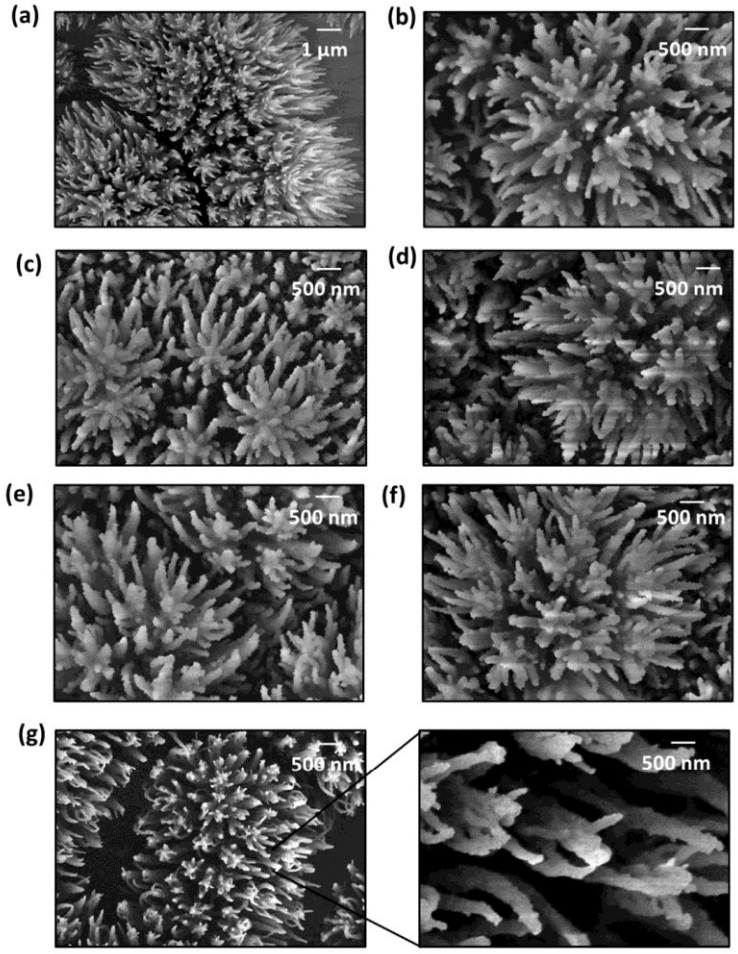

Figure S3: SEM images of the hierarchically designed 3D flower-like composite nanostructures with (a) 0, (b) 10, (c) 20, (d) 30, (e) 40, (f) 50, (g) 60 nm silver deposition.

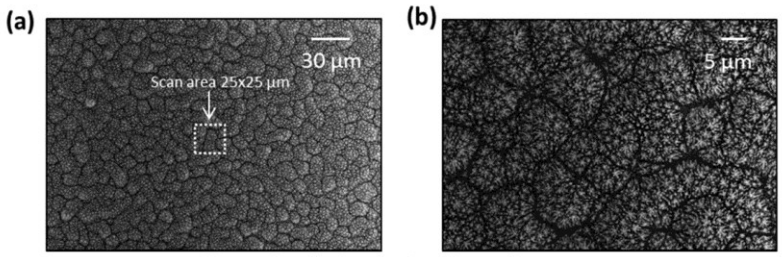

Figure S4: SEM images of hierarchically designed 3D flower-like composite nanostructures that is fabricated with 135 cycles of PE-ALD (a) showing the measurement scan with an area of 25x25µm. (b) The same surface is illustrated with a lower magnification.

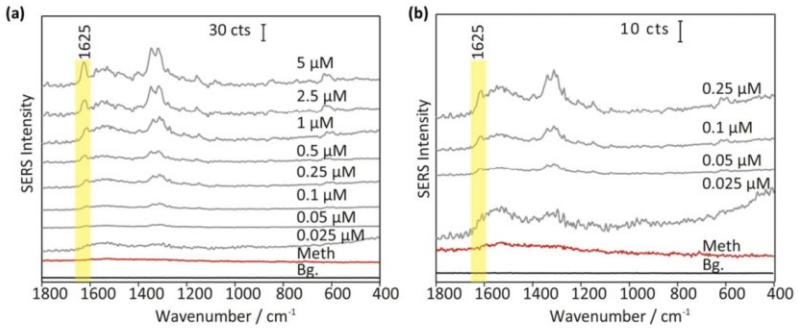

Figure S5: Average SERS spectra of the riboflavin concentration ranging from (a) 5-0.025 µM, (b) 0.25-0.025 µM, pure methanol (Meth.) and the background (Bg.) of the SERS template.

4.4 Microwave-assisted silver nanoparticle film formation for SERS applications [SY4]

Guido Soliveri, Silvia Ardizzone, Sezin Yüksel, Dana Cialla-May, Jürgen Popp, Ulrich S. Schubert, Stephanie Hoeppener.

The Journal of Physical Chemistry C, 2016, **120**, p. 1237-1344
DOI: 10.1021/acs.jpcc.5b10833

*both authors contributed equally

Autorenschaft der Publikation

Guido Soliveri	*Concept development* *Nanoparticle synthesis and its characterization* *Data analysis and interpretation* *Writing the manuscript*
Silvia Ardizzone	Project management Discussion of concepts and results Proof reading of manuscript
Sezin Yüksel	Experimental design Raman measurements *Data analysis and interpretation* Writing the manuscript Proof reading of manuscript
Dana Cialla-May	Proof reading of manuscript
Jürgen Popp	Project management Discussion of concepts and results Proof reading of manuscript
Ulrich S. Schubert	Project management Discussion of concepts and results Proof reading of manuscript
Stephanie Hoeppener	Discussion of experimental concept and results Proofreading of manuscript

*both authors contributed equally

Erklärung zu den Eigenanteilen der Promovendin sowie der weiteren Doktoranden/ Doktorandinnen als Koautoren an der Publikation und Zweitpublikationsrechten bei einer kumulativen Dissertation

Publication: **Guido Soliveri, Silvia Ardizzone, Sezin Yüksel, Dana Cialla-May, Jürgen Popp, Ulrich S. Schubert, Stephanie Hoeppener.** ***Microwave-assisted silver nanoparticle film formation for SERS applications*** **The Journal of Physical Chemistry C, 2016, 120(2), p.1237-1244**		
Beteiligt an		
	Guido Soliveri	**Sezin Yüksel**
Konzeption des Forschungsansatzes	**X**	
Planung der Untersuchungen	**X**	**X**
Datenerhebung	**X**	**X**
Datenanalyse und -interpretation	**X**	**X**
Schreiben des Manuskripts	**X**	**X**
Vorschlag Anrechnung Publikationsäquevalente	**1.0**	**0.75**

*both authors contributed equally

THE JOURNAL OF PHYSICAL CHEMISTRY C

Article

pubs.acs.org/JPCC

Microwave-Assisted Silver Nanoparticle Film Formation for SERS Applications

Guido Soliveri,[†] Silvia Ardizzone,[†] Sezin Yüksel,[‡,⊥] Dana Cialla-May,[‡,⊥] Juergen Popp,[‡,⊥] Ulrich S. Schubert,[§,∥] and Stephanie Hoeppener*[,§,∥]

[†]Dipartimento di Chimica, Università degli Studi di Milano, Via Golgi 19, 20133 Milano, Italy

[‡]Institute of Physical Chemistry and Abbe Center of Photonics, Friedrich Schiller University Jena, Albert-Einstein-Str. 9, 07745 Jena, Germany

[⊥]Leibniz-Institut of Photonic Technology, Albert-Einstein-Str. 9, 07745 Jena, Germany

[§]Laboratory of Organic and Macromolecular Chemistry (IOMC), Friedrich Schiller University Jena, Humboldtstr. 10, 07743 Jena, Germany

[∥]Jena Center for Soft Matter (JCSM), Friedrich Schiller University Jena, Philosophenweg 7, 07743 Jena, Germany

Supporting Information

ABSTRACT: Stable Ag nanoparticle (NP) films bear relevance to a large variety of applications due to their unique properties such as the surface-plasmon-resonance modes of their conduction electrons. Here a simple and fast one-step procedure is presented to obtain Ag NPs films by microwave irradiation of aqueous silver salt solutions. Ethanol, ethylene glycol, and glycerol are used as reducing agents in the absence of any other capping or stabilizing agent. Optical and morphological properties were accessed by UV−vis spectroscopy, X-ray diffraction, transmission, and scanning electron microscopy. Different substrates with different wettability and chemical nature, reactant compositions, and reaction conditions were tested to tailor the film properties. The mechanisms of particle and film formation were evaluated. The obtained surfaces represent promising SERS activity, e.g., for the model analyte riboflavin which can be detected down to the nanomolar range.

INTRODUCTION

The actual relevance of silver (Ag) nanoparticles (NPs) is testified by the abundance of publications in the past few years reporting results on the topic. The interest results from several distinctive properties, such as a good conductivity, optical peculiarity, chemical stability, and catalytic and antibacterial activity. Silver is widely known as an important industrial catalyst, as e.g., in the case of the oxidation of methanol to ethylene oxide and formaldehyde.[1] Recently, Fuku et al.[2] described the synthesis of size controlled Ag NPs supported on mesoporous silica, and for the first time, the enhancement of the catalytic activity assisted by localized surface plasmon resonance (LSPR) was reported. The plasmonic resonance is associated with the collective oscillation of conduction electrons of typically noble metal NPs; Ag exhibits, among all, the highest efficiency of excitation.[3] Antimicrobial, antibacterial, and anticancerous cell activity is one of the additional reasons for the high commercial interest in this material.[4,5] Sharma et al.[6] recently reported an explanation of the nature of the interactions between the bacteria cell membrane and Ag nanoparticles. Next to these, other applications of Ag NPs in electronics, photonics, optoelectronics, and sensing have to be mentioned.[7,8]

Several approaches have been reported for the synthesis of Ag NPs. The most extensively adopted procedures are traditional solution phase reductions, mostly performed in the presence of capping agents, stabilizers, and organic solvents, which might imply risks for the environmental ecosystem or biological systems.[8,9] More recently, the use of microwave irradiation (MW) for the synthesis of Ag NPs has been proposed as a more environmentally friendly approach allowing a rapid and uniform heating and a lower energy consumption.[10,11] Over the past 25 years, microwave chemistry has moved from a laboratory curiosity to a well-established synthetic technique applied in many academic and industrial laboratories. MW heating provides reaction conditions that, thanks to the speed and homogeneity of the locally produced heating, allow for a rapid synthesis of nanostructures with high control of shape and dimensions. This is experimentally demonstrated by Horikoshi et al.,[12] where the authors performed the same reduction, with the same experimental conditions, by both MW and traditional heating. Different reaction procedures supported by MW irradiation have been recently reported to obtain Ag NPs in suspension. Liu et al.[13] reported a facile method to synthesize stable Ag nanoparticles (Ag NPs) with a narrow size distribution in water by using

Received: November 5, 2015
Revised: December 11, 2015
Published: January 11, 2016

DOI: 10.1021/acs.jpcc.5b10833
J. Phys. Chem. C 2016, 120, 1237−1244

quaternized carboxymethyl chitosan as both stabilizing and reducing agent. Raveendran et al.[14] introduced the use of glucose and starch respectively as reducing and protecting agent. Hu[7] combined amino acids and soluble starch, while Nadagouda[10] reviewed the use of polyvinylpyrrolidone in the polyol synthesis.

Studies on the direct reduction and deposition of Ag NPs in films, by either traditional heating or MW irradiation, are so far not reported in literature, although the exclusive properties of Ag NPs have recently shown their relevance also in the field of surface modification and film reactivity. In particular, films of Ag NPs have been investigated as surface enhanced Raman spectroscopy (SERS) substrates.[15,16] Literature data concerning the preparation of Ag NPs films, by chemical procedures, are mostly related to different procedures on the deposition of preformed particles. In the case of SERS applications Zhang et al.[17] analyzed the effect of different shapes and dimensions of Ag NPs prepared in solution that were deposited onto silicon wafers, and Lu et al.[18] suggested a Langmuir−Blodgett method to deposit Ag NPs onto polymer membranes. In the case of applications for electric circuits, Magdassie et al.[19] studied the sintering of preformed Ag NPs by a spontaneous 3D coalescence process supported by charge neutralization and stabilizer desorption. Long et al.[20] described a complex process for the deposition of particles, with a sublayer of dopamine, and a subsequent immersion in a plating solution. The MW irradiation was adopted by Schubert et al.[21,22] to promote the sintering of commercial Ag NPs deposited by inkjet printing, for applications in microelectronics. Hu et al.[7] instead deposited Ag NPs obtained in solution by MW irradiation by drop-casting; homogeneity of the film, in this case, could only be obtained in small and localized areas.

Major problems associated with the use of Ag NPs is related to the separation between the Ag NPs themselves and the reducing/stabilizing agents being part of the traditional synthetic route, as underlined by Liu et al.[13] That may critically limit applications in many fields, particularly those connected with biomaterials and medical devices.[23]

Here a facile, fast, and environmentally friendly method is reported for the production of thin and robust films, composed of nanoparticles, without the use of any stabilizing or strong reducing agent. The film can be obtained from silver acetate and an ethanol/water mixture; the formation and the deposition of the nanoparticles proceed simultaneously supported by microwave radiation. Reducing agents different from ethanol were also tested. Morphological, structural, and optical characterizations of the films were performed, and the critical process parameters were investigated; substrates with different degree of hydrophilicity are tested as well. The formation of stable films homogeneously covering objects with different shape and size is documented. As a representative practical application, the SERS activity of the obtained Ag NPs covered substrate was tested.

■ EXPERIMENTAL SECTION

Film Synthesis. Microscopy glass slides, cut into rectangular pieces of 0.8 cm × 1.25 cm size, were used as standard substrates for the synthesis. Before the reaction, an argon plasma treatment (300 W, Diener Electronic) was applied to the substrates to remove organic residues and to obtain a hydrophilic surface. Different reaction conditions were tested, i.e., temperature (150 to 190 °C), reagent ratio, and reducing agents (ethanol, ethylene glycol, and glycerol). The MW vial was filled with a total amount of 3 mL of solvent, composed of distilled water, the reducing agent (ethanol, ethylene glycol, or glycerol), and dissolved silver acetate. The treated glass support was immersed in the solution. The vial was then capped and exposed to microwave radiation (Biotage Initiator) with 2.45 GHz frequency under magnetic stirring. The power rise of the irradiation protocol was programmed to allow a mild heating of the solution (Figure S1, Supporting Information), and the irradiation was stopped and was quenched by a flow of compressed air until room temperature was reached. The sample was cleaned with distilled water and dried under nitrogen flow.

To test the effect of the hydrophilicity of the substrate, the wettability of the glass slide was switched from hydrophilic to hydrophobic by the formation of a *n*-octadecyltrichlorosilane (OTS) monolayer, adopting the procedure reported by Hoeppener et al.[24]

Characterization. Scanning electron microscopy images were acquired with a LEO 1530 Gemini (Zeiss) scanning electron microscope with InLense detector. The samples were carbon coated before the analysis. For transmission electron microscopy, a CM 120 (Philips) with 120 kV acceleration voltage or a FEI Tecnai G^2 20 was used. Samples were prepared on Quantifoil grids (R2/2) to reduce background signals. The film was mechanically removed from the substrate and suspended in water. 15 μL of the solution was blotted onto the grid.

Room-temperature X-ray diffraction (XRD) patterns were collected between 20° and 90° with a Siemens D500 diffractometer, using Cu Kα radiation. The average diameter of the crystallites was estimated from the most intense reflection (111) using the Scherrer equation.

UV−vis analysis of the films was obtained from a microplate reader (Genios Pro, Tecan GmbH), while of the suspensions were analyzed by a Specord 250 spectrophotometer (Analytic Jena). Water contact angle analysis was performed on a Dataphysics CA10 system.

The mechanical stability was tested both by tape adhesion test and by immersion of the coated substrates in water and applying ultrasonication. In the former test the sample was half covered with a tape (MAGIC 3G). When the tape was removed, both the difference between the two parts and the amount of layer left on the tape was evaluated by optical inspection. The difference between tested and nontested parts of the film was evaluated additionally by SEM analysis.

The SERS activity of the nanoparticle layers was tested on Ag NPs films synthesized on glass substrates, in ethanol at 170 °C. The test was performed with riboflavin.

Riboflavin was purchased from Sigma-Aldrich (Steinheim, Germany). 10 mM stock solution of riboflavin in distilled water was prepared, and aliquots of the solution were diluted to obtain the appropriate concentrations.

SERS spectra were measured by using a confocal Raman microscope (WITec GmbH, Ulm, Germany) equipped with 488 nm laser excitation. The Raman signal was collected by the same objective which is used for irradiation. The spectrometer has a 600 lines/mm grating with a 1024 × 127 pixel CCD camera at a working temperature of 200 K. SERS spectra of riboflavin were recorded with a 100× Olympus objective (NA: 0.9), and the incident laser power onto the surface was 30 μW. Each substrate was incubated 30 min with the target molecule; then, the substrates were washed with distilled water and dried with pressurized air. SERS spectra were recorded within a 60 ×

DOI: 10.1021/acs.jpcc.5b10833
J. Phys. Chem. C 2016, 120, 1237−1244

60 μm area, and 400 spectra with 0.2 s of integration time were collected.

RESULTS AND DISCUSSION

Optimization of the Experimental Conditions. The aim of the present work was to develop a simple and facile method to synthesize and homogeneously self-assemble Ag NPs at the surface of a glass support, utilizing nonhazardous chemicals by MW irradiation. We directed our efforts toward achieving an adequately robust film, composed of small and well packed nanoparticles and utilization of the superficial sintering to preserve the properties of the NPs.

Three different solvents acting as reducing agents were studied: ethanol, ethylene glycol, and glycerol. Alcohols generally show high dielectric loss for MW irradiation at 2.546 GHz and possess a strong reduction ability. Therefore, they are regarded as ideal solvents for MW rapid reduction reactions.[25] Silver acetate was used as silver source, and glass substrates were utilized as routine supports. The first part of the article exclusively deals with results obtained using ethanol as a reducing agent.

Capped MW vials with the glass substrate immersed in the reaction solution were exposed to microwave irradiation under stirring, and the temperature was gradually raised up to 170 °C. The temperature was maintained for different irradiation times and was then quenched by an air flow. Mild conditions were applied to avoid overheating and excessive sintering of the NPs; this was achieved by a slow rise of the microwave power in the heating phase of the irradiation process. A typical power/temperature/pressure plot of such a synthesis process is reported in the Supporting Information (Figure S1).

At the end of the reaction, the internal wall of the vial and the glass substrate were covered with a yellowish metallic or an even shiny layer (Figure 1).

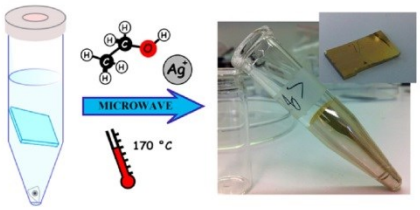

Figure 1. Photo shows the used glass vial and the glass support (inset) at the end of the synthesis. The synthesis was performed at 170 °C for 2 min; the reaction mixture was composed by 2 mL of water, 1 mL of ethanol, and 1 mg of silver acetate.

The remaining reaction solution in the vial was transparent, and no evidence of significant changes was detected by UV−vis spectroscopy compared to the starting prereaction mixture indicating that only very few or even no nanoparticles are present in the reaction mixture. TEM images (reported in Supporting Information Figure S2) obtained by blotting the final solution directly onto a TEM grid revealed only very few small particles.

The choice of the specific conditions to be adopted in order to obtain a homogeneous and compact layer was investigated first. The role of temperature, Ag salt concentration, and reducing agent amount is discussed in the Supporting Information (Figures S3−S5). Based on these results, the optimal reaction conditions could be determined resulting in densely packed, homogeneous films. A reaction mixture of 1 mL of ethanol, 2 mL of water, and 1 mg of silver acetate, reacted at a temperature of 170 °C, resulted in compact and well-defined silver film formation.

With those parameters, the particle formation kinetics during the time of irradiation was investigated in detail. The irradiation process can be divided into two distinct phases: a temperature raising step of about 2.6 min; after that the power of irradiation was controlled to ensure a constant temperature inside the vial. The MW irradiation was stopped 1, 2, 3, and 4 min after the start of the irradiation, and the samples were quickly cooled to room temperature. The top view SEM images (Figure 2a−d) were compared with the sample kept for 2 min at 170 °C (that corresponds to 4.6 min of total irradiation time, Figure 2e); the latter were identified as optimum reaction conditions. Figure 2f shows the variation of temperature and pressure during the course of the reaction; the Supporting Information displays the pictures of the obtained films (Figure S6). In the first minute ($T \sim 110$ °C, $p \sim 1$ bar), the film was still totally transparent (Figure S6a); only few particles were present on the surface. The dimension of these particles was approximately 30 nm (Figure 2a). After 2 min ($T \sim 150$ °C, $p \sim 7$ bar), the surface was well covered with nanoparticles, and the substrate was changing to a yellowish color (Figure S6b). The particles diameter was in the range of 30 to 40 nm (Figure 2b). After 3 min ($T \sim 170$ °C, $p \sim 12$ bar), the temperature reached the optimal value of 170 °C. At this stage the film was not transparent anymore (Figure S6c). The dimension of the individual particles on the surface was still small; however, the films appeared to be more homogeneous and the particles are more densely packed (Figure 2c). After 4 min total irradiation time ($T \sim 170$ °C, $p \sim 13$ bar), the particle sizes strongly increased; the particles lost the round shape and revealed a more aggregated appearance (Figure 2d). Figure 2e (and Figure S6e) shows the best homogeneity of the film compared to the previous ones. No changes were recorded at the surface by further increasing the reaction time. The SEM picture of the sample obtained at 170 °C for 10 min is reported in the Supporting Information (Figure S7). To summarize, 2 min (plus the initial heating time of 2.6 min) at 170 °C was the shortest time that resulted in good particle coverage at the surface with only negligible remaining Ag salt amounts in the reaction mixture.

Film Characterization. Figure 3 shows the UV−vis spectrum of the covered substrate (obtained at 170 °C for 2 min + initial heating time corresponding to Figure 2e). The peak around 390 nm is identified as an optical resonance, associated with the collective oscillation of conduction electrons typical for noble-metal nanoparticles (NPs), commonly know as surface plasmon resonance (SPR).[3] Such plasmonic resonances identify the presence of Ag NPs with dimensions much smaller than the wavelength of the irradiation light. As reported by Evanoff et al.,[3,26] the surrounding medium as well as size, shape, and material of the nanostructures critically affects the profile and position of the peak. Nevertheless, the peak could be associated with particles with a dimension of approximately 30 to 40 nm. The high noise present in the high wavelength portion can be associated with scattering and optical phenomena due to the interface between the substrate and the film.

DOI: 10.1021/acs.jpcc.5b10833
J. Phys. Chem. C 2016, 120, 1237−1244

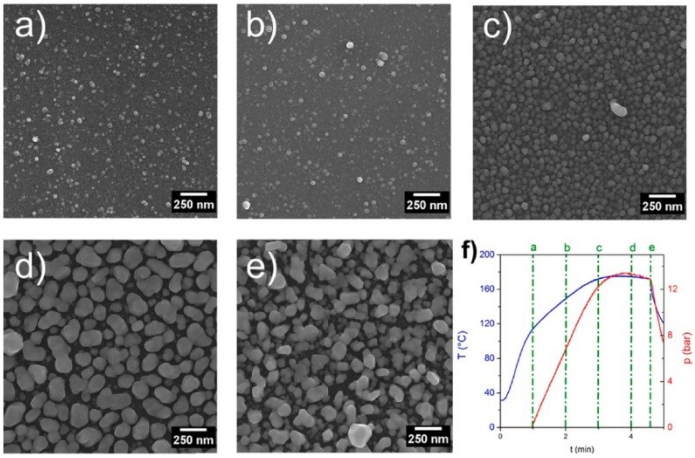

Figure 2. (a–d) SEM top-view pictures of films obtained after 1, 2, 3, and 4 min from the beginning of the MW irradiation. (e) SEM top-view pictures of the film at the end of the programmed reaction (2 min at a constant temperature of 170 °C + initial heating time of 2.6 min). (f) Temperature/pressure plot vs time of irradiation.

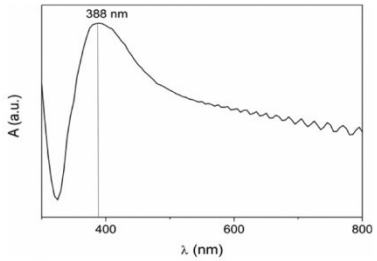

Figure 3. UV–vis spectroscopy of the sample obtained after 2 min at 170 °C using ethanol as reducing agent.

SEM (top view) pictures disclosed the presence of particle aggregates of dimensions in the range from 100 to 150 nm at the surface (Figure S8). The substrate was totally covered and the presence of underlying layers of particles is slightly visible at higher magnification (Figure S8).

SEM cross-section analyses of the same films are reported in Figure 4a–c. Figure 4a shows an Ag layer thickness between 5 and 6 μm; the layer depth appeared to be constant all along the cross section and was reproducible for different samples. Figure 4b displays the existence of large aggregates between 1 and 2 μm. Higher magnifications showed the presence of much smaller round-shaped particles, which form the aggregates and appear to be well packed. Those particles, with a quite reproducible diameter from 30 to 35 nm (Figure 4c), were found to be homogeneous along all the section. Those latter particles are supposed to be the ones dominating the obtained optical results presented above.

A further proof of the shape and dimensions of the Ag NPs in the inner part of the layer was obtained by high resolution

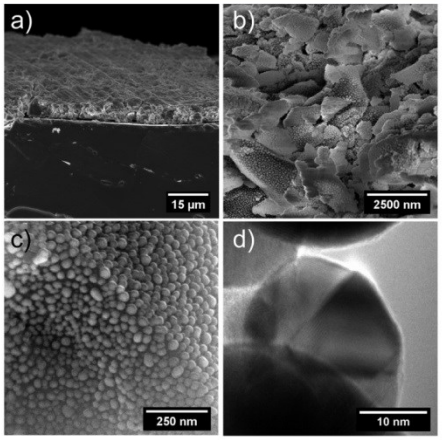

Figure 4. (a–c) SEM cross-section pictures of the sample obtained after 2 min at 170 °C, using ethanol as the reducing agent at different magnifications. (d) HR TEM picture of the same sample scratched.

transmission electron microscopy (HR TEM). The film was scratched as to investigate the particles inside the layer. Figure 4d reports the TEM picture of a few Ag NPs packed together. The clear and uniform lattice fringes revealed the highly crystallinity of the particles. The lattice spacing of ~0.23 nm corresponds to the (111) planes of silver.

This finding was supported by the X-ray diffraction pattern of the NPs film (Figure 5) confirming the face-centered cubic (fcc) silver crystal structure (JCPDS Card No. 04-0783). The

DOI: 10.1021/acs.jpcc.5b10833
J. Phys. Chem. C 2016, 120, 1237–1244

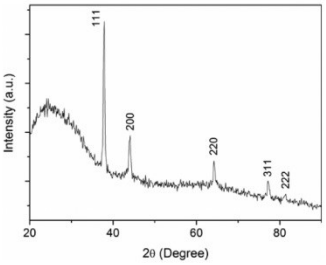

Figure 5. X-ray diffraction pattern of the sample obtained after 2 min at 170 °C, using ethanol as reducing agent.

lattice constant calculated from this pattern was 4.080 Å, which is a value very close to the reported one (a = 4.086 Å, JCPDS Card No. 04-0783). Calculated over the (111) reflection, using the Scherrer equation,[27] the average crystallite diameters was founded to be ∼28 nm. This result shows that the pristine Ag NPs observed by the SEM and TEM analysis are actually single crystals. This latter occurrence justifies the shape and the narrow controlled dimensions of such particles. The calculated crystallite size was slightly smaller compared to those estimated by electron microscopy. Chen et al.[27] reported that the Scherrer equation generally tends to underestimate the real size of the NPs, probably due to the contribution of other components to the broadening of line width (structural stress of Ag NPs, instrumental effects, etc.).

Additionally, an aging test of the surface was performed. The coverage with a carbon coating and the SEM analysis was performed both 2 h after the synthesis and after 1 week. No significant differences were found by inspection of the surface by electron microscopy.

Mechanical tests of the film were also performed by Scotch tape tests. After the tape removal, no changes were observed by the naked eye at the surface. Only a small amount of particles was visible on the tape. Sonication in water for 10 min did not provoke the detachment of a significant amount of particles to the solution, thus suggesting good adhesion properties of the silver nanoparticles on the glass substrates.

Different Reducing Agents. Based on these promising results for the coating of glass substrates with uniform Ag NPs, different alternative reducing agents were tested. Based on the chemical similarity and existing literature data, the same procedure was applied using ethylene glycol and glycerol as reducing agents. Ethylene glycol is a well-known reducing agent for the synthesis of Ag NPs for MW controlled reactions. This solvent is used, for example, for the polyol synthesis, in which the nucleation and growth of silver atoms are performed in solution to produce a wide range of different shapes.[28,29] The temperature-dependent reducing power, the high boiling point, the high relative permittivity,[25] and the ability to solvate many metal precursors make ethylene glycol perfectly suited for the synthesis of a large variety of metal nanoparticles. However, in the present case, the reaction did not yield a satisfying, robust film as in the case of ethanol. The substrate became only lightly yellowish (SEM picture in Figure S9), while the reaction occurred mainly in suspension, without any control of shape and size of the particles. Possibly this outcome is the result of the quite good suspending ability of ethylene glycol[30] which promotes the nucleation and grow of the particles preferentially in suspension and not their deposition onto the substrate.

Results related to the synthesis of metal NPs in glycerol have been far less frequently reported in the literature compared to ethanol and ethylene glycol. The solvent is generally reported both as a reducing agent as well as the reaction medium, occasionally combined with a protective agent, like poly-(vinylpyrrolidone) (PVP).[31] Ullah et al.[32] reported that the stability of the Ag NPs synthesized in glycerol without a stabilizing surfactant is generally much higher compared to the ones, for example, in ethylene glycol. This higher stability in glycerol is explained by the higher viscosity of ethylene glycol leading to a slower diffusion. In the present work, films were obtained at the same conditions than the previous ones. Only the amount of silver acetate had to be lowered to 0.5 mg to obtain a more homogeneous film. However, the results of these preparations were significantly different compared to the two previous systems.

The solution was not transparent anymore; a yellowish-white suspension was obtained. The first observation on the substrate was a clear change in color: greenish-metallic with a strong yellowish reflection. The apparent change in color was supported by UV−vis spectroscopy investigations of the film. Figure 6c shows a broader peak with a maximum at 443 nm. This can be associated with larger NPs, about 90 to 100 nm in diameter, due to a higher scattering component.[3]

The top view of the layer obtained by SEM (Figure 6a) showed the presence of a rather broad size distribution, between 80 and 150 nm, with an average spherical shape. The layer seems not to completely cover the substrate, and no underlayer of particles was evident. The cross section of the

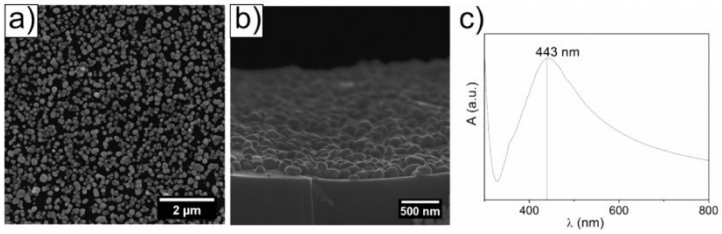

Figure 6. (a) Top-view and (b) cross-section SEM pictures of the sample obtained using glycerol as reducing agent. (c) UV−vis spectrum of the same sample.

DOI: 10.1021/acs.jpcc.5b10833
J. Phys. Chem. C 2016, 120, 1237−1244

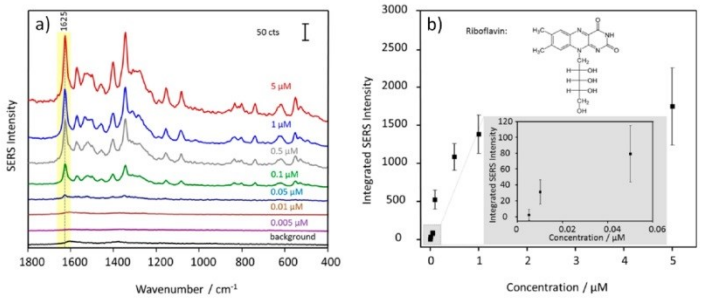

Figure 7. Average SERS spectra of riboflavin with different concentrations (a) and integrated SERS intensity at 1625 cm^{-1} of riboflavin (b). The inset highlights the low concentration regime and indicates the limit of detection.

sample (Figure 6b) revealed the same observations. The particles were self-assembled at the surface, not forming a robust and packed 3D layer, but only a submonolayer. This behavior could be extremely interesting in applications and investigations that require only a very small amount of isolated Ag NPs at the surface.

Covering Surfaces with Different Chemical Nature. In order to investigate the role of the support surface on the interaction and the subsequent deposition of the NPs, different conditions of wettability of the glass plate were tested. First, the hydrophilicity/hydrophobicity of the support was tested. The glass substrate (at the beginning hydrophilic) was covered by a self-assembled monolayer of OTS, as e.g. reported by Hoeppener et al.,[24] in order to make the surface hydrophobic (contact angle about 108°), without change in the surface morphology. After the Ag NPs synthesis (reducing agent ethanol), the final layer was investigated both by UV−vis spectroscopy (Figure S10) and SEM analysis (Figure S11). Both methods showed the formation of an Ag NPs film totally comparable with the one previously prepared on to the hydrophilic glass. On the contrary, a Teflon sheet placed in the reaction vial was poorly covered by Ag NPs.

Both of these surfaces are highly hydrophobic. This observation may suggest that the self-assembly behavior of Ag NPs is not correlated with the hydrophilicity but to the polar momentum of the surface. Literature reports suggest that the momenta of siloxanes are far from zero,[33,34] while polytetrafluoroethylene has a very low dielectric constant. That observation is in total agreement with the prediction of a reaction route that goes through the formation of hot spots on the surface under MW radiation, as reported by Tsuji et al.[25]

The feasibility to cover further insulating or semiconductor materials was briefly investigated. Good results were obtained both on a silicon wafer and on a thin titanium dioxide layer supported, in its turn, on a glass slide.[35]

Based on the results reported above, the major steps involved in the Ag NPs film formation can be discussed. As suggested by Tsuji et al.,[25] in the case of MW synthesis, the high dielectric (and dielectric loss) constant of the groups at the surface of the support may give rise to hot spots that effectively promote the preferential nucleation of silver clusters. The formation of those hot spots at the surface, as described by Zhang et al.,[36] could locally increase the temperature up to 100 to 200 °C above the bulk temperature, hence dramatically changing the thermodynamics of reactions; they are highly correlated with the momenta of atoms and molecules at the surface (native or adsorbed), but not with the wettability of the material. The local high temperature is reached very quickly and promotes the formation of round shaped small, single crystalline particles. The electrostatic charge of the substrate may support the formation of a compact and robust layer. Further, the first deposited layers of metal particles themselves develop local hot spots at the surface, favoring the nucleation of new particles. That proceeds up to the total consumption of the Ag salt in solution. At that point, possibly, the temperature at the water/Ag NPs interface locally increases, promoting the sintering process in the first layers and, hence, the formation of aggregates consisting of individual particles. That critically influences all the properties described above, imparting chemical and mechanical stability without affecting the optical and technological advantages connected to the small NPs kept inside the layer.

The large differences in the layer formation observed by passing from ethanol to ethylene glycol and glycerol could be ascribed to the noticeable differences in physical constants of the solvents (reported in Supporting Information, Table S1). The heating process of a liquid under MW radiation is highly correlated with its dielectric loss constant.[25] As shown in the data reported in the table, ethanol is characterized by the lowest dielectric loss constant. Associated with the lowest viscosity and surface tension, this suggests that Ag nanoclusters may nucleate directly at the surface and, at the same time, self-assemble without any obstacle. In the case of glycerol, the high dielectric loss constant causes a prevalence of NP formation in solution. The high viscosity of the medium and the protecting power of glycerol molecules adsorbed around the small Ag clusters[37] may prevent coalescence, leading to aggregates at the surface. Concurrently, the absence of an overheated area (on the surface), due to the lack of accumulation of metallic NPs (like in the case of ethanol), may slow down the kinetics of nucleation and create stable and long life clusters in solution, next to the formation of larger particles. Ethylene glycol presents all intermediate properties. Reasonably, in this case, the nucleation and growth proceeds both on the surface and in the liquid phase with particles showing different shapes and dimensions (different nucleation spots and local temperature). The suspending power is not high enough and agglomerates tend to form, attracted by the surface.

Emerging Possibilities and Applications. The film formation is independent of the particular shape of the

DOI: 10.1021/acs.jpcc.5b10833
J. Phys. Chem. C 2016, 120, 1237−1244

substrate (unlike other coating techniques, i.e., evaporation[20,38,39]) and potentially allows also the covering of concave and hollow objects. This might provide new aspects and enables the straightforward and reliable coating of complex object. Silver nanoparticle films are frequently employed to enhance the sensitivity of Raman measurements. For this purpose, uniform nanoparticles and dense films are frequently used. As such the fabricated substrates were tested for their SERS sensitivity. This was done by application of a 10^{-4} M solution of riboflavin onto the surfaces and analysis of the Raman signal. Figure 7a shows the average SERS spectra of riboflavin with different concentrations. The most dominant C−C stretching vibrational mode at 1625 cm^{-1} of riboflavin is integrated and plotted versus various different concentrations (see Figure 7b). It is cearly visible that the signal intensity increases as a function of the concentration until a plateau is reached for concentrations higher than 1 μM. This is attributed to the saturation of all free binding sites on the metallic surface by riboflavin. Concentrations down to 0.01 μM are detectable. Thus, microwave-assisted silver nanoparticles are promising SERS substrates for analytical detection schemes of concentrations down to the sub-micromolar and nanomolar range.

CONCLUSION

A simple and fast method for the controlled synthesis of AgNP films has been developed using a MW-assisted synthesis approach to establish the direct fabrication of Ag films.

The employment of MW irradiation allowed to avoid the use of additional chemicals and stabilizing agents, which are usually difficult to remove in postreaction treatments. Ethanol, ethylene glycol, and glycerol were alternatively tested as reducing agents, and significant differences in the film formation characteristics were observed. These could be related to the MW adsorption properties of the utilized reducing agents.

As a consequence of the results obtained in this work, we propose that the presented reaction is ruled by a balance between surface and solution effects. MW irradiation promotes the formation of hot spots on the surface of the support. The local high temperature allows a fast kinetic of nucleation close to the surface and a subsequent self-assembly on it. By changing the reducing agents (from ethanol to ethylene glycol and glycerol), we investigated the influence of the physical properties of these solvents, like the reported suspending power of Ag nanoclusters and the high dielectric loss constant, that promotes the nucleation in the bulk solution instead on the surface.

Consequently, by changing the reaction conditions, tailored films for different applications can be obtained. The mechanically robust films obtained in water/ethanol mixtures, in the absence of any adsorbed organic species, represent excellent candidates for bio and medical applications; high SERS activity could open up their application in the field of trace sensing. In particular, the absence of a stabilizing coating, which is required for avoiding aggregation and precipitation of solvent processed nanoparticles, is an important property of the introduced nanoparticle synthesis protocol, as functionalization of the layers can be directly performed on the bare plasmonic particles. As such, the obtained layers might be suitable to study plasmon-driven chemical reactions,[40,41] without the presence of any stabilizing agents.

ASSOCIATED CONTENT

Supporting Information

The Supporting Information is available free of charge on the ACS Publications website at DOI: 10.1021/acs.jpcc.5b10833.

Pressure−power−temperature diagrams of the microwave process; TEM images of the Ag particles; a discussion of the chosen experimental parameters; UV−vis investigations of the Ag nanoparticle solutions; a comparative SEM study of the film morphology obtained at different temperatures and for different concentrations and film morphologies at different experimental conditions; photographs of the coated substrates and a summary of the properties of different solvents (PDF)

AUTHOR INFORMATION

Corresponding Author

*E-mail: s.hoeppener@uni-jena.de (S.H.).

Notes

The authors declare no competing financial interest.

ACKNOWLEDGMENTS

G.S. acknowledges the financial support from Università degli Studi di Milano (PhD school in Chemical Sciences). This work is part of the PhoNa project funded by the German Ministery of Education and Research (BMBF) in the framework of the excellence initiative "Spitzenforschung in den Neuen Ländern". TEM measurements were performed at the TEM facilities of the JCSM (funded by DFG and EFRE). Furthermore, the research project "JBCI 2.0'" (03IPT513Y, InnoProfile-Transfer, Unternehmen Region), supported by the Federal Ministry of Education and Research (BMBF) Germany, is gratefully acknowledged.

REFERENCES

(1) Nagy, A.; Mestl, G. High Temperature Partial Oxidation Reactions over Silver Catalysts. *Appl. Catal., A* **1999**, *188*, 337−353.

(2) Fuku, K.; Hayashi, R.; Takakura, S.; Kamegawa, T.; Mori, K.; Yamashita, H. The Synthesis of Size- and Color-Controlled Silver Nanoparticles by Using Microwave Heating and Their Enhanced Catalytic Activity by Localized Surface Plasmon Resonance. *Angew. Chem., Int. Ed.* **2013**, *52*, 7446−7450.

(3) Evanoff, D. D.; Chumanov, G. Synthesis and Optical Properties of Silver Nanoparticles and Arrays. *ChemPhysChem* **2005**, *6*, 1221−1231.

(4) Tran, H. V.; Tran, L. D.; Ba, C. T.; Vu, H. D.; Nguyen, T. N.; Pham, D. G.; Nguyen, P. X. Synthesis, Characterization, Antibacterial and Antiproliferative Activities of Monodisperse Chitosan- Based Silver Nanoparticles. *Colloids Surf., A* **2010**, *360*, 32−40.

(5) Xue, C.-H.; Chen, J.; Yin, W.; Jia, S.-T.; Ma, J.-Z. Superhydrophobic Conductive Textiles with Antibacterial Property by Coating Fibers with Silver Nanoparticles. *Appl. Surf. Sci.* **2012**, *258*, 2468−2472.

(6) Sharma, V. K.; Yngard, R. A.; Lin, Y. Silver Nanoparticles: Green Synthesis and Their Antimicrobial Activities. *Adv. Colloid Interface Sci.* **2009**, *145*, 83−96.

(7) Hu, B.; Wang, S.-B.; Wang, K.; Zhang, M.; Yu, S.-H. Microwave-Assisted Rapid Facile "Green" Synthesis of Uniform Silver Nanoparticles: Self-Assembly Into Multilayered Films and Their Optical Properties. *J. Phys. Chem. C* **2008**, *112*, 11169−11174.

(8) Saponjic, Z. V.; Csencsits, R.; Rajh, T.; Dimitrijevic, N. M. Self-Assembly of TOPO-Derivatized Silver Nanoparticles into Multilayered Film. *Chem. Mater.* **2003**, *15*, 4521−4526.

DOI: 10.1021/acs.jpcc.5b10833
J. Phys. Chem. C 2016, 120, 1237−1244

(9) Jana, N. R.; Peng, X. Single-Phase and Gram-Scale Routes toward Nearly Monodisperse Au and Other Noble Metal Nanocrystals. *J. Am. Chem. Soc.* **2003**, *125*, 14280−14281.
(10) Nadagouda, M. N.; Speth, T. F.; Varma, R. S. Microwave-Assisted Green Synthesis of Silver Nanostructures. *Acc. Chem. Res.* **2011**, *44*, 469−478.
(11) Bilecka, I.; Niederberger, M. Microwave Chemistry for Inorganic Nanomaterials Synthesis. *Nanoscale* **2010**, *2*, 1358−1374.
(12) Horikoshi, S.; Abe, H.; Torigoe, K.; Abe, M.; Serpone, N. Access to Small Size Distributions of Nanoparticles by Microwave-Assisted Synthesis. Formation of Ag Nanoparticles in Aqueous Carboxymethylcellulose Solutions in Batch and Continuous-Flow Reactors. *Nanoscale* **2010**, *2*, 1441−1447.
(13) Liu, B.; Li, X.; Zheng, C.; Wang, X.; Sun, R. Facile and Green Synthesis of Silver Nanoparticles in Quaternized Carboxymethyl Chitosan Solution. *Nanotechnology* **2013**, *24*, 235601.
(14) Raveendran, P.; Fu, J.; Wallen, S. L. A Simple and "green" Method for the Synthesis of Au, Ag, and Au−Ag Alloy Nanoparticles. *Green Chem.* **2006**, *8*, 34−38.
(15) Orendorff, C. J.; Gole, A.; Sau, T. K.; Murphy, C. J. Surface-Enhanced Raman Spectroscopy of Self-Assembled Monolayers: Sandwich Architecture and Nanoparticle Shape Dependence. *Anal. Chem.* **2005**, *77*, 3261−3266.
(16) Xia, L.; Wang, H.; Wang, J.; Gong, K.; Jia, Y.; Zhang, H.; Sun, M. Microwave-Assisted Synthesis of Sensitive Silver Substrate for Surface-Enhanced Raman Scattering Spectroscopy. *J. Chem. Phys.* **2008**, *129*, 134703.
(17) Zhang, J.; Li, X.; Sun, X.; Li, Y. Surface Enhanced Raman Scattering Effects of Silver Colloids with Different Shapes. *J. Phys. Chem. B* **2005**, *109*, 12544−12548.
(18) Lu, Y.; Liu, G. L.; Lee, L. P. High-Density Silver Nanoparticle Film with Temperature-Controllable Interparticle Spacing for a Tunable Surface Enhanced Raman Scattering Substrate. *Nano Lett.* **2005**, *5*, 5−9.
(19) Magdassi, S.; Grouchko, M.; Berezin, O.; Kamyshny, A. Triggering the Sintering of Silver Nanoparticles at Room Temperature. *ACS Nano* **2010**, *4*, 1943−1948.
(20) Long, Y.; Wu, J.; Wang, H.; Zhang, X.; Zhao, N.; Xu, J. Rapid Sintering of Silver Nanoparticles in an Electrolyte Solution at Room Temperature and Its Application to Fabricate Conductive Silver Films Using Polydopamine as Adhesive Layers. *J. Mater. Chem.* **2011**, *21*, 4875−4881.
(21) Perelaer, J.; de Gans, B.-J.; Schubert, U. S. Ink-Jet Printing and Microwave Sintering of Conductive Silver Tracks. *Adv. Mater.* **2006**, *18*, 2101−2104.
(22) Perelaer, J.; Klokkenburg, M.; Hendriks, C. E.; Schubert, U. S. Microwave Flash Sintering of Inkjet-Printed Silver Tracks on Polymer Substrates. *Adv. Mater.* **2009**, *21*, 4830−4834.
(23) Raveendran, P.; Fu, J.; Wallen, S. L. Completely "Green" Synthesis and Stabilization of Metal Nanoparticles. *J. Am. Chem. Soc.* **2003**, *125*, 13940−13941.
(24) Meroni, D.; Ardizzone, S.; Schubert, U. S.; Hoeppener, S. Probe-Based Electro-Oxidative Lithography of OTS SAMs Deposited onto Transparent ITO Substrates. *Adv. Funct. Mater.* **2012**, *22*, 4376−4382.
(25) Tsuji, M.; Hashimoto, M.; Nishizawa, Y.; Kubokawa, M.; Tsuji, T. Microwave-Assisted Synthesis of Metallic Nanostructures in Solution. *Chem. - Eur. J.* **2005**, *11*, 440−452.
(26) Evanoff, D. D.; White, R. L.; Chumanov, G. Measuring the Distance Dependence of the Local Electromagnetic Field from Silver Nanoparticles. *J. Phys. Chem. B* **2004**, *108*, 1522−1524.
(27) Chen, M.; Feng, Y.-G.; Wang, X.; Li, T.-C.; Zhang, J.-Y.; Qian, D.-J. Silver Nanoparticles Capped by Oleylamine: Formation, Growth, and Self-Organization. *Langmuir* **2007**, *23*, 5296−5304.
(28) Wiley, B.; Sun, Y.; Xia, Y. Synthesis of Silver Nanostructures with Controlled Shapes and Properties. *Acc. Chem. Res.* **2007**, *40*, 1067−1076.
(29) Sun, Y.; Xia, Y. Shape-Controlled Synthesis of Gold and Silver Nanoparticles. *Science* **2002**, *298*, 2176−2179.
(30) Jiang, H.; Moon, K.; Zhang, Z.; Pothukuchi, S.; Wong, C. P. Variable Frequency Microwave Synthesis of Silver Nanoparticles. *J. Nanopart. Res.* **2006**, *8*, 117−124.
(31) Nirmala Grace, A.; Pandian, K. One Pot Synthesis of Polymer Protected Pt, Pd, Ag and Ru Nanoparticles and Nanoprisms under Reflux and Microwave Mode of Heating in glycerol—A Comparative Study. *Mater. Chem. Phys.* **2007**, *104*, 191−198.
(32) Ullah, M. H.; Il, K.; Ha, C.-S. Preparation and Optical Properties of Colloidal Silver Nanoparticles at a High Ag+ Concentration. *Mater. Lett.* **2006**, *60*, 1496−1501.
(33) Cappelletti, G.; Ardizzone, S.; Meroni, D.; Soliveri, G.; Ceotto, M.; Biaggi, C.; Benaglia, M.; Raimondi, L. Wettability of Bare and Fluorinated Silanes: A Combined Approach Based on Surface Free Energy Evaluations and Dipole Moment Calculations. *J. Colloid Interface Sci.* **2013**, *389* (1), 284−291.
(34) Soliveri, G.; Annunziata, R.; Ardizzone, S.; Cappelletti, G.; Meroni, D. Multiscale Rough Titania Films with Patterned Hydrophobic/Oleophobic Features. *J. Phys. Chem. C* **2012**, *116*, 26405−26413.
(35) Maino, G.; Meroni, D.; Pifferi, V.; Falciola, L.; Soliveri, G.; Cappelletti, G.; Ardizzone, S. Electrochemically Assisted Deposition of Transparent, Mechanically Robust TiO_2 Films for Advanced Applications. *J. Nanopart. Res.* **2013**, *15* (2087), 1−10.
(36) Zhang, X.; Hayward, D. O.; Mingos, D. M. P. Apparent Equilibrium Shifts and Hot-Spot Formation for Catalytic Reactions Induced by Microwave Dielectric Heating. *Chem. Commun.* **1999**, *11*, 975−976.
(37) Rele, M.; Kapoor, S.; Sharma, G.; Mukherjee, T. Reduction and Aggregation of Silver and Thallium Ions in Viscous Media. *Phys. Chem. Chem. Phys.* **2004**, *6*, 590−595.
(38) Sheel, D. W.; Brook, L. A.; Yates, H. M. Controlled Nanostructured Silver Coated Surfaces by Atmospheric Pressure Chemical Vapour Deposition. *Chem. Vap. Deposition* **2008**, *14*, 14−24.
(39) Ling, X. Y.; Yan, R.; Lo, S.; Hoang, D. T.; Liu, C.; Fardy, M. A.; Khan, S. B.; Asiri, A. M.; Bawaked, S. M.; Yang, P. Alumina-Coated Ag Nanocrystal Monolayers as Surfaceenhanced Raman Spectroscopy Platforms for the Direct Spectroscopic Detection of Water Splitting Reaction Intermediates. *Nano Res.* **2014**, *7*, 132−143.
(40) Fang, Y.; Li, Y.; Xu, H.; Sun, M. Ascertaining p,p′-Dimercaptoazobenzene Produced from p-Aminothiophenol by Selective Catalytic Coupling Reaction on Silver Nanoparticles. *Langmuir* **2010**, *26*, 7737−7746.
(41) Dong, B.; Fang, Y.; Chen, X.; Xu, H.; Sun, M. Substrate-, Wavelength-, and Time-Dependent Plasmon-Assisted Surface Catalysis Reaction of 4-Nitrobenzenethiol Dimerizing to p,p′-Dimercaptoazobenzene on Au, Ag, and Cu Films. *Langmuir* **2011**, *27*, 10677−10682.

DOI: 10.1021/acs.jpcc.5b10833
J. Phys. Chem. C 2016, 120, 1237−1244

WILEY-VCH

Supporting Information

Microwave-assisted Silver Nanoparticle Film Formation for SERS applications

*Guido Soliveri, Silvia Ardizzone, Sezin Yüksel, Dana Cialla-May, J. Popp, Ulrich S. Schubert, Stephanie Hoeppener**

Guido Soliveri, Prof. Silvia Ardizzone

Dipartimento di Chimica, Università degli Studi di Milano, Via Golgi 19, 20133 Milano, Italy

Sezin Yüksel, Dr. Dana Cialla-May, J. Popp

Leibniz-Institut of Photonic Technology, Albert-Einstein-Str. 9, 07745 Jena, Germany;

Institute of Physical Chemistry and Abbe Center of Photonics, Friedrich Schiller University Jena, Helmholtzweg 4, 07743 Jena, Germany

Prof. Dr. Ulrich S. Schubert, Dr. Stephanie Höppener

Laboratory of Organic and Macromolecular Chemistry (IOMC), Friedrich Schiller University Jena, Humboldtstr. 10, 07743 Jena, Germany and

Jena Center for Soft Matter (JCSM), Friedrich Schiller University Jena, Philosophenweg 7, 07743 Jena, Germany

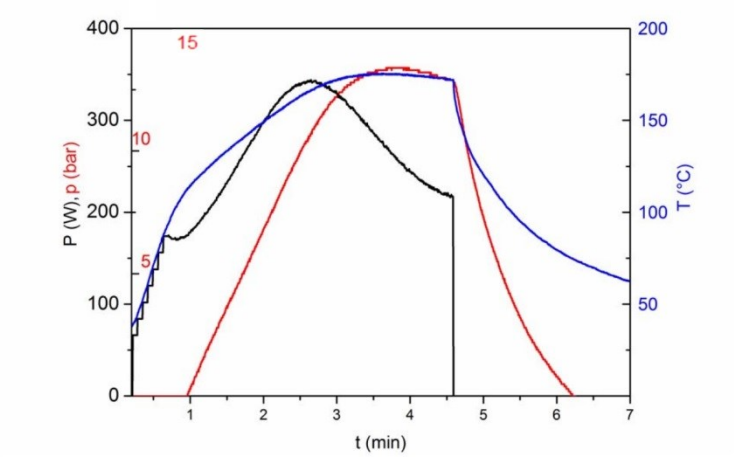

Figure S1: Pressure (p) / power (P) / temperature (T) plot *vs.* time of irradiation of the sample obtained after two minutes at 170 °C, using ethanol as the reducing agent.

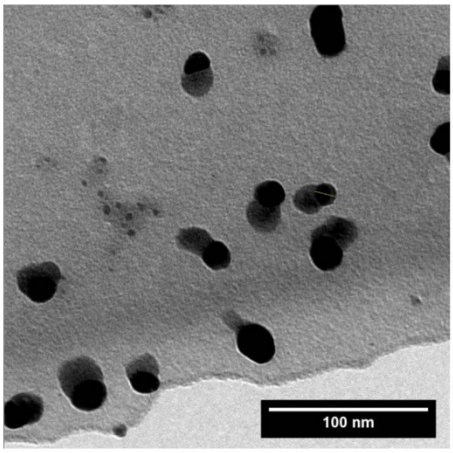

Figure S2: TEM picture obtained by blotting the final solution directly on the TEM grid. Sample obtained after two minutes of irradiation at 170 °C using ethanol as reducing agent.

Choice of experimental conditions: Temperature and amount of reactants

The choice of the specific conditions to be adopted was first investigated. The role of temperature, the dependence of the Ag salt concentration and the amount of reducing agent are here summarized.

Temperature

The temperature range between 150 to 190 °C was investigated. The synthesis was planned in such a way to heat the reaction mixture for two minutes at a constant desired temperature. Figure S3 shows the UV/vis spectra of the sample heated at 150, 170, 180 and 190 °C, while Figure S4 shows the SEM top-view pictures of the corresponding samples. In the case of the sample heated at 150 °C, no clear-cut plasmonic resonance was observed. The other samples revealed a similar peak position, with a slight blue-shift associated with increasing temperature. SEM pictures of the 150 °C sample displayed agglomerates attached to the surface. The sample at 170 °C was homogeneous, with quite small, well packed particles at the surface. By increasing the temperature, the particles grew and the layer became less homogeneous and less packed. The chosen temperature of 170 °C was a good compromise between plasmonic resonance and desired properties at the surface.

Amount of silver acetate and ethanol

We optimized the silver acetate / water + ethanol / water ratios in such a way to obtain the best film. The conditions reported in the manuscript (1 mL of ethanol, 2 mL of water and 1 mg of silver acetate) were chosen on the grounds of the investigation of syntheses carried out changing the concentrations of ethanol and silver salt. In the case of a lower amount of ethanol (0.5 mL), no film formation was observed. Figure S5 shows SEM pictures of films obtained by utilizing different reaction mixtures. We evaluated by electron microcopy and observation with the bare eye the best condition for our purpose. As shown in Figure S5, only in (c) the particles were rather spherical and well packed.

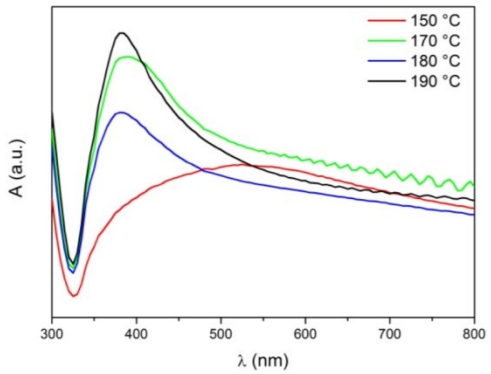

Figure S3: UV-vis spectroscopy of the sample obtained after two minutes at different temperatures using ethanol as reducing agent.

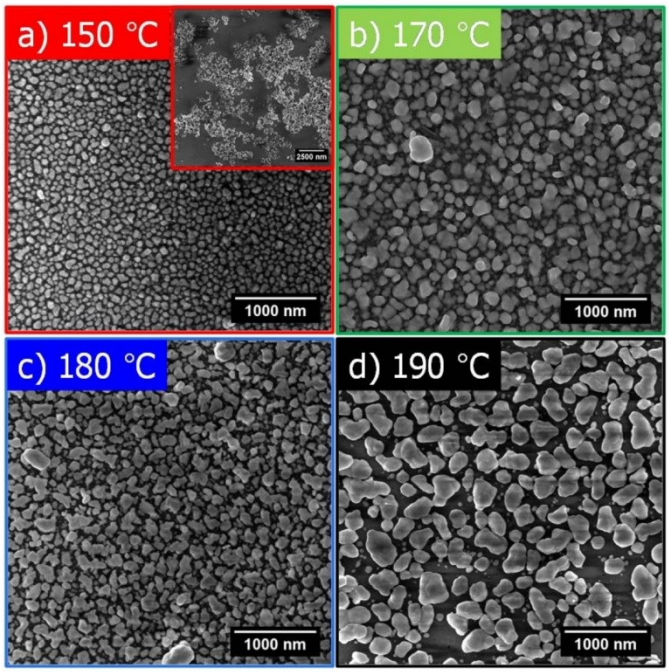

Figure S4: SEM of the samples obtained after two minutes at different temperatures, using ethanol as reducing agent.

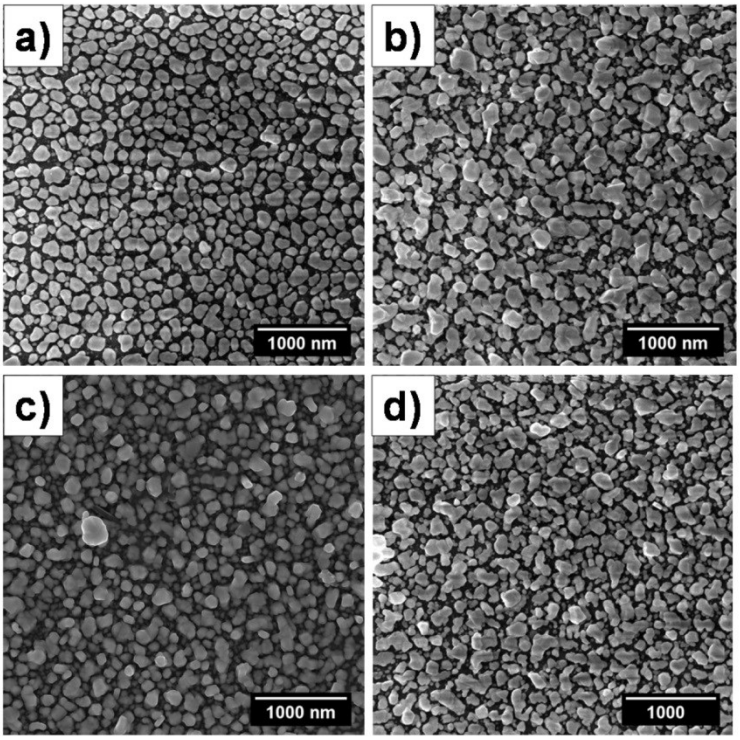

Figure S5: SEM of the samples obtained after two minutes at 170 °C: (a) 0.5 mg and (b) 1.5 mg of Ag acetate on 1 mL of ethanol; (c) 1 mg of Ag acetate and 1mL of ethanol; (d) 1 mg of Ag acetate and 1.5 mL of ethanol.

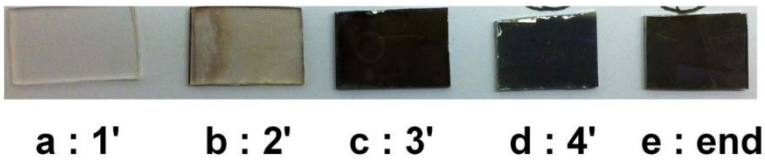

Figure S6: (a-d) Photograph of the samples in which the reaction was quenched after 1, 2, 3 or 4 minutes from the beginning of the MW irradiation and (e) of the film at the end of the optimized reaction (two minutes at 170 °C).

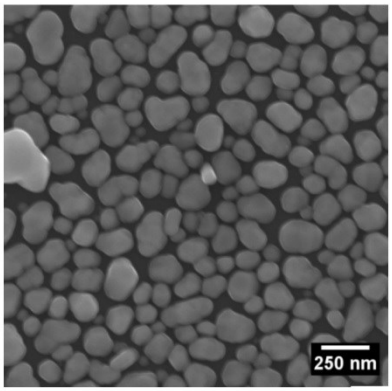

Figure S7: SEM of the sample obtained after 10 minutes at 170 °C using ethanol as reducing agent.

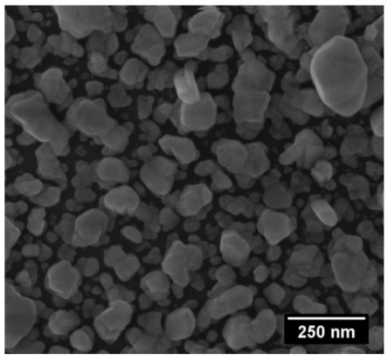

Figure S8: SEM of the sample obtained after two minutes at 170 °C, using ethanol as the reducing agent (magnification).

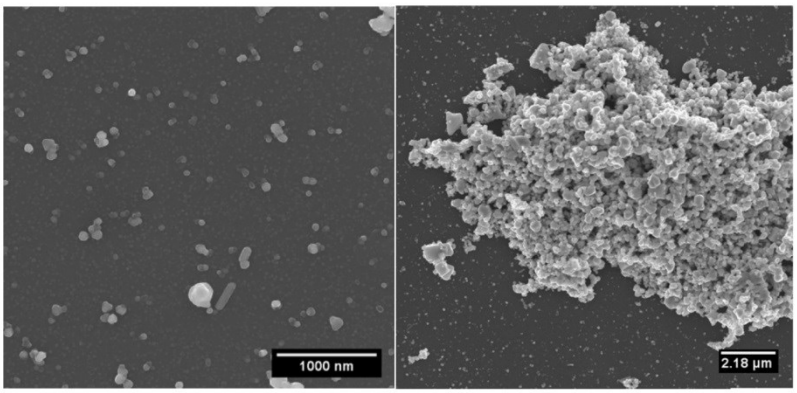

Figure S9: SEM of the sample obtained after two minutes at 170 °C using ethylene glycol as the reducing agent; two different areas.

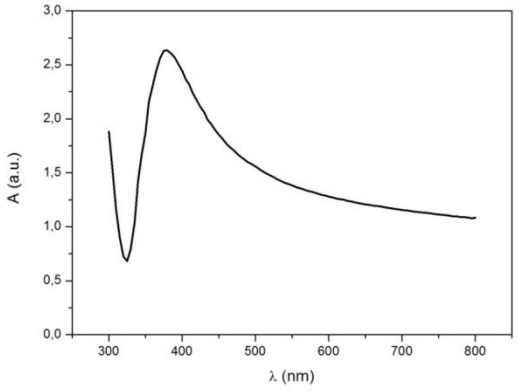

Figure S10: UV-Vis spectroscopy of the sample obtained after two minutes at 170 °C, using ethanol as the reducing agent on a hydrophobic silanized glass lamina as a support.

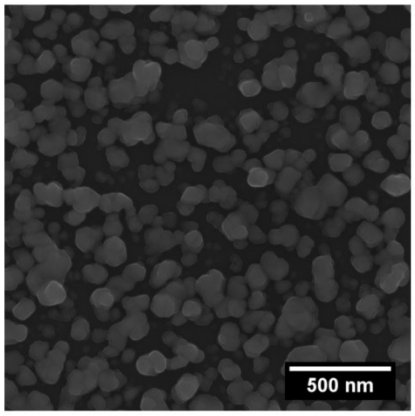

Figure S11: SEM of the sample obtained after 2 minutes at 170 °C, using ethanol as the reducing agent an a hydrophobic silanized glass lamina as a support.

Table T1.

	Ethanol	Ethylene glycol	Glycerol
Viscosity / cP	12	161	1412
Boiling point / °C	78	197	290
Density / kgL^{-1}	0.789	1.113	1.261
Dielectric constant	24	37	42
Surface tension / nMm^{-1}	22	48	63

4.5 Trace detection of tetrahydrocannabinol (THC) with a SERS-based capillary platform prepared by the in situ microwave synthesis of AgNPs [SY5]

S. Yüksel*, Almut M. Schwenke*, Guido Soliveri, Silvia Ardizzone, Karina Weber, Dana Cialla-May, Stephanie Hoeppener, Jürgen Popp.

Analytica Chimica Acta, *2016*, ***939***, p. 93-100,

http://dx.doi.org/10.1016/j.aca.2016.08.033

*both authors contributed equally

Autorenschaft der Publikation

*Sezin Yüksel**	*Concept development* *Experimental design* *Raman measurements* *Data analysis and interpretation* *Writing the manuscript*
*Almut M. Schwenke**	Concept development Experimental design Nanoparticle synthesis and its characterization Data analysis and interpretation Writing the manuscript
Guido Soliveri	Experimental design Proof reading of manuscript
Silvia Ardizzone	Proof reading of manuscript
Karina Weber	Discussion of experimental concept and results Proofreading of manuscript
Dana Cialla-May	Discussion of experimental concepts and results Proof reading of manuscript
Stephanie Hoeppener	Discussion of experimental concepts and results Proof reading of manuscript
Ulrich S. Schubert	Project management Discussion of concepts and results Proof reading of manuscript
Jürgen Popp	Project management Discussion of concepts and results Proof reading of manuscript

*both authors contributed equally

Erklärung zu den Eigenanteilen der Promovendin sowie der weiteren Doktoranden/ Doktorandinnen als Koautoren an der Publikation und Zweitpublikationsrechten bei einer kumulativen Dissertation

Publication: **S. Yüksel*, A. M. Schwenke*, G. Soliveri, S. Ardizzone, K. Weber, D. Cialla-May, S. Hoeppener, U. S. Schubert and J. Popp.** ***Trace detection of tetrahydrocannabinol (THC) with a SERS-based capillary platform prepared by the in situ microwave synthesis of AgNPs*** **Analytica Chimica Acta, 2016, 939, p.93-100**		
Beteiligt an		
	Sezin Yüksel*	**Almut M. Schwenke***
Konzeption des Forschungsansatzes	**X**	**X**
Planung der Untersuchungen	**X**	**X**
Datenerhebung	**X**	**X**
Datenanalyse und -interpretation	**X**	**X**
Schreiben des Manuskripts	**X**	**X**
Vorschlag Anrechnung Publikationsäquevalente	**1.0**	**1.0**

*both authors contributed equally

Analytica Chimica Acta 939 (2016) 93–100

Contents lists available at ScienceDirect

Analytica Chimica Acta

journal homepage: www.elsevier.com/locate/aca

Trace detection of tetrahydrocannabinol (THC) with a SERS-based capillary platform prepared by the *in situ* microwave synthesis of AgNPs

Sezin Yüksel [a, b, c, 1], Almut M. Schwenke [d, e, 1], Guido Soliveri [f], Silvia Ardizzone [f], Karina Weber [a, b, c], Dana Cialla-May [a, b, c, *], Stephanie Hoeppener [d, e, **], Ulrich S. Schubert [d, e], Jürgen Popp [a, b, c, e]

[a] Leibniz Institute of Photonic Technology Jena (IPHT), Jenaer BioChip Initiative, Albert-Einstein-Straße 9, 07745 Jena, Germany
[b] Institute of Physical Chemistry and Abbe Center of Photonics, Friedrich Schiller University Jena, Helmholtzweg 4, 07743 Jena, Germany
[c] InfectoGnostics Forschungscampus Jena, Zentrum für Angewandte Forschung, Philosophenweg 7, 07743 Jena, Germany
[d] Laboratory of Organic and Macromolecular Chemistry (IOMC), Friedrich Schiller University Jena, Humboldtstrasse 10, 07743 Jena, Germany
[e] Jena Center for Soft Matter (JCSM), Friedrich Schiller University Jena, Philosophenweg 7, 07743 Jena, Germany
[f] Dipartimento di Chimica, Università degli Studi di Milano, Via Golgi 19, 20133 Milano, Italy

HIGHLIGHTS

- An ultra-sensitive and highly reproducible novel SERS-based capillary platform.
- Glass capillaries were coated with Ag nanoparticles by utilizing microwave-assisted synthesis in a batch fabrication process.
- A high point-to-point and batch-to-batch SERS reproducibility.
- 1 nM of tetrahydrocannabinol (THC) is detected.

GRAPHICAL ABSTRACT

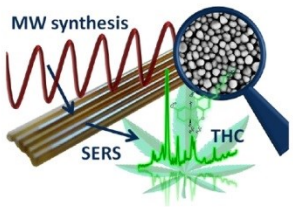

ARTICLE INFO

Article history:
Received 24 May 2016
Received in revised form
25 July 2016
Accepted 20 August 2016
Available online 26 August 2016
Dedicated to Professor Dr. Gerhard Bringmann on the occasion of his 65th birthday.

ABSTRACT

In the present study, an ultra-sensitive and highly reproducible novel SERS-based capillary platform was developed and utilized for the trace detection of tetrahydrocannabinol (THC). The approach combines the advantages of microwave-assisted nanoparticle synthesis, plasmonics and capillary forces. By employing a microwave-assisted preparation method, glass capillaries were reproducibly coated with silver nanoparticles in a batch fabrication process that required a processing time of 3 min without needing to use any pre-surface modifications or add surfactants. The coated capillaries exhibited an excellent SERS activity with a high reproducibility and enabled the detection of low concentrations of target molecules. At the same time, only a small amount of analyte and a short and simple incubation process was required. The developed platform was applied to the spectroscopic characterization of

* Corresponding author. Leibniz Institute of Photonic Technology Jena (IPHT), Jenaer BioChip Initiative, Albert-Einstein-Straße 9, 07745 Jena, Germany.
** Corresponding author. Laboratory of Organic and Macromolecular Chemistry (IOMC), Friedrich Schiller University Jena, Humboldtstrasse 10, 07743 Jena, Germany.
E-mail addresses: dana.cialla-may@uni-jena.de (D. Cialla-May), s.hoeppener@uni-jena.de (S. Hoeppener).
[1] Both authors contribute equally to the paper.

http://dx.doi.org/10.1016/j.aca.2016.08.033
0003-2670/

Keywords:
Microwave-assisted synthesis
SERS
Drug monitoring
Capillary
THC

tetrahydrocannabinol (THC) and its identification at concentration levels down to 1 nM. Thus, a highly efficient detection system for practical applications, e.g., in drug monitoring/detection, is introduced, which can be fabricated at low cost by using microwave-assisted batch synthesis techniques.

1. Introduction

The detection of trace amounts of compounds is an essential challenge for quality control, diagnostics and sensing [1]. This includes, e.g., the analysis of very low amounts of trace compounds. There is a constantly increasing desire for easily applicable, cheap and reliable test devices that provide excellent sensitivity and low detection limits. Some of these applications focus on monitoring illegal drugs and drug consumption, such as Cannabis sativa L., with its main component being tetrahydrocannabinol (THC) [2–6]. Generally, the amount of THC and its metabolites in the human body can be quantified by urinalysis and hair follicle drug testing [7–12]. However, these sophisticated approaches require complex chemical analysis with advanced equipment, specialized expertise and long processing times. Alternatively, presumptive tests are commercially available that allow for measurements to be made from blood serum and saliva matrices and can be used for onsite detection. However, these methods cannot provide quantitative information but can only confirm the presence of the suspected substance with some certainty. In this context, surface enhanced Raman scattering (SERS) serves as an emerging and promising tool for bioanalytical applications [13–23]. This technique relies critically on the development of suitable measurement platforms that can be applied in routine analytics, ideally by non-expert users. In this respect, capillary-based systems offer advantages as they allow for easy sample preparation and minimize the required amount of test substance. Additionally, capillary-based system provides a large surface area in the focus volume. As a result, the number of SERS-active sites increases; thus, more reproducible and reliable measurement conditions are obtained [24–34]. Furthermore, the capillary forces enable the transportation of the target analyte to plasmonic sensors within a few seconds. Thus, an effective and rapid detection scheme is obtained. One common technique to fabricate capillary-based SERS platforms is to coat the inside of a capillary with metal nanoparticles (NPs). In the literature, different approaches are reported that usually include the *ex situ* synthesis of silver or gold nanoparticles and thereafter the immobilization of the particles on the inner surface of the capillaries. The binding can be promoted by either a self-assembled monolayer, for example, 3-aminopropyl trimethoxysilane (APTMS) [35,36] or an alkanethiol [37], or a polyelectrolyte coating [38,39]. These preparation protocols typically consist of multiple time-consuming processes, including several cleaning steps with, e.g., concentrated acids or different solvents, as well as require long binding times. Thus, the overall preparation time ranges from several hours to days. Furthermore, polymer-capped metal nanoparticles can be deposited on the inside of a capillary, for example, poly(ethylene imine) capped AuNPs [40] and AgNPs [41] or poly(vinyl pyrrolidone)-coated Ag nanowires [42]. All of these approaches require the application of organic additives, which will potentially contribute to the background signal during Raman analysis. In the present study (the experimental outline is summarized in Fig. 1), we improved the fabrication of nanoparticle-coated capillaries by utilizing a microwave-assisted *in situ* synthesis approach to directly form homogenous monolayers of silver nanoparticles in a capillary. This approach provides several advantages over the previously introduced methods [43]. Homogenously sized nanoparticles are achieved without the addition of any surfactant, and by applying microwave irradiation; only extremely short processing times are required. Moreover, the batch synthesis of many nanoparticle-coated capillaries can be performed in one step, thereby utilizing a simple set-up with accessible control of the reaction. Next, for a detailed morphological characterization of the capillaries, the SERS reproducibility was investigated by point-to-point as well as batch-to-batch measurements. The extraordinary sensitivity of the capillary-based sensor was demonstrated by the detection and spectroscopic characterization of THC – a molecule that has been rarely investigated by means of SERS and that has a high significance for practical applications. To the best of our knowledge, this is the first report on a SERS-based sensor platform for the monitoring of THC down to nanomolar concentrations, as well as the first report of microwave-assisted *in situ* synthesis of AgNPs inside a capillary tube, which enables a fast and reliable workflow for a SERS-based drug sensor.

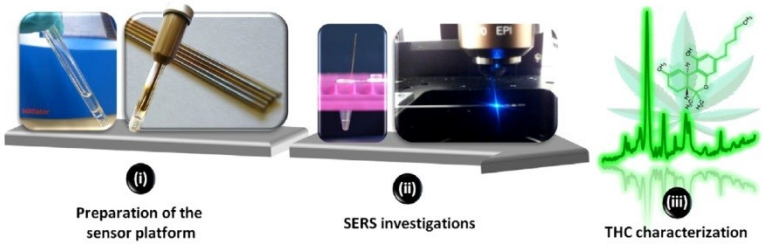

Fig. 1. Schematic representation of the experimental procedure: **(i)** The AgNP coating was realized by adding a batch of five bare glass capillaries to a reaction vial filled with a silver salt solution. Upon microwave irradiation, AgNPs developed on the glass wall. **(ii)** After analyte incubation, the SERS-characteristics of the sensor platform and the system's point-to-point and batch-to-batch reproducibility were investigated. **(iii)** Finally, the platform was applied to the detection and spectroscopic characterization of THC.

2. Results and discussion

2.1. Preparation and morphology of AgNP-coated glass capillaries

In this study, commercially available glass capillaries, e.g., those used for thermal analysis or blood sample collection, were functionalized with a silver nanoparticle coating to obtain a plasmonic-active structure. The fabrication process was performed by adjusting a recently reported microwave-assisted synthesis method [44] to the demands of coating the inner surface of the glass capillaries. In this context, microwave heating provides the advantages of rapid heating rates and, consequently, short reaction times, as well as the possibility for automation and batch processing [45].

The precursor for the preparation of the AgNP coating consists of an aqueous solution of silver acetate mixed with ethanol, which serves as the reducing agent. Neither stabilizers, additional reducing agents nor stirring are required to support the formation of uniform silver nanoparticles.

AgNP synthesis was performed by utilizing a designated laboratory single-mode microwave. In contrast to the previously introduced method [44], in which a defined reaction temperature was utilized, the microwave was operated in the power-controlled mode; thus, a constant irradiation power was applied for the duration of the reaction time. By continuously using the maximum power of the microwave oven, the heating ramp time was minimized, and as a result, the overall processing time was shortened. Hence, in this study, only 90 s of microwave irradiation was required, and the whole microwave process, including the cooling time, was completed in less than 3 min (for a detailed discussion of the chosen synthesis parameters see **SI 1**). During the reaction, a typical temperature of 190–200 °C and pressure of 10–15 bar were measured, with slight variations occurring among the different batches that were fabricated (Fig. S1). Five capillaries were always prepared in one batch. A homogenous coating was consistently obtained, as seen from the characteristic yellowish color of AgNPs that was visible along all five capillaries in Fig. 1(i).

By scanning electron microscopy (SEM), the morphology of the AgNP-coatings was investigated (Fig. 2). The microwave-assisted reduction reaction of the precursor solution resulted in the development of AgNPs that formed a dense monolayer on the glass surface (Fig. 2(A-C)) and homogenously covered the substrate over a large area (Fig. 2(B, D)). In Fig. 2(E), a photograph of a representative capillary is displayed along with SEM images (Fig. 2(D)) taken at three different areas of the capillary, as marked in the photograph. In Fig. 2(F), the related particle size distributions are shown. It can be observed that a homogenous and dense coating of AgNPs was obtained over a range of more than 3 cm. In this area, the nanoparticles feature an approximate size of 45 ± 15 nm and are separated from each other.

Generally, the size of the nanoparticles can be tuned by changing the reaction time or the concentration of the precursor solution with an increase in concentration and reaction time leading to larger nanoparticles. Moreover, the concentration of silver salt in the precursor not only has an effect on the particle size but also influences the microwave absorption of the precursor solution. A higher concentration of silver acetate results in a more efficient MW absorption, thus accelerating the heating and decreasing the required synthesis time (alternative synthesis protocols are discussed in Figs. S2 and S3). Another factor that influences the required reaction time is the filling level of the solution in the reaction vial. In contrast to conventional heating processes, in which a larger volume of reactants usually requires a longer heating time, microwave-assisted reactions with a larger volume, i.e., a.

higher filling level of the reactants, provides a larger absorption area and thus a more efficient heating of the reactants in the vial [46].For our synthesis approach, we identified 0.3 mL to be the optimum filling level in terms of the fast heating of the reactants and in accordance with a minimum consumption of the precursor solution. The filling level of the reaction vial has, however, no direct.

influence on the coated area at the inside of the capillary, i.e., the height at which a homogenous coating is obtained. Although the filling level in the vial was approximately 1.5 cm, the liquid level inside the capillary was several centimeters because of capillary force. Consequently, AgNPs were homogenously formed on the inner glass walls of the capillaries over a large range.

Thus, by optimizing the reaction conditions, a reliable and fast microwave-assisted batch fabrication process for the preparation of silver nanoparticle-coated glass capillaries was developed. After simply rinsing with water and wiping off the outer surface, the capillaries were ready to be applied as SERS substrates.

2.2. SERS characterization of AgNP-coated capillaries

After investigating the morphology of the AgNP coating and its homogeneity across a large spatial range, the SERS activity of the platform was evaluated. This included the determination of the optimal SERS measurement conditions, as well as the point-to-point and batch-to-batch SERS reproducibility of the capillaries. This was performed by utilizing adenine as a model analyte.

For the determination of the optimal SERS measurement conditions, 0.1 mM of adenine in aqueous solution (as a non-resoanant molecule) is used in order to avoid the resonance Raman effect. The capillaries were filled with an adenine solution (as a model analyte) by utilizing capillary action. Because of the thin inner diameter of the capillary, only 4 μL of analyte was required to incubate a substrate with a length of 3 cm. Fig. 3(A) shows the SERS background of the capillary and the SERS spectrum of adenine, which were recorded from a single point with an integration time of 0.5 s and 10 s by focusing the laser beam through the capillary wall. The characteristic bands of adenine can be reliably detected without any significant background contribution from the capillary. Comparing the adenine spectra recorded at 0.5 s with that recorded at 10 s, it is clear that with a longer measurement time the carbon spectrum between 1200 cm^{-1} and 1600 cm^{-1} appears to be much more intense. This intense carbon spectrum is due to the twenty times longer laser exposure time. Furthermore, this is caused by decomposition (i.e., burning effects) of the molecule at the nanoparticle surface with relatively long integration time at a single point. To conclude, while the carbon background increases with the long exposure time, the signal-to-noise ratio of the characteristic band of the adenine decreases. The adenine spectrum features the characteristic aromatic ring breathing mode [47] at 733 cm^{-1}. This Raman mode was integrated and plotted as a function of time to investigate the stability of the SERS signal (Fig. 3(B)). It can be observed that the maximum SERS intensity was obtained over a time period of 10 s with a nearly stable SERS value and then started to decrease dramatically. These SERS intensity fluctuations can be caused by changes in the substrate's morphology, e.g., because of the heating of the substrate caused by the magnified local field of electromagnetic enhancement [48]. Furthermore, changes to the effective molecular configuration of the surface, such as the desorption, re-orientation, and surface diffusion of adsorbates, can be an important contributor to SERS intensity fluctuations over the course of the investigation.

To prevent the burning effect and, at the same time, to increase the signal to noise ratio, subsequent SERS investigations used a short integration time per spot while scanning along the capillary. Thus, a higher number of measured SERS spectra was obtained,

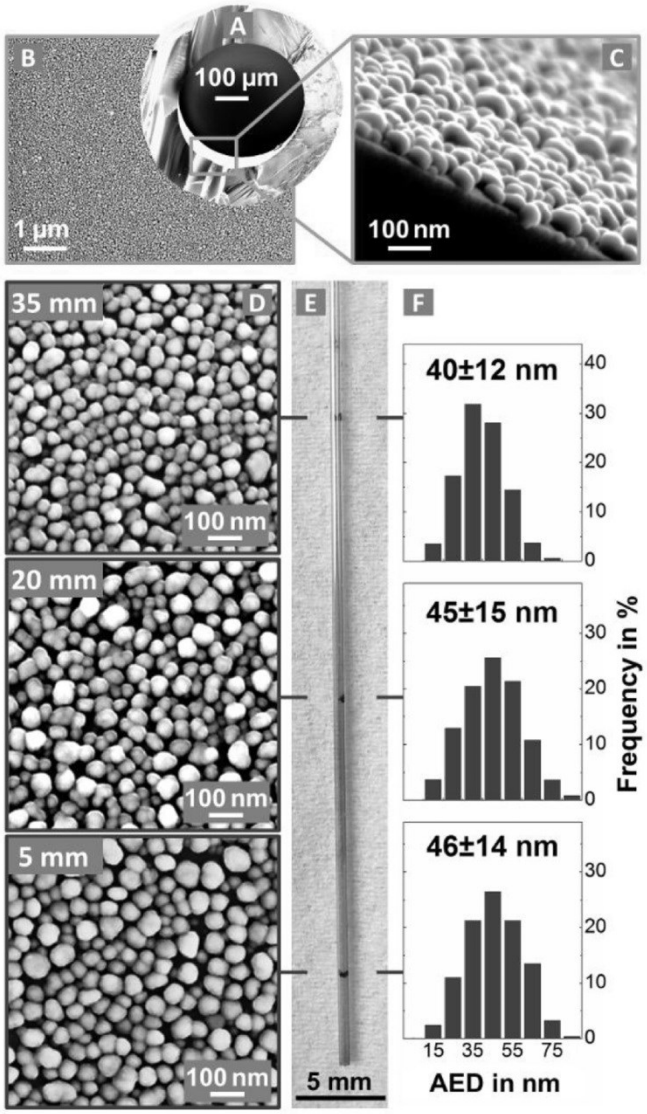

Fig. 2. Morphology of the AgNP coatings: SEM images showing the cross-section of a capillary **(A)** and its homogeneously coated interior **(B)**, which consists of a monolayer of silver nanoparticles **(C)**. The SEM images **(D)** and particle size-distributions **(F)** of the marked areas in the photograph of the capillary **(E)**, reveals the long-range uniformity of the silver nanoparticles. In the size distributions, the area equivalent diameter (AED) of the particles is plotted.

which improved the statistics of the data. However, this method requires a high point-to-point reproducibility along the capillary. Despite the fact that SERS substrates offer great potential with respect to their high sensitivity and specificity, two major drawbacks of bottom-up produced arrays are the lack of spatial reproducibility and poor large area fabrication [49].

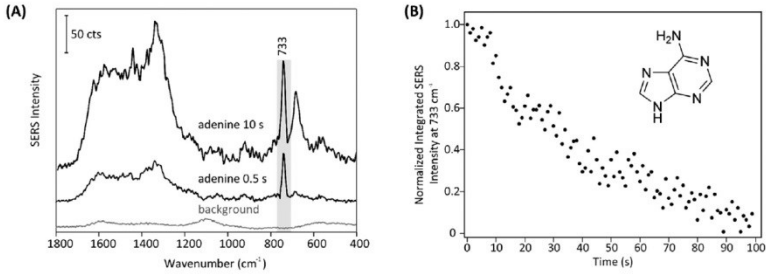

Fig. 3. **(A)** SERS spectra of adenine recorded with an integration time of 10 s and 0.5 s and the SERS spectrum of the capillary background. **(B)** Single-point measurement of SERS signal fluctuations as a function of time after introducing 0.1 mM of adenine. The normalized integrated SERS intensity at 733 cm^{-1} is plotted as a function of time.

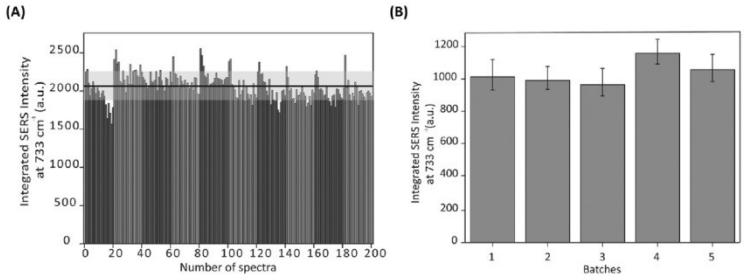

Fig. 4. **(A)** Point-to-point SERS reproducibility of 0.1 mM of adenine obtained from randomly selected spots along a single capillary. The black line shows the average intensity, and the light gray area represents the standard deviation of the obtained spectra. **(B)** The batch-to-batch SERS reproducibility of 5 different batches of capillaries.

SEM analysis of the AgNP coatings already showed the morphological homogeneity across a large segment of the capillary (see Fig. 2). To investigate the SERS signal uniformity along the capillary wall, SERS spectra were collected along 40 μm line from 20 different measurement points which was repeated at 10 randomly chosen areas. Fig. 4(A) presents the point-to-point SERS reproducibility of the measurements. The characteristic Raman mode of adenine at 733 cm^{-1} was integrated for 200 individual spectra and plotted as a function of the spectrum number. The relative standard deviation (RSD) of the SERS intensity was approximately 8.1%, which is shown as the light gray area. It is clear that the variations of most of the recorded SERS spectra are located within this area. This observation illustrates, that scanning the laser along the capillary is a reliable method to decrease the measurement time per point, thereby preventing the observed burning effects, and to improve the signal to noise ratio. Additionally, several batches of capillaries were prepared (see Fig. S4) to investigate the batch-to-batch SERS reproducibility. Similarly, as for the point-to-point analysis, the ring breathing mode at 733 cm^{-1} was integrated and plotted for individual batches of capillaries. (see Fig. 4(B)). The RSD of the five different batches were between 6.6 and 9.2%. These investigations reveal the potential of the introduced method to fabricate silver-coated glass capillaries supporting a high point-to-point and batch-to-batch reproducibility of the SERS intensity.

2.3. Potential in analytical science: SERS-based detection of THC

To demonstrate the potential of the developed capillary platform for drug monitoring, the main psychoactive component of cannabis, the (−)-trans-Δ^9-tetrahydrocannabinol (THC) molecule, was studied. Its chemical structure is depicted in Fig. 5(A). The reliable and convenient measurement of cannabinoids is highly important for pharmacokinetic studies, drug treatment, drug testing and traffic sobriety checks.

In Fig. 5(B), the measured SERS spectra of THC in methanol, pure methanol and the background of the capillary are shown. Since there is no detailed vibrational assignment of the THC molecule in the literature, density functional theory (DFT) calculations were performed to assign the Raman modes in the SERS spectrum. The calculated Raman vibrational modes of the THC molecule exhibit a large number of well-defined Raman modes. However, most of the Raman bands involve the vibration of several atoms and their precise assignment to particular vibrational modes is demanding. Thus, the calculated and measured signals are displayed in Table 1 together with a tentative assignment. The characteristic Raman modes of the THC molecule are centered at 1390 cm^{-1}, 1236 cm^{-1}, 1006 cm^{-1} and 712 cm^{-1}, which can be ascribed, respectively, to the (=C–H) deformation, (C–H) deformation, (CC) stretching and (C–H) deformation. It can be clearly seen that there is no significant background contribution from the capillary to the SERS spectrum of the THC. However, the characteristic SERS bands at 1033 cm^{-1} and 1590 cm^{-1} of pure methanol might interfere with the THC spectrum. The quantitative relation between the SERS activity and THC concentration is illustrated in Fig. 5(C-D). The SERS signal at 1390 cm^{-1} was integrated and normalized as a function of the concentration.

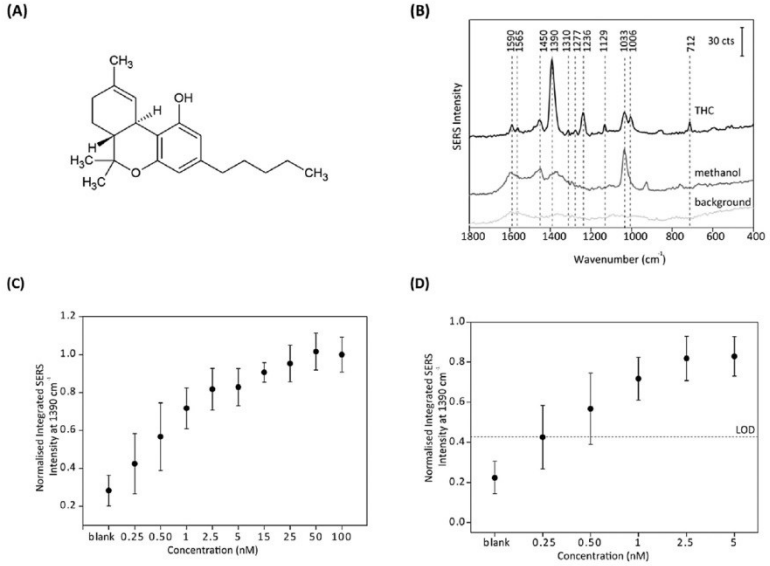

Fig. 5. **(A)** Chemical structure of (−)-trans-Δ^9-tetrahydrocannabinol (THC). **(B)** Measured SERS spectra of 320 nM THC in methanol, pure methanol and the background of the capillary marked with significant vibrational bands. The limit of detection (LOD) for THC: **(C)** The normalized integrated SERS intensity of the peak at 1393 cm^{-1} *versus* the different concentrations of THC. **(D)** A detailed view of the LOD for low concentrations in comparison with the background contribution. The calculated LOD is given by the black dashed line.

THC was detected in the range of 100 to 0.25 nM (see Fig. 5(C)). For better visibility, Fig. 5(D) presents the normalized integrated SERS intensity at 1393 cm^{-1} *versus* the low concentration range between 0.25 nM and 5 nM. To determine the limit of detection (LOD) and to maintain a 99.8% confidence level of the data points, according to the IUPAC definition, the value of three times the standard deviation (+3σ) of the mean value of the background was used to set a threshold and is shown as a black dashed line (see Fig. 5(D)). The comparison of the data with the LOD proves that by employing this SERS-based sensor platform, THC can reliably be detected down to a concentration of 1 nM. Based on the capillary approach, this measurement requires only a few microliters of the THC sample and a very short incubation time.

3. Conclusion

The microwave-assisted synthesis of silver nanoparticle coatings on glass capillaries was identified as a fast and simple method for the preparation of a highly sensitive SERS-based sensor platform. Silver nanoparticle coatings were formed within a reaction time of only 90 s, preparing five capillaries within one reaction batch. No surfactants are required for the formation of the nanoparticles, and only an aqueous silver acetate solution and ethanol were utilized as the reactants. The capillary-based platform exhibits the advantages of requiring a short analyte incubation time and smaller sample consumption compared with well-established planar and bottom-up fabricated SERS substrates. Furthermore, the developed SERS platform is characterized by easy handling, pointing towards an application in routine analytics. With their high point-to-point and batch-to-batch reproducibility, the coated capillaries exhibit high potential as a sensor platform. Applying this platform to a SERS-based detection scheme, THC, as a relevant analyte molecule in illegal drug monitoring, was quantitatively detected in trace concentrations down to 1 nM.

Table 1
Selected experimental SERS wavenumbers of THC in methanol together with the calculated Raman wavenumbers of THC.

Calculated Raman wave numbers [cm^{-1}]	Experimental SERS wave numbers [cm^{-1}]	Band assignments
731	712	CH deformation
1021	1006	CC stretching
1029	1033	CC stretching
1257	1236	CH deformation
1281	1277	CH deformation
1302	1310	CH deformation
1394	1390	=C–H deformation
1479	1450	C–H deformation
1616	1590	C=C stretching

4. Experimental section

4.1. Chemicals and materials

Silver acetate (≥99%), adenine (≥99%) as well as 3.2 mM stock solution of (−)-Δ^9-tetrahydrocannobinol (THC) in methanol were purchased from Sigma-Aldrich (Steinheim, Germany), and ethanol (99%) was obtained from Brenntag (Mühlheim, Germany). Adenine was diluted in distilled water to a final concentration of 0.1 mM, and the required concentrations of THC were prepared in methanol. Glass capillary tubes (for the determination of melting point) with outer dimensions of 80 mm × 0.6 mm and an inner diameter of 0.42 mm were purchased from Marienfeld Laboratory Glassware (Lauda-Königshofen, Germany).

4.2. Preparation of capillaries

Before the coating procedure, the glass capillaries were shortened to approximately 6 cm and cleaned with oxygen plasma (Diener electronic, Ebhausen, Germany) for 5 min in the upright position to increase wettability and homogeneity.

A 12 mM aqueous solution of silver acetate was prepared as the precursor solution and mixed with ethanol as a reducing agent at a ratio of 2:1. A 300 μL aliquot of this solution was placed into a microwave vial (volume: 0.2–0.5 mL, Biotage, Uppsala, Sweden), and five capillaries were added to the vial. The microwave-assisted synthesis process was carried out without a stirring bar. Thus, no sophisticated support was required to hold the glass capillaries, but they could be directly placed at the bottom of the reaction vial (see Fig. 1(i), Fig. S1(A)). Due to the capillary force, the precursor solution ascended the capillary to a height of several centimeters. The vial was capped and heated utilizing a single-mode microwave oven (Biotage Initiator, Uppsala, Sweden) at a full power of 400 W. After 90 s of irradiation, the *in situ* development of AgNPs on the glass surface was quenched by cooling the vial with a stream of air. During the MW process, the temperature was recorded by an external infrared sensor mounted at a height of 1.5 cm, and the pressure was detected by the extension of the septum in the cap. After the synthesis, the outer part of the capillaries was wiped with a tissue and the inside of the capillary was cleaned from precursor residues and loosely bounded AgNPs by rinsing with distilled water.

4.3. Morphology investigation

Scanning electron microscopy imaging was performed with a field emission SEM (Sigma VP, Carl Zeiss AG, Jena, Germany) at 3 kV utilizing the In-lens detector at a working distance of approximately 3 mm. To investigate the morphology of the nanoparticle coatings on the inside of the capillaries, the samples had to be fragmented and pieces from selected areas were affixed to a conductive adhesive carbon tab. All of the samples were coated with a thin layer of carbon to eliminate charging effects.

Image processing and analysis was performed with ImageJ. For the determination of the nanoparticle size distributions, the median filter, a background subtraction by the rolling ball algorithm, binarization with a manual threshold and a watershed to separate connected particles were applied to the SEM images. A size of more than 1000 particles per sample was determined by the particle analysis algorithm. The area equivalent diameter (AED, $d_{AED} = \sqrt{4A/\pi}$) was plotted and used for the calculation of the average particle size [50].

4.4. Raman measurement and calculation

The capillaries were filled with the target analyte containing solution within few seconds employing capillary forces and SERS measurements were carried out using a confocal Raman microscope (WITec GmbH, Ulm, Germany) equipped with a 488-nm excitation laser line, focusing the laser beam through the capillary wall. For the irradiation of the samples, a 20 × Olympus objective (NA: 0.40) with a laser power of 10 mW was utilized. The same objective was used for recording the backscattered light with a spectrometer equipped with a 600 line/mm grating and a 1024 × 127 pixel CCD camera, which was cooled down to 208 K. 10 measurements with an integration time of 0.5 s were collected along 40 μm line scans from 20 different measurement spots.

A density functional theory (DFT) calculation of THC was performed by using Gaussian 09 at the B3LYP level of theory and employing the 6-31G (d, p) basis set. The spectrum was calculated as a convolution with a Lorentzian line shape having the half width of 20 cm^{-1}. In this work a factor of 0.97 was used for scaling the wavenumbers.

Acknowledgements

Funding of the research projects "JBCI 2.0" (03IPT513Y) within the framework "Unternehmen Region - InnoProfile Transfer" as well as "PhoNa" (03IS2101A) within the framework of the excellence program 'Spitzenforschung & Innovation in den Neuen Ländern', the Federal Ministry of Education and Research, Germany (BMBF) is gratefully acknowledged. The SEM facilities of the Jena Center for Soft Matter (JCSM) were established with a grant from the German Research Council (DFG) and the European Funds for Regional Development (EFRE). Moreover, G. Soliveri acknowledges the financial support from Università degli Studi di Milano. Finally, the authors would like to thank Dr. Dirk Bender (IPC, Friedrich Schiller University Jena, Germany) for the theoretical Raman calculation of the THC molecule.

Appendix A. Supplementary data

Supplementary data related to this article can be found at http://dx.doi.org/10.1016/j.aca.2016.08.033.

References

[1] European Monitoring Centre for Drugs and Drug Addiction (EMCDDA), EuropeanDrug Report. Trends and Developments, 2015.
[2] United Nations Office on Drugs and Crime, World Drug Report, 2014.
[3] N. Lau, P. Sales, S. Averill, F. Murphy, S.-O. Sato, S. Murphy, Int. J. Drug Policy 26 (2015) 709.
[4] R.P. Ogeil, J.G. Phillips, S.M.W. Rajaratnam, J.H. Broadbear, Hum. Psychopharmacol. Clin. Exp. 30 (2015) 356.
[5] S. Dubois, N. Mullen, B. Weaver, M. Bédard, Forensic Sci. Int. 248 (2015) 94.
[6] European Monitoring Centre for Drugs and Drug Addiction (EMCDDA), Characteristics of Frequent and High-risk Cannabis Users, 2015.
[7] H. Miller Coyle, T. Palmbach, N. Juliano, C. Ladd, H.C. Lee, An overview of DNA methods for the identification and individualization of Marijuana, Croat. Med. J. 44 (2003) 315.
[8] B.J. Buchan, M. L Dennis, F.M. Tims, G.S. Diamond, Cannabis use: consistency and validity of self-report, on-site urine testing and laboratory testing, Addiction 97 (2002) 108.
[9] S.L. Kacinko, A. Xu, J. W.Homan, M. McMullin, D.M. Warrington, B.K. Logan, J. Anal. Toxicol. 35 (2011) 386.
[10] T.A. Halgren, Chem. Biol. Drug Des. 69 (2007) 146.
[11] N. Galand, D. Ernouf, F. Montigny, J. Dollet, J. Pothier, J. Chromatogr. Sci. 42 (2004) 130.
[12] S. Fedchak, Presumptive Field Testing Using Portable Raman Spectroscopy, 2014.
[13] M. Jahn, S. Patze, I.J. Hidi, R. Knipper, A.I. Radu, A. Mühlig, S. Yüksel, V. Peksa, K. Weber, T. Mayerhöfer, D. Cialla-May, J. Popp, Analyst 141 (2016) 756.
[14] G.M. Santos, F. Zhao, J. Zeng, M. Li, W.C. Shih, J. Biophot. 8 (2015) 855.
[15] K. Hering, D. Cialla, K. Ackermann, T. Dörfer, R. Möller, H. Schneidewind, R. Mattheis, W. Fritzsche, P. Rösch, J. Popp, Anal. Bioanal. Chem. 390 (2008) 113.
[16] I.A. Larmour, D. Graham, Analyst 136 (2011) 3831.
[17] S. Schlücker, Angew. Chem. Int. Ed. 53 (2014) 4756.
[18] R.A. Alvarez-Puebla, L. Liz-Marzán, Chem. Soc. Rev. 41 (2012) 43.
[19] D. Cialla-May, S. Pollok, C. Steinbrücker, K. Weber, J. Popp, Nanophotonics 3 (2014) 383.
[20] T. Vo-Dinh, H.N. Wang, J. Scaffidi, J. Biophot. 3 (2010) 89.
[21] R. Buividas, N. Dzingelevičius, R. Kubiliute, P.R. Stoddart, V.K. Truong, E.P. Ivanova, S. Juodkazis, J. Biophot. 8 (2015) 567.
[22] S. Pahlow, A. März, B. Seise, K. Hartmann, I. Freitag, E. Kämmer, R. Böhme, V. Deckert, K. Weber, D. Cialla, J. Popp, Eng. Life Sci. 12 (2012) 131.
[23] U.S. Dinish, G. Balasundaram, Y.T. Chang, M. Olivo, J. Biophot. 7 (2014) 956.
[24] X. Fan, I.M. White, Nat. Photonics 5 (2011) 591.
[25] Y. Deng, M.N. Idso, D.D. Galvan, Q. Yu, Anal. Chim. Acta 863 (2015) 41.
[26] W. Huttner, K. Christou, A. Gohmann, V. Beushausen, H. Wackerbarth, Microfluid. Nanofluidics 12 (2012) 521.
[27] C. Lim, J. Hong, B.G. Chung, A.J. deMello, J. Choo, Analyst 135 (2010) 837.
[28] C. Escobedo, Lab. Chip 13 (2013) 2445.
[29] D. Sinton, R. Gordon, A.G. Brolo, Microfluid. Nanofluidics 4 (2008) 107.
[30] C. Escobedo, A.G. Brolo, R. Gordon, D. Sinton, Nano Lett. 12 (2012) 1592.
[31] I.M. White, S.H. Yazdi, W.W. Yu, Microfluid. Nanofluidics 13 (2012) 205.
[32] S.H. Yazdi, I.M. White, Anal. Chem. 84 (2012) 7992.
[33] A.a. Yanik, M. Huang, O. Kamohara, A. Artar, T.W. Geisbert, J.H. Connor,

H. Altug, Nano Lett. 10 (2010) 4962.
[34] Y. Yin, T. Qiu, W. Zhang, P.K. Chu, J. Mater. Res. 26 (2011) 170.
[35] F.Y. Chen, W.C. Chang, R.S. Jian, C.J. Lu, Anal. Chem. 86 (2014) 5257.
[36] W. Wang, Q. Guo, M. Xu, Y. Yuan, R. Gu, J. Raman Spectrosc. 45 (2014) 736.
[37] Z. Zhang, R. Xiao, T. Yang, X. Bo, S. Wang, Laser Phys. Lett. 11 (2014) 356031.
[38] Y. Guo, M.K.K. Oo, K. Reddy, X. Fan, ACS Nano 6 (2012) 381.
[39] M.K. Khaing Oo, Y. Guo, K. Reddy, J. Liu, X. Fan, Anal. Chem. 84 (2012) 3376.
[40] K. Kim, J.W. Lee, H.B. Lee, K.S. Shin, Langmuir 25 (2009) 9697.
[41] J.W. Lee, H.B. Lee, K. Kim, K.S. Shin, Anal. Bioanal. Chem. 397 (2010) 557.
[42] J.W. Liu, J.L. Wang, W.R. Huang, L. Yu, X.F. Ren, W.C. Wen, S.H. Yu, Sci. Rep. 2 (2012) 9871.
[43] H.K. Park, H.B. Lee, K. Kim, Appl. Spectrosc. 61 (2007) 19.
[44] G. Soliveri, S. Ardizzone, S. Yüksel, D. Cialla-May, J. Popp, U.S. Schubert, S. Hoeppener, J. Phys. Chem. C 120 (2016) 1237.
[45] I. Bilecka, M. Niederberger, Nanoscale 2 (2010) 1358.
[46] R. Hoogenboom, T.F.A. Wilms, T. Erdmenger, U.S. Schubert, Aust. J. Chem. 62 (2009) 236.
[47] B. Giese, D. McNaughton, J. Phys. Chem. B 106 (2002) 101.
[48] E. Le Ru, P. Etchegoin, Principles of Surface-enhanced Raman Spectroscopy, Elsevier, 2008.
[49] D. Cialla, A. März, R. Böhme, F. Theil, K. Weber, M. Schmitt, J. Popp, Anal. Bioanal. Chem. 403 (2012) 27.
[50] G. Landini, Advanced shape analysis with ImageJ, in: Presented at Proceedings of the Second ImageJ User and Developer Conference, Luxembourg, 6-7 November, 2008.

Supporting Information

Trace Detection of THC with a SERS-based capillary platform prepared by the *in situ* microwave synthesis of AgNPs

Sezin Yüksel,[abc‡] Almut M. Schwenke,[de‡] Guido Soliveri,[f] Silvia Ardizzone,[f] Karina Weber,[abc] Dana Cialla-May,[abc] Stephanie Hoeppener,[de*], Ulrich S. Schubert,[de] and Jürgen Popp[abce]*

[a]Leibniz Institute of Photonic Technology Jena (IPHT), Jenaer BioChip Initiative, Albert-Einstein-Straße 9, 07745 Jena, Germany

[b]Institute of Physical Chemistry and Abbe Center of Photonics, Friedrich Schiller University Jena, Helmholtzweg 4, 07743 Jena, Germany

[c]InfectoGnostics Forschungscampus Jena, Zentrum für Angewandte Forschung, Philosophenweg 7, 07743 Jena, Germany

[d]Laboratory of Organic and Macromolecular Chemistry (IOMC), Friedrich Schiller University Jena, Humboldtstrasse 10, 07743 Jena, Germany

[e]Jena Center for Soft Matter (JCSM), Friedrich Schiller University Jena, Philosophenweg 7, 07743 Jena, Germany

[f]Dipartimento di Chimica, Università degli Studi di Milano, Via Golgi 19, 20133 Milano, Italy

[‡]Both authors contribute equally to the paper.

[*]Corresponding authors:

Dr. Dana Cialla-May, Phone: +49 (0)3641-206309, Fax: +49 (0)3641-206399
E-mail: dana.cialla-may@uni-jena.de
[*]Dr. Stephanie Höppener, Phone: +49 (0) 3641-948596, Fax: +49 (0) 3641-948202,
E-mail: s.hoeppener@uni-jena.de

Keywords: Microwave-assisted synthesis, SERS, drug monitoring, capillary, THC

1. Discussion of synthesis parameters

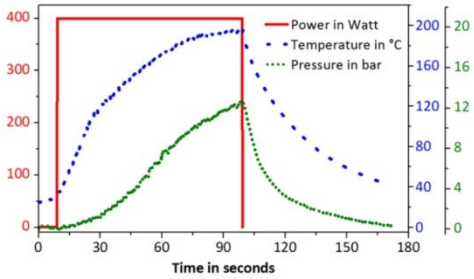

Figure S1: Power, temperature and pressure data as recorded during a typical microwave synthesis.

Dedicated laboratory microwave ovens offer the possibility to choose either a temperature- or a power-controlled synthesis mode and many microwave synthesis protocols are typical performed in the temperature control mode.[1,2] However, the available tools for temperature measurement are not suitable for the exact and fast determination of the temperature when heterogeneous reaction mixtures and highly microwave absorbing components are involved.[3] This situation is found in case of the AgNP synthesis on glass surfaces. Thus, the microwave-assisted synthesis of silver nanoparticles was performed in constant power mode instead of operating with an arbitrary power adjustment based on the measured temperature. The temperature and pressure data recorded during a typical synthesis process are displayed in Figure S1. The final temperature and pressure data thereby provide a valuable insight into the course of the reaction with the exceedance of a certain limit, with this set-up around 180 °C and 8 bar, being a reliable sign for a successful synthesis process, i.e. a batch of homogenously coated capillaries. It has to be noted that microwave ovens from different suppliers can possess very different heating performances. Thus, the power levels are often not comparable and the irradiation time needs to be optimized for the specific microwave set-up.

2. Alternative synthesis approaches

In the reported synthesis approach, bare glass capillaries are immersed in a vial filled with silver acetate precursor solution and the precursor is ascending in the capillaries due to capillary forces (Figure S2A). In contrast to the set-up described and used in the main text, two alternative synthesis protocols were tested. In these approaches the precursor solution was applied to the capillaries before they were placed in the reaction vial. In method B, the capillaries were placed in an empty vial without any liquid reservoir (Figure S2B). In method C the capillaries were added to a vial that was previously filled with 0.3 mL of a water-ethanol mixture, thus a similar solution than method A, just without silver acetate (Figure S2C).

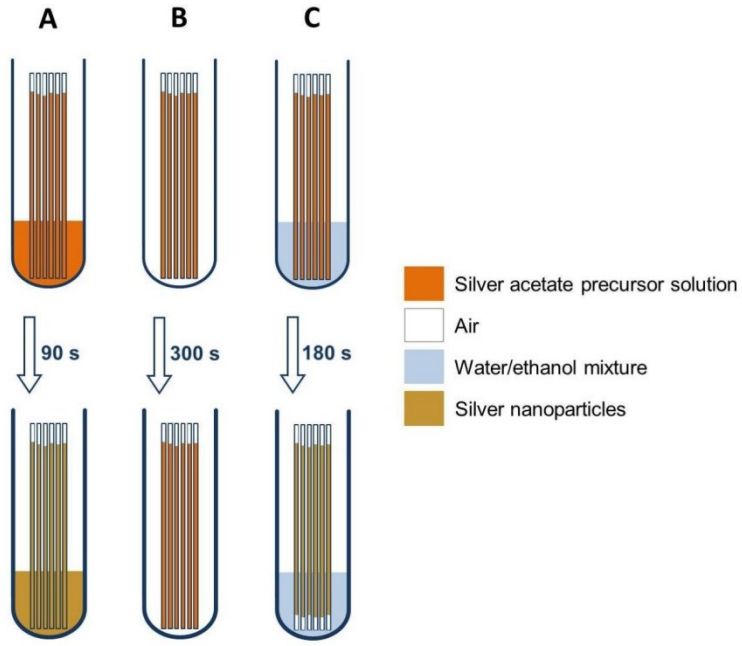

Figure *S2:* Schematic presentation of the tested synthesis approaches. In method A, the capillaries are immersed in precursor solution. In method B and C the capillaries are filled with precursor solution before they are added to the reaction vial.

With method B no AgNP formation was obtained. Presumably, heat dissipation effects and the small absorption cross-section prevented the required temperature increase for the reduction reaction. However, an AgNP coating was formed, when the precursor-filled capillaries were added to a vial filled with a water-ethanol mixture (method C). Since water and ethanol exhibit intermediate microwave heatability the heating of the reactants is improved and the heat dissipation is reduced without requiring additional silver salt. As a result, similar coatings as obtained with the original synthesis protocol (method A) were generated (compare Figure S3C with Figure 2D). However, the irradiation time had to be increased to 180 s, since the microwave absorption of water and ethanol is not as efficient as that of the silver salt solution in method A. Furthermore, when surrounded with only a water-ethanol mixture, the very bottom of the capillaries remains uncoated and the particle size distribution is less uniform over a long range, which can be traced back on diffusion effects (Figure S3A,B). Nevertheless, due to the fast heating by the microwave irradiation, only short reaction times are required, thus, satisfactory coatings can be also obtained by this approach. However, since the addition of silver acetate solution in the vial (method A) was found to shorten the required synthesis time as well as to improve the homogeneity of the coating it was, consequently, applied for the reproducible preparation of the capillary-based sensor platform.

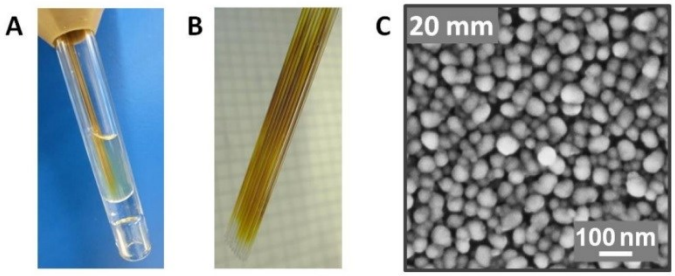

Figure S3: Images of capillaries that were prepared with method C. Photographs of a reaction vial right after the synthesis process (A) and two batches of capillaries after cleaning and drying (B). C) SEM picture showing the morphology of the nanoparticles inside a capillary at 2 cm height.

3. Homogenous and reproducible batch fabrication

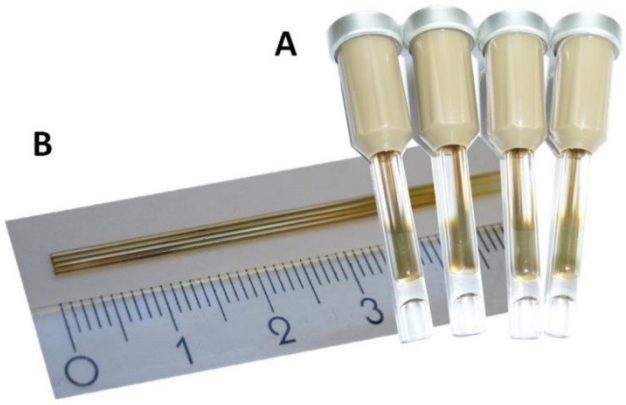

Figure S4: Photographs of four batches of capillaries. A) The four batches right after the synthesis process. B) One capillary of each batch together with a ruler with cm scale.

References

[1] C. O. Kappe, D. Dallinger, S. S. Murphree, *Practical Microwave Synthesis for Organic Chemists: Strategies, Instruments, and Protocols*, Wiley-VCH, Weinheim, **2009**.

[2] Y. J. Zhu, F. Chen, *Chem. Rev.* **2014**, *114*, 6462–6555.

[3] C. O. Kappe, *Chem. Soc. Rev.* **2013**, *42*, 4977–4990.

5. References

1. Wang, H.B., W. D.; Nordlander, P.; Halas, J. N., *Plasmonic Nanostructures: Artificial Molecules.* Accounts of Chemical Research, 2007. **40**: p. 53-62.
2. Szunerits, S.B., R. , *Introduction to Plasmonics Advances ad Applications.* Pan Standford Publishing, 2015.
3. Pavan Kumar, G.V., *Plasmonic Nano-Architectures for Surface Enhanced Raman Scattering: A Review.* Journal of Nanophotonics, 2012. **6**(1): p. 064503.
4. Kreuter, J., *Nanoparticles-A Historical Perspective.* Int J Pharm, 2007. **331**(1): p. 1-10.
5. Sreeprasad, T.S.P., T., *Noble Metal Nanoparticles.* 2013: p. 303-388.
6. Thompson, D., *Michael Faraday's Recognition of Ruby Gold: the Birth of Modern Nanotechnology.* Gold Bulletin, 2007. **40/4**: p. 267-269.
7. Heiligtag, F.J.M.N., *The Fascinating World of Nanoparticle Research.* Materials Today, 2013. **16**(7-8): p. 262-271.
8. Tweney, R.D., *Discovering Discovery: How Faraday Found the First Metallic Colloid.* Perspectives on Science, 2006. **14**(1): p. 97-121.
9. Tripp, R.A., R.A. Dluhy, and Y. Zhao, *Novel nanostructures for SERS biosensing.* Nano Today, 2008. **3**(3-4): p. 31-37.
10. Edwards, P.P.T., J. M., *Gold in a Metallic Divided State-From Faraday to Present-Day Nanoscience.* Angew Chem Int Ed Engl, 2007. **46**(29): p. 5480-6.
11. Polte, J., *Fundamental Growth Principles of Colloidal Metal Nanoparticles – a New Perspective.* CrystEngComm, 2015. **17**: p. 6809-6830.
12. Brown, R.J.C. and M.J.T. Milton, *Nanostructures and nanostructured substrates for surface-enhanced Raman scattering (SERS).* Journal of Raman Spectroscopy, 2008. **39**(10): p. 1313-1326.
13. Kleinman, S.L., et al., *Creating, characterizing, and controlling chemistry with SERS hot spots.* PhysChemChemPhys, 2013. **15**(1): p. 21-36.
14. Willets, K.A.V.D., R. P., *Localized Surface Plasmon Resonance Spectroscopy and Sensing.* Annu Rev Phys Chem, 2007. **58**: p. 267-97.
15. Stark, W.J., et al., *Industrial Applications of Nanoparticles.* Chem. Soc. Rev., 2015. **44**: p. 5793-5805.
16. Wang, A.X.K., X., *Review of Recent Progress of Plasmonic Materials and Nano-Structures for Surface-Enhanced Raman Scattering.* Materials (Basel), 2015. **8**(6): p. 3024-3052.
17. Moskovits, M., *Surface-enhanced Raman spectroscopy: a brief retrospective.* Journal of Raman Spectroscopy, 2005. **36**(6-7): p. 485-496.
18. Halas, N.J.M., M., *Surface-Enhanced Raman Spectroscopy: Substrates and Materials for Research and Applications.* MRS Bulletin, 2013. **38**(08): p. 607-611.
19. Alvarez-Puebla, R.A.L.-M., L. M., *Traps and Cages for Universal SERS Detection.* Chem Soc Rev, 2012. **41**(1): p. 43-51.
20. Tian, Z.Q., *Surface-Enhanced Raman Spectroscopy: Advancements and Applications.* Journal of Raman Spectroscopy, 2005. **36**(6-7): p. 466-470.
21. Le Ru, E.C.E., P. G., *Single-Molecule Surface-Enhanced Raman Spectroscopy.* Annu Rev Phys Chem, 2012. **63**: p. 65-87.
22. Jahn, M., et al., *Plasmonic nanostructures for surface enhanced spectroscopic methods.* Analyst, 2016. **141**(3): p. 756-93.

23. Cialla, D., et al., *SERS-based detection of biomolecules.* Nanophotonics, 2014. **3**(6).
24. Pahlow, S.M., A.; Seise, B.; Hartmann, K.; Freitag, I.; Kämmer, E.; Böhme, R.; Deckert, V.; Weber, K.; Cialla, D.; Popp, J., *Bioanalytical Application of Surface- and Tip-Enhanced Raman Spectroscopy.* Engineering in Life Sciences, 2012. **12**(2): p. 131-143.
25. Cialla, D.M., A.; Böhme, R.; Theil, F.; Weber, K.; Schmitt, M.; Popp, J., *Surface-Enhanced Raman Spectroscopy (SERS): Progress and Trends.* Anal Bioanal Chem, 2012. **403**(1): p. 27-54.
26. Schlucker, S., *Surface-enhanced Raman spectroscopy: concepts and chemical applications.* Angew Chem Int Ed Engl, 2014. **53**(19): p. 4756-95.
27. Schüler, T., et al., *Enzyme-induced growth of silver nanoparticles studied on single particle level.* Journal of Nanoparticle Research, 2008. **11**(4): p. 939-946.
28. Allen, C.S.S., G. C.; Van Duyne, R. P., *Tunable Laser Excitation Profile of Surface Enhanced Raman Scattering From Pyridine Adsorbed on a Copper Electrode Surface.* Chemical Physics Letters, 1980. **75**(2): p. 201-205.
29. Lin, X.M.C., Y.; Xu, Y. H.; Ren, B.; Tian, Z. Q., *Surface-Enhanced Raman Epectroscopy: Substrate-Related Issues.* Anal Bioanal Chem, 2009. **394**(7): p. 1729-45.
30. Larmour, I.A.G., D., *Surface enhanced optical spectroscopies for bioanalysis.* Analyst, 2011. **136**(19): p. 3831-53.
31. Yang, L., P. Liab, and J. Liuab, *Progress in multifunctional surface-enhanced Raman scattering substrate for detection.* RSCAdvances, 2014. **4**: p. 49635–49646 |.
32. Sharma, B., et al., *High-performance SERS substrates: Advances and challenges.* MRS Bulletin, 2013. **38**(08): p. 615-624.
33. Muehlethaler, C.L., M.; Lombardi, J. R., *Review of Surface Enhanced Raman Scattering Applications in Forensic Science.* Anal Chem, 2016. **88**(1): p. 152-69.
34. Cialla, D.P., S.; Steinbrücker, C.; Weber, K.; Popp, Jürgen, *SERS-Based Detection of Biomolecules.* Nanophotonics, 2014. **3**(6).
35. Sharma, B.C., F. M.; Kleinman, S. L.; Greeneltch, N. G.; Frontiera, R. R.; Blaber, M. G.; Schatz, G. C.; Van Duyne, R. P., *High-performance SERS substrates: Advances and challenges.* MRS Bulletin, 2013. **38**(08): p. 615-624.
36. Sharma, B.F., R. R.; Henry, A. I.; Ringe, E.; Van Duyne, R. P., *SERS: Materials, Applications, and the Future.* Materials Today, 2012. **15**(1-2): p. 16-25.
37. Wood, R.W., *XLII.On a Remarkable Case of Uneven Distribution of Light in a Diffraction Grating Spectrum.* Philosophical Magazine Series 6, 1902. **4**(21): p. 396-402.
38. Mie, G., *Beiträge zur Optik trüber Medien, Speziell Kolloidaler Metallösungen.* Annalen der Physik., 1908. **4**: p. 377-445.
39. Fano, U., *Atomic Theory of Electromagnetic Interactions in Dense Materials.* Physical Review, 1956. **103**(5): p. 1202-1218.
40. Pines, D., *Collective Energy Losses in Solids.* Reviews of Modern Physics, 1956. **28**(3): p. 184-198.
41. Cunningham, S.L.M., A. A.; Wallis, R. F., *Effect of a Charge Layer On the Surface-Plasmon-Polariton Dispersion Curve.* Physical Review B, 1974. **10**(8): p. 3342-3355.
42. Barnes, W.L.D., A.; Ebbesen, T. W., *Surface Plasmon Subwavelength Optics.* Nature, 2003. **424**: p. 824-830.
43. Specht, M.P., J. D.; Heckl, W. M.; Hansch, T. W., *Scanning Plasmon Near-Field Microscope.* Phys Rev Lett, 1992. **68**(4): p. 476-479.
44. Jensen, L.A., C. M.; Schatz, G. C., *Electronic Structure Methods for Studying Surface Enhanced Raman Scattering.* Chem Soc Rev, 2008. **37**(5): p. 1061-73.

45. Lu, X., et al., *Chemical synthesis of novel plasmonic nanoparticles.* Annu Rev Phys Chem, 2009. **60**: p. 167-92.
46. Wilson, A.J.W., K. A., *Molecular Plasmonics.* Annu Rev Anal Chem (Palo Alto Calif), 2016. **9**(1): p. 27-43.
47. Hayashi, S.O., T., *Plasmonics: Visit the Past to Know the Future.* Journal of Physics D: Applied Physics, 2012. **45**(43): p. 433001.
48. Zhang, J.Z., L. and W. Xu, *Surface Plasmon Polaritons:Pphysics and Applications.* Journal of Physics D: Applied Physics, 2012. **45**(11): p. 113001.
49. Fan, M., G.F. Andrade, and A.G. Brolo, *A review on the fabrication of substrates for surface enhanced Raman spectroscopy and their applications in analytical chemistry.* Analytica Chimica Acta, 2011. **693**(1-2): p. 7-25.
50. Etchegoin, P.G.L.R., E. C. , *Basic Electromagnetic Theory of SERS, in Surface Enhanced Raman Spectroscopy: Analytical, Biophysical and Life Science Applications.* Wiley-VCH Verlag GmbH & Co. KGaA, Weinheim, Germany. , 2010: p. 1-38.
51. Le Ru, E.C.M., M.; Blackie, E.; Etchegoin, P. G., *Advanced Aspects of Electromagnetic SERS Enhancement Factors at a Hot Spot.* Journal of Raman Spectroscopy, 2008. **39**(9): p. 1127-1134.
52. Brolo, A.G.I., D. E.; Smith, B. D., *Applications of surface enhanced Raman scattering to the study of metal-adsorbate interactions.* Journal of Molecular Structure, 1997. **405**: p. 29-44.
53. Cialla, D.P., J.; Hubner, U.; Schneidewind, H.; Zeisberger, M.; Mattheis, R.; Pertsch, T.; Schmitt, M.; Moller, R.; Popp, J., *Investigation on the Second Part of the Electromagnetic SERS Enhancement and Resulting Fabrication Strategies of Anisotropic Plasmonic Arrays.* Chemphyschem, 2010. **11**(9): p. 1918-24.
54. Le Ru, E.C., Etchegoin, P. G., *Rigorous Justification of the |E|4 Enhancement Factor in Surface Enhanced Raman Spectroscopy.* Chemical Physics Letters, 2006. **423**(1-3): p. 63-66.
55. Jahn, M.P., S.; Hidi, I. J.; Knipper, R.; Radu, A. I.; Muhlig, A.; Yüksel, S.; Peksa, V.; Weber, K.; Mayerhofer, T.; Cialla-May, D.; ,Popp, J., *Plasmonic Nanostructures for Surface Enhanced Spectroscopic Methods.* Analyst, 2016. **141**(3): p. 756-93.
56. Lu, X.R., M.; Skrabalak, S. E.; Wiley, B.; Xia, Y., *Chemical Synthesis of Novel Plasmonic Nanoparticles.* Annu Rev Phys Chem, 2009. **60**: p. 167-92.
57. Wiley, B.S., Y.; Xia, Y., *Synthesis of Silver Nanostructures with Controlled Shapes and Properties.* Acc. Chem. Res., 2007. **40**: p. 1067-1076.
58. Rycenga, M.C., C. M.; Zeng, J.; Li, W.; Moran, C. H.; Zhang, Q.; Qin, D.; Xia, Y., *Controlling the Synthesis and Assembly of Silver Nanostructures for Plasmonic Applications.* Chem Rev, 2011. **111**(6): p. 3669-712.
59. Barcikowski, S. and G. Compagnini, *Advanced Nanoparticle Generation and Excitation by Lasers in Liquids.* Phys Chem Chem Phys, 2013. **15**(9): p. 3022-6.
60. Amendola, V. and M. Meneghetti, *What Controls the Composition and the Structure of Nanomaterials Generated by Laser Ablation in Liquid Solution?* Phys Chem Chem Phys, 2013. **15**(9): p. 3027-46.
61. Betz, J.F.Y., W. W.; Cheng, Y.; White, I. M.;,Rubloff, G. W., *Simple SERS Substrates: Powerful, Portable, and Full of Potential.* Phys Chem Chem Phys, 2014. **16**(6): p. 2224-39.
62. Leiterer, C., et al., *Fast self-assembly of silver nanoparticle monolayer in hydrophobic environment and its application as SERS substrate.* Journal of Nanoparticle Research, 2014. **16**(9).

63. Chen, Y., *Nanofabrication by Electron Beam Lithography and Its Applications: A Review.* Microelectronic Engineering, 2015. **135**: p. 57-72.
64. Altissimo, M., *E-beam Lithography for Micro-Nanofabrication.* Biomicrofluidics, 2010. **4**(2).
65. Ma, L., et al., *Ag Nanorods Coated with Ultrathin TiO2 Shells as Stable and Recyclable SERS Substrates.* Sci Rep, 2015. **5**: p. 15442.
66. Grigorescu, A.E. and C.W. Hagen, *Resists for Sub-20-nm Electron Beam Lithography with a Focus on HSQ: State of the Art.* Nanotechnology, 2009. **20**(29): p. 292001.
67. Bilenberg, B.S., M.; Shi, P.; Schmidt, M. S.; Bøggild, P.; Fink, M.; Schuster, C.; Reuther, F.; Gruetzner, C.; Kristensen A., *Comparison of high resolution negative electron beam resists.* Journal of Vacuum Science & Technology B: Microelectronics and Nanometer Structures, 2006. **24**(4): p. 1776.
68. Okazaki, S., *High Resolution Optical Lithography or High Throughput Electron Beam Lithography: The Technical Struggle From the Micro to the Nano-Fabrication Evolution.* Microelectronic Engineering, 2015. **133**: p. 23-35.
69. Liddle, J.A.G., G. M., *Nanomanufacturing: A Perspective.* ACS Nano, 2016. **10**(3): p. 2995-3014.
70. Patze, S.H., U.; Weber, K.; Cialla-May, D.; Popp, J., *TopUp Plasmonic Arrays for Surface-Enhanced Raman Spectroscopy.* Advanced Materials Interfaces, 2016. **3**(19): p. 1600549.
71. Marz, A.A., K. R.; Malsch, D.; Bocklitz, T.; Henkel, T.; Popp, J., *Towards a Quantitative SERS Approach--Online Monitoring of Analytes in a Microfluidic System with Isotope-edited Internal Standards.* J Biophotonics, 2009. **2**(4): p. 232-42.
72. Le Ru, E.C., et al., *Advanced Aspects of Electromagnetic SERS Enhancement Factors at a Hot spot.* Journal of Raman Spectroscopy, 2008. **39**(9): p. 1127-1134.
73. Hidi, I.J.M., A.; Jahn, M.; Liebold, F.; Cialla, D.; Weber, K.; Popp, J., *LOC-SERS: Towards Point-of-Care Diagnostic of Methotrexate.* Analytical Methods, 2014. **6**(12): p. 3943.
74. Walter, A.M., A.; Schumacher, W.; Rosch, P.; Popp, J., *Towards a Fast, High Specific and Reliable Discrimination of Bacteria on Strain Level by Means of SERS in a Microfluidic Device.* Lab Chip, 2011. **11**(6): p. 1013-21.
75. Huebner, U., et al., *Microfabricated SERS-arrays with sharp-edged metallic nanostructures.* Microelectronic Engineering, 2008. **85**(8): p. 1792-1794.
76. Yoshida, K.I., T.; Tamaru, H.; Biju, V.; Ishikawa, M.; Ozaki, Y., *Quantitative Evaluation of Electromagnetic Enhancement in Surface-Enhanced Resonance Raman Scattering from Plasmonic Properties and Morphologies of Índividual Ag Nanostructures.* Physical Review B, 2010. **81**(11).
77. Cialla, D., et al., *Probing innovative microfabricated substrates for their reproducible SERS activity.* ChemPhysChem, 2008. **9**(5): p. 758-62.
78. Giovannozzi, A.M.R., F.; Sega, M.; Abete, M. C.; Marchis, D.; Rossi, A. M., *Rapid and Sensitive Detection of Melamine in Milk with Gold Nanoparticles by Surface Enhanced Raman Scattering.* Food Chem, 2014. **159**: p. 250-6.
79. Leopold, N.L., B., *A New Method for Fast Preparation of Highly Surface-Enhanced Raman Scattering (SERS) Active Silver Colloids at Room Temperature by Reduction of Silver Nitrate with Hydroxylamine Hydrochloride.* J. Phys. Chem. B, 2003. **107**(5723-5727).
80. Larmour, I.A.F., K.; Graham, D., *SERS Activity and Stability of the Most Frequently Used Silver Colloids.* Journal of Raman Spectroscopy, 2012. **43**(2): p. 202-206.

81. Cozar, O.B., I.; Szabó, L.; Cozar, I. B.; Chiş, V.; David, L., *IR and ESR study of copper(II) complexes with 15N-labelled lysine and ornithine.* Journal of Molecular Structure, 2011. **993**(1-3): p. 397-403.
82. Bebu, A.S., L.; Leopold, N.; Berindean, C.; David, L., *IR, Raman, SERS and DFT study of amoxicillin.* Journal of Molecular Structure, 2011. **993**(1-3): p. 52-56.
83. del Puerto, E.D., C.; Garcia Ramos, J. V.; Sanchez-Cortes, S., *Adsorption Study and Detection of the High Performance Organic Pigments Quinacridone and 2,9-Dimethylquinacridone on Ag Nanoparticles by Surface-Enhanced Optical Spectroscopy.* Langmuir, 2014. **30**(3): p. 753-61.
84. Mircescu, N.E.Z., H.; Leopold, N.; Chis, V.; Ivleva, N. P.; Niessner, R.; Wieser, A.; Haisch, C., *Towards a Receptor-Free Immobilization and SERS Detection of Urinary Tract Infections Causative pathogens.* Anal Bioanal Chem, 2014. **406**(13): p. 3051-8.
85. Zhang, P., et al., *Dual-Peak Electrogenerated Chemiluminescence of Carbon Dots for Iron Ions Detection.* Anal Chem, 2014. **86**(12): p. 5620-3.
86. Shautsova, V.I.Z., V. A.; Korolik, O. V.; Novikau, A. G.; Shevchenko, G. P.; Gaiduk, P. I., *Effect of Interparticle Field Enhancement in Self-Assembled Silver Aggregates on Surface-Enhanced Raman Scattering.* Plasmonics, 2014. **9**(5): p. 993-999.
87. Harper, M.M.D., J. A.; Shand, N. C.; Graham, D.; Faulds, K., *Detection of SERS active labelled DNA based on surface affinity to silver nanoparticles.* Analyst, 2012. **137**(9): p. 2063-8.
88. Ito, S.F., S.; Kusumi,T.; Ishibashi,Y.; Miyasaka,H.; Goto,Y.; Ikai,M.; Tani,T.;Inagaki, S.|, *Microscopic Structure and Mobility of Guest Molecules in Mesoporous Hybrid Organosilica: Evaluation with Single-Molecule Tracking.* J. Phys. Chem. C, 2009. **113**: p. 11884–11891.
89. Hajduková, N.P., M.; Štěpánek, J.; Špírková, M., *Chemically Reduced and Laser-Ablated Gold Nanoparticles Immobilized to Silanized Glass Plates: Preparation, Characterization and SERS Spectral Testing.* Colloids and Surfaces A: Physicochemical and Engineering Aspects, 2007. **301**(1-3): p. 264-270.
90. Procházka, M.Š., P.; Hajduková-Šmídová, N., *SE(R)RS Microspectroscopy of Porphyrins on Immobilized Au Nanoparticles: Testing Spectral Sensitivity and Reproducibility.* Colloids and Surfaces A: Physicochemical and Engineering Aspects, 2012. **402**: p. 24-28.
91. Potara, M.G., A. M.; Astilean, S., *Solution-Phase, Dual LSPR-SERS Plasmonic Sensors of High Sensitivity and Stability Based on Chitosan-Coated Anisotropic Silver Nanoparticles.* Journal of Materials Chemistry, 2011. **21**(11): p. 3625.
92. Wustholz, K.L.H., A. I.; McMahon,J. M.; Griffith Freeman, R.; Valley, N.; Piotti, M. E; Natan, M. J.; and G.C.V.D. Schatz, R. P., *Structure-Activity Relationships in Gold Nanoparticle Dimers and Trimers for Surface-Enhanced Raman Spectroscopy.* JACS, 2010. **132**: p. 10903–10910.
93. Lim, D.-K.K.-S.J., K-S.;Kim, H. M.; Nam, J-M.; Suh, Y. D., *Nanogap-Engineerable Raman-Active Nodumbbells for Single-Molecule Detection.* Nature Materials, 2009. **9**: p. 60-67.
94. Jin, Y.J., C.; Huang, S. W.; O'Donnell, M.; Gao, X., *Multifunctional Nanoparticles as Coupled Contrast Agents.* Nat Commun, 2010. **1**: p. 41.
95. Mulvaney, S.P.M., M. D.; Keating, C. D.; Natan, M. J., *Glass-Coated, Analyte-Tagged Nanoparticles: A New Tagging System Based on Detection with Surface-Enhanced Raman Scattering.* Langmuir, 2003. **19**: p. 4784-4790.

96. Gole, A.A., N.; Nagaria, P.; Wyatt, M. D.; Murphy, C. J., *One-Pot Synthesis of Silica-Coated Magnetic Plasmonic Tracer Nanoparticles.* Chem Commun (Camb), 2008(46): p. 6140-2.
97. Deng, W.J., D.; Drozdowicz-Tomsia, K.; Yuan, J.; Wu, J.; Goldys, E. M., *Ultrabright Eu-doped Plasmonic Ag@SiO2 Nanostructures: Time-Gated Bioprobes with Single Particle Sensitivity and Negligible Background.* Adv Mater, 2011. **23**(40): p. 4649-54.
98. Cecchini, M.P.T., V. A.; Paget, J.; Kornyshev, A. A.; Edel, J. B., *Self-Assembled Nanoparticle Arrays for Multiphase Trace Analyte Detection.* Nature Materials, 2012. **12**: p. 165-171.
99. Kang, Y.S., M.; Zhu, Y.; Miao, L.; Xu, G., *Surface-Enhanced Raman Scattering (SERS) Spectra of Hemoglobin of Mouse and Rabbit with Self-Assembled Nano-Silver Film.* Spectrochim Acta A Mol Biomol Spectrosc, 2013. **108**: p. 177-80.
100. Freeman, G.R.G., K. C.; Allison, K. J.; Bright, R. M.; Davis, J. A.; Gutherie, A. P.; Hommer, M. B.; Jackson, M. A.; Smith, P. C.; Walter, D. G.; Natan, M. J., *Self-Assembled Metal Colloid Monolayers: An Approach to SERS substratese.* Science, 1995. **267**: p. 1629-1632.
101. Fan, M.B., A. G., *Silver Nanoparticles Self Assembly as SERS Substrates with Near Single Molecule Detection Limit.* PCCP, 2009. **11**: p. 7381–7389.
102. Carles, R.F., C.; Bonafos, C.; Benassayag, G.; Bayle, M.; Benzo, P.; Groenen, J.; Zwick, A., *Three Dimensional Design of Silver Nanoparticle Assemblies Embedded in Dielectrics for Raman Spectroscopy Enhancement and Dark-Field Imaging.* ACS Nano, 2011. **11**: p. 8774–8782
103. Xia, Y.G., B.; Yin, Y.; Lu, Y., *Monodispersed Colloidal Spheres: Old Materials with New Applications.* Advanced Materials, 2000. **10**: p. 693-713.
104. Dick, L.S.M., A. D.; Haynes, K. L.; Van Duyne, R. P., *Metal Film over Nanosphere (MFON) Electrodes for Surface-Enhanced Raman Spectroscopy (SERS): Improvements in Surface Nanostructure Stability and Suppression of Irreversible Loss.* J. Phys. Chem. B, 2002. **106**: p. 853-860.
105. Farcau, C.A., S., *Mapping the SERS Efficiency and Hot-Spots Localization on Gold Film over Nanospheres Substrates.* J. Phys. Chem. C, 2010. **114**: p. 11717–11722.
106. Peksa, V.J., M.; Stolcova, L.; Schulz, V.; Proska, J.; Prochazka, M.; Weber, K.; Cialla-May, D.; Popp, J., *Quantitative SERS Analysis of Azorubine (E 122) in Sweet Drinks.* Anal Chem, 2015. **87**(5): p. 2840-4.
107. McGilvray, K.L.F., C.; Bueno-Alejo, C. J.; Schwartz-Narbonne, R.; Scaiano, J. C., *Photochemical Strategies for the Seed-Mediated Growth of Gold and Gold-Silver Nanoparticles.* Langmuir, 2012. **28**(46): p. 16148-55.
108. Barbosa, S.A., A.; Rodriguez-Lorenzo, L.; Pastoriza-Santos, I.; Alvarez-Puebla, R. A.; Kornowski, A. Weller, H.; Liz-Marzan, L. M., *Tuning Size and Sensing Properties in Colloidal Gold Nanostars.* Langmuir, 2010. **26**(18): p. 14943-50.
109. Yen, C.W.M., M. A.; El-Sayed, M. A. , *Photocatalysis in Gold Nanocage Nanoreactors.* J. Phys. Chem. A, 2009. **113**: p. 4340–4345.
110. Le Guevel, X.W., F. Y.; Stranik, O.; Nooney, R.; Gubala, V; McDonagh, C.; MacCraith, B. D., *Synthesis, Stabilization, and Functionalization of Silver Nanoplates for Biosensor Applications.* J. Phys. Chem. C, 2009. **113**: p. 16380-16386.
111. Roh, J.Y., J.; Kim, Y., *Rapid, Reversible Preparation of Size-Controllable Silver Nanoplates by Chemical Redox.* Langmuir, 2010. **26**(14): p. 11621-3.

112. Dong, Z.-G.L., H.; Xu, M.-X.; Li, T.; Wang, S.-M.; Zhu, S.-N.; Zhang, X., *Plasmonically Induced Transparent Magnetic Resonance in a Metallic Metamaterial Composed of Asymmetric Double Bars.* OSA, 2010. **18229-18234**.
113. Ye, X.J., L.; Caglayan, H.; Chen, J.; Xing, G.; Zheng, C.; Doan-Nguyen, V.; Kang, Y.; Engheta, N.; Kagan, C. R.; Murray, C. B., *Improved Size-Tunable Synthesis of Monodisperse Gold Nanorods through the Use of Aromatic Additives.* ACS Nano, 2012. **6**: p. 2804-2817.
114. Kattumenu, R.L., C. H.; Tian, L.; McConney, M. E.; Singamaneni, S., *Nanorod Decorated Nanowires as Highly Efficient SERS-Active Hybrids.* Journal of Materials Chemistry, 2011. **21**(39): p. 15218.
115. Chou, Y.-C.W., W. W.; Lee, C.-Y.; Liu, C.-Y.; Chen, L.-J.;Tu, K.-N., *Heterogeneous and Homogeneous Nucleation of Epitaxial NiSi2 in [110] Si Nanowires.* J. Phys. Chem. C 2, 2010. **115**: p. 397–401.
116. Jones, M.R.O., K. D.; Macfarlane, R. J.; Langille, M. R.; Mirkin, C. A., *Templated Techniques for the Synthesis and Assembly of Plasmonic Nanostructures.* Chem Rev, 2011. **111**(6): p. 3736-827.
117. Haes, A.J.H., C. L.; McFarland, A. D., Schatz, G. C.; Van Duyne, R. P.; Zou, S., *Plasmonic Materials for Surface-Enhanced Sensing and Spectroscopy.* MRS BULLETIN 2005. **30**: p. 356-375.
118. Anker, J.N.H., P. W.; Lyandres, O.; Shah, N. C.; Zhao, J.; Van Duyne, R. P., *Biosensing with Plasmonic Nanosensors.* Nature Materials, 2008. **7**: p. 442-453.
119. Hulteen, J.C.V.D., R. P., *Nanosphere Lithography: A Materials General Fabrication Process for Periodic Particle Array Surfaces.* J. Vac. Sci. Technol. A, 1995. **13**: p. 1153-1558.
120. Jensen, T.R.D., M. L.; Kelly, K. L.; Lazarides, A. A.; Schatz, G. C.; Van Duyne, R. P., *Nanosphere Lithography: Effect of the External Dielectric Medium on the Surface Plasmon Resonance Spectrum of a Periodic Array of Silver Nanoparticles.* J. Phys. Chem. B, 1999. **103**: p. 9846-9853.
121. Baia, M.B., L.; Astilean, S., *Gold Nanostructured Films Deposited on Polystyrene Colloidal Crystal Templates for Surface-Enhanced Raman Spectroscopy.* Chemical Physics Letters, 2005. **404**(1-3): p. 3-8.
122. L. Baia, L.B., M.; Popp, J.; Astilean, S., *Gold Films Deposited over Regular Arrays of Polystyrene Nanospheres as Highly Effective SERS Substrates from Visible to NIR.* J. Phys. Chem. B, 2006. **110**: p. 23982-23986.
123. Sherry, L.J.J., R.; Mirkin, C. A.; Schatz, G. C.; Van Duyne, R. P., *Localized Surface Plasmon Resonance Spectroscopy of Single Silver Triangular Nanoprisms.* Nano Letters, 2006. **6**: p. 2060-2065.
124. Haes, A.J.Z., S.; Zhao,J.; Schatz, G. C.; Van Duyne, R. P., *Localized Surface Plasmon Resonance Spectroscopy Near Molecular Resonances.* JACS, 2006. **128**: p. 10905-10914.
125. Whitney, A.V.E., J. W.; Zou, S.; Zinovev, A. V., Peter C. Stair, P. C.; Schatz, G. C.; Van Duyne, R. P. , *Localized Surface Plasmon Resonance Nanosensor: A High-Resolution Distance-Dependence Study Using Atomic Layer Deposition.* J. Phys. Chem. B, 2005. **109**: p. 20522-20528.
126. Ye, X. and L. Qi, *Recent Advances in Fabrication of Monolayer Colloidal Crystals and Their Inverse Replicas.* Science China Chemistry, 2013. **57**(1): p. 58-69.

127. Xu, Z.D., G.; Zhang, H.; Wang, Y.; Xu, L.; Cai, W., *In Situ Synthesis of Porous Array Films on a Filament Induced Micro-Gap Electrode Pair and Their Use As Resistance-Type Gas Sensors With Enhanced Erformances.* Nanoscale, 2015. **7**(34): p. 14264-71.
128. Huebner, U.W., K.; Cialla, D.; Haehle, R.; Schneidewind, H.; Zeisberger, M.; Mattheis, R.; Meyer, H.-G.; Popp, J., *Microfabricated Polymer-Substrates for SERS.* Microelectronic Engineering, 2012. **98**: p. 444-447.
129. Kohler, J.M.M., A.; Popp, J.; Knauer, A.; Kraus, I.; Faerber, J.; Serra, C., *Polyacrylamid/Silver Composite Particles Produced via Microfluidic Pphotopolymerization for Single Particle-Based SERS Microsensorics.* Anal Chem, 2013. **85**(1): p. 313-8.
130. Liu, M.L., X.; Karuturi, S. K.; Tok, A. I.; Fan, H. J., *Atomic Layer Deposition for Nanofabrication and Interface Engineering.* Nanoscale, 2012. **4**(5): p. 1522-8.
131. Kresge, C.T.L., M. E.; Roth, W. J.; Vartuli, J. C.; Beck, J. S., *Ordered Mesoprous Molecular Sieves Synthesized by a Liquid-Crystal Template Mechanism.* Nature Materials, 1992. **359**: p. 710-712.
132. Lang, X.Q., Teng and W.Y. Zhang, Y.; Chu, P. K., *Tunable Silver Nanocap Superlattice Arrays for Surface-Enhanced Raman Scattering.* The Journal of Physical Chemistry C, 2011. **115**(49): p. 24328-24333.
133. Jernshoj, K.D.H., S.; Hansen, R. S.; Krohne-Nielsen, P., *Experimental Study on Polarized Surface Enhanced Resonance Raman Scattering of Rhodamine 6G Adsorbed on Porous Al2O3 Substrates.* J Chem Phys, 2011. **135**(12): p. 124514.
134. Li, Z.C., S. W.; Nam, J. M.; Ginger, D. S.; Mirkin, C. A., *Living Templates for the Tierarchical Assembly of Gold Nanoparticles.* Angew Chem Int Ed Engl, 2003. **42**(20): p. 2306-9.
135. Homola, J., S.S. Yee, and G. Gauglitz, *Surface plasmon resonance sensors: review.* Sensors and Actuators B, 1999. **54**: p. 3-15.
136. George, A.M., *Atomic Layer Deposition: An Overview.* Chem. Rev., 2010. **110**: p. 111-131.
137. Im, H.W., N. J.; Lindquist, N. C.; Oh, S. H., *Atomic Layer Deposition (ALD): A Versatile Technique for Plasmonics and Nanobiotechnology.* J Mater Res, 2012. **27**(4): p. 663-671.
138. Marin, E.L., A.; Andreatta, F.; Lekka, M.; Guzman, L.; Fedrizzi, L., *Atomic Layer Deposition: State-of-the-Art and Research/Industrial Perspectives.* Corrosion Reviews, 2011. **29**(5-6).
139. Miikkulainen, V., et al., *Crystallinity of Inorganic Films Grown by Atomic Layer Deposition: Overview and General Trends.* Journal of Applied Physics, 2013. **113**(2): p. 021301.
140. Schüler, T.S., A.; Festag, G.; Möller, R,; Fritzsche, W., *Enzyme-Induced Growth of Silver Nanoparticles Studied on Single Particle Level.* Journal of Nanoparticle Research, 2008. **11**(4): p. 939-946.
141. Schneidewind, H.S., T.; Strelau, K. K.; Weber, K.; Cialla, D.; Diegel, M.; Mattheis, R.; Berger, A.; Moller, R.; Popp, J., *The morphology of silver nanoparticles prepared by enzyme-induced reduction.* Beilstein J Nanotechnol, 2012. **3**: p. 404-14.
142. Hering, K.K.M., R.; Fritzsche, W.; Popp, J., *Microarray-Based Detection of Dye-Labeled DNA by SERRS Using Particles Formed by Enzymatic Silver Seposition.* Chemphyschem, 2008. **9**(6): p. 867-72.

143. Katharina Konstanze Strelau, et al., *Detection of PCR products amplified from DNA of epizootic pathogens using magnetic nanoparticles and SERS.* Journal of Raman Spectroscopy, 2011. **42**(3): p. 243-250.
144. Barhoumi, A.H., N. J., *Label-Free Detection of DNA Hybridization Using Surface Enhanced Raman Spectroscopy.* JACS, 2010. **132**: p. 12792-12793.
145. Julich, S.R., M.; Kielpinski, M.; Urban, M.; Kretschmer, R.; Wagner, S.; Fritzsche, W.; Henkel, T.; Moller, R.; Werres, S., *Development of a Lab-On-a-Chip Device for Diagnosis of Plant Pathogens.* Biosens Bioelectron, 2011. **26**(10): p. 4070-5.
146. Milesa, T.D.G., J. M.; Jaroszb, A. M.; Schildera A. M. C., *The Effect of Environmental Factors on Infection of Blueberry Fruit by Colletotrichum Acutatum.* Plant Pathology, 2013. **62**: p. 1238–1247.
147. Meng Chen, M.F., Y.-G.; Wang, X.; Li,T.-C.; Zhang,J.-Y. Qian, D:-J., *Silver Nanoparticles Capped by Oleylamine: Formation, Growth, and Self-Organization.* Langmuir 2007. **23**: p. 5296-5304.

6. Publications, Patents and Conference Contributions

Publications

- **Trace detection of tetrahydrocannabinol (THC) with a SERS-based capillary platform prepared by the in situ microwave synthesis of AgNPs**
  S. Yüksel*, Almut M. Schwenke*, Silvia Ardizzone, Karina Weber, Dana Cialla-May, Stephanie Hoeppener, Jürgen Popp.
  Analytica Chimica Acta, 2016, **939**, p. 93-100
- **Microwave-assisted silver nanoparticle film formation for SERS applications**
  Guido Soliveri, Silvia Ardizzone, Sezin Yüksel, Dana Cialla-May, Jürgen Popp, Ulrich S. Schubert, Stephanie Hoeppener.
  The Journal of Physical Chemistry C, 2016, **120**, p. 1237-1344
- **Label-free detection of Phytophthora ramorum using surface-enhanced Raman spectroscopy**
  Sezin Yüksel*, Lydia Schwenkbier*, Sibyll Pollok, Karina Weber, Dana Cialla-May, Jürgen Popp.
  Analyst, 2015, **140**, p.7254-7262
- **Background-free Bottom-up plasmonic arrays with increased sensitivity, specificity and shelf life for SERS detection schemes**
  Sezin Yüksel, Mario Ziegler, Sebastian Goerke, Uwe Hübner, Kilian Pollok, Falko Langenhorst, Karina Weber, Dana Cialla-May, and Jürgen Popp.
  The Journal of Physical Chemistry C, 2015, **119**, p. 13791-13798
- **Plasmonic nanostructures for surface enhanced spectroscopic methods**
  Martin Jahn, Sophie Patze, Izabella Hidi, Richard Knipper, Andreea Radu, Anna Mühlig, Sezin Yüksel, Vlastimil Peksa, Karina Weber, Thomas Meyerhöfer, Dana Cialla-May, Jürgen Popp.
  Analyst, 2015, 141, 756-793
- **Growth of hierarchically 3D Silver-Silica hybrid nanostructures by metastable state assisted atomic layer deposition (MS-ALD)**

Mario Ziegler*, Sezin Yüksel*, Sebastian Goerke, Karina Weber, Dana Cialla-May, Jürgen Popp, Kilian Pollok, Dong Wang, Falko Langenhorst, Uwe Hübner, Peter Schaaf, Hans Georg Meyer.
Advanced Material Technologies, 2017, 2, 1700015-17

- **Hierarchically designed 3D flower-like composite nanostructures as an ultra-stable, reproducible and sensitive SERS substrate**
  Sezin Yüksel*, Mario Ziegler*, Sebastian Goerke, Uwe Hübner, Karina Weber, Dana Cialla-May, Peter Schaaf, Hans Georg Meyer, Jürgen Popp.
  *ACS Applied Materials & Interfaces, 2017, **9**, 38854-38862*

Patents

- **Aktivierte 3-D-Nanooberfläche, Verfahren zu Ihrer Herstellung und Ihrer Verwendung**
  Mario Ziegler, Sezin Yüksel, Dana Cialla-May.
  September 2016, DE 10 2016 118 440.3

Conference Contribution

- **Improved stability of enzymatically generated silver nanoparticles (EGNPs) for surface enhanced Raman spectroscopy (SERS) using ultra-thin film technique**
  International Conference on Raman spectroscopy (24ICORS), 10-15 August 2014, Jena, Germany (Poster)
  Sezin Yüksel, Mario Ziegler, Uwe Hübner, Karina Weber, Dana Cialla-May, and Jürgen Popp.
- **3D Flower-Like Nanostructures as an Efficient and Reproducible template for Surface Enhanced Raman Spectroscopy (SERS)**
  10-15 August 2014, International Conference on Raman spectroscopy (24ICORS), Jena, Germany (Poster)
  Sezin Yüksel, Mario Ziegler, Uwe Hübner, Karina Weber, Dana Cialla-May, and Jürgen Popp.
- **Particle based approaches for enriching microorganisms and low molecular weight substances for subsequent Raman spectroscopic analysis**
  International Conference on Raman spectroscopy (24ICORS), 10-15 August 2014, Jena, Germany (Talk)

Karina Weber, Martha Schwarz, Sezin Yüksel, J. Michael Köhler, Dana Cialla, and Jürgen Popp.

- **Improved stability of enzymatically generated silver nanoparticles (EGNPs) for surface enhanced Raman spectroscopy (SERS) using ultra-thin film technique**
  Surface Enhanced Spectroscopies (SES), 7-10 August 2014, Chemnitz, Germany (Poster)
  Sezin Yüksel, Mario Ziegler, Uwe Hübner, Karina Weber, Dana Cialla-May, and Jürgen Popp.
- **3D flower-like nanostructures as an efficient and reproducible SERS substrate** SPIE Photonics Europe, Brussels, 14-17 April 2014, Belgium (Talk)
  Sezin Yüksel, Mario Ziegler, Uwe Hübner, Karina Weber, Dana Cialla, Jürgen Popp.
- **Enzymatically Generated Silver-Nanoparticles (EGNPs) as a Powerful Platform for Surface Enhanced Spectroscopy (SERS)**
  7th International Conference on Advanced Vibrational Spectroscopy (ICAVS-7), 25-30 August 2013, Kobe, Japan (Poster)
  Sezin Yüksel, Mario Ziegler, Uwe Hübner, Dana Cialla, Karina Weber, Jürgen Popp.
- **3D Flower-Like Nanostructures as an Efficient and Reproducible Surface Enhanced Raman Spectroscopy Substrate (SERS)**
  Molecular Plasmonic, 23-25 May 2013, Jena, Germany (Poster)
  Sezin Yüksel, Mario Ziegler, Uwe Hübner, Dana Cialla, Karina Weber, Jürgen Popp.
- **SERS As analytical Tool**
  SAVVY Workshop, 30 August 2013, San Sebastian, Spain (Talk)
  Dana Cialla, Martin Jahn, Sophie Patze, Anna Hauser, Sezin Yüksel, Andreea Radu, Izabella Hidi, Karina Weber, Jürgen Popp.

Acknowledgement

I would like to express my sincere gratitude to Prof. Dr. Jürgen Popp for giving me the opportunity to be part of his research group. His guidance and immense of knowledge helped me all the time during the research and writing of papers and this thesis.
Besides my advisor, I would like to thank my two my two supervisors, Dr. Dana Cialla-May and Dr. Karina Weber for their continuous and intensive help, support and advices for the last four years. I have developed and learned a lot because of their constructive and creative ideas as well as my organizational skills were strongly shaped by their expertise.
I would like to thank Prof. Dr. Sibyll Pollok for her friendly support and help. I was so lucky to share the office with her and all the friendly discussions helped me to understand "biology world" much way easier as being a physicist. I
Furthermore, I would like to thank Prof. Dr. Falko Langenhorst for sharing his valuable knowledge with me. And my gratitude goes to Dr. Kilian Pollok for the TEM, XRD measurement as well as long helpful discussions that made easier to understand material characterization part during the thesis.
I want to thank Dr. Dirk Bender for the DFT calculations for the THC molecule and also, I would like to express my gratitude to Andrea Dellith and Dr. Jan Dellith for providing SEM, EDX measurement. I really appreciated for their kind consideration, patience to me for answering my tones of questions.
I would like to thank Prof. Dr. Schubert, Dr. Stephanie Höppener and Prof. Dr. Silvia Ardizzone for their kind collaboration, manuscript correction and useful discussions. Moreover, I want to thank Almut Schwenke and Dr. Guido Soliveri for being nice co-workers, for the TEM measurements and for providing MW-assisted AgNPs for me.
I would like to thank to "clean room team", Dr. Uwe Hübner, Mario Ziegler and Sebastian Goerke for providing clean room and ALD facilities.
I am very grateful for the nice working atmosphere and the continues support of my colleagues of the SERS and biochip group, Dr. Lydia Lehniger, Vera Dugandzic, Dr. Andreea Radu, Sophie Patze, Richard Knipper, Dr. Izabella Hidi, Martin Jahn, Olga Zukovskaja, Dr. Barbara Seise, Dr. Xiao-Shan Zheng, and Sabine Schimdt. I am really appreciated for the being the part of this working group and many thanks for the nice moments, lots of funs, chats, dinners and coffee times.
I would particularly thank to and point out "Jena girls" (Vera, Lydia, Sapna, Darya, Melina, Andreea and Nazrin) for being always ready for me. I have been great times with you girls!

Last, but not the least, I would like to thank to my close friends Emin and Gökhan for being always supportive and friends being more than ten years.
Last but not least, I would like to express my gratitude to my both two families from Istanbul (my daddy, my mommy and Secil and Orkun) and from Paris (Talin, Murat and Audrey) for supporting me through out my whole life. Without their support, I cannot imagine this could happen. Love you all to the moon and back <3

Curriculum Vitae (CV)

Personal Information:

Name	: Sezin Yüksel
Address	: Eichendorffweg 3
	07745, Jena
Date of Birth	: 29 January 1986
Place of Birth	: Istanbul/Turkey
Marital Status	: Single

Education:

Since 11/2012	*Doctoral student* Institute of Physical Chemistry (IPC), Friedrich-Schiller University and , Jena, Germany The Leibniz Institute of Photonic Technology (IPHT), Jena, Germany.
09/2011 – 09/2012	*Master in Optics, Matter and Plasma* (double degree/Optics in Science and Technology (OpSciTec)) University Paris Sud 11, Institut d'Optique Graduate School co-accredited with Ecole Polytechnique, Paris, France.
10/2010 – 09/2011	*Master of Science in Photonics* (double degree/Optics in Science and Technology (OpSciTec)) Friedrich-Schiller University, Jena, Germany.
08/2008 – 08/2009	*Bachelor in Physics* Groningen University, Groningen, the Netherlands.
09/2005-01/2010	*Bachelor in Physics* Yeditepe University, Istanbul, Turkey.
09/2001-06/2004	*High School diploma specialized in natural science* Acibadem Science High School, Istanbul, Turkey.

Work Experience:

Since 11/2012	*Research Assistant*, at Institute of Physical Chemistry (IPC), Friedrich-Schiller University and , Jena, Germany The Leibniz Institute of Photonic Technology (IPHT), Jena, Germany, under the supervision of Prof. Dr. Jürgen Popp.
03/2009 – 09/2010	*Research Assistant*, at Laboratoire Physique et Etude des Matériaux ESPCI, CNRS, UPMC UMR, Paris, France. Under the supervision of Assoc. Prof. Alexandra Fragola.
04/2011 – 08/2011	*Internship*, at Leibniz-Institut für Photonische Technologien Jena, Germany. Under the supervision of Prof. Dr. Jürgen Popp.
01/2010-08/2010	*Research Assistant*, at Polymer Research Laboratory, Yildiz Technical University, Istanbul, Turkey. Under the supervision of Dr. Cenk Denktas.
08/2009-01/2010, 03/2008-08/2008	*Research Assistant*, at Yeditepe University, Istanbul, Turkey. Under the supervision of Assoc. Prof. Dr. S. Ipek Karaaslan.
06/2009-08/2009	*Internship*, at The Scientific and Technological Research Council of Turkey (TUBITAK), National Metrology Institute (UME), Kocaeli, Turkey. Under the supervision of Assoc. Prof. Ramiz Hamid.
06/2009-08/2009	*Internship*, at Biomedical Engineering Institute, Biomedical optics laboratory, Bogazici University, Istanbul, Turkey. Under the supervision of Prof. Dr. Ata Akin.
09/2008-02/2009	*Internship*, at Optical Condensed Matter Physics Group, The Zernike Institute for Advanced Materials, Groningen University, Groningen, the Netherlands.

Under the supervision of Prof. Paul H. M. van Loosdrecht.

Awards and Scholarship:

09/2010-09/2012	48.000 € for Optics in Science and Technology (OpSciTech) Master Programme (double degree), in the frame of Erasmus Mundus program, The Education, Audiovual and Culture Executive Agency (EACEA), European Union Commission.
09/2004-01/2010	35.000 € for bachelor in physics, from Ministry of National Education (MEB) Turkey.
08/2008 – 08/2011	7.000 € for bachelor in physics, in the frame of Socrates-Erasmus exchange program, The Education, Audiovual and Culture Executive Agency (EACEA), European Union Commission.
09/2001-06/2004	25.000 € for the high school studies specialized in natural sciences, from Istanbul Education and Culture Foundation (ISTEK) scholarship committee.

Jena, den

_____

Sezin Yüksel

Declaration/ Selbstständigkeitserklärung

Ich erkläre, dass ich die vorliegende Arbeit selbstständig und unter Verwendung der angegebenen Hilfsmittel, persönlichen Mitteilungen und Quellen angefertigt habe.

Ort, Datum:

Unterschrift:

Erklärung zu den Eigenanteilen der Promovendin sowie der weiteren Doktoranden/ Doktorandinnen als Koautoren an den Publikationen und Zweitpublikationsrechten bei einer kumulativen Dissertation

Für alle in dieser kumulativen Dissertation verwendeten Manuskripte liegen die notwendigen Genehmigungen der Verlage („*Reprint permissions*“) für die Zweitpublikation vor.

Bestätigung des Einverständnisses der Koautoren

Die Co-Autoren der in dieser kumulativen Dissertation verwendeten Manuskripte sind sowohl über die Nutzung, als auch über die oben angegebenen Eigenanteile informiert und stimmen dem zu.

Die Anteile der Co-Autoren an den Publikationen sind vor der jeweiligen Publikation aufgeführt.

Jena, den _____

Einverständniserklärung des Betreuers

Ich bin mit der Abfassung der Dissertation als publikationsbasiert, d.h. kumulativ, einverstanden und bestätige die vorstehenden Angaben. Eine entsprechend begründete Befürwortung mit Angabe des wissenschaftlichen Anteils der Doktorandin an den verwendeten Publikationen werde ich parallel an den Rat der Fakultät der Chemisch-Geowissenschaftlichen Fakultät richten.

Jena, den _____

Prof. Dr. Jürgen Popp